COSTA, 1

MINISTÉRIO DAS OBRAS PÚBLICAS, TRANSPORTES E COMUNICAÇÕES

Laboratório Nacional de Engenharia Civil

THREE-DIMENSIONAL MODELLING OF COHESIVE SEDIMENT TRANSPORT IN ESTUARINE ENVIRONMENTS

Liverpool, May 1995

Rui Carlos Faria Gameiro da Costa

Dissertação apresentada na Universidade de Liverpool
para obtenção do grau de Doctor in Philosophy

I&D
TESE
HIDRÁULICA

Ministério das Obras Públicas Transportes e Comunicações
Laboratório Nacional de Engenharia Civil

Departamento de Hidráulica
Núcleo de Estuários

Proc. 604/11/10637

University of Liverpool

Faculty of Engineering

Department of Civil Engineering

THREE-DIMENSIONAL MODELLING OF COHESIVE SEDIMENT TRANSPORT IN ESTUARINE ENVIRONMENTS

Rui Carlos Faria Gameiro da Costa

Licenciado em Eng.ª Civil pelo Instituto Superior Técnico
Mestre em Coastal and Oceanographic Engineering pela University of Florida, Gainesville

Dissertação submetida à Universidade de Liverpool
para obtenção do grau de Doctor of Philosophy

Liverpool, Maio 1995

ACNOWLEDGEMENTS

The author would like to express his gratitude to his academic supervisor Prof. B.A. O'Connor for his continued guidance and advice during the author's study period at the University of Liverpool. The author's appreciation is extended to Dr. John Nicholson, for his encouragement and many helpful discussions, and to Dr. Kamil Ali and Mr. Martin Crapper who provided data and useful information on their fluid mud experiments. Thanks are also due to Prof. Ramiro Neves from the Technical University of Lisbon, Drs. Ashish Mehta from the University of Florida and António Baptista from the Oregon Graduate Institute for their fruitful suggestions and to the numerous european researchers participating in the MAST II G8M-Project 4 on cohesive sediments, led by Dr. Charles Teisson, for their friendly cooperation from which this work also benefited.

The author is indebted to Hydraulics Research Ltd. who provided data for running the numerical models developed in this thesis and, in particular, to Drs. Nicholas Odd, Alan Cooper, John Baugh and William Roberts for their assistance and their helpful suggestions. The author would also like to thank the Mersey Barrage Company and, in particular, its assistant general manager, Mr. Adam Wilson, for allowing access to its archives and the use of data produced for the company.

Support for the author's doctoral studies in the UK by the portuguese National Council for Science and Technology Research (JNICT), under scholarship BD/673/90-IG, and

the British Council, under award LIS/2260/09(90/91), is gratefully acknowledged. The author would also like to thank his employer, the portuguese National Laboratory for Civil Engineering (LNEC), where most of the programming and application work took place, for authorising and supporting his project of doctoral studies. The continued encouragement of Messrs. Jaime Melo Baptista, Head of the Hydraulics Department, Eduardo Oliveira, Head of the Estuaries Division and of Dr. Afonso Covas, chairman of the local supervisory committee is acknowledged. Special thanks are due to Mrs. Esmeralda Costa, Messrs. Eleutério Vieira, Fernando Brito and Fernando Barreto, from the Hydraulics Department, who produced most of the drawings and to Mrs. Palmira Cruz and Mrs. Beatriz Carmo, from the Computer Centre, who carried out three-dimensional visualisation and drawing production.

Finally, the author wishes to thank his family, friends and colleagues for their support, encouragement and patience during this special period of his life.

ABSTRACT

Patterns of flow and cohesive sediment transport in estuarine environments under tidal action are extremely complex. Both the geometric irregularity of estuaries and the importance of vertical phenomena in cohesive sediment transport require that such phenomena are described in three dimensions.

In the present investigation a theoretical formulation for describing the transport in three dimensions of suspended sediment, treated as a single representative class, in low concentration environments was developed, which incorporated a generic vertical coordinate transformation. The use of specific forms of the transformation will allow fine vertical discretisations in areas of the domain where large concentration gradients occur which, in the case of cohesive sediment, is expected to happen near the estuary bed. A numerical model, aimed at engineering applications, was developed based on this formulation and applied to the Mersey Estuary, UK. The model successfully reproduced the expected features of a cohesive sediment concentration field under tidal action, namely its overall vertical structure and the settling/deposition and erosion/re-suspension sequences around slack water. Model application also led to the conclusion that the simulation of the finer details of the vertical concentration structure would require a more complex description of settling and turbulence, although improved data sets will be necessary to test such formulations.

The description of the dynamics of near-bed mobile high-concentration layers (fluid mud) was also considered essential, as such layers significantly change the fluxes at the lower interface of low concentration layers and are the cause for significant advective transport. A depth-averaged formulation describing the dynamics of fluid mud was developed and a pilot numerical model, corresponding to this formulation, was tested using a laboratory experiment which is representative of layer formation through rapid settling. Model application successfully simulated the main features of the experiment and allowed the identification of the settling fluxes (and associated layer formation mechanisms) and fluid mud viscosity as the the main factors controlling fluid mud behaviour. It is expected that further research on such aspects and the definition of a practical criterion (other than concentration alone) for the identification of fluid mud will allow the coupling of this type of models with those describing transport in low concentration layers and, therefore, ensure the applicability of such modelling systems to most estuarine environments.

TABLE OF CONTENTS

LIST OF TABLES

LIST OF FIGURES

LIST OF SYMBOLS

a	Settling parameter, depth-averaged part of generic variable α, lower diagonal element in a tri-diagonal matrix
a'	Deviation from depth-average value of generic variable α
$a(\cdot),...,i(\cdot)$	Generic form of coefficients in advection-diffusion equation
A	Bed layer critical erosive stress parameter, entrainment parameter, generic numerical coefficient, final concentration at the origin of vertical coordinate in Dobbins solution
A_h	Horizontal area
A_x	Vertical area perpendicular to the x axis
A_y	Vertical area perpendicular to the y axis
AEC	Anion Exchange Capacity
b	Settling parameter, buoyancy or reduced gravity, intensive property of a system, main diagonal element in a tri-diagonal matrix, depth-averaged part of generic variable β
b'	Deviation from depth-average value of generic variable β
bf	Subscript denoting bed formation
B	Bed layer critical erosive stress parameter, extensive property of a system, generic numerical coefficient
B_{BM}	Settling coefficient for Brownian motion
B_{DS}	Settling coefficient for differential settling
B_{SH}	Settling coefficient for velocity gradients
c	Upper diagonal element in a tri-diagonal matrix
C	Mass concentration (of generic constituent or of suspended sediment)
$\bar{C}$	Time-averaged concentration

C_0	Initial concentration
C_1	Upper limit of the free-settling range
C_2	Upper limit of the hindered settling range
C_3	Concentration corresponding to the peak settling flux
C_4	Concentration corresponding to negligible settling velocity
C_b ,C_b^i	Near-bed sediment concentration, near-bed concentration of sediment class i
C_D	Drag coefficient
C_f	Residual concentration in a deposition test
C^i	Initial concentration
C_m	Concentration of fluid mud
C_R	Reference concentration in kinematic viscosity formulation
Cu	Courant number
$C_{x^* y^* \sigma}$	Nodal concentration value for interpolation
$C_{x^* \sigma}$	Concentration value resulting from interpolation in y* direction
C_σ	Concentration value resulting from interpolation in y* , x* directions
C'	Deviation of concentration from its time-mean value
C', C_0'	Non-dimensional concentration, characteristic maximum
C^*,C^{**},C^{***}	Intermediate concentrations resulting from fractional step method
CD	Chart Datum
CEC	Cation Exchange Capacity
CS	Control surface
CV	Control volume
d	Depth-averaged part of generic variable δ

d_0, d_m , d_b	Thickness of low concentration layer, thickness of mobile fluid mud layer, thickness of bed layer
d_i	Advection distance along a characteristic line
d_i , d_j , d_{ij}	Diameters of the i and j classes of particles, sum of diameters of classes i and j
d'	Deviation from depth-average value of generic variable δ
D	Grain diameter, total depth, flow depth, entrainment parameter, generic numerical coefficient
D_m	Fickian molecular diffusion coefficient
e, e_0	Bed void ratio, reference void ratio
e_m , e_b , e_f	Fluid mud voids ratio, bed voids ratio, floc voids ratio
en	Subscript denoting entrainment
er	Subscript denoting erosion
E	Non-dimensional entrainment rate
E, E_1, E_2	Generic numerical coefficients
$E(Ri_B)$	Entrainment coefficient
f	Coriolis parameter
$f(\zeta/H)$	Vertical effective viscosity vertical distribution function
$f(z)$	Generic function of the cartesian vertical coordinate
f_0	Friction factor at the clear water/fluid mud interface
f_m	Friction factor at the fluid mud/cohesive bed interface
F	Superscript denoting values at the formation stage of a bed layer, entrainment parameter
$F(z)$	Generic function
F, F_1, F_2	Generic numerical coefficients

F_b	Flux at the bed or lower interface
F_{dz}	Vertical Reynolds flux
F_e	Erosion flux
F_n	Turbulent mass diffusion flux in the n direction, term in summation in Dobbins solution
F_p	Deposition flux
F_s	Settling flux, turbulent mass diffusion flux in the s direction
F_t	Total turbulent mass diffusion flux
F_x	Turbulent mass diffusion flux in the x direction, x component of body forces
F_y	Turbulent mass diffusion flux in the y direction
F_z	Turbulent mass diffusion flux in the z direction
F_σ	Transformed turbulent vertical mass diffusion flux
g	Acceleration of gravity
$g(Z)$	Generic function of the vertical coordinate obtained through the use of the Phillips transformation
G	Entrainment parameter, amplification factor, absolute velocity gradient
h	Flow depth in a deposition test
H	Total depth
H	Height of control surface, characteristic estuarine depth, water depth
HW	High water
i, I	Reference of grid node in the longitudinal direction
$\vec{i}$	Longitudinal unit base vector

ib	Subscript denoting an inflow boundary
$\vec{j}$	Lateral unit base vector
j, J	Reference of grid node in the lateral direction
k	Boltzmann constant, mean turbulence energy, settling parameter, reference of grid node in the vertical direction
$\vec{k}$	Vertical unit base vector
k_1	Flocculation settling parameter
$\bar{k}_2, k_2$	Hindered settling parameters
k_s	Water retention coefficient during settling into fluid mud layer
K	Concentration at the origin of vertical coordinate in Dobbins solution
$K(d_i, d_j)$	Collision frequency function corresponding to a given collision mechanism
K_{BM}	Collision frequency function for the case of Brownian motion
K_{DS}	Collision frequency function for the case of differential settling
K_i	Mass diffusivity constants
K_{SH}	Collision frequency function for the case of velocity gradients
l_c, l_{cn}, l_{cs}	Mass mixing length, mass mixing lengths for neutral and stratified conditions
l_m, l_{mn}, l_{ms}	Momentum mixing length, momentum mixing lengths for neutral and stratified conditions
l_n, l_s	Geometric scales of normal and tangential motions
L	Length, characteristic estuarine length
L_A	Advection operator in fractional step method

L_C	Lateral operator in fractional step method
L_L	Longitudinal operator in fractional step method
L_V	Vertical operator in fractional step method
L_x , L_y	Dimensions of domain in advection test case
LBD	Liverpool Bay Datum
LW	Low water
m	Mass, mass per unit area, deposition parameter, settling parameter, integer
m_1, m_2, m_3	Parameters in empirical settling function
m_e	Erosion constant
m_f, m_w	Mass of flocs, mass of water
m_i	Mass per unit area released at each source i in analytical solution used in advection test case
m_{sys}	Total mass in a system
M	Number of Δx intervals in length L_x
M_{sf}	Solids mass within a floc
$M_z(x, y, t)$	Vertical effective viscosity function
n	Bed porosity, time level, settling parameter, normal direction to a solid surface
n_1	Flocculation settling parameter
n_2	Hindered settling parameter
n_i , n_j	Number concentrations (volume^{-1}) of the i and j classes of particles
N	Numerical solution
$\vec{N}$	Net sediment flux vector

$\vec{N}_A$	Advective component of net sediment vector
$\vec{N}_D$	Diffusive component of net sediment vector
N_{ij}	Collision frequency
$\vec{N}_S$	Settling component of net sediment vector
N_z	Vertical momentum effective viscosity
N_z , N_σ	Net vertical sediment fluxes
OD(N)	Ordnance Datum (Newlyn)
p	Probability of sediment deposition, entrainment parameter, subscript denoting a particle's trajectory, integer
p , p_a	Pressure, atmospheric pressure
p_i	Probability of deposition for sediment of class i
P	Number of Δy intervals in length L_y
q	Buoyancy flux, integer
$\vec{q}$	Fluid velocity vector
$\bar{\vec{q}}$	Time-mean value of fluid velocity vector
$\vec{q}'$	Deviation from time-mean value of fluid velocity vector
Q	Non-dimensional buoyancy flux, number of $\Delta\sigma$ intervals in length L_σ
r	Re-entrainment coefficient, first step concentration values in the Barakat and Clark method
$r(Rf)$	Stratification function
$r(Ri)$	Generic function
R	Residual terms resulting from Taylor series expansion

$R(\partial p/\partial z)$	Generic function
Re , Re_s	Reynolds number, grain Reynolds number
Ri ,Rf ,Rc, Ri_c	Gradient Richardson number, flux Richardson number, critical value of the flux Richardson number, critical Richardson number
$R_p R_x R_y R_\sigma R_v$	Depth-averaging residuals
s	Second step concentration values in the Barakat and Clark method, subscript denoting settling
s_x	x* standard deviation of two-dimensional gaussian distribution
s_y	y* standard deviation of two-dimensional gaussian distribution
sb	Subscript denoting a solid boundary
$S(\partial C/\partial z)$	Generic function
S_t , S_{t0}	Schmidt number, Schmidt number calculation constant
t	Time
t_0	Initial time
t', t_0	Non-dimensional time, reference time
t^*	Time coordinate in transformed domain
T	Period, absolute temperature
T_v	Stress acting in a vertical plane
u, U	x component of the velocity
$\bar{u}$	Time averaged x velocity component
$\langle u \rangle$	Depth-mean x component of the velocity
u_0, u_m	x depth-averaged velocity in low concentration layer, x depth-averaged velocity in mobile fluid mud layer
u_*	Friction velocity
u'	Deviation of x velocity component from its time-mean value

u', u_0	Non-dimensional x velocity, characteristic x velocity
U	Integral of the x velocity over the mobile fluid mud layer
v, V	y component of velocity
$\bar{v}$	Time averaged y velocity component
v_0, v_m	y depth-averaged velocity in low concentration layer, y depth-averaged velocity in mobile fluid mud layer
v_n , v_s	Velocity scales of normal and tangential motions
v_n	component of velocity vector normal to the area elements of a control surface
v'	Deviation of y velocity component from its time-mean value
V, V_w , V_f, V_s	Total volume, volume of water, volume of flocs, volume of solids
V_{bf}	Bed formation velocity
V_e	Entrainment velocity
V_i	Low concentration suspension/fluid mud interface lowering velocity
V_{tf} ,V_{wf} , V_{sf}	Total volume of a floc, volume occupied by water within a floc, volume occupied by solids within a floc
w	z component of velocity
$\bar{w}$	Transformed z velocity component, time averaged z velocity component
w'	Deviation of z velocity component from its time-mean value
w', w_0	Non-dimensional z velocity, characteristic z velocity
w_{us},w_{uw}	Upsloping vertical velocity, upwelling vertical velocity
W_r	Reference settling velocity
W_s,W_s^i	Settling velocity, settling velocity of sediment class i
W_{s50}	Median settling velocity

$\bar{W}_s$	Mean settling velocity
$\bar{W}_{s0}$, W_{s0}	Peak settling velocity, modified peak settling velocity
W_s', W_{s0}	Non-dimensional settling velocity, characteristic maximum settling velocity
W_s^{max}, W_s^{min}	Upper value of the settling velocity classes, lower value of the settling velocity classes
x , x^*	Longitudinal cartesian coordinate, longitudinal coordinate in transformed domain
x'	Non-dimensional longitudinal coordinate
x_{0i}	Position of each source i in analytical solution used in advection test case
x_c^*, x_0^*	x* coordinate of centre of domain in advection test case, x* coordinate of centre of two-dimensional gaussian distribution
x_i	x coordinates of measuring stations
y, y^*	Lateral cartesian coordinate, lateral coordinate in transformed domain
y_c^*,y_0^*	y* coordinate of centre of domain in advection test case, y* coordinate of centre of two-dimensional gaussian distribution
Y_n	Term in summation in Dobbins solution
z , z^*	Vertical cartesian coordinate, vertical coordinate in transformed domain
z_b	Vertical coordinate of the bed or lower interface of a low concentration suspension
Z	Bed depth below initial surface, vertical coordinate in transformed domain using Phillips transformation
α	Generic variable
α , α'	Stratification parameters
α_1 ,...,α_n	Erosion resistance defining parameters

α_n	Coefficient in summation in Dobbins solution
A	Sigma transformation parameter (derivative with respect to x)
A', A_0	Normalised longitudinal transformation parameter, characteristic value of longitudinal transformation parameter
β , β'	Stratification parameters
β	Parameter of sigma transformation, generic variable
B	Sigma transformation parameter (derivative with respect to y)
γ	Coefficient in Barakat and Clark method, coefficient in kinematic viscosity formulation
γ_m , γ_p , γ_q	Frequencies
$\dot{\gamma}$	Shear rate
Γ	Sigma transformation parameter (derivative with respect to z)
Γ', Γ_0	Normalised longitudinal transformation parameter, characteristic value of longitudinal transformation parameter
δ	Generic variable
$\delta_1,...,\delta_5$	Bed shear strength parameters
Δb	Interfacial buoyancy step
Δt , Δt^*	Time steps
ΔU	Interfacial velocity jump
Δx , Δx^*	Longitudinal steps
Δy , Δy^*	Lateral steps
Δz^* , $\Delta\sigma$	Vertical steps
$\Delta\rho$	Interfacial density jump
$\Delta\rho_i$, $\Delta\rho_j$	Difference between the densities of particles of classes i and j and the density of water

ε	Total energy dissipated per unit mass, dissipation rate of turbulence energy, error
$\bar{\varepsilon}_i$	Depth-averaged turbulent mass diffusivities
ε_0 , ε_1	Mass vertical effective viscosity parameters
ε_h	Horizontal turbulent mass diffusivity
ε_n , ε_s	Mass diffusivities in the normal and tangential directions to a coordinate line
ε_x , ε_y , ε_z	Turbulent mass diffusivities in the x, y, z directions
ε_{x^*} , ε_s	Turbulent mass diffusivities in the x*, s directions
ε_{xx} , ε_{xy}	Momentum diffusivities in the x direction
ε_{yx} , ε_{yy}	Momentum diffusivities in the y direction
ε_x', ε_z'	Non-dimensional x mass diffusivity, non-dimensional z mass diffusivity
ε_v , $\bar{\varepsilon}_v$	Vertical and modified vertical turbulent mass diffusivities
ε_z	Vertical mass effective viscosity
ζ	Initial y* coordinate of particle in backtracking process, time dependent component of numerical error, elevation from the bottom
$\zeta_1,\ldots,\zeta_5$	Bed shear strength parameters
η	Free surface position
η_w ,η_m ,η_b	Position of low concentration suspension free surface, position of fluid mud surface, position of bed surface
θ	Schmidt number calculation constant, argument of trigonometric function
κ	von Karman constant
λ	Coefficient in Barakat and Clark method
μ	Dinamic viscosity

ν	Kinematic viscosity
ξ	Normalised x coordinate, initial σ coordinate of particle in backtracking process
$\overline{\rho}$	Time-averaged density
ρ^*	Bed bulk density
ρ_0	Depth-averaged density of low concentration suspension
ρ_i , ρ_j	Densities of particles of classes i and j
ρ_m	Depth-averaged density of fluid mud, density of fluid mud
ρ_r , ρ_l	Reference density, density of arbitrary fluid
ρ_s	Particle density
ρ_w , ρ_f , ρ_s	Density of water, density of flocs, density of solids
σ	Vertical coordinate in transformed domain
σ',σ_0	Non-dimensional vertical coordinate, characteristic estuarine transformed depth
σ_{ii}	Viscous stresses
τ	Initial t* coordinate of particle in backtracking process
τ_b	Time mean bottom shear stress, bottom shear stress
τ_{bf}	Critical shear stress for bed formation
τ_{bx} , τ_{by}	Stresses at the fluid mud/bed interface in the x, y directions
τ_{cl},τ_{cM}	Lower value of critical shear stress for deposition, upper value of critical shear stress for deposition
τ_{cd} ,τ_{ci}	Critical shear stress for deposition, critical shear stress for deposition of sediment of class i
τ_{ce}	Critical shear stress for erosion, critical erosive stress of a bed layer
τ_{dm}	Critical shear stress for settling into fluid mud

τ_{fs}	Floc shear strength
τ_i ,τ_{ix} , τ_{iy}	Shear stress at low concentration suspension/fluid mud interface, stresses at the low concentration/fluid mud interface in the x, y directions
τ_s	Bed shear strength
τ_{zx}	Reynolds stress in z plane and in x direction
T	Sigma transformation parameter (derivative with respect to t)
T', T_0	Normalised time transformation parameter, characteristic value of time transformation parameter
ϕ	Angle between a sigma surface and the horizontal
$\Phi(W_s^i)$	Frequency distribution of the settling velocity classes
χ	Initial x* coordinate of particle in backtracking process
Ω	Angular velocity in advection test case, exact numerical solution

CHAPTER 1
INTRODUCTION

1.1 Problem Significance

Coastal areas have traditionally offered significant advantages for human settlement. It is estimated that some two thirds of the world's population live in areas distant less than 80 km from the coastline and at elevations less than 15 m relative to mean sea level. Estuaries, in particular, have witnessed the development of numerous urban centres on their banks (most of the world's largest cities are located around estuaries), due to the valued combination of sea accessibility, sheltered harbours and the possibility of inland navigation with the availability of fresh water from the upland rivers. Population growth and the rapid industrial development of many estuarine centres has led to intensive use of estuarine waters and to competing demands. In fact, the needs associated with port development, navigation and wastewater disposal soon became contradictory with those related to recreational uses and to the preservation of natural aquatic diversity.

Estuaries are meeting places, transitional areas, between land and sea, providing support to a wide variety of life forms due to the natural nutrient wealth of their waters and surrounding wetlands. Sensitive areas in estuarine environments usually include fish spawning grounds, invertebrate habitats and bird reproduction areas. Estuaries can also act either as collecting areas or conveying routes for suspended and dissolved materials, originating either from rivers or the sea.

Among the many problems related to anthropogenic activities in estuarine environments those related to sediment dynamics are often of very significant economic and ecologic importance. Such aspects include:

a) Problems related to changes in estuarine topography, due to land reclamation or dock construction, and in the nature of the estuarine environment, due to wetland drainage and urban development.

b) Problems related to changes in estuarine bathymetry due to dredging of navigation channels and port basins, dumping of dredged materials and scouring or shoaling of estuary channels due to hydrodynamic modifications.

c) Issues related to the effectiveness and safety of man-made structures and to operation costs in estuarine ports and harbours.

d) Water quality problems, due to adsorption or desorption of pollutants by fine grained sediment which can affect invertebrates and fish; such effects can either be caused by physico-chemical changes in the water or by mechanical action (dredging).

e) Water quality problems due to increased turbidity, thus inhibiting light penetration, causing a decrease in phytoplankton production and, consequently, in the amounts of food available for fish consumption.

In general terms it can be stated that sediment dynamics conditions the configuration and overall behaviour of estuaries and that the knowledge of sediment distribution and the ability to predict changes in the patterns of sediment circulation are of fundamental importance for the global management of such water bodies. In particular, the knowledge of the behaviour of the finer fractions of estuarine sediment is paramount, since aggregation of particles (related to the cohesive properties of the clay mineralogic fraction and to the presence of organic matter and microorganisms in the water) determines the behaviour of most estuarine sediments (commonly known as *muds*), even when a large percentage of the sediment is non-cohesive.

1.2 Objectives and Methodology

Studies of sediment dynamics in estuaries have commonly been performed in the past through field studies and physical and numerical modelling. Such studies have generally been carried out by using an appropriate combination of the above methods, their choice being conditioned by the purpose of the study, the costs involved and, in the case of engineering studies, the desired degree of accuracy of the project.

Field studies can be used either as a way to provide data and validate model applications or, by themselves, aiming at identifying and solving particular problems. The costs involved and the practical difficulties connected with large scale synoptic studies prevent the latter approach from being fully effective, while the first is always a fundamental contribution to the success of modelling efforts.

Physical modelling provides a *global* picture (i.e. individual processes are not isolated) and has been successfully applied in the past to solve hydrodynamics problems, although sediment dynamics problems have been studied less effectively. In particular, the complex physico-chemical nature of the finer, cohesive, fractions of sediment and of the cohesion forces between particles have prevented, so far, a suitable type of model sediment to be found and used in such studies.

Numerical modelling of estuarine systems (or *system modelling*) is strongly dependent on the state of knowledge that exists at a particular time, on sediment processes and how these are described in mathematical terms (*process modelling*). In the particular case of cohesive sediment the need to describe, as accurately as possible, a large number of interacting processes, i.e. processes in which flow and sediment mutually influence themselves to various degrees is certainly an additional difficulty.

Numerical modelling has been extensively applied in the past to solve estuarine problems and is still an active field of research. In an ideal situation, fully three-dimensional tidal models, solving a coupled set of momentum and continuity equations for water and several transport equations for salt, sediment and other pollutants, including the associated equations for turbulence description, some of which must incorporate modules for chemical and biological reactions, should be used. Moreover, in wide estuaries, wetting and drying of tidal flats should be accounted for, as should the effects of waves and winds and their interactions with currents and turbulence, in order to achieve a complete description of the phenomena involved. The

computational complexity of such a methodology and the lack of basic knowledge to describe a large number of physical and chemical processes involved, as well as limitations of computer hardware, currently prevent the use of such an approach for a complete estuary.

Present philosophy is to neglect many interactions and to reproduce only dominant processes in models; in this way it is possible to combine together a series of system models to study estuarine fine sediment movements in three dimensions. An example of such an approach is the TIDEFLOW System of Hydraulics Research Ltd. (HR). While the TIDEFLOW System is able to study parts of large estuaries and the whole of small estuaries, it can only use a limited number of layers to describe the averaged flow and sediment concentrations over each one of them (typically eight to ten layers are used over the maximum flow depth). In many situations, however, it is necessary to have much more detailed information of near-bed processes. Moreover, in high tidal range estuaries with large fine sediment inflows, it is necessary not only to consider the separate motion of high concentration fluid mud layers (as in model FLUIDMUD-2D of HR) but also to describe sediment exchanges between such layers and the lower concentration layers above, as part of the models to be developed.

The main purpose, therefore, of the present investigation was to develop theoretical formulations and numerical models to describe cohesive sediment transport in three dimensions, incorporating recent research results related to the pertinent physical processes, and numerically formulated using the techniques most adequate to each

process, in order to improve accuracy relative to existing models. The description of the dynamics of fluid mud layers was considered essential as also was the need to be able to use a fine vertical discretisation in areas of the domain where large concentration gradients are to be expected. The research was also developed keeping in mind the need for practical engineering tools aimed at solving particular problems with adequate accuracy.

1.3 Organisation of Thesis

A summary of the different physical processes related to cohesive sediment dynamics in low to medium concentration estuarine environments is presented in Chapter 2. Process modelling results obtained to date are reviewed and evaluated from an engineering modelling approach, i.e. from the viewpoint of their applicability in models with predictive capabilities within reasonable computational requirements.

In Chapter 3 the transport of cohesive sediment in suspension is introduced from the mathematical viewpoint, modelling options are reviewed and the formulation of a three-dimensional model is presented. The methods used in the development of the numerical model and test results of the main computational units are described in Chapter 4. The application of the model to the simulation of suspended fine sediment transport in a tidal channel (the Mersey Narrows, in the UK) is presented in Chapter 5.

Chapter 6 deals with the transport of near-bed high-concentration suspensions. The physics of such suspensions and the assumptions for mathematically formulating the movement of sediment under those conditions are presented and a numerical model is developed. Application of the latter model to a laboratory situation is presented and discussed in the same chapter.

A summary of the research, the pertinent conclusions and recommendations for future work are presented in Chapter 7.

CHAPTER 2
ASPECTS OF FINE SEDIMENT DYNAMICS IN ESTUARIES

2.1 Introduction

Field measurements of suspended sediment concentrations in estuaries and coastal areas where fine sediments are predominant usually show long periods of near-constant concentration, interrupted by relatively short periods of rapid variation; such periods, which occur around slack water, can still be divided into settling-dominated periods, in which concentrations abruptly decrease, and re-entrainment-dominated periods, in which a sudden increase in concentration restores its previous level.

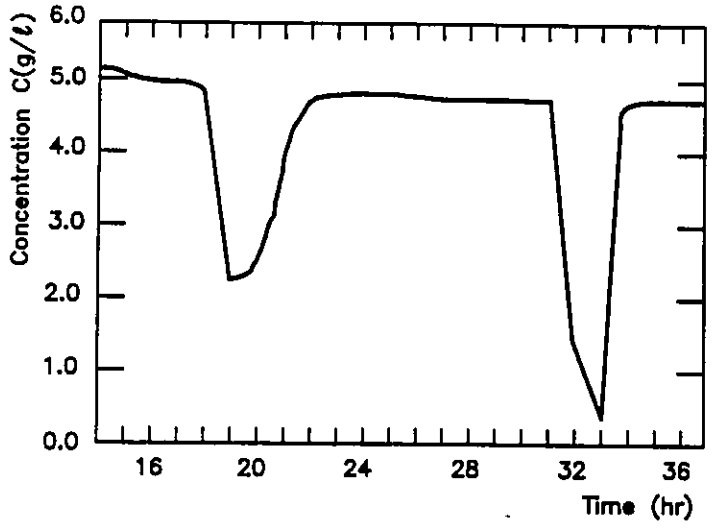

Figure 2.1 Suspended sediment concentration as a function of time in a high concentration environment (Hangzhou Bay - People's Republic of China). Adapted from Feng (1990).

Figure 2.1 (Feng, 1990) obtained during a neap tide in Hangzou Bay (People's Republic of China), a high turbidity, fine sediment environment, gives a good description of the phenomenon, although the hourly intervals between measurements prevent a finer representation. A general framework for the description of fine sediment transport processes in estuaries will, therefore, identify two main components:

(i) a *horizontal transport* component, in connection with horizontal advection phenomena, which is dominant during most of the tidal cycle and is expressed through measured concentration values at any given point which are almost constant in time;

(ii) a *vertical transport* component, in connection with vertical settling and diffusion and with sediment exchanges with the bed, whose effect is dominant around slack water, when sudden variations in concentration are apparent.

From the above two transport components, the latter combines the physical phenomena which make fine sediment transport distinctive in relation to the transport of dissolved constituents (salt, for example) and, to a lesser extent, of coarse sediments. Furthermore, and although the vertical component of transport is only dominant during relatively short periods within the tidal cycle, it is within these periods that most exchanges with the bed take place. Therefore, it is crucial for an accurate description of fine sediment dynamics in estuarine environments that the physical processes

contributing to the vertical component of transport are correctly identified and modelled and, in particular, those processes through which sediment is exchanged between the bed and the water column.

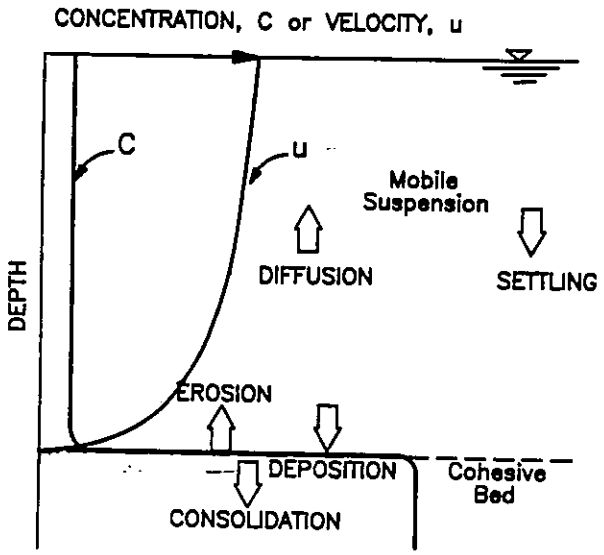

Figure 2.2 *Classical* definition of water column/sediment bed transition and of the vertical sediment fluxes (adapted from Mehta, 1989).

Schematic descriptions of the phenomena involved in the vertical dynamics of fine sediment under the action of tidal currents are presented in figures 2.2 and 2.3. Figure 2.2 shows the *classical* process description, commonly associated with low and medium concentration environments, in which a sharp transition is assumed between the water column and the cohesive bed. Figure 2.3 presents an idealised profile and flux definition for the cases in which the transition between the water column and the cohesive bed is made by a high concentration layer, known as fluid mud, which exchanges sediment with the water column and the bed through different processes than in the first case. Such layers, with thicknesses ranging from tens to hundreds of centimeters, have been detected in high concentrations environments and it has been

hypothesised that they may represent a more widespread feature in estuarine environments than currently thought.

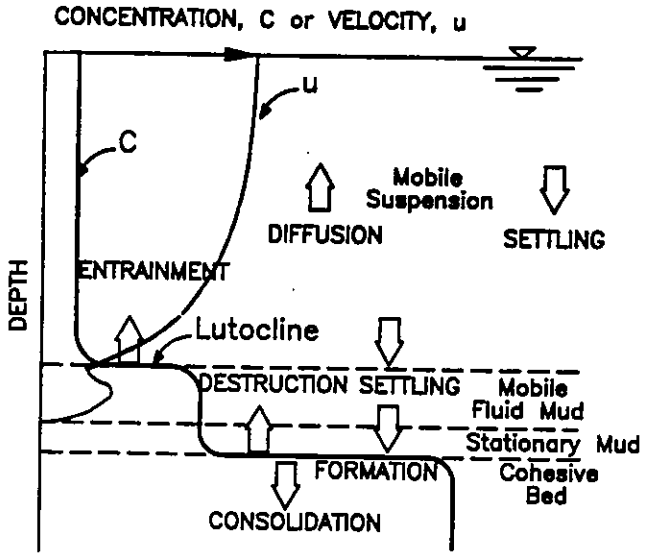

Figure 2.3 Idealised definition of water column/sediment bed transition and of the vertical sediment fluxes, in the presence of fluid mud (adapted from Mehta, 1989).

In this chapter a review of the physical processes of interest for the *classical* description of fine sediment dynamics, as shown in figure 2.2, will be presented. However, the higher complexity of the near-bed processes (and corresponding fluxes) associated with figure 2.3 strongly recommends that the properties of fluid mud layers are investigated, so that an improved bed boundary condition can be introduced in transport models. The generation, dynamics and destruction of fluid mud layers and the pertinent physical processes will, therefore, be separately described in Chapter 6.

2.2 General Properties of Fine Estuarine Sediments

The most commonly found sediments in many estuaries are generally described as *muds*. Typically these are mixtures of fine sediment fractions (in the clay and silt grain size ranges), organic matter of diverse nature, salt or brackish water and, in certain cases, even small amounts of coarser sediment size fractions (fine sand, mainly). The behaviour of muddy sediments in aquatic environments is complex as, unlike coarser sediments, it is not uniquely determined by grain size distribution (Berlamont et al., 1993); in fact, not only the physico-chemical properties of both mud components and the surrounding fluid are relevant, but flow characteristics have also to be considered.

Regarding the sediment fraction of muddy materials two different criteria can be applied: (i) a grain size classification; (ii) a mineralogic classification, related to particle *activity* or ability to interact with other particles, forming aggregates.

In terms of the grain size classification of sediment, coarse fractions are defined as those having particle sizes greater than 63 μm, while the fine fractions can be divided into silt (coarse silt: 20-63 μm; medium silt: 6-20 μm; fine silt: 2-6 μm) and clay (particle sizes less than 2 μm).

In terms of the mineralogic criterion a less well defined boundary, in the size range of 20 to 40 μm, separates *active* or cohesive materials, i.e. materials for which

interparticle attraction forces may become higher than gravitational forces, from *inert* or cohesionless sediments. This difference in behaviour results from the mineral composition of the sediment and should not be directly related to particle size, although most cohesive particles actually have sizes in the clay grain size range (Mehta et al., 1989). Cohesive particles are generally of clayey mineralogic nature, which presents particle sizes usually less than 10 μm and, typically, less than 2 μm (Gorsline, 1984), although it has been reported by Unsöld in 1982 that quartz particles of sizes less than 10 μm also present cohesive properties in water (McCave, 1984).

In a mineralogic sense, clays are composed of a family of silicate minerals with sheet structures and possess the property of ion exchange, reflecting the existence of unsatisfied bonds on and within the sheet structures (Gorsline, 1984). This property provides a mechanism for transfer of organics and metal ions (a fundamental aspect for environmental studies) and is the primary factor for aggregation of clay particles in marine environments. Common clay groups are kaolinites, montmorillonites and illites. From the viewpoint of their mineralogy, silts are typically heterogeneous mixtures of detrital primary minerals of which quartz is most common, and feldspars and ferromagnesian minerals are common accessories (Gorsline, 1984).

Organic matter found in muddy sediments can have different origins, natures and molecular shapes but is particularly important in forming aggregates and in binding mineral particles, through processes known as organic aggregation and bioflocculation (when living organisms are intimately associated with the aggregates). Formation of

organic aggregates in estuarine waters is a common phenomenon where high levels of dissolved organic matter exist and seems to be predominantly due to polysaccharides, polymers produced by micro-organisms (van Leussen, 1988).

The main differences in behaviour between muds and coarse sediments are, consequently, due to the ability of the primary particles of the former to cluster or aggregate, producing larger particles, called flocs or aggregates[1]; this is due to the cohesive properties of the *active* sediment fraction in salt water, to the binding action of the organic molecules and to strong biological *glues* produced through bioflocculation processes. The process of aggregation does not continue indefinitely, however. Flocs are destroyed under the shearing action of the surrounding turbulent fluid, leading to the existence of upper values for the floc sizes under given hydrodynamic conditions.

Floc aggregation and breakup largely control the transport of mud particles in estuaries as the properties of the flocs, such as floc size, floc size distribution, floc density and floc strength, influence most phenomena relevant for a description of transport and its modelling to a much larger extent than the properties of primary particles. In very general terms floc properties influence settling fluxes (through their dependence on the settling velocity) as well as deposition fluxes (through their dependence on the settling velocity and on the probability of deposition) and erosion fluxes (through the bed

[1]In this work the clustering of particles is indistinctly called *flocculation* or *aggregation* and the resulting clusters are also indistinctly referred to as flocs or aggregates. Both descriptions appear in the literature.

intergrain cohesive strength and susceptibility to crushing or re-arrangement due to overburden).

In order to understand floc creation and destruction and the properties of the existing suspended flocs, at a given time, it is useful to decompose such processes into three main components: collision mechanisms and aggregation mechanisms, which lead to the binding of particles, and breakup mechanisms, leading to the destruction of flocs (van Leussen, 1988).

When primary cohesive particles exist in suspension it is necessary, for aggregates to be formed, that such particles are brought together close enough so that attractive forces become dominant. The collision frequency, N_{ij} (number of collisions occurring per unit time and per unit volume) between two classes of particles of diameters d_i and d_j can be written as

$$N_{ij} = K(d_i, d_j) n_i n_j \tag{2.1}$$

where n_i and n_j are the number concentrations (volume^{-1}) of the i and j particles and $K(d_i, d_j)$ is the collision frequency function corresponding to a given collision mechanism (van Leussen, 1988). The main collision mechanisms are (Krone, 1978; van Leussen, 1988):

(a) Brownian motion, which is the irregular and random motion of colloidal particles hit by thermally agitated water molecules. This is an important

mechanism at the beginning of the flocculation process, when the particles are still very small. Brownian motion produces aggregates having a ragged structure, weak and easily broken by low velocity gradients in the fluid or crushed in a deposit. Flocculation caused by this mechanism is called perikinetic flocculation and the corresponding collision frequency function is

$$K_{BM} = \frac{2kTd_{ij}^2}{3\mu d_i d_j} \tag{2.2}$$

where $d_{ij}=d_i+d_j$, k is the Boltzmann constant, T is the absolute temperature and μ is the dynamic viscosity of the liquid.

(b) Velocity gradients in the surrounding turbulent fluid, which are particularly important in the mixing zone of an estuary. They tend to produce spherical aggregates, which are stronger than those formed by other collision mechanisms. The frequency of collisions due to this mechanism is proportional to both the particle size and the velocity gradient. Flocculation caused by velocity gradients is called orthokinetic flocculation and the corresponding collision frequency function is

$$K_{SH} = \frac{(d_i+d_j)^3}{6} G \tag{2.3}$$

where G is the absolute velocity gradient

$$G = \sqrt{\frac{\varepsilon}{\nu}} \qquad (2.4)$$

ε is the total energy dissipated per unit mass and ν is the kinematic viscosity of the fluid.

(c) Differential settling of the suspended particles, which is most effective for larger particles and contributes to the rapid clarification of waters during near-slack periods in high concentration mixing zones. There is little stress on aggregates colliding under such conditions and, as a result, they are ragged, weak (easily dispersed by low velocity gradients) and have low density. The corresponding collision frequency function is

$$K_{DS} = \frac{\pi g}{72 \nu \rho_w} (d_i + d_j)^2 (\Delta \rho_i d_i^2 - \Delta \rho_j d_j^2) \qquad (2.5)$$

where, besides the symbols already defined, g is the acceleration of gravity, ρ_w, ρ_i and ρ_j are the densities of water, i particles and j particles, respectively, and $\Delta\rho_i = \rho_i - \rho_w$, $\Delta\rho_j = \rho_j - \rho_w$.

Comparison between the number of collisions due to Brownian motion and velocity gradients, based on the respective collision frequency functions, seems to indicate that, for estuarine conditions, velocity gradients are a much more important mechanism than Brownian motion, although the latter can be important at the beginning of the flocculation process of very fine particles, of about 1 μm. For larger dimensions, 5 μm or higher, differential settling is, generally, the dominant mechanism amongst the

three, with velocity gradients showing similar collision frequencies only for high values (10 s^{-1}) of the absolute velocity gradient, which mainly occur near the bottom (van Leussen, 1988).

Once cohesive particles are brought close enough for some floc formation to take place, a certain percentage of collisions must result in adhesion of particles, through aggregation mechanisms. The effectiveness of the collisions in forming aggregates is a measure of the stability of the suspended particles and the suspension is called *stable* or *deflocculated* when the dispersed particles are capable of remaining independent entities within the suspension (van Leussen, 1988). The main aggregation mechanisms are salt flocculation, organic aggregation and bioflocculation.

Clay sediment particles show electric surface forces: in general terms, negative charges are found on particle faces, due to isomorphic substitutions of divalent ions by trivalent or tetravalent ions, and positive charges are found on the edges due to the existence of exposed cations. The negative charges are measured by their capacity to attract cations, neutralising them. This is known as the Cation Exchange Capacity (CEC), and is usually expressed in terms of milliequivalents per 100 grams of the clay mineral. Higher values of the CEC denote less stable clay minerals (see table 2.1). Similarly, an Anion Exchange Capacity (AEC) can be determined, although the corresponding laboratory techniques have been reported to be less reliable. The ratio CEC/AEC ranges from 0.5 for kaolinite to 6.7 for montmorillonite (Grimm, 1962). Furthermore, a second attractive force results from instantaneous dipole attraction

between atoms for each other, the omnidirectional Van der Waals force (Krone, 1978). This force is generated within the mass of the particles and decays very rapidly with distance (Partheniades, 1973). An additional bonding mechanism is chemical cementation due to the presence of, among others, iron oxides (Partheniades, 1973).

Table 2.1
Cation Exchange Capacity of Typical Clay Minerals (Adapted from Grimm, 1962).

Clay Mineral	CEC (meq / 100 g)
Kaolinite	3 -15
Haloisite $2H_2O$ [a]	5 -10
Illite	10 - 40
Montmorillonite	80 - 150

[a] Haloisite $2H_2O$ is the low hydration form of the mineral, commonly found in nature.

When clay particles are suspended in waters with very low salt concentration, positive edges are attracted to negatively charged faces and an open floc structure results. In saline or brackish environments, however, the negatively charged faces attract cations, while, less importantly, edges attract anions. The adsorbed ions, due to to their thermal motion, surround the plate-like clay particles, forming what is known as a double layer, of thickness dependent on ion size and valence, and causing particles to repulse one another. If the concentration of dissolved ions in the suspending water increases, the difference in ion concentration between the double layer and the surrounding fluid diminishes and particles are allowed to get closer before repulsion is effective: attractive surface and van der Waals forces can

then cause aggregation to occur (Krone, 1978). Cohesion of clay particles in salt water rapidly develops at salinities between 0.6 and 2.4 g/l, depending on clay mineral type (Krone, 1978). This simple aggregation mechanism is, however, further complicated due to the existence of metallic or organic coatings on most estuarine particles which, effectively, blanket the electrostatic properties of the original materials (van Leussen, 1988).

Organic aggregates found in estuaries have sizes from a few micrometers to several millimeters. Such aggregates consist of mineral particles and organic matter, strongly bound together, often with the inclusion of living organisms (i.e. bacteria, phytoplankton), as reported by Eisma (1986). Two types of organic aggregates have been observed in estuaries: microflocs, up to 125 μm, which consist of mineral particles and organic matter, and macroflocs, up to 4 mm, which are clusters of microflocs and mineral particles. However, much larger aggregates (called macroscopic aggregates or *marine snow*) have been observed in the open ocean; these are very fragile and do not withstand common sampling methods, their sizes ranging from a few millimeters to several meters (van Leussen, 1988).

In shallow inshore waters (like estuaries), where the levels of dissolved organic matter are high, microorganisms produce polymers which can be adsorbed at the surface of colloidal particles, in one or more sites, and increase in size, through bacterial colonization and growth and subsequent adsorption of more dissolved organic matter. The long polymer molecules extend into the solution and if they are

able to interact with other colloidal particles (i.e. if they are longer than the repulsive layer thicknesses at the particle's surfaces) will adsorb at the surface of other particles and form aggregates (bridging mechanism). Organic flocculation can happen at low polymeric concentration. For polymers with the same charge it requires the presence of a dissolved salt, the concentration of which is, however, much lower than that needed for salt flocculation (van Leussen, 1988).

The size growth of the flocs formed either by salt flocculation or organic and biological aggregation, is limited by breakup mechanisms. Different modes of floc destruction have been proposed in the literature: (i) floc fracture, producing smaller flocs; (ii) surface erosion by turbulent drag, taking place particle by particle. As larger floc sizes having higher settling velocities also have lower strengths they are unable to resist the increasingly high shear stresses in the lower layers, as they settle. In practice, as shown by several studies, the maximum floc size, at a given level, is in the same range of dimensions as the smallest turbulence eddies, although it is still impossible to quantitatively predict the maximum floc size in a given turbulent system (van Leussen, 1988). Breakup of flocs is mainly related to turbulent processes in the region close to the bottom (wall region or inner region) where the strongest shear and lift forces occur, thus controlling the size and shear strength distribution of both suspended and deposited aggregates (Mehta and Partheniades, 1975).

Under the influence of turbulence and due to the properties of the sediment fractions and organic matter a continuous process of floc generation and breakup takes place in the water column and may originate, for a given tidal condition, a quasi-equilibrium situation characterised by floc sizes, a floc size distribution, floc densities and floc strengths. Aggregates, either formed through salt flocculation or organic and biological aggregation, present an ordered structure, i.e. they occur in several orders of aggregation and show discontinuities in the values of their properties.

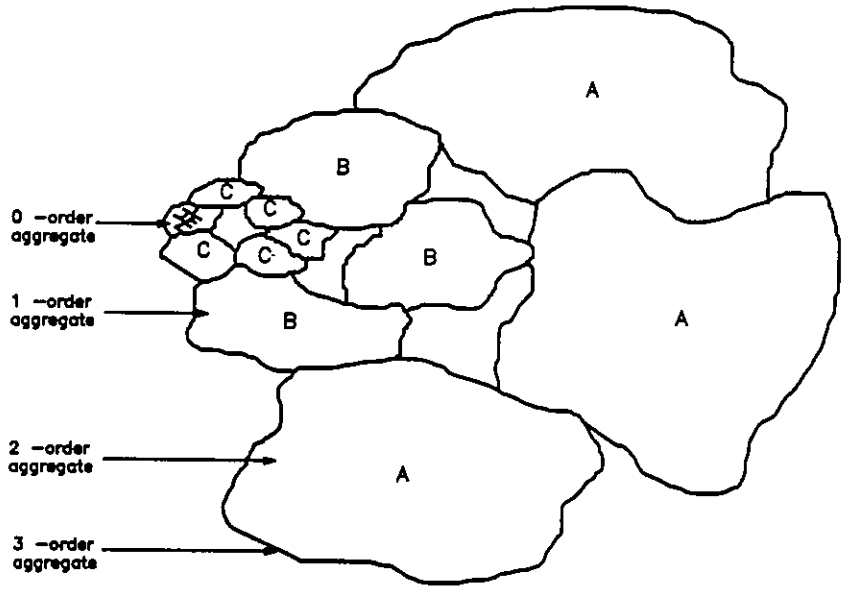

Figure 2.4 Orders of aggregation of sediment for the case of salt flocculation (adapted from Krone, 1978).

Orders of aggregation of sediment due to salt flocculation (figure 2.4) were studied by Krone: assemblages of primary particles form zero order aggregates (particle aggregates, *pa*) while first order aggregates (particle aggregate aggregate, *paa*) consist of aggregates of several zero order aggregates. Aggregates of first order aggregates are

called second order aggregates (*paaa*), etc. Increasing orders of aggregation are designated *pna* with *n-1* identifying the order of aggregation (Krone, 1978).

Both aggregate densities and shear strengths decrease with increasing order of aggregation (table 2.2). In estuarine environments lower order, stronger, aggregates are formed close to the bottom in zones of high shear while higher order, weaker, aggregates are formed in upper layers which, in the absence of wind, are zones of lower shear.

Table 2.2
Properties of Suspended Aggregates Formed Through Salt Flocculation (Adapted from Krone, 1978).

Aggregate Order	S. Francisco Bay		Philadelphia District		Brunswick Harbour		Gulfport Channel		White River (saline)	
	ρ_f	τ_{fs}	ρ_f	τ_{fs}	ρ_f	τ_{fs}	ρ_f	τ_{fs}	ρ_f	τ_{fs}
0	1269	2.2	1250	2.1	1164	3.4	1205	4.6	1212	4.9
1	1179	0.39	1132	0.94	1090	0.41	1106	0.69	1109	0.68
2	1137	0.14	1093	0.26	1067	0.12	1078	0.47	1079	0.47
3	1113	0.14	1074	0.12	1056	0.062	1065	0.18	1065	0.19
4	1098	0.082								
5	1087	0.036								
6	1079	0.020								

Note: Floc density ρ_f in kg/m^3, floc shear strength τ_{fs} in Pa. Floc densities are for interstitial fluid ρ_w= 1025 kg/m^3.

Observations by Eisma (1986) also indicate that, similarly to what happens with salt flocculation, there are two levels of organic and biological aggregation: the weak macroflocs are built of smaller and more resistant microflocs and of single mineral particles, all of them undergoing a continuous process of breaking up and reformation. Microflocs consist of mineral particles and organic matter and their formation is strongly related to the origin of the latter, to the organisms producing it and to shear dominated resuspension and deposition conditions. Stability of the microflocs is likely to be determined by the binding strength of the organic matter in relation to the total mass of the floc. Macroflocs are formed under conditions of less turbulent flow and, due to their fragility, are probably held together by organic coatings on the building particles, rather than by strong organic glues (Eisma, 1986). Although data on aggregate densities and shear strengths does not seem to be available regarding organic aggregates, variations in such properties with respect to the order of aggregation which are similar to those of salt flocculation aggregates would be expected.

2.3 Settling Velocities and Settling Fluxes

2.3.1 General Aspects

Settling of sediment particles is usually described by a terminal settling velocity, which combines together the effects of gravitational forces, viscous drag on the particles and interparticle interactions. Due to the salinity levels in estuarine

environments, fine sediment particles are generally found in a flocculated condition, as a result of the collision, aggregation and breakup mechanisms described in the previous section. Therefore, the settling velocity is a highly time dependent parameter, given the influence of tidal hydrodynamics and sediment concentrations on such processes. Typical values of the settling velocity for marine and estuarial environments, as reported by several authors range from 10^{-4} to 1 mm/s (Mehta et al., 1989) although Berlamont et al. (1993) indicate higher values, in the range 10^{-2} to 10 mm/s.

Flocs differ from primary sediment particles in three main aspects, which are relevant for settling:

(i) their size is larger than that of primary particles;

(ii) their density is lower than that of the primary particles, due to the existence of trapped interstitial water;

(iii) their shape is generally more spherical than the plate-like shape of the primary particles, which corresponds to reduced drag.

From the above factors, the increase in fall diameter and the reduction of drag are more significant than the decrease in density and, consequently, the settling velocities of the flocs are substantially higher than those of individual particles. The magnitude

of the aggregate diameter and of the settling velocity are, moreover, only slightly dependent on the primary particle diameter.

The settling velocities of cohesive sediment particles (primary particles and flocs) have been found to be strongly dependent on the mass concentration (a convenient bulk parameter indirectly expressing the multiple factors related to aggregation) and, if secondary effects such as those of temperature and salinity are neglected, fall within three ranges (figure 2.5): free settling, flocculation settling and hindered settling. A summary of the physical features of each settling regime is presented in the next subsections.

2.3.2 Free Settling

Free settling occurs for low concentrations, i.e. below a free settling limit, C_1, of, typically, 100 to 300 mg/l (Mehta, 1989). In this range the particles settle independently, without mutual interference; their terminal settling velocity is a result of the force balance between drag and net negative buoyancy. In the viscous range ($Re_s<1$, where $Re_s=W_sD/\nu$) the drag coefficient is

$$C_D=\frac{24}{Re_s} \tag{2.6}$$

and the terminal settling velocity for spherical particles is (Vanoni, 1975)

$$W_s = \frac{D^2}{18}\left(\frac{\rho_s - \rho_w}{\mu}\right) g \qquad (2.7)$$

where D is the grain diameter, ρ_s and ρ_w are the particle and fluid densities, g is the acceleration of gravity, and μ and ν the dynamic and kinematic viscosities of the fluid, respectively. Fine estuarial sediment in dispersed or quiescent conditions typically falls within these conditions although the shape of the particles requires the use of an effective particle diameter (Ross, 1988).

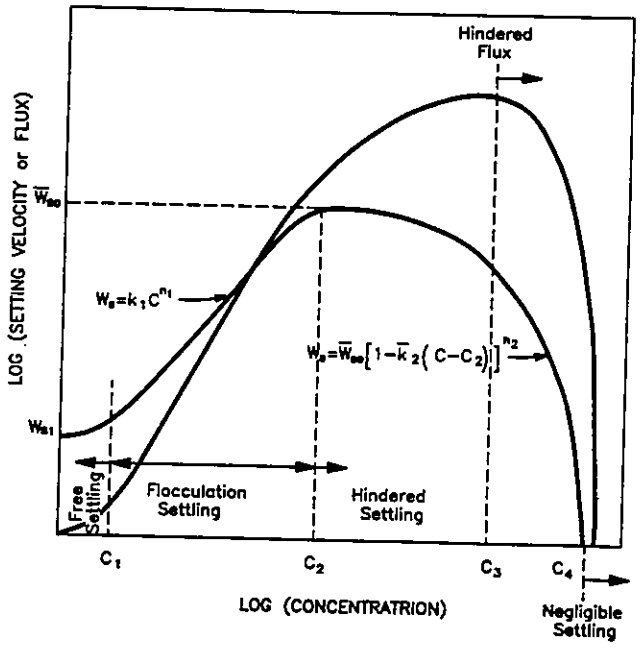

Figure 2.5 A general description of settling velocity and settling flux variation with suspended concentration of fine sediment (adapted from Costa, 1989).

2.3.3 Flocculation Settling

When the suspension concentration becomes higher than the free settling limit C_1, increased frequency of interparticle collision causes an increase in aggregation and

higher settling velocities. The general expression for the settling velocities in the flocculation range is

$$W_s = k_1 C^{n_1} \tag{2.8}$$

The theoretical value of n_1, based on the kinetics of flocculation, is 4/3 (Krone, 1962) but, in practice, it has been found to vary between 1 and 2 (Mehta, 1986). The coefficients in equation 2.8 may be determined in laboratory settling columns or in field tests; values determined by the latter procedure have been found to be higher by as much as an order of magnitude than those corresponding to the former, using the same sediment (Owen, 1971). This is due to the effect of local flow shearing rate on the aggregation conditions which is expressed through coefficient k_1.

2.3.4 Hindered Settling

For concentrations higher than a value C_2 of about 2 to 5 g/l the settling velocity decreases with the concentration. This is a result of hindered settling, a phenomenon in which aggregates become so closely packed that the fluid is forced to flow between them, through increasingly small pores, for settling to continue. The general expression for the settling velocity in the hindered settling range is

$$\begin{aligned} W_s &= \bar{W}_{s0}[1-\bar{k}_2(C-C_2)]^{n_2} \\ &= W_{s0}(1-k_2 C)^{n_2} \end{aligned} \tag{2.9}$$

where $\bar{W}_{s0}$ is the settling velocity that corresponds to C_2, i.e. the maximum velocity of the flocculation range, $\bar{k}_2$ is the inverse of the concentration in excess of C_2 at which $W_s=0$ and n_2 is usually taken as 4.65, based on the work of Richardson and Zaki (1954) on the settling of systems of particles whose formulation directly corresponds to the second form of equation 2.9. Coefficients in equation 2.9 are usually determined from laboratory settling tests as the rate of upward escape of interstitial water becomes dominant over the effects of flow shearing on aggregation. For concentrations higher than C_4 settling becomes negligible.

2.3.5 Alternative Formulations

While equations 2.7 to 2.9 are commonly used to describe the settling velocities, other formulations have also been used by different authors. An expression for the combined flocculation and settling ranges, resulting from a modification to an expression originally proposed by Wolansky et al. (1989) was used by Hwang (1989) as

$$W_s=\frac{aC^n}{(C^2+b^2)^m} \qquad (2.10)$$

where a , b , n and m are settling parameters. Curves obtained by the same author for sediment from Lake Okeechobee (Florida, U.S.A.) are presented in figure 2.6.

Hayter and Pakala (1989) used an empirical relationship obtained by Farley and Morel (1986) to derive the following expression, valid for low concentration suspensions

$$W_s=(B_{DS}C^{2.3}+B_{SH}C^{1.9}+B_{BM}C^{1.3})\Delta z\ /\Delta C \qquad (2.11)$$

where B_{DS}, B_{SH} and B_{BM} are the coefficients for the differential settling rate, internal shear rate and Brownian motion, respectively, obtained by Farley and Morel and ΔC is the difference in concentration between two vertical points (grid nodes in a numerical model) separated by a distance Δz. In the hindered settling range Hayter and Pakala used the Richardson and Zaki (1954) equation as

$$W_s=W_r(1-kC)^5 \qquad (2.12)$$

where, again, W_r is a reference settling velocity and k the inverse of the hypothetical fully settled sediment concentration. The reference settling velocity is obtained by the same authors by equating both settling velocity expressions (equations 2.11 and 2.12) at $C=C_2$.

In an attempt to improve the description of settling by considering several size fractions and recognising the need to describe the interactions between size fractions Krishnappan (1990) developed a vertical transport model which included a flocculation component as well as a transport component solving the one dimensional advection-diffusion equation. The flocculation component of the model uses a coagulation equation which expresses the rate of change of the number of particles per unit

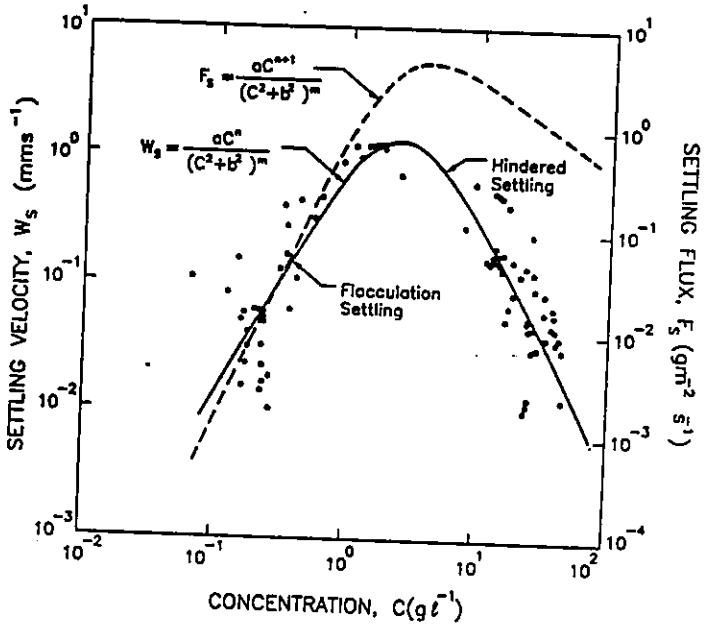

Figure 2.6 Settling velocity curve corresponding to equation 2.10 and settling flux curve determined using the same equation (adapted from Hwang, 1989).

volume of a particular size class *i* as a result of collisions with particles of all other classes *j;* the rate of change is, in turn, a function of the number concentrations for each size class and of the collision frequency functions between two classes, which measure the probability of collision in unit time.

Assumptions used in the flocculation component allow only binary collision processes (i.e. those involving two particles) while setting a unity probability of coalescence (or coagulation factor) for every pair of particles that collide and imposing conservation of the volume of collided particles. Furthermore, as the model was applied to the simulation of sediment settling in a stagnant water column, only differential settling was considered, using a formulation similar to that in equation 2.5. Particles, assumed spherical, are divided in discrete ranges, each range being materialised in a bin, in such a way that the mean particle volume in a bin is twice that in the preceding bin;

collisions between particles of bins i and j ($j<i$) are assumed to produce new particles fitting into bins i and $i+1$, through allocation functions, computed from the particle volumes in the bins involved. Application of the calculation procedure to each bin produces the new particle size distibution over a time step.

The model was applied to the simulation of settling tests in quiescent water solutions with sediment in both flocculated and unflocculated conditions (in which case the flocculation component of the model was not used). Comparison of the time evolution of the total concentrations at a given level of the settling bottle used in the tests with model predictions showed a good fit for both the flocculated and unflocculated sediment tests. Comparison of the time evolution of the measured and computed size distributions at the same level also showed good agreement for the unflocculated tests

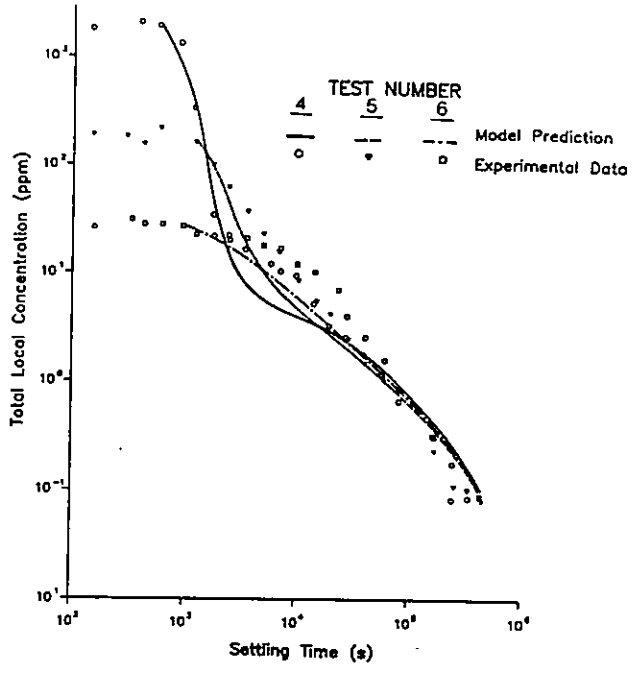

Figure 2.7 Time evolution of total volume concentration for the settling column tests simulated by Krishnappan using a model with a flocculation component (adapted from Krishnappan, 1990).

but a similar comparison for the flocculated tests which would allow full evaluation of the model's flocculation component was not possible due to floc breakup by the instrument used for size analysis in the laboratory.

Discrepancies found between laboratory data and model simulations can reasonably be attributed to the nature of some of the assumptions used: in the model two colliding spherical particles will always coallesce to produce a new spherical particle, whose volume will be equal to the sum of the volumes of the initial particles, will have the same density of those particles and will settle with a velocity given by Stokes law without any correction for shape.

Despite the good agreement with laboratory data for the cases in which comparisons were possible, the difficulties found by Krishnappan in verifying his model, even for the case of a relatively simple experiment seem to indicate that a *settling by class* modelling approach, although promising, will not be of immediate use for engineering applications.

2.3.6 Settling Flux

The behaviour of the settling flux, itself, can be seen in figure 2.5, according to equations 2.7 to 2.9. The settling flux grows with the concentration within the flocculation settling range and for the lower concentrations of the hindered settling range. However, within the hindered settling zone, the settling flux reaches a

maximum, for $C=C_3$, and decreases for higher concentrations. This phenomenon is known as hindered settling flux. The settling flux curve produced using the settling velocities calculated through equation 2.10 is also presented in figure 2.6.

2.4 Vertical Diffusive Transport

In a water column, settling is counterbalanced by the vertical transport of mass resulting from turbulent fluctuations of both the vertical velocity and the concentration field. In most modelling applications variables are averaged over a time scale larger than that of the turbulent fluctuations and, in a similar way to the description of the turbulent fluxes of momentum, known as the Reynolds stresses, turbulent mass fluxes (or Reynolds fluxes) must be described in terms of known or calculable quantities. The set of approximations used to describe Reynolds stresses and fluxes is known as a turbulence closure model. Such models can, generally, be divided into effective viscosity models and turbulent stress/flux models (Smith and Takhar, 1979). The latter provide differential transport equations for each component of the mean Reynolds stress tensor and each mean Reynolds flux (Smith and Takhar, 1979) and produce rather complex systems of equations (see also, for example, Sheng, 1986).

If the Reynolds stress (τ_{xx}) and the vertical Reynolds flux (F_{dz}) are expressed, through the use of Fick's Law, in terms of the time-averaged values (denoted by overbars) of the horizontal velocity (u) and concentration (C), effective viscosity formulations are obtained as

$$\tau_{zx} = -\bar{\rho}\,\overline{u'w'} = \bar{\rho} N_z \frac{\partial \bar{u}}{\partial z} \qquad (2.13)$$

$$F_{dz} = \overline{w'C'} = -\varepsilon_z \frac{\partial \bar{C}}{\partial z} \qquad (2.14)$$

where primed variables denote deviations from time-average values, w is the vertical flow velocity, ρ is the fluid density, z is the vertical coordinate and N_z and ε_z are the momentum and mass effective viscosities (also called eddy diffusivities or turbulent diffusion coefficients in the literature).

Eddy diffusivities are scalar functions of the turbulence structure and can be taken, in the simplest case, as constants, or as functions of the mean flow field (as in mixing length formulations) or, in a rather more complex approach, as functions of the mean turbulence energy (k) and of its dissipation rate (ε) for which two additional differential equations must be written (see, for example, Smith and Takhar, 1979). In tidal applications the values of the eddy diffusivities are strongly dependent on the flow velocity, the relative roughness of the flow channel and the degree of vertical stratification and can vary over several orders of magnitude at a fixed point in an estuary during a tidal cycle (Odd and Rodger, 1978). In particular, as slack water is approached, there is a considerable reduction in the magnitude of the eddy diffusivities (Smith and Takhar, 1979). Formulations relating turbulent fluxes to mean flow and concentration gradients, as in equations 2.13 and 2.14, assume that there are no phase lags between such quantities, as noted by Smith and Takhar (1981).

The momentum mixing length, a concept due to Prandtl, is a local function of the flow field and measures the length scales of turbulence. These lengths can be used as indicators of the eddy size or of the average distance traveled by fluid parcels in their random movements. In a mixing length approach, eddy viscosities for momentum and mass are obtained as functions of both the mixing length and the local, time dependent, velocity gradients $\partial u/\partial z$ (Odd and Rodger, 1978)

$$\tau_{zx}=\bar{\rho}N_z\frac{\partial\bar{u}}{\partial z}=\bar{\rho}l_m^2\left|\frac{\partial\bar{u}}{\partial z}\right|\frac{\partial\bar{u}}{\partial z} \tag{2.15}$$

$$F_{dz}=-\varepsilon_z\frac{\partial\bar{C}}{\partial z}=-l_c l_m\left|\frac{\partial\bar{u}}{\partial z}\right|\frac{\partial\bar{C}}{\partial z} \tag{2.16}$$

where l_m and l_c are the mixing lengths for momentum and mass fluxes, respectively. For a logarithmic velocity profile and a linear shear stress variation in the water column the momentum mixing length is obtained as

$$l_m=\kappa\zeta\left(\frac{H-\zeta}{H}\right)^{1/2} \tag{2.17}$$

where κ is the von Karman constant, ζ the elevation from the bottom and H the total depth. Bowden and Hamilton (1975) used a mixing length approach in trial runs of their model of estuarine circulation and concluded that instabilities developed due to unavoidable inaccuracies in representing $\partial u/\partial z$ in finite difference form.

The ratio between momentum and mass eddy viscosities in the same spatial direction is called the turbulent Schmidt number (see, for example, Harleman, 1988) and can be expressed using the mixing length concept as

$$S_t = \frac{N_z}{e_z} = \frac{l_m^2 \left|\frac{\partial \bar{u}}{\partial z}\right|}{l_c l_m \left|\frac{\partial \bar{u}}{\partial z}\right|} = \frac{l_m}{l_c} \tag{2.18}$$

According to Teeter (1986) most experimental evidence suggests that the Schmidt number can be taken as unity for particles in the Stokes range of settling, which includes sediment smaller than about 100 μm; this should be, at least, the case for neutral or non-stratified conditions (Odd and Rodger, 1978). In the presence of stable density stratification conditions, which can be produced by salt, temperature or suspended sediment, vertical turbulent motions are damped and the vertical diffusion of mass and momentum is affected, since a proportion of the energy in excess of that required to maintain the mean field is used to perform work against the vertical density gradient (Odd and Rodger, 1978). Furthermore, momentum and mass diffusivities (and mixing lengths) are not affected in the same way , the former having larger values (Oduyemi, 1986). Costa (1989) computed the turbulent Schmidt number for three 10 minute velocity and sediment concentration data blocks from Hangzhou Bay (P.R. China) and obtained values of 0.94, 2.45 and 2.40. For local equilibrium turbulence conditions the ratio between the rate of work done against gravity and the rate of production of turbulent energy by the action of the Reynolds stresses (both per unit volume) measures the efficiency of conversion from turbulent kinetic to potential

energy and is known as the flux Richardson number (Odd and Rodger, 1978; Abraham, 1989)

$$Rf = \frac{-g\overline{\rho' w'}}{\bar{\rho}\,\overline{u' w'}\,\frac{\partial \bar{u}}{\partial z}} = \frac{l_c}{l_m}\,\frac{-g\frac{\partial \bar{\rho}}{\partial z}}{\bar{\rho}\left(\frac{\partial \bar{u}}{\partial z}\right)^2} = \frac{Ri}{S_t} \tag{2.19}$$

where ***Ri*** is the gradient Richardson number, which measures the relative importance of the stabilising gravitational forces to the destabilising, shear induced, turbulence forces.

Relationships between the momentum mixing lengths for stratified (denoted by subscript *s*) and neutral conditions (denoted by subscript ***n***) have the general form (Ross, 1988)

$$l_{ms} = \frac{l_{mn}}{(1+\beta' Ri)^{\alpha'}} \tag{2.20}$$

where α' and β' are positive constants, either empirical or resulting from assumptions concerning conservation of turbulent kinetic and potential energy. For the case of mixing lengths for mass flux a similar relationship has been used, in the form

$$l_{cs} = \frac{l_{cn}}{(1+\beta Ri)^{\alpha}} \tag{2.21}$$

where α and β are now different from α' , β' (Ross, 1988).

Smith and co-workers (see Smith, 1982 and Smith and Kirby, 1989, for details) by analogy with the self-similarity properties of the momentum eddy viscosity vertical distribution, which can be written as

$$N_z = M_z(x,y,t)\, f\left(\frac{\zeta}{H}\right) \tag{2.22}$$

(where M_z is proportional to the depth-mean value of N_z and expresses the space and time variability of the momentum eddy viscosity and f represents its vertical distribution) defined the mass diffusivity, as

$$\varepsilon_z\left(\frac{\zeta}{H}, Rf\right) = \varepsilon_0\, f\left(\frac{\zeta}{H}\right) r(Rf) \tag{2.23}$$

in which ε_0 is a constant, ζ is the elevation from the bottom, H is the total depth and

$$f\left(\frac{\zeta}{H}\right) = \frac{32}{5}\frac{\zeta}{H}\exp\left(-\frac{16}{5}\frac{\zeta}{H}\right) \tag{2.24}$$

$$r(Rf) = \frac{1-\frac{Rf}{Rc}}{S_t} \tag{2.25}$$

$$S_t = S_{t0}\frac{1-2Rf}{1-\theta\frac{Rf}{Rc}} \tag{2.26}$$

In equations 2.25 and 2.26 Rc is a critical value of the flux Richardson number at which vertical turbulent transfer of mass is zero and S_{t0} and θ are constants, taking values of 0.75 and 1.0, respectively. However, given the functional form of M_z in equation 2.22, ε_0 should, more appropriately, depend on x, y and t. Smith and Kirby (1989) also indicate that function 2.25, similarly to 2.21, actually leads to

$$r(Rf) \approx r(Ri) = \frac{1}{(1+\beta Ri)^{\alpha}} \tag{2.27}$$

with $\alpha = 3/2$ and β a constant of order 1.

Bowden and Hamilton (1975), while recognising that, for estuarine flows, the assumption of diffusion and dispersion coefficients independent of time is physically

unrealistic, used two formulations for the salt transport equation of their width-averaged model, in the form

$$\varepsilon_z=\varepsilon_0+\varepsilon_1 H|\langle u\rangle| \tag{2.28}$$

$$\varepsilon_z=\varepsilon_0+\varepsilon_1 H|\langle u\rangle|(1+\beta Ri)^{-\alpha} \tag{2.29}$$

where $\langle u\rangle$ is the depth mean velocity, H the water depth, ε_0 and ε_1 are constants (taken as 0.025 and 0.00125, respectively for the Mersey estuary), α and β are stratification parameters, and Ri is an overall Richardson number based on the salinity differences between the bottom and the surface.

2.5 Fluxes at the Bed

2.5.1 General Aspects

In order to describe the transport of fine suspended sediment in low concentration environments it is necessary to model the processes through which the *active* (i.e. periodically resuspended) portion of the bed directly exchanges sediment with the water column; of related importance is the characterisation of the active portion of the bed, itself, in terms of its thickness, density and resistance variation at the timescale of the required simulation. In the following sections, the classically adopted erosion and deposition formulations are described, while some of the problems related to their application are also discussed.

2.5.2 Erosion

Active estuarial cohesive sediment beds typically have time-dependent thicknesses ranging from 10^{-2} to 1 m; such beds can be divided into two zones (Parchure and Mehta, 1985):

(i) an upper zone of high water content (*soft bed*), showing depth stratification with respect to cohesive properties, possessing very low mechanical strength and undergoing consolidation; the density and shear strength of this zone of the bed increase with time for a period ranging from a few days to a week or two;

(ii) a lower zone, showing relatively uniform cohesive properties with depth (*uniform bed*).

Erosion of sediment from estuarial cohesive beds has been observed to occur in one of two modes: *floc by floc* and *mass* erosion. In mass erosion portions of the bed which became unstable through processes like fluidisation, liquefaction, generalised bed failure (occurring in layers below the bed surface) or local detachment of large pieces of a hard bed are resuspended almost instantaneously in large masses. Floc by floc or surface erosion is, however, the most common erosional mechanism in estuaries: flocs separate from the bed in an individual basis, as a result of hydrodynamic erosional forces exceeding cohesive bonding, frictional and gravitational

forces. Under the action of bottom shear stresses higher than the shear strength of the exposed bed layers, removal of particles and decrease in bed elevation (scour) will proceed until a bed layer of higher strength, equal to the applied stress, is found.

The increase in bed shear strength with depth is due to consolidation and associated physico-chemical changes due to overburden and to the variation of particle size with depth; as a consequence of overburden the deposited aggregates are successively crushed into smaller, denser, more resistant aggregates, until an aggregate size is reached that is difficult to be broken without an external compressive force (Parchure and Mehta, 1985). This strength developing mechanism is expected to produce a step-like increase of the shear strength with depth, although such steps are not always recognised in strength profiles measured in the laboratory.

The time rate of increase of the suspended sediment mass per unit area of the bed (rate of erosion) can, in general, be described as

$$F_e = \left.\frac{dm}{dt}\right|_e = f(\tau_b, \tau_s, \alpha_1, \alpha_2, \ldots, \alpha_n) \qquad (2.30)$$

where τ_b is the time mean bottom shear stress, τ_s the bed shear strength and the α_i are other erosion resistance defining parameters. It has been found that resistance to erosion is influenced, among other factors, by the bed temperature, pH, water and gas content, sediment type and total salt concentration and ionic species in the pore fluid, which control swelling and permeability. Algae and microorganisms were found to increase the bed shear stength in an annular flume experiment (Parchure and Mehta, 1985) and, generally, benthic processes are expected to have an important contribution

for the bed strength in low energy areas but to be much less significant in high energy environments and in zones subjected to frequent dredging. In broad terms resistance of a cohesive bed should be affected by any factors that change the interparticle electrochemical bond strength or influence the production of biological secretions which cause adhesion of particles and stabilise the bed. The size distribution of bed sediment and the interaction between sizes may also be important in the prediction of bed resistance: relatively robust fecal pellets may be much easier to move than much smaller aggregates, while very large aggregates, having large potential lift surfaces and perhaps held by only a few weak bonds, may be eroded *en masse* at relatively low shear stresses (McLean, 1985).

The difference τ_b-τ_s, known as the excess shear stress, is one of the common features of some of the existing formulas for the erosion flux, such as that proposed by Kandiah (1974) for uniform beds, which can be expressed as

$$F_e=\alpha_1\left(\frac{\tau_b-\tau_s}{\tau_s}\right) \qquad \tau_b \geq \tau_s$$
$$F_e=0 \qquad \tau_b<\tau_s \tag{2.31}$$

where α_1 is an empirical erosion parameter which depends on the interparticle bond strength and is defined as

$$\alpha_1=F_e\big|_{\tau_b=2\tau_s} \tag{2.32}$$

Values of α_1 typically range from 10^{-3} to 10^{-1} kg m^{-2} min^{-1} (Mehta, 1991a). For non-uniform (soft) beds Parchure and Mehta (1985) proposed

$$F_e=\alpha_2\exp\{\alpha_3[\tau_b-\tau_s(Z)]^{1/2}\} \quad \tau_b\geq\tau_s$$
$$F_e=0 \quad \tau_b<\tau_s \tag{2.33}$$

where Z is the bed depth below its initial surface, α_2 is known as the floc erosion rate

$$\alpha_2=F_e|_{\tau_b=\tau_s} \tag{2.34}$$

and α_3 is a factor which is inversely proportional to the absolute temperature. It should be noted that τ_b is defined as a mean value and, consequently, some sediment particles will still be eroded when it equals the shear strength. This is taken into account by equation 2.33 but not by equation 2.31. Another expression for non-uniform beds was proposed by Thorn and Parsons (1980) as

$$F_e=\alpha_4(Z)[\tau_b-\tau_s(Z)] \quad \tau_b\geq\tau_s$$
$$F_e=0 \quad \tau_b<\tau_s \tag{2.35}$$

in which the erosion parameter α_4 is also observed to vary with the depth of erosion. Equation 2.31 has also been applied to non-uniform beds by taking a constant α_1 and the bed shear strength as the local value within the deposit (O'Connor and Tuxford, 1980), an approach which is identical to that of equation 2.35 if the erosion parameter in the latter is defined as $\alpha_4(Z) = \alpha_1/\tau_s(Z)$.

Laboratory determined values for the critical shear stress for erosion (i.e. shear strength of the top bed layer) of soft estuarine muds are usually in the range 0.1-2 Pa (Berlamont et al. 1993), but can vary from almost zero for organic floc layers to 10 Pa for very hard soils (Mehta, 1991a).

2.5.3 Deposition

Deposition of cohesive sediment from a suspension to the bed depends on a combination of different sediment and flow related factors of which floc shear resistance and settling velocity, the sediment near-bed concentration and the bottom shear stress are the most important.

It has been observed that for uniform sediment (i.e. sediment having uniform properties in a suspension and, in particular, a single settling velocity) in flume tests, in which sediment, initially suspended at high flow velocities with initial concentration C_0, is allowed to deposit at lower velocities, the ratio C_f/C_0 (C_f being the residual concentration that corresponds to a given bottom stress) is independent of C_0 and given by (Krone, 1962)

$$\frac{C_f}{C_0} = \exp[-p\frac{W_s}{h}t] \tag{2.36}$$

where h is the flow depth, p is the probability of sediment deposition and W_s the settling velocity. The probability of deposition is defined as

$$\begin{aligned} p &= 1 - \frac{\tau_b}{\tau_{cd}} && \tau_b < \tau_{cd} \\ p &= 0 && \tau_b \geq \tau_{cd} \end{aligned} \tag{2.37}$$

where τ_b and τ_{cd} are the bottom shear stress and a critical shear stress for deposition (i.e. the bed shear stress above which no deposition occurs), respectively.

The probability of deposition concept reflects the fact that the deposition of flocs is controlled by near bed turbulence and, more specifically, by the rate of shearing $\partial u/\partial z$ at the bottom. For a flock to stick to the bed it must be strong enough to withstand the near bed shear stress, weaker flocs being disrupted and resuspended. Consequently, the deposition process also acts as an effective sorting mechanism.

For the case of non-uniform sediments, i.e. those having a relatively broad size and settling velocity distribution, complete deposition will only occur if τ_b drops below a critical lower value τ_{cl}. For increasing bottom shear stresses a residual concentration C_f (less than the initial C_0) will remain, as long as τ_b is less than an upper critical value τ_{cM} (for $\tau_{cl}<\tau_b<\tau_{cM}$ the ratio C_f/C_0 is a function of τ_b only and increases with it). The equation for the case of non-uniform sediment is (Mehta and Lott, 1987)

$$\frac{C_f}{C_0}=\sum_{i=1}^{n}\Phi(W_s^i)\exp\left\{-\left[\left(1-\frac{\tau_b}{\tau_{cl}}\right)\left(\frac{W_s^{\min}}{W_s^i}\right)^m\right]\frac{W_s^i}{h}t\right\} \tag{2.38}$$

where

$$m=\frac{\ln\left(\frac{\tau_{cM}}{\tau_{cl}}\right)}{\ln\left(\frac{W_s^{\max}}{W_s^{\min}}\right)} \tag{2.39}$$

$\Phi(W_s^i)$ is the frequency distribution of W_s^i (settling velocity class), W_s^{min} and W_s^{max} being the extreme values that define the range of the settling velocities.

Values for the critical shear stresses for deposition are usually in the range 0.05 - 0.2 Pa but for a distributed sediment, larger aggregates will generally begin to deposit at higher shear stresses of 0.2 - 1 Pa (Berlamont et al., 1993). The critical shear stress for deposition is usually determined through laboratory flume tests.

The time rate of sediment deposition per unit bed area (or deposition flux) F_p is defined for uniform sediments as (Krone, 1962)

$$F_p = \left.\frac{dm}{dt}\right|_p = pW_s C_b \tag{2.40}$$

where C_b is the near bed sediment concentration.

For the case of non-uniform sediments, the deposition flux will be calculated as a result of flux summation over all the settling classes (Mehta et al. 1989)

$$F_p = \left.\frac{dm}{dt}\right|_p = \sum_{i=1}^{n} p_i W_s^i C_b^i \tag{2.41}$$

where W_s^i is the settling velocity of settling class i, C_b^i the concentration of class i near the bed, while the probability of deposition for each class i will, in this case be expressed as

$$\begin{aligned} p &= 1 - \frac{\tau_b}{\tau_{ci}} && \tau_b < \tau_{ci} \\ p &= 0 && \tau_b \geq \tau_{ci} \end{aligned} \tag{2.42}$$

which, again, corresponds to a *deposition by class* concept: for a given fraction i of the suspended sediment, if τ_b is greater than τ_{ci} (but less than τ_{cM}) no sediment will deposit while another class j, of stronger sediment may have $\tau_{cj} >> \tau_b$ and virtually no sediment of that class will remain in suspension. For non-uniform sediments the size

distribution of the suspended sediment is, therefore, not only a function of the bottom shear stress but also of the initial size distribution and deposition properties of each sediment class.

It should be noted that the equivalent fall velocity to be used in the description of deposition using a single class approach, if the W^i, C^i_b are known, should be the mean fall velocity, determined as,

$$\bar{W}_s = \frac{\sum_{i=1}^{n} W_s^i C_s^i}{\sum_{i=1}^{n} C_s^i} \tag{2.43}$$

instead of the commonly used median fall velocity (W_{s50}). As reported by van Leussen and Cornelisse (1993), field measurements in the Ems estuary indicated the former is significantly higher, due to the contribution of large macroflocs to the settling flux which affects the mean settling velocity significantly.

Two models using the deposition formulations for uniform and non-uniform sediments were developed by Ockenden (1993) and tested using a laboratory deposition experiment with mud from Eastham Dock, in the Mersey estuary, and field measurements of deposition at the same location. The distributed sediment model was found to give a better representation of deposition in a decelerating flow in the closed system of the laboratory annular flume but did not produce a better fit to the field data than the uniform sediment model. This was attributed to additional influences which are present in the field and, in particular, to advective effects which are not

represented by the models. Nevertheless, since both models reproduced reasonably well the field data, Ockenden suggested that for complex engineering applications, where assumptions often have to be made for practical reasons, a uniform sediment model may still be adequate.

Krone (1993) re-analysed the data and concepts associated with early settling and deposition experiments and defined five transport regimes (table 2.3) of which the first four are related to deposition: regimes I, II and III are linked to the three settling ranges described in Section 2.3, while regime IV seems to be linked with fluid mud and bed formation phenomena. Krone reemphasised in his analysis the importance of selecting the correct transport regime when selecting a deposition relation and the need for further research in order to relate settling velocity to velocity gradients, besides concentration, in ranges I and II (flocculation and hindered settling) as currently done.

Finally, the differences between settling phenomena, as observed in laboratory flumes (and, in particular, in annular flumes) and in the field should be mentioned. For example, strong settling fluxes on natural or dredged slopes, leading to higher slopes than the sediment's equilibrium slopes under the applied fluid forces has been linked to the formation and flow of fluid mud.

Table 2.3
Cohesive Sediment Transport Regimes (Adapted from Krone, 1993)

Regime	Description	Typical Solids[a] Conc. (g/l)	Collision Frequency in Shear	Settling Velocity
I	Dilute suspended aggregates	< 0.3	Infrequent	Constant
II	Suspended aggregates	0.3 to 10	Frequent f (C, du/dz)	Flocculation settling W_s (C, du/dz)
III	Concentrated suspended aggregates	10 to 20+	Very frequent f (C, du/dz)	Hindered settling W_s (C, du/dz)
IV	Homogeneous matrix or slurry	20 to 100	Continuous deformation	Consolidation
V	Homogeneous gel structure	> 100	Static	Static

[a] The mass concentration limits depend on the density of the aggregates. Note: temperature affects settling velocities and, at high concentrations, frequency of collision.

2.5.4 Discussion

Although the use of the erosion and deposition formulations described in the two previous subsections is, at present, common practice when dealing with low concentration environments, a number of related issues are still the subject of debate.

A direct consequence of the description, in terms of bulk parameters, of the exchange processes at the bed is that their dependence on the suspended sediment, bed and

eroding fluid physico-chemical properties and local biological conditions is not explicitly considered and, therefore, specific process characterisation tests are necessary for each application. A first group of issues is, then, related to the accuracy to which the determination of the erosion/deposition critical shear stresses and other process defining parameters is carried out in the laboratory. This is usually done through the use of annular flumes, for which the mean bottom shear stresses are determined as a result of preliminary tests in clear water, in which additional measurements of turbulent quantities are usually not carried out. The extent to which these turbulent quantities and the mean flow parameters are affected by suspended sediment in actual characterisation tests remains largely unknown. A related problem has to do with the possibility of reproducing in a laboratory environment realistic field conditions in terms of sediment mixtures, turbulence and flocculation, biological effects, etc; this problem is particularly important for erosion studies for which it is virtually impossible to reproduce an undisturbed natural bed in the laboratory. Field instruments for measuring erosion parameters of natural beds have been developed (see Berlamont et al.,1993, for details) but their use presents a higher degree of complexity than that of laboratory devices.

A second issue, in connection with the definition of the fluxes at the bed, is related to the range of bottom shear stresses over which a given process can occur. As noted by Sandford and Halka (1993) a paradigm of cohesive sediment transport research is that erosion and deposition of sediment are mutually exclusive. For cohesive sediments numerous laboratory studies have indicated that the bed stresses which are necessary

to keep sediment in suspension are much lower than those necessary to erode it and that, consequently, the threshold for erosion is higher than the threshold for deposition. A recent study by Lau and Krishnappan (1994) using a laboratory annular flume and a particle size analyser confirmed that for low shear stresses (i.e. depositional conditions) erosion and deposition did not take place simultaneously, in agreement with the mechanism proposed by Partheniades and co-workers (see, for example, Partheniades, 1986), according to which flocs that deposit are only the ones able to withstand the near bed shearing rate and, once deposited, will only be eroded at higher shear.

Sandford and Halka (1993) analysed data from different locations in upper Chesapeake Bay and concluded that suspended sediment concentrations began to decrease shortly after the velocity began to decrease and long before the velocity fell below the point at which erosion (and, therefore, deposition) had begun; such a feature seems to have been confirmed in many other American and European estuaries. This led Sandford and Halka, while using a single sediment class approach, to model resuspension and deposition of cohesive sediment without considering a deposition threshold (effectively making the probability of deposition always unity), thus allowing erosion and deposition to occur simultaneously. The improved fit to the field data obtained through this formulation, relative to the classically exclusive erosion/deposition approach previously used by the same authors, was explained by Sandford and Halka (1993) as, possibly, resulting from three causes:

(i) a constant exchange of fine sediment particles between the bed and the water column;

(ii) scaling problems between the laboratory and the field, related to the non-uniformity of the bottom shear stresses, to the non existence in laboratory flumes of zones of low shear where large aggregates may develop and to biogenic binding, which is important in situ;

(iii) the possibility that sediments are behaving as an admixture of particle classes with a sequence of increasing critical erosion and deposition stresses, such that the last class eroded deposits very soon after the shear stress begins to decrease.

As noted by the same authors the first possibility is the least conceptually attractive of the three, as it contradicts most of the currently available body of laboratory evidence. The success of a single particle class modelling approach with a unity probability of deposition is, therefore, regarded by Sandford and Halka as an operational rather than a conceptual improvement, in the absence of a more refined modelling framework; at the same time, it highlights the need for careful evaluation of the performance of models in which major simplifications in the modelling of key processes are allowed.

Finally, a third issue is related to the characterisation of the active bed layers in relation to their erodibility, as considerable progress has recently been made in consolidation studies. Alexis et al. (1992) analysed consolidation theories developed in the fields of chemical and mechanical analysis and proposed a tree of theoretical studies in which the historical and conceptual links between theories are identified. Within mechanical analysis the one-dimensional, vertical, consolidation of soft soils was shown to be described in its most general form by the geotechnical formulation of Gibson et al. (1967), in terms of the void ratio, which contains as particular cases the classical formulations separately used by hydraulicians and geotechnicians. The solution of Gibson's equation requires the use of constitutive laws, i.e. the characterisation of the dependence of both the effective stress and the permeability on the void ratio. An hydraulics-based formulation, in terms of the excess bulk density relative to that of water, was also presented by Toorman (1992) and is shown to be completely complementary to that of Gibson et al. (1967) for saturated soils. Again, constitutive laws are needed for the effective stress and permeability, in this case as functions of the density. As noted by both Alexis et al. (1992) and Toorman (1992) both formulations can encompass both settling and consolidation as a continuous process if an adequate condition, in terms of the effective stress, is introduced at the settling zone/consolidation zone boundary. The constitutive relations required by both models were separately inverstigated by Alexis et al. (1992) and Berlamont et al. (1992) but, in each case, the need for further research on the effects of additional parameters (like the initial density and height of consolidation, load history, organic matter, temperature, sediment composition, etc.) was emphasised. Furthermore, spatial

variability in load history and three-dimensional effects in the consolidation processes of actual estuarine beds should also be important in actual engineering applications.

Le Hir and Karlikow (1992) linked a consolidation model to a cross-sectionally averaged sediment transport model in order to investigate the role of consolidation processes in the sediment dynamics of the macrotidal Loire estuary. Their simulations showed that the sediment transport patterns, as indicated by the tidally-averaged magnitude and location of the turbidity maximum and of the deposited mud (fluid and partly consolidated), showed little dependence on consolidation. As expected consolidation influenced the time lags between hydrodynamics forcing and sediment response and, ultimately, the residual (i.e. at the spring/neap cycle scale) deposition or erosion of mud.

It is also recognised that the bulk parameters (such as the density) and the shear strength of a cohesive bed cannot be uniquely correlated and that, in fact, their relationship is very approximate (Mehta et al., 1989); the bed shear strength, which globally expresses the strength of existing bonds between aggregates, depends not only on aggregate packing and on their respective densities but also on all the other physico-chemical properties of the flocculated solids and of the interstitial water; therefore the same shear strength can correspond to different packing densities. This is confirmed by the differences in the formulations for the bed shear strength derived from laboratory experiments using natural muds, as shown in the review of Møller-Jensen (1993) and summarised in table 2.4.

Table 2.4
Formulas for the Determination of the Bed Shear Strength as a Function of Bed Parameters

	Formula	Reference
(2.44)	$\tau_s=\zeta_1 C^{\delta_1}$	Owen (1970)
(2.45)	$\tau_s=\left(\frac{e}{e_0}\right)^{\delta_2}$	Bain (1981)
(2.46)	$\tau_s=\zeta_3 C$	DHI (1990)
(2.47)	$\tau_s=\zeta_4(\rho^*-1)$	Villaret and Paulic (1986)
(2.48)	$\tau_s=\zeta_5(1-n)^{\delta_5}$	Kusuda et al. (1985)

Note: τ_s - bed shear strength (Pa); C - bed dry density (kg/m^3); ρ^* - bed bulk density (g/cm^3); e - bed void ratio; e_0 - reference void ratio; n - porosity; ζ_i , δ_i - parameters.

A plot of the bed shear strength as a function of the bed bulk density extending that produced by Møller-Jensen is presented in figure 2.8, using the different relationships in table 2.4 and several sets of parameters found in the litterature. In the figure, curves 1, 2 and 3 correspond to the parameters determined by Owen (1970), Thorn and Parsons (1980) and HR (1989b), respectively, while curves 4, 5 and 6 correspond to the use of a modified version of equation 2.45

$$\tau_s = \left(\frac{\rho_s - C}{e_0 C} \right)^{\delta_2} \qquad (2.45')$$

with values determined by Bain (1981). Curves 7, 8 and 9 were obtained using the parameters determined by their respective authors, although equation 2.48 had to be transformed, for consistency, into

$$\tau_s = \zeta_5 \left(\frac{C}{\rho_s} \right)^{\delta_5} \qquad (2.48')$$

It should also be noted that parameters in curves 3 and 4 were obtained with sediment from the Mersey Estuary. Despite the fact that site fluid was not used in all tests, figure 2.8 clearly shows that variations between the results of the several relationships are very large. The virtual impossibility of reproducing cohesive beds in the laboratory, which are similar to those found in the field, has, again, to be considered when interpreting such results.

Le Hir and Karlikow (1992) also pointed out the strong influence of the relationship between sediment density and (strength-related) erodibility on their results. As noted by the same authors and confirmed by Møller-Jensen's review, the current knowledge on this crucial aspect is so poor that even a very accurate prediction of the bed density, through a consolidation model, combined with a strength/density relationship, would become almost useless for that reason. Therefore, direct determinations of erosion parameters, in laboratory tests or, preferably, in in-situ tests, still seems a better approach.

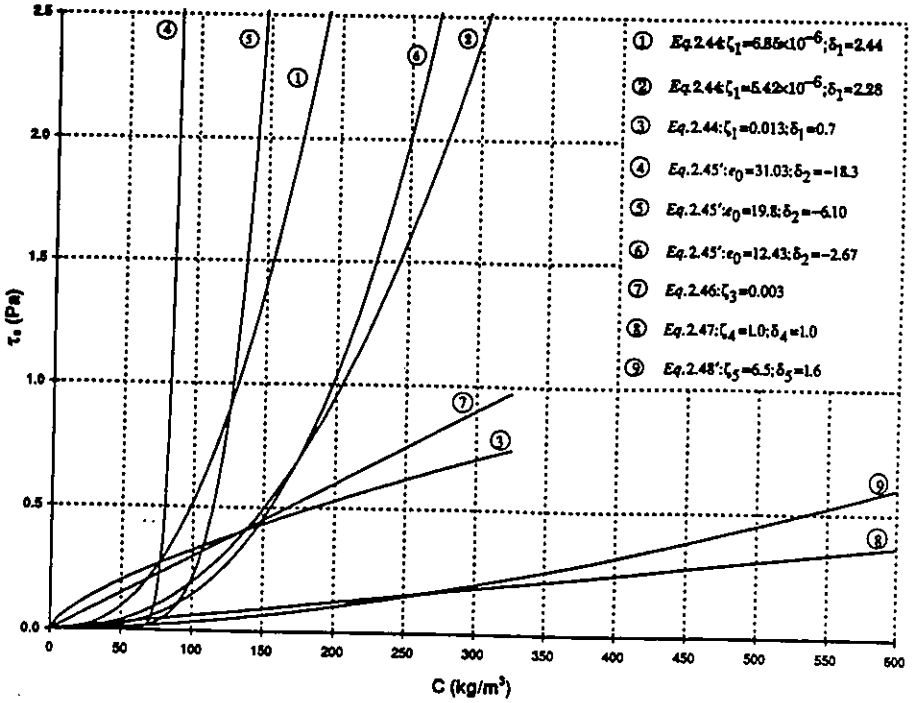

Figure 2.8 Results obtained using several relationships between the bed shear strength and the bed dry density.

2.6 Conclusions

The possibility of describing cohesive sediment dynamics using a number of particle size classes instead of a single class approach, although conceptually adequate is, at present, extremely difficult. For example, Lavelle (1993) developed a one-dimensional vertical transport model in which only two particle populations (fine particles and marine snow) were considered, since field based exchange rates between a large set of particle classes are still not known for natural marine systems. A consequence of such an approach is, in fact, the need to model collision, aggregation and breakup mechanisms in the water column, leading to the definition of exchange coefficients between particle classes and allowing the source/sink terms, in the mass transport

equations written for each class, to be specified. Lick and Huang (1993) pointed out that the numerical computations involved in their model of collision, aggregation and breakup using several floc classes, although relatively simple, often required a great deal of computer time. As mentioned by the same authors this problem will be magnified if such computational modules are used in conjunction with transport models applied to real cases, involving thousands of grid nodes and long simulation periods. Furthermore, the need to accurately and finely model the turbulent diffusion processes of mass and momentum which couple the advection and diffusion processes of mass and momentum (McLean, 1985), taking into account flow-sediment interactions (i.e. stratification), lags in sediment response and hysteresis effects between turbulent and mean flow properties, is an important pre-requisite if multiple class sediment dynamics is to be correctly described. Other areas of research for a multiple class approach include modelling the effects of organics and biological glues in flocculation processes, their interaction with saline flocculation and, in general the relation between the cohesive components and the coarser fractions of mud.

The need for information on floc size, density, settling velocity and shear strength distributions in the water column, both in relatively simple laboratory situations and in the field, in connection with the practical problems found in sampling undisturbed large flocs (Berlamont et al., 1993) is also a major difficulty. While the deposition flux can easily be described in terms of sediment classes (as in equation 2.41) a parallel formulation taking into account sizes, densities and shear strengths of particles, for example, does not seem to have been proposed until present, for the case

of surface erosion. The need to determine a large number of class-dependent critical shear stresses for both deposition and erosion, given the limitations of currently available instruments in sampling and analysing flocs, and of the methods to determine such stresses is another source of difficulty. Furthermore, the study of the erosional behaviour of mixed mud and sand beds (see, for example Williamson and Ockenden, 1993) is still in a very early stage.

Finally, the dependence of most phenomena of interest for cohesive sediment dynamics on a wide range of spatial and temporal scales and the dependence of such phenomena on flow and sediment properties suggests that large numbers of tests and measurements will be necessary for the application of a multiple sediment class model.

Given that a generalised increase in modelling complexity does not, necessarily, imply more accurate results, especially if a large number of simplifications in process models is introduced, it seems reasonable that realistic improvements in key components are gradually attempted, instead. As noted by Sandford and Halka (1993) and Ockenden (1993), the current difficulties in developing an effective multi-class modelling alternative suggest that improved models, treating sediment as a single representative size class, are still more useful for engineering purposes, even if they are physically less realistic. This approach will, therefore, be adopted in the formulation of the transport model described in Chapter 3.

CHAPTER 3
FORMULATION OF A SUSPENDED SEDIMENT TRANSPORT MODEL

3.1 General Aspects

Suspended sediment dynamics in a water body is mathematically described by an advection-diffusion equation. Formally this equation differs only from those describing the dynamics of conservative dissolved substances by the need to account for sediment settling, since sediment particles are not neutrally buoyant. Moreover, specific boundary conditions must be considered, describing the conditions at the water surface and the interaction between suspended sediment and the sediment bed or near-bed high-concentration layers. In this chapter the formulation of a three-dimensional numerical transport model for suspended cohesive sediment, treated as a single representative size class, as discussed in Chapter 2, is described. The appropriate advection-diffusion equation for a cartesian coordinate system is presented in Section 3.2. A review of modelling approaches is carried out in Section 3.3, in which the general modelling options adopted given the physics of the problem and the nature of the intended applications are also indicated. The equation described in Section 3.2 is then transformed into a more convenient computational form (Section 3.4), its terms being re-analysed and grouped according to the corresponding physical processes, in order to allow the use of adequate numerical methods for modelling purposes. Finally the main conclusions of the chapter are summarised in Section 3.5. The development and component testing of the model whose formulation is described in the present

chapter are presented in Chapter 4, while an application to an estuarine channel is described in Chapter 5.

3.2 The Transport Equation in the Physical Domain

The advection-diffusion equation for suspended sediment represented as a single class, which describes mass conservation, can be derived, in a cartesian coordinate system (x longitudinal, y lateral and z in the gravity direction, i.e. vertical, positive upwards from a given datum below the water surface - figure 3.1) by considering an elemental control volume and equating the time rate of sediment accumulation inside the volume to the net flux of sediment through its boundaries (see, for example, Mehta, 1973 for

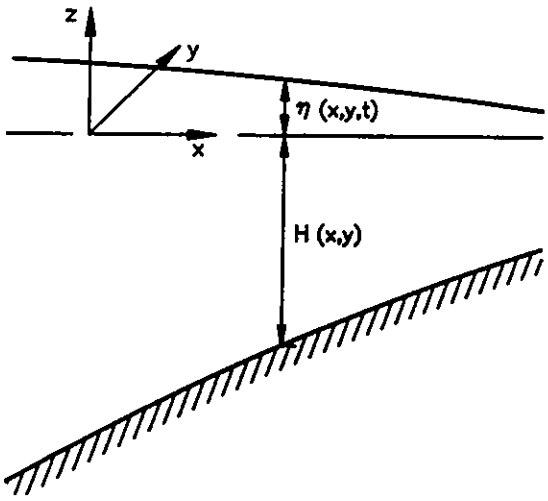

Figure 3.1 Definition of the cartesian coordinate system and symbols used in the derivation of the transport equation.

details). The application of this global continuity principle is a consequence of the assumption that, despite the continuous process of sediment floc formation and

destruction within the control volume, the overall sediment size distribution can be taken as constant and, therefore, there is no net generation or destruction of the flocs of any particular size (Mehta, 1973). As a result a single equation can be written (instead of a set of equations, one for each sediment class, with the corresponding production and decay terms) and suspended sediment can be treated as a whole and assumed to be conservative. The equation is then

$$\frac{\partial C}{\partial t} = -\nabla \cdot \vec{N} \tag{3.1}$$

where C is the instantaneous sediment mass concentration (mass of sediment/volume of suspension) and $\vec{N}$ is the sediment flux vector. This vector can be decomposed into an advective component ($\vec{N}_A$) a molecular diffusion component ($\vec{N}_D$) and, since the sediment is not neutrally buoyant, a settling component ($\vec{N}_S$), such that

$$\begin{aligned} \vec{N}_A &= \vec{q}C \\ \vec{N}_D &= -D_m \nabla C \\ \vec{N}_S &= -W_S C \vec{k} \end{aligned} \tag{3.2}$$

where $\vec{q} = u\vec{i} + v\vec{j} + w\vec{k}$ is the fluid velocity vector, D_m the Fickian molecular diffusion coefficient (assumed isotropic), W_s the terminal settling velocity of the sediment particles or flocs and $\vec{i}, \vec{j}, \vec{k}$ the longitudinal, lateral and vertical unit base vectors. Again, since several sediment sizes are actually present, and despite the assumption of a constant size distribution, the overall settling flux should be interpreted as representing the sum of the partial fluxes corresponding to the different sizes.

Equations 3.1 and 3.2 lead to

$$\frac{\partial C}{\partial t} = -\nabla \cdot (\vec{q} C - D_m \nabla C - W_s C \vec{k}) \tag{3.3}$$

Due to the turbulent characteristics of natural flows and to the impossibility of tracking individual particle movements, flow velocity components and concentrations are usually decomposed into time-averaged parts (over a longer period than the turbulent time scales involved), denoted by an overbar, and fluctuating components, denoted by a prime; for example:

$$\begin{aligned} u &= \bar{u} + u' \\ C &= \bar{C} + C' \end{aligned} \tag{3.4}$$

for the x component of the velocity vector in the cartesian coordinate system and the mass concentration, respectively. Inserting such terms into equation 3.3, expanding, averaging over time (using the same time scale as before) and using the fluid continuity equation, the following equation is obtained:

$$\frac{\partial \bar{C}}{\partial t} + \bar{\vec{q}} \cdot \nabla \bar{C} = D_m \nabla^2 \bar{C} + \nabla \cdot (W_S \bar{C} \vec{k}) + \nabla \cdot (-\overline{q' C'}) \tag{3.5}$$

which can also be written as

$$\begin{aligned} \frac{\partial \bar{C}}{\partial t} + \bar{u} \frac{\partial \bar{C}}{\partial x} + \bar{v} \frac{\partial \bar{C}}{\partial y} + \bar{w} \frac{\partial \bar{C}}{\partial z} = D_m \left(\frac{\partial^2 \bar{C}}{\partial x^2} + \frac{\partial^2 \bar{C}}{\partial y^2} + \frac{\partial^2 \bar{C}}{\partial z^2} \right) + \frac{\partial}{\partial z} (W_s \bar{C}) \\ - \frac{\partial}{\partial x} (\overline{u' C'}) - \frac{\partial}{\partial y} (\overline{v' C'}) - \frac{\partial}{\partial z} (\overline{w' C'}) \end{aligned} \tag{3.6}$$

The last three terms in equation 3.6 correspond to gradients of turbulent diffusion fluxes (or Reynolds fluxes) and are commonly modelled, by analogy with the molecular diffusion case as (see Section 2.4):

$$\frac{\partial}{\partial x}(\overline{u'C'})=\frac{\partial}{\partial x}\left(-\varepsilon_x\frac{\partial \overline{C}}{\partial x}\right)$$
$$\frac{\partial}{\partial y}(\overline{v'C'})=\frac{\partial}{\partial y}\left(-\varepsilon_y\frac{\partial \overline{C}}{\partial y}\right) \qquad (3.7)$$
$$\frac{\partial}{\partial z}(\overline{w'C'})=\frac{\partial}{\partial z}\left(-\varepsilon_z\frac{\partial \overline{C}}{\partial z}\right)$$

where ε_x, ε_y and ε_z are the turbulent mass diffusivities in the x, y, z directions, respectively. Turbulent diffusion coefficients are, however, much larger than the molecular diffusivities and the terms corresponding to the latter phenomenon can be neglected in equation 3.6 (Harleman, 1988). Consequently, and omitting the overbars which denote time average values, for clarity, the transport equation for single class suspended cohesive sediment in a cartesian coordinate system becomes:

$$\frac{\partial C}{\partial t}+u\frac{\partial C}{\partial x}+v\frac{\partial C}{\partial y}+w\frac{\partial C}{\partial z}-\frac{\partial}{\partial z}(W_sC)= \\ =\frac{\partial}{\partial x}\left(\varepsilon_x\frac{\partial C}{\partial x}\right)+\frac{\partial}{\partial y}\left(\varepsilon_y\frac{\partial C}{\partial y}\right)+\frac{\partial}{\partial z}\left(\varepsilon_z\frac{\partial C}{\partial z}\right) \qquad (3.8)$$

Information on the velocity field, which is necessary to solve equation 3.8, can be obtained from field measurements or from the results of physical or numerical models. In the first two cases and whenever hydrodynamics and transport numerical models are not run interactively sediment transport modelling is considered to be decoupled from that of water flows, a reasonable assumption in low to moderate concentration environments which will be adopted in the present work. Equation 3.8 belongs to the group of parabolic equations that contain first order spatial derivatives and are called convection-diffusion equations or advection-diffusion equations. The names given to such equations are due to the type of physical processes they describe (Smith, 1979); the latter is applied when the scalar being transported does not significantly interact

with the velocity field, and will, therefore, be adopted in this work. A brief discussion of the nature of equation 3.8 in connection with cohesive sediment transport is presented in Appendix A.

Equation 3.8 is valid in the water column (between the *bed* - settled bed or near-bed high concentration layer - and the water surface) and its solution requires appropriate boundary and initial conditions.

Boundary Conditions

(i) *Bed* Boundary Condition

At the bed or lower interface, $z=z_b$ a flux term F_b (mass of sediment per unit area per unit time) must be defined, corresponding to a source or sink for the suspended sediment in conditions, respectively, of erosion/entrainment or deposition/hindered settling. Consequently, in the z direction, and at the lower interface:

$$N_z(z_b,t)=F_b=F_e-F_p \tag{3.9}$$

where F_e and F_p are the erosion and deposition fluxes, respectively (erosion and deposition should in this case be the taken in a broad sense and include erosion/deposition from/to a settled bed and entrainment/hindered settling from/to a fluid mud layer).

(ii) Free-surface Boundary Condition

At the water surface, $z=\eta$ the boundary condition is

$$N_z(\eta,t)=W_s C|_\eta+\varepsilon_z\frac{\partial C}{\partial z}|_\eta=0 \tag{3.10}$$

(see, for example, O'Connor, 1971 and Nicholson and O'Connor, 1986) which corresponds to imposing a zero net vertical flux at the free surface, the diffusive flux always balancing the settling flux.

(iii) Solid Boundary Condition

At solid boundaries diffusion is not allowed in the normal direction to the boundary:

$$\varepsilon_n\frac{\partial C}{\partial n}|_{sb}=0 \tag{3.11}$$

where n is the direction normal to the solid boundary (denoted by subscript sb). The same boundary condition will be applied at outflow boundaries, which are assumed to be located in zones of negligible concentration gradient, far from the main areas of interest.

(iv) Inflow Boundary Condition

At inflow boundaries the input concentration is prescribed, for $t>0$, as

$$C(x_{ib},y_{ib},z_{ib},t)=C_{ib}(x_{ib},y_{ib},z_{ib},t) \quad (3.12)$$

where C_{ib} denotes the inflow concentration and subscript ib denotes a boundary point.

Initial Condition

At $t=t_0$ an initial concentration field C_0 is prescribed as

$$C(x,y,z,t_0)=C_0(x,y,z) \quad (3.13)$$

To summarise, it can be stated that the description of cohesive sediment dynamics in a given water body, using a cartesian coordinate system, is obtained through the solution of equation 3.8, with boundary conditions 3.9, 3.10, 3.11 and 3.12 and initial condition 3.13. However, the complexity of the equation, given the nature of its parameters, boundary and initial conditions, prevents its analytical solution for most application cases and numerical methods have to be used. Transformation of equation 3.8 in order to allow the development of a numerical model is presented in Section 3.4.

3.3 A Review of Modelling Approaches

Under the set of assumptions leading to its derivation (in particular, a single class approach for sediment) it can be considered that equation 3.8 represents the most general framework for the description of cohesive sediment dynamics in estuarine environments. In fact, the complex structures of both flow and sediment transport patterns require that full three-dimensional (3D) models are used in most practical

applications, a demand which is nowadays possible to satisfy, given the current computing capabilities and cost levels, at least for short term simulations. This was not always the case, however, and most early modelling efforts were heavily conditioned by the available computing resources. Simplifications in model formulations had, therefore, to be adopted, namely in order to reduce the dimensions of the problems to be solved, leading to unavoidable losses in modelling performances. For this reason, and although testing of modelling improvements is usually best carried out in such simplified models, the usefulness of most early formulations for application cases is, at present, rather limited.

Historically the first attempt at cohesive sediment modelling was that of Odd and Owen (1972) who modelled the Thames estuary using a two-layer approach. In their model Odd and Owen assumed rectangular cross-sections, with width increasing exponentially with the longitudinal coordinate, and divided them into two unequal horizontal layers, the lower layer having constant thickness and being much smaller than the upper. Cross-sectional averaging was carried out over the layers but the main effects of the vertical gravitational circulation were still retained by the model. Despite its limitations it can be considered that this early model included a better description of sediment movement than later one-dimensional, cross-sectionally averaged models (1DH).

Ariathurai and Krone (1976), recognising that most estuaries are shallow and extensive horizontally, developed the first two-dimensional depth-averaged (2DH) transport

model using a finite element technique. 2DH models became popular in the late seventies and early eighties (see, for example, O'Connor and Tuxford, 1980, O'Connor and Nicholson, 1988 and Teisson, 1991, for details) and were considered to simulate adequately the conditions found in moderate concentration and in vertically well mixed environments. However, the lack of vertical resolution in such models, for example, prevents the reproduction of gravitational circulation effects, a serious problem for sediment transport simulations. Furthermore a major difficulty found in the application of any formulation that includes depth-averaging (2DH and 1DH models) is related to the definition of the deposition fluxes, since the independent variable in such models is a depth or cross-sectionally averaged concentration, whose relation to the near-bed concentrations is, in principle, not known. This relation has to be established through field observations or, for the case of 2DH models, through an analytical expression, in terms of depth-averaged quantities (Teeter, 1986).

Given the limitations of 2DH models, it can be considered that two-dimensional width-averaged models (2DV) are a much better approach than 2DH models, as the vertical structure of the concentration field is computed (see, for example, O'Connor, 1975 and Smith and O'Connor, 1979). 2DV models can be used in relatively narrow or laterally well mixed estuaries and tidal rivers, as described by Odd (1988). However, 2DV and 1DH models cannot accurately simulate the effects of irregular lateral boundaries. One-dimensional, vertical models (1DV) have also been developed, mainly for research purposes (Ross, 1988; Krishnappan, 1991) and are particularly

useful for investigating the physical processes associated with the vertical component of sediment transport.

Finally, when spatial variability of sediment properties can be neglected, models considering only the time dependence of the variables, zero-dimensional models (0D) which solve the bed mass continuity equation, have been successfully applied to the prediction of rates of sedimentation (see, for example, O'Connor and Tuxford, 1980). A review of the advantages and disadvantages of the several types of models, in terms of their expected accuracy and costs of operation, for the description of cohesive sediment transport and the long-term prediction of siltation rates is presented in O'Connor and Nicholson (1988).

Three-dimensional models solving equation 3.8 have been developed, beginning in the eighties, and are not affected by the shortcomings of the formulations which are averaged in one or more dimensions. Different numerical methods have been used: finite differences, for example by Nicholson and O'Connor (1986), and finite elements, for example by Hayter and Pakala (1989). However, as noted by Teisson (1991), modelling shortcomings are linked to a much greater extent to the poor knowledge of the physical processes than to the efficiency of the numerical techniques. In fact, processs formulations used so far by the several models have shown little differences. The model developed by Nicholson (Nicholson and O'Connor, 1986) can, in this regard, be considered as fairly representative of existing 3D engineering models.

In Nicholson and O'Connor's (1986) model transport is decoupled from hydrodynamics and, therefore, u, v, w have to be provided. Settling is represented by settling velocities whose dependence on the concentration is similar to that described by equations 2.7 to 2.9, coefficients being determined in the laboratory or, preferably, through field tests; this approach, through which sediment and flow effects on flocculation are indirectly taken into account is, generally, adopted instead of the more theoretical description of equations 2.11 and 2.12. Mass diffusion in a given direction i is, in the same model, described through depth-averaged coefficients which are functions of the friction velocity (u_*) and the flow depth (D) in the form

$$\bar{\varepsilon}_i = K_i u_* D \tag{3.14}$$

where the K_i are constants. However, given the importance of the mass diffusivity vertical distribution and of stratification effects in vertical mass diffusion, ε_z should, more appropriately, be described in the form of 2.23 (as in the model by Hayter and Pakala, 1989), possibly with a time-varying form of ε_0 for tidal applications. Erosion and deposition fluxes corresponding to the classical description of near-bed phenomena (see figure 2.2) are included in Nicholson and O'Connor (1986) model in the form of equations similar to 2.31 and 2.40, respectively. The critical erosive stress of bed layers at depth Z below the initial bed surface is given by a relationship in the form

$$\tau_{ce}(Z) = \tau_{ce}^{F} + A[\rho(Z) - \rho^{F}]^{B} \tag{3.15}$$

where ρ is the bed layer bulk density, A and B are parameters incorporating the effects of mud type and salinity and superscript F denotes values corresponding to the formation stage of a layer. The bulk density of homogeneous bed layers is computed

by a simple model which keeps track of layer densities and thicknesses. Hayter and Pakala (1989) also determined the bed shear strengths from bed density profiles but, in their case, the latter were computed from void ratios obtained through the solution of the Gibson equation (Gibson et al., 1967). Finally, a further process (slump) was considered by Nicholson and O'Connor (1986), representing the flow of disturbed bed material following the failure of an underwater slope, which could be caused by oversteepening due to dredging or deposition or by the destruction of bed layers through wave action. This process was characterised in terms of the strength of the sediment and can be recognised as an early attempt to simulate fluid mud dynamics.

Equation 3.8 was solved by Nicholson and O'Connor (1986) in the cartesian coordinate system, using a fractional step method: three-dimensional advection was modelled by a simple characteristics technique in which particles located at the grid nodes are backtracked with the nodal velocity (i.e. without time or space updating) along a straight line for the duration of the time step, concentrations being obtained at the end points through three-dimensional second order interpolation; combined vertical diffusion and settling were modelled by an implicit finite difference scheme; finally, both lateral and longitudinal diffusion are described by an explicit finite difference scheme.

Requirements for the improvement of numerical modelling technology were discussed by a specialised panel during the Estuarine Cohesive Sediment Workshop, held in St. Petersburg, Florida, USA, in April 1991, as reported by Mehta (1991b). Topics

discussed were grouped into: (i) mud processes; (ii) model grids; (iii) long term predictions; (iv) ways of using models; (v) particulate contaminants. Panel members recognised the difficulties associated with items (iii) and (v) and emphasised the 3D nature of mud transport and the need for calibration steps and sensitivity analyses (item iv). Regarding item (i) the need for more research on basic processes was stressed, while in item (ii) the need for the selection of appropriate grids for the representation of major mechanisms was emphasised.

In this work the panel's conclusions regarding items (i) and (ii) are interpreted in the light of the research needs associated with the vertical component of cohesive sediment transport, for the reasons described in Section 2.1. Modelling improvements will, therefore, be sought in two main aspects: the selection of a grid which is appropriate to describe vertical phenomena (Section 3.4) and the development of a fluid mud model, eventually leading to a generalised *bed* boundary condition for suspended sediment (Chapter 6).

3.4 The Transport Equation in the Computational Domain

One of the main problems in numerical modelling of transport in coastal and estuarine environments is found when large variations in the value of the variables being studied exist with depth and, in particular, when such variations occur over small vertical distances, giving rise to large gradients. This problem becomes particularly important in the application of 3D models to large areas: if, in the interest of accuracy, the

vertical grid spacing is made uniformly small enough to resolve the smallest spatial scales of interest, not only the computational costs may become excessive but large amounts of unnecessary information are generated, as well; in contrast, however, if the spatial discretisation is not fine enough, the numerical computations may be grossly in error.

Problems of similar nature and those related to the representation of irregular solid boundaries in natural flows have led investigators to search alternative methods to the classical finite difference techniques on rectangular grids, used in most numerical modelling early studies: finite element methods; finite difference methods using curvilinear grids, stretched rectangular grids, triangular grids and boundary fitted coordinates; finite volume methods (Spaulding, 1984; Capitão, 1989). However, the generally recognized simplicity, intuitiveness in development and facility in modification of the classical finite difference methods has also led researchers to attempt retaining the benefits of such methods: a possible way to accomplish this is by solving transformed versions of the original equations in rectangular grids, defined in a transformed domain resulting from mapping the physical domain of interest (Spaulding, 1984).

In general terms, given a cartesian space (x, y, z, t), a geometric coordinate transformation (time remaining unchanged) could be arbitrarily defined, so that a new space, in the form (x^*, y^*, z^*, t) was obtained. As an example, a method for horizontally mapping the physical domain into a space such that all boundaries

coincide with coordinate lines is presented by Spaulding (1984) for a two dimensional model and could also be used as part of a generalised coordinate transformation scheme for three dimensional models. However, a restrictive approach, widely used when solving for unknowns whose variability is much higher vertically than horizontally is to perform a vertical transformation alone, the well known σ-type transformation used in metereology and oceanography, allowing all other cartesian components and time to remain unchanged.

In σ-type transformations applied to coastal areas a depth varying domain is mapped into a computational domain of constant depth (bottom and free surface becoming coordinate planes of constant sigma values), while a new vertical velocity is defined, accounting for both the cartesian velocity and the effect of changes in water depth, due to water level variations (the bottom level is assumed not to change at the time scale of simulations). The most widely used form of the σ transformation is

$$Z=\frac{z-\eta}{\eta+H} \tag{3.16}$$

where H is the bottom depth (see figure 3.1), which keeps the vertical uniformity in grid spacing in both the physical and the transformed domain (figure 3.2b). Advantages of conventional σ-type transformations include: a more efficient use of computer resources; a direct way of accounting for the impermeability of marine bottom and surface in hydrodynamic models; the possibility of using centered horizontal differencing in the vicinity of the bottom and surface; a better representation of the bathymetry, in the case of staggered grid models (Phillips, 1957; Deleersnijder and Beckers, 1992).

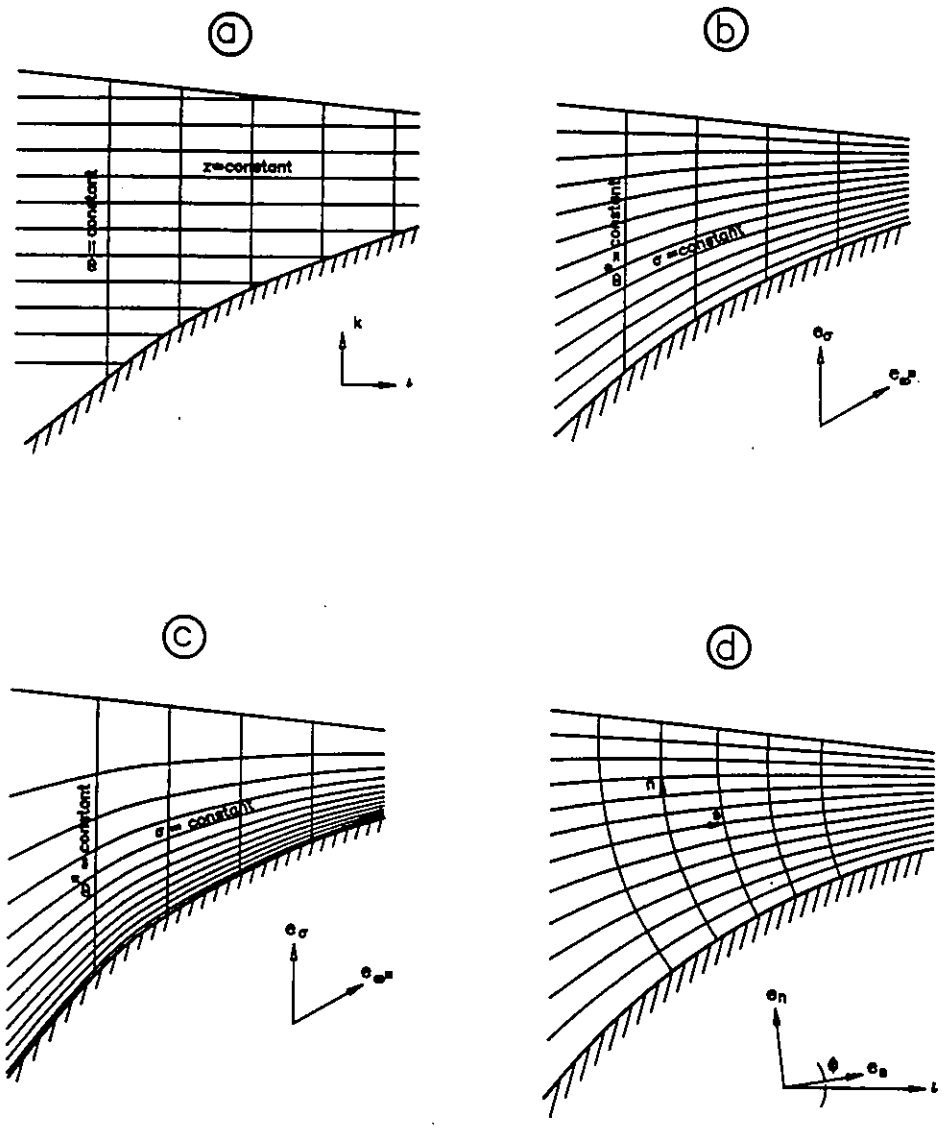

Figure 3.2 Definition of coordinate systems in the vertical plane: a) conventional cartesian; b) conventional sigma; c) modified sigma with clustering of points near the bottom; d) orthogonal curvilinear.

Furthermore, as seen in the previous chapter, cohesive sediment dynamics in estuaries is determined by two transport components: a horizontal (advective) component and a vertical component. Around slack water the vertical component is dominant and leads to large vertical concentration gradients, usually near the estuary bed. Hence models must be able to correctly reproduce strong vertical variations of the concentration over small length scales, i.e. fine discretisations are needed. However, and since the bulk of this variation usually happens in layers close to the lower boundary, it is inefficient to represent the concentration numerically by its values on a uniformly spaced computational mesh as the very fine spacing required in the bottom layers is unnecessarily accurate close the surface where gradients are mild.

Based on the previous discussion and in an attempt to improve modelling accuracy in the description of suspended cohesive sediment dynamics, while benefitting from other advantages of σ-type transformations, a vertical coordinate transformation was used in the present work. For that purpose a generic space x^*, y^*, σ, t^* was defined as

$$\begin{aligned} t^* &= t \\ x^* &= x \\ y^* &= y \\ \sigma &= \sigma(x,y,z,t) \end{aligned} \tag{3.17}$$

where $\sigma=\sigma(x,y,z,t)$ is a function to be specified later but will have the generic form (see Appendix C)

$$\sigma = \sigma[Z(x,y,z,t)] = \sigma\left(\frac{z-\eta}{\eta+H}\right) \tag{3.18}$$

through which, and for the case of suspended cohesive sediment modelling, as discussed before, a refinement of the grid close to the lower boundary will be sought.

Using 3.18, time and space derivatives become:

$$\begin{aligned}
\frac{\partial}{\partial t} &= \frac{\partial}{\partial t^*} + \frac{\partial \sigma}{\partial t}\frac{\partial}{\partial \sigma} = \frac{\partial}{\partial t^*} + \mathrm{T}\frac{\partial}{\partial \sigma} \\
\frac{\partial}{\partial x} &= \frac{\partial}{\partial x^*} + \frac{\partial \sigma}{\partial x}\frac{\partial}{\partial \sigma} = \frac{\partial}{\partial x^*} + \mathrm{A}\frac{\partial}{\partial \sigma} \\
\frac{\partial}{\partial y} &= \frac{\partial}{\partial y^*} + \frac{\partial \sigma}{\partial y}\frac{\partial}{\partial \sigma} = \frac{\partial}{\partial y^*} + \mathrm{B}\frac{\partial}{\partial \sigma} \\
\frac{\partial}{\partial z} &= \frac{\partial \sigma}{\partial z}\frac{\partial}{\partial \sigma} = \Gamma\frac{\partial}{\partial \sigma}
\end{aligned} \tag{3.19}$$

where T, A, B and Γ are transformation parameters.

Introducing the above derivatives in equation 3.8 the following equation is obtained:

$$\begin{aligned}
\frac{\partial C}{\partial t^*} + \mathrm{T}\frac{\partial C}{\partial \sigma} = & -u\left(\frac{\partial C}{\partial x^*} + \mathrm{A}\frac{\partial C}{\partial \sigma}\right) - v\left(\frac{\partial C}{\partial y^*} + \mathrm{B}\frac{\partial C}{\partial \sigma}\right) - w\left(\Gamma\frac{\partial C}{\partial \sigma}\right) \\
& + \Gamma\frac{\partial (W_s C)}{\partial \sigma} \\
& + \frac{\partial}{\partial x^*}\left[\varepsilon_x\left(\frac{\partial C}{\partial x^*} + \mathrm{A}\frac{\partial C}{\partial \sigma}\right)\right] + \mathrm{A}\frac{\partial}{\partial \sigma}\left[\varepsilon_x\left(\frac{\partial C}{\partial x^*} + \mathrm{A}\frac{\partial C}{\partial \sigma}\right)\right] \\
& + \frac{\partial}{\partial y^*}\left[\varepsilon_y\left(\frac{\partial C}{\partial y^*} + \mathrm{B}\frac{\partial C}{\partial \sigma}\right)\right] + \mathrm{B}\frac{\partial}{\partial \sigma}\left[\varepsilon_y\left(\frac{\partial C}{\partial y^*} + \mathrm{B}\frac{\partial C}{\partial \sigma}\right)\right] \\
& + \Gamma\frac{\partial}{\partial \sigma}\left[\varepsilon_z\left(\Gamma\frac{\partial C}{\partial \sigma}\right)\right]
\end{aligned} \tag{3.20}$$

Re - arranging again:

$$\frac{\partial C}{\partial t^*} = -u\frac{\partial C}{\partial x^*} - v\frac{\partial C}{\partial y^*} - (\mathrm{T} + u\mathrm{A} + v\mathrm{B} + w\Gamma)\frac{\partial C}{\partial \sigma}$$
$$+\Gamma\left[\frac{\partial}{\partial \sigma}(W_s C) + \frac{\partial}{\partial \sigma}\left(\varepsilon_z \Gamma \frac{\partial C}{\partial \sigma}\right)\right]$$
$$+\frac{\partial}{\partial x^*}\left(\varepsilon_x \frac{\partial C}{\partial x^*}\right) + \frac{\partial}{\partial x^*}\left(\varepsilon_x \mathrm{A}\frac{\partial C}{\partial \sigma}\right) + \varepsilon_x \mathrm{A}\frac{\partial^2 C}{\partial x^* \partial \sigma} + \mathrm{A}\frac{\partial}{\partial \sigma}\left(\varepsilon_x \mathrm{A}\frac{\partial C}{\partial \sigma}\right) \tag{3.21}$$
$$+\frac{\partial}{\partial y^*}\left(\varepsilon_y \frac{\partial C}{\partial y}\right) + \frac{\partial}{\partial y^*}\left(\varepsilon_y \mathrm{B}\frac{\partial C}{\partial \sigma}\right) + \varepsilon_y \mathrm{B}\frac{\partial^2 C}{\partial y^* \partial \sigma} + \mathrm{B}\frac{\partial}{\partial \sigma}\left(\varepsilon_y \mathrm{B}\frac{\partial C}{\partial \sigma}\right)$$

It is obvious from equation 3.21 that, in the computational domain x^*, y^*, σ, t^*, and by analogy with the physical domain, a transformed vertical velocity can be defined as:

$$\begin{aligned}\bar{w} &= \mathrm{T} + u\mathrm{A} + v\mathrm{B} + w\Gamma \\ &= \frac{\partial \sigma}{\partial t} + u\frac{\partial \sigma}{\partial x} + v\frac{\partial \sigma}{\partial y} + w\frac{\partial \sigma}{\partial z} \\ &= \frac{d\sigma}{dt}\end{aligned} \tag{3.22}$$

An interpretation of this transformed velocity and its relationship with the vertical velocity that is measured or computed in the physical domain can be done by writing

$$\begin{aligned}w &= \frac{\bar{w}}{\Gamma} - \frac{\mathrm{T}}{\Gamma} - u\frac{\mathrm{A}}{\Gamma} - v\frac{\mathrm{B}}{\Gamma} \\ &= \frac{\bar{w}}{\Gamma} + w_{us} \\ &= w_{uw} + w_{us}\end{aligned} \tag{3.23}$$

where the two components of the physical velocity in the physical domain w_{uw} and w_{us} are called the upwelling and upsloping (or vertical geometric) velocities, respectively (Deleersnijder, 1989).

The upwelling velocity is not a consequence of surface or bottom gradients and can be taken as the *real* vertical velocity of a particle free from geometric constraints, as happens in the transformed domain; in terms of the particle's Lagrangian velocity in the transformed domain:

$$\bar{w} \equiv \frac{d\sigma}{dt^*} = \frac{\partial\sigma}{\partial z}\frac{dz}{dt^*} = \Gamma w_{uw} \tag{3.24}$$

Conversely, the upsloping velocity is the component of the vertical velocity that results from constraints, imposed through continuity, on the particle movement by the geometry of the domain (bottom and surface gradients), i.e. it expresses the vertical movement of a particle that would move, in the real domain along a surface of constant σ, $\bar{\sigma} = f(x,y,z,t)$, for which $F = \bar{\sigma} - f(x_p,y_p,z_p,t)$ is zero (where subscript p denotes the particle's trajectory) and, consequently

$$\frac{dF}{dt} = -\frac{\partial f}{\partial t} - u\frac{\partial f}{\partial x} - v\frac{\partial f}{\partial y} - w\frac{\partial f}{\partial z} = 0$$

$$w\frac{\partial f}{\partial \sigma}\frac{\partial \sigma}{\partial z} = -\frac{\partial f}{\partial \sigma}\frac{\partial \sigma}{\partial t} - u\frac{\partial f}{\partial \sigma}\frac{\partial \sigma}{\partial x} - v\frac{\partial f}{\partial \sigma}\frac{\partial \sigma}{\partial y} \tag{3.25}$$

$$\Gamma w = \Gamma w_{us} = -\mathrm{T} - u\mathrm{A} - v\mathrm{B}$$

as $\partial f/\partial\sigma = 1$, function f being the transformation itself.

Equation 3.22 consequently shows that the transformed vertical velocity is the natural choice when the effects of geometrical constraints are removed (as in a σ domain) and is fully consistent with the physics of the phenomena being described.

From equation 3.21 the complexity of the horizontal diffusion terms resulting from applying the coordinate transformation to equation 3.8 is also apparent. An order-of-

magnitude analysis of equation 3.21 (Appendix B) indicates that such terms are much smaller ($O(10^{-6})$ for normal estuarine conditions) than the remaining terms (O(1)) and, in principle, they could be discarded in favor of horizontal advection and vertical terms, without major losses in accuracy. A general hypothesis of similar nature is discussed by Mellor and Blumberg (1985) for all the cases in which the horizontal length scale of mean property variation is large relative to the vertical scale, provided the vertical grid resolution is fine enough. This hypothesis was confirmed by the same authors, after modelling currents and salinities in New York Harbour and Estuary with a grid of horizontal size 500 m and vertical size 6 m or smaller (a conventional σ coordinate system was used). In their study, despite the fact that no horizontal diffusivities were required, the correspondence with observed values was reported to be very good. However, and in order to ensure full generality of the model developed in the present work, it was decided to retain the horizontal diffusion terms, while attempting their transformation into simpler forms, less susceptible of introducing large errors due to their numerical computation.

As a first step, the terms on the right-hand side of equation 3.8, which represent turbulent mass diffusion can be written as:

$$\nabla \cdot F_t = \frac{\partial}{\partial x}\left(\varepsilon_x \frac{\partial C}{\partial x}\right) + \frac{\partial}{\partial y}\left(\varepsilon_y \frac{\partial C}{\partial y}\right) + \frac{\partial}{\partial z}\left(\varepsilon_z \frac{\partial C}{\partial z}\right) = \\ = \frac{\partial}{\partial x} F_x + \frac{\partial}{\partial y} F_y + \frac{\partial}{\partial z} F_z \qquad (3.26)$$

which, by performing the coordinate transformation, becomes:

$$\nabla \cdot F_t = \frac{\partial}{\partial x^*} F_x + \mathrm{A} \frac{\partial}{\partial \sigma} F_x + \frac{\partial}{\partial y^*} F_y + \mathrm{B} \frac{\partial}{\partial \sigma} F_y + \Gamma \frac{\partial}{\partial \sigma} F_z \tag{3.27}$$

A transformed vertical flux can be defined as:

$$F_\sigma = F_z + \frac{\mathrm{A}}{\Gamma} F_x + \frac{\mathrm{B}}{\Gamma} F_y \tag{3.28}$$

Following Mellor and Blumberg (1985) the divergence of the turbulent mass fluxes is defined as:

$$\nabla \cdot F_t = \frac{1}{\eta + H} \frac{\partial}{\partial x^*} \left[(\eta + H) F_x \right] + \frac{1}{\eta + H} \frac{\partial}{\partial y^*} \left[(\eta + H) F_y \right] + \Gamma \frac{\partial}{\partial \sigma} F_\sigma \tag{3.29}$$

Substituting for F_σ , as defined in 3.28, and making use of the relation

$$\frac{\partial}{\partial x} (\eta + H) = \frac{\partial}{\partial x^*} (\eta + H) \tag{3.30}$$

recalling 3.18 and that, for such transformations:

$$\begin{aligned} \mathrm{A} &= \frac{\partial \sigma}{\partial x} = \frac{\partial \sigma}{\partial Z} \frac{\partial Z}{\partial x} \\ \mathrm{B} &= \frac{\partial \sigma}{\partial y} = \frac{\partial \sigma}{\partial Z} \frac{\partial Z}{\partial y} \\ \Gamma &= \frac{\partial \sigma}{\partial z} = \frac{\partial \sigma}{\partial Z} \frac{\partial Z}{\partial z} \end{aligned} \tag{3.31}$$

and, consequently:

$$\begin{aligned} \frac{\mathrm{A}}{\Gamma} &= \frac{\frac{\partial H}{\partial x}(\eta - z) - \frac{\partial \eta}{\partial x}(H + z)}{H + \eta} \\ \frac{\mathrm{B}}{\Gamma} &= \frac{\frac{\partial H}{\partial y}(\eta - z) - \frac{\partial \eta}{\partial y}(H + z)}{H + \eta} \end{aligned} \tag{3.32}$$

equation 3.27 is recovered, i.e. formulations described by equations 3.29 and 3.27 are equivalent if definition 3.28 is used. The formulation corresponding to equation 3.29 will, therefore, be adopted.

As a second step, a choice of expressions for F_x , F_y and F_σ , taking into consideration the conditions found in estuarine applications is necessary. For this purpose it is of interest to consider the curvilinear orthogonal system represented in figure 3.2d, in which coordinate s is parallel and coordinate n is perpendicular to both the bottom and surface. This system is the most adequate to represent surface and bottom variability but, due to the small bottom slopes found in estuarine applications it is, in fact, very similar to the σ system in figure 3.2c. Following Mellor and Blumberg (1985) and by analogy with their formulation for momentum it can be considered that:

$$\begin{aligned} F_s &= -\varepsilon_s \frac{\partial C}{\partial s} \\ F_n &= \varepsilon_n \frac{\partial C}{\partial n} \end{aligned} \tag{3.33}$$

where subscripts s and n denote tangential (or parallel) and normal directions. Mass diffusivities can be defined on physical grounds, as

$$\begin{aligned} \varepsilon_s &\equiv \nu_s l_s \\ \varepsilon_n &\equiv \nu_n l_n \end{aligned} \tag{3.34}$$

In these ν_n and ν_s are velocity scales corresponding to the unresolved subgrid parallel motions and to the small scale turbulent normal motions, respectively, and have a similar magnitude. However the geometric scale of parallel motion l_s is O(Δs), where Δs is the grid spacing in the tangential direction (see figure 3.2d), while the scale of motion normal to solid surfaces (i.e. bottom), l_s is O(1 m) and, consequently $\varepsilon_s \gg \varepsilon_n$ (Mellor and Blumberg, 1985). Formulation 3.34 is in agreement with this scaling, as can be confirmed near the bottom, since the normal flux is not influenced by any

contribution arising from horizontal diffusion, as would happen if an additional larger term depending on $\partial C/\partial n$ and ε_s was present in the latter (as in equation 3.21).

In order to transform F_s , F_n into F_x , F_σ it is useful to consider (figure 3.3a) the angle, ϕ, between the s surface (which approximately coincides with a σ surface) and the horizontal which, for the mild bottom slopes found in estuarine applications (usually less than 1:20) is very small and can be taken as

$$\phi \approx \sin\phi \approx \frac{\Delta z}{\Delta x} \approx \frac{A}{\Gamma} \tag{3.35}$$

Mass balance for the elementary wedge MOP of unit thickness (see figure 3.3a), in terms of fluxes F_s, F_n and F_x alone (i.e. in the absence of any other forms of transport) leads to

$$\begin{aligned} F_x &= F_s\cos^2\phi + F_n\sin^2\phi \\ &\approx F_s(1-\phi^2) + F_n\phi^2 \\ &\approx F_s \end{aligned} \tag{3.36}$$

i.e. F_x (and F_y) can be replaced by F_s in 3.29. Since coordinate systems d and c in figure 3.2 are, locally, very similar

$$F_s = \varepsilon_s\frac{\partial C}{\partial s} \approx \varepsilon_x \cdot \frac{\partial C}{\partial x^*} = \varepsilon_h\frac{\partial C}{\partial x^*} \tag{3.37}$$

Repeating the mass balance calculations for the elementary wedge of unit thickness LQP (figure 3.3b)

$$\begin{aligned} F_z &= F_s\sin^2\phi + F_n\cos^2\phi \\ &\approx \phi^2 F_s + (1-\phi^2)F_n \\ &\approx F_n \end{aligned} \tag{3.38}$$

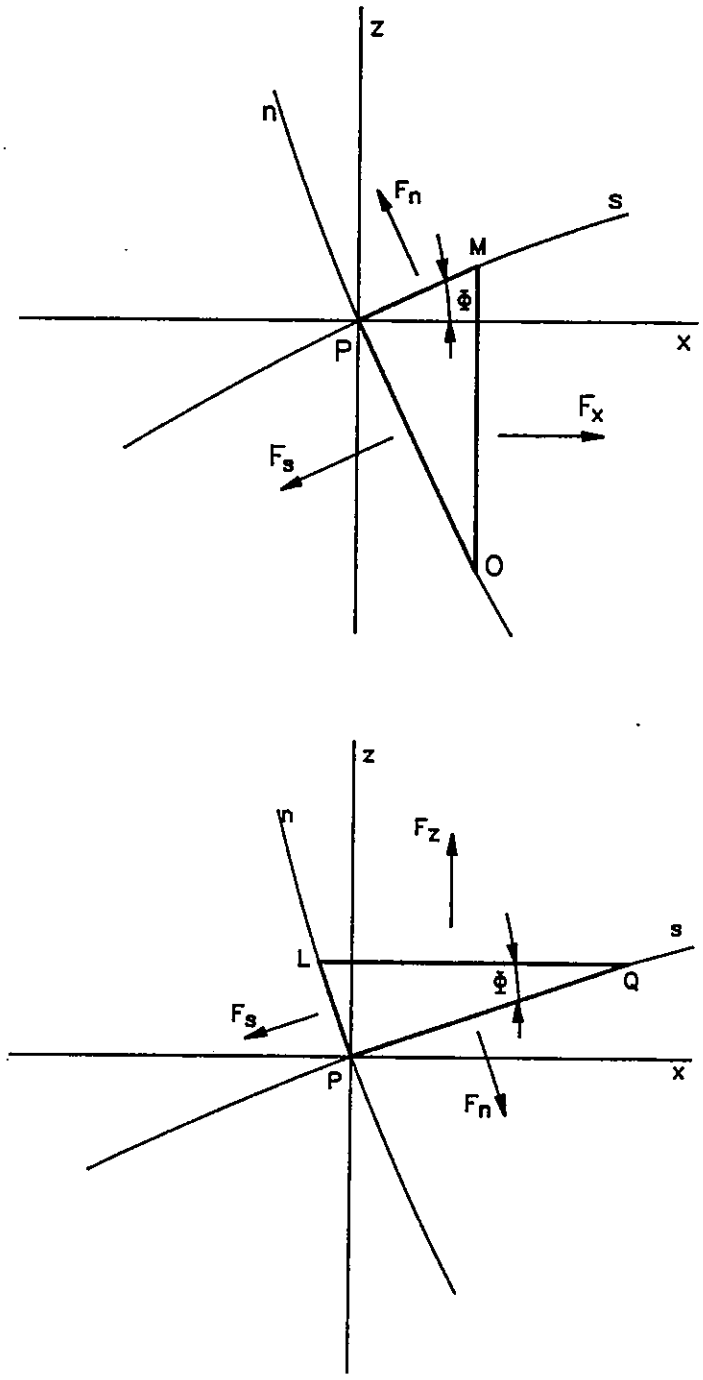

Figure 3.3 Definition of axes, cross sections of elementary surfaces and diffusive fluxes.

Given the small magnitude of the two last terms in 3.28, since not only A/Γ and B/Γ are very small for typical estuarine applications, but the horizontal fluxes are small as well (see 3.32 and Appendix A), and taking into account the form of F_z given by 3.38, it is possible to write:

$$F_\sigma \approx F_z = \varepsilon_v \frac{\partial C}{\partial z} = \varepsilon_v \Gamma \frac{\partial C}{\partial \sigma} \tag{3.39}$$

i.e. diffusion flux formulations which are, formally, similar to those of equation 3.8, can be used.

Equation 3.20 can, consequently, be rewritten in its final, simpler, form as

$$\begin{aligned} \frac{\partial C}{\partial t^*} = & -u\frac{\partial C}{\partial x^*} - v\frac{\partial C}{\partial y^*} - \bar{w}\frac{\partial C}{\partial \sigma} \\ & + \Gamma\left[\frac{\partial}{\partial \sigma}(W_s C) + \frac{\partial}{\partial \sigma}\left(\varepsilon_v \Gamma \frac{\partial C}{\partial \sigma}\right)\right] \\ & + \frac{1}{\eta + H}\frac{\partial}{\partial x^*}\left[(\eta + H)\varepsilon_h \frac{\partial C}{\partial x^*}\right] \\ & + \frac{1}{\eta + H}\frac{\partial}{\partial y^*}\left[(\eta + H)\varepsilon_h \frac{\partial C}{\partial y^*}\right] \end{aligned} \tag{3.40}$$

while boundary and initial conditions can be rewritten as:

(i) *Bed* Boundary Condition

$$N_\sigma\left[\sigma(z_b), t^*\right] = F_b = F_e - F_p \tag{3.41}$$

(ii) Free-surface Boundary Condition

$$N_\sigma[\sigma(\eta),t^*]=W_s C|_{\sigma(\eta)}+\Gamma\varepsilon_v\frac{\partial C}{\partial\sigma}|_{\sigma(\eta)}=0 \tag{3.42}$$

(iii) Solid Boundary Condition

$$\begin{aligned}\varepsilon_h\frac{\partial C}{\partial x^*}|_{sbx^*}&=0\\ \varepsilon_h\frac{\partial C}{\partial y^*}|_{sby^*}&=0\end{aligned} \tag{3.43}$$

where sbx^* and sby^* denote boundaries perpendicular to x^* and y^*, respectively.

(iv) Inflow Boundary Condition

$$C(x^*_{ib},y^*_{ib},\sigma_{ib},t^*)=C_{ib}(x^*_{ib},y^*_{ib},\sigma_{ib},t^*) \tag{3.44}$$

Initial Condition

$$C(x^*,y^*,\sigma,t_0)=C_0(x^*,y^*,\sigma) \tag{3.45}$$

Finally, it is necessary to specify the form of transformation σ, given that equation 3.40 was derived only with the restriction of condition 3.18. In the present case, since grid refinement near the estuarine bed was sought, the following form for the transformation was adopted (see Appendix C):

$$\sigma = 1 - \frac{\ln[(\beta - Z)/(\beta + Z)]}{\ln[(\beta + 1)/(\beta - 1)]} \tag{3.46}$$

where β ($\beta \neq 1$) is the parameter of the transformation, which vertically transforms a physical domain, ranging from $-H$ to η into a computational domain ranging from $\sigma=0$ to $\sigma=1$ (see figures 3.1 and 3.2c). The expression for the inverse transformation is

$$z = \eta + (H+\eta)Z(\sigma) = \eta + (H+\eta)\frac{\beta - \beta[(\beta+1)/(\beta-1)]^{1-\sigma}}{\{[(\beta+1)/(\beta-1)]^{1-\sigma}\}+1} \tag{3.47}$$

and the derivatives which are defined in equation 3.19 are, respectively

$$\begin{aligned}
T &= \frac{\partial \sigma}{\partial t} = K\left[-\frac{\partial \eta}{\partial t}\frac{(H+z)}{(H+\eta)^2}\right] \\
A &= \frac{\partial \sigma}{\partial x} = K\left[\frac{\partial H}{\partial x}\frac{(\eta - z)}{(H+\eta)^2} - \frac{\partial \eta}{\partial x}\frac{(H+z)}{(H+\eta)^2}\right] \\
B &= \frac{\partial \sigma}{\partial y} = K\left[\frac{\partial H}{\partial y}\frac{(\eta - z)}{(H+\eta)^2} - \frac{\partial \eta}{\partial y}\frac{(H+z)}{(H+\eta)^2}\right] \\
\Gamma &= \frac{\partial \sigma}{\partial z} = K\left[\frac{1}{(H+\eta)}\right]
\end{aligned} \tag{3.48}$$

where

$$K = K(Z) = \frac{2\beta}{\ln[(\beta+1)/(\beta-1)](\beta^2 - Z^2)} \tag{3.49}$$

The above derivatives are only functions of the transformation parameter β, and of variables which are known at each time step (η and H) and their respective derivatives with respect to the independent variables in the cartesian domain.

3.5 Conclusions

In this chapter the cartesian three-dimensional form of the advection-diffusion equation describing suspended cohesive sediment transport in estuarine environments was presented together with the corresponding boundary and initial conditions. Analysis of current cohesive sediment modelling practice recommends that the 3D form of the equation is retained, due to the complex nature of estuarine flow and sediment transport patterns. Furthermore, the need to correctly reproduce vertical concentration profiles showing zones of strong variation, usually located near the bed, requires that appropriate grids are used in numerical simulations. The 3D advection-diffusion equation was, therefore, re-written for a computational domain, through the use of a generic vertical coordinate transformation. A modified form of the vertical velocity, which is shown to be consistent with the use of such transformation, was also introduced. Finally, an appropriate form for the mass diffusion fluxes in the computational domain was presented, based on the physics of the phenomena being modelled and on the geometry of estuarine bottom slopes. The final equation is valid for a generic class of vertical transformations, i.e. all those which are obtained from the classical form of the sigma transformation proposed by Phillips (1957) through the application of any formula which refines the grid in specific zones of the domain. For the particular case of cohesive sediments a version of the transformation, allowing grid refinement in near-bed zones without the need for an excessively fine discretisation in upper layers of the domain, was adopted. The development of the model whose formulation was described in this chapter is presented in Chapter 4.

CHAPTER 4
DEVELOPMENT OF A SUSPENDED SEDIMENT TRANSPORT MODEL

4.1 General Aspects

The mathematical formulation for a suspended cohesive sediment transport model written for a computational σ domain was presented in Chapter 3, based on currently available formulations for the pertinent physical processes, as described in Chapter 2. In this chapter the development of a numerical model (SUSMUD3), based on the formulation of Chapter 3 is presented. Process-splitting, the basic approach followed in the development of the model, is described in Section 4.2, while the numerical formulation of each of the steps into which the original equation was divided is detailed in Section 4.3. Tests carrried out with each of the model steps are described in Section 4.4, while the main conclusions are summarised in Section 4.5.

4.2 Process-Splitting in the Computational Domain

As described in Appendix A, the complex nature of equation 3.8 whose solution, depending on the relative magnitude of its terms, may behave as the solutions of the extreme hyperbolic (advection dominated) or parabolic (diffusion dominated) cases makes it difficult to find a single numerical method which is equally adequate for both situations. Equation 3.40, which resulted from equation 3.8 through a coordinate transformation, obviously presents the same properties.

A convenient solution for this problem is the use of a fractional step method (Yanenko, 1971; Verboom, 1975), as suggested by O'Connor (1971) and used by Nicholson and O'Connor (1986). In this method each time step is broken into a number of partial or fractional steps, each containing some of the terms of the original equation. Each partial step is then separately solved through a specific numerical scheme, independent from those used to solve the other steps, thus avoiding any restrictions regarding the time and space resolutions resulting from terms not included in the partial step being solved. Consistency and stability of the method are ensured if each partial step is consistent and stable (Verboom, 1975). The advantages of the fractional step method may also include the reduction of the dimensionality of the problem to be solved and improved accuracy, if the split of the initial equation into partial steps is done in correspondence with actual physical processes and adequate numerical methods are used. Considering the properties of the method, equation 3.40 was split into four partial steps (as in Nicholson and O'Connor, 1986) which correspond to the following grouping of terms:

(i) three-dimensional advection step;

(ii) vertical step, which includes vertical diffusion and settling;

(iii) longitudinal diffusion step;

(iv) lateral diffusion step;

or, in terms of operators,

$$\frac{\partial C}{\partial t} = \{L\}(C) = \{L_A + L_V + L_L + L_C\}(C) \tag{4.1}$$

where the L_i correspond to the four indicated steps. Following Verboom (1975) and treating the L_i as ordinary parameters, locally constant in time, and integrating over a time step Δt ($n\Delta t$ to $(n+1)\Delta t$, where n is an integer value)

$$\begin{aligned} \int_{n\Delta t}^{(n+1)\Delta t} \frac{dC}{C} &= \int_{n\Delta t}^{(n+1)\Delta t} L\,dt \\ C^{n+1} &= \exp(\Delta t.L)C^n \\ &= \exp[\Delta t.(L_A + L_V + L_L + L_C)]C^n \end{aligned} \tag{4.2}$$

which can be split into component equations as:

$$\begin{aligned} C^* &= \exp(\Delta t.L_A)C^n \\ C^{**} &= \exp(\Delta t.L_V)C^* \\ C^{***} &= \exp(\Delta t.L_L)C^{**} \\ C^{n+1} &= \exp(\Delta t.L_C)C^{***} \end{aligned} \tag{4.3}$$

In the above expressions C^*, C^{**} and C^{***} are intermediate concentrations having no physical meaning and, consequently, the boundary conditions must be evaluated from those at time steps n and $n+1$. Moreover, if the L_i do not commute, then they should be used in a sequence of all possible permutations in order to maintain the order of the truncation error (Verboom, 1975). This means, in the case of 4.3, as in the case of the similar process-splitting used by Nicholson (1983), that model operation would be carried out in cycles of 24 time steps, a rather impractical requirement. Nicholson (1983) discussed the consequences of non-commutability for his splitting scheme and concluded that these should be negligible if the model was satisfactorily verified.

4.3 The Numerical Formulation of the Model

4.3.1 General

It follows, from the nature of the fractional step method and of the problem to be solved, that the following conditions should be observed regarding the choice of numerical methods:

a) Methods chosen for the solution of each step should be suitable for each type of phenomenon (i.e. advection or diffusion).

b) In a likely situation, the model will have to be run for long periods (a fortnightly tidal cycle, for example): in order to minimize the computational effort, Δt should be as large as possible (within the bounds imposed by the physical meaning of the solution) and unconditionally stable schemes should therefore be used.

c) Due to the large number of grid points involved (particularly in the horizontal directions), methods involving the inversion of large matrices should be avoided whenever possible.

The numerical formulations adopted for each of the model's partial steps are presented in the following sections. The type of grid used in model development is illustrated in figures 4.1, 5.10 and 5.12 and discussed in Section 5.4.

4.3.2 The Advection Step

In order to identify an accurate method to solve the advection step it is useful to consider the physics it represents and the properties of characteristic lines. A characteristic line (or, simply, characteristic) can be defined as the path followed by a property or physical state when propagating through a solution domain. The concept can be applied to a wide range of phenomena given its initial conditions, its governing laws and the integration conditions of such laws in the domain where propag- occurs (Abbott, 1966), producing an integral or solution surface. In the presen the propagation of mass concentration in a tidal, turbulence-averaged, velocity field is considered. This phenomenon is described, in a cartesian domain, as (see equation 3.8)

$$\frac{\partial C}{\partial t}+u\frac{\partial C}{\partial x}+v\frac{\partial C}{\partial y}+w\frac{\partial C}{\partial z}=0 \tag{4.4}$$

which states that, for a purely advective case, the concentration remains constant along characteristic lines that follow the flow and are mathematically defined by

$$\begin{aligned}\frac{dx}{dt}&=u(x,y,z,t)\\ \frac{dy}{dt}&=v(x,y,z,t)\\ \frac{dz}{dt}&=w(x,y,z,t)\end{aligned} \tag{4.5}$$

which are the flow particles' Lagrangian velocities.

The advection step in the transformed domain takes the form (see equation 3.21):

$$\frac{\partial C}{\partial t^*}+u\frac{\partial C}{\partial x^*}+v\frac{\partial C}{\partial y^*}+(\mathrm{T}+u\mathrm{A}+v\mathrm{B}+w\Gamma)\frac{\partial C}{\partial \sigma}=0 \qquad (4.6)$$

Considering now, in the x^*, y^*, σ, t^* (transformed) space, a surface of constant C, the total differential along that surface will be:

$$dC=\frac{\partial C}{\partial t^*}dt^*+\frac{\partial C}{\partial x^*}dx^*+\frac{\partial C}{\partial y^*}dy^*+\frac{\partial C}{\partial \sigma}d\sigma=0 \qquad (4.7)$$

Dividing by dt^*:

$$\frac{\partial C}{\partial t^*}+\frac{\partial C}{\partial x^*}\frac{dx^*}{dt^*}+\frac{\partial C}{\partial y^*}\frac{dy^*}{dt^*}+\frac{\partial C}{\partial \sigma}\frac{d\sigma}{dt^*}=0 \qquad (4.8)$$

Locally it can be considered that:

$$\begin{aligned}\frac{dx^*}{dt^*}&=\frac{dx}{dt}=u\\ \frac{dy^*}{dt^*}&=\frac{dy}{dt}=v\end{aligned} \qquad (4.9)$$

which are Lagrangian velocities; also, given that $d\sigma/dt^*=d\sigma/dt$:

$$\frac{d\sigma}{dt^*}=\frac{d\sigma}{dt}=\frac{\partial \sigma}{\partial t}+u\frac{\partial \sigma}{\partial x}+v\frac{\partial \sigma}{\partial y}+w\frac{\partial \sigma}{\partial z}=\mathrm{T}+u\mathrm{A}+v\mathrm{B}+w\Gamma=\bar{w} \qquad (4.10)$$

Equation 4.8 can, then, be rewritten as:

$$\frac{\partial C}{\partial t^*}+u\frac{\partial C}{\partial x^*}+v\frac{\partial C}{\partial y^*}+\bar{w}\frac{\partial C}{\partial \sigma}=0 \qquad (4.11)$$

effectively recovering equation 4.6. Again, equation 4.11 states that in a flow with velocity field $u,v,\bar{w}$ in the space x^*,y^*,σ,t^* a given concentration distribution is

advected by the flow, with no change in its values along characteristic lines, during an interval Δt^*, along distances defined, for each point i of the domain, by

$$d_i=\sqrt{(u_i\Delta t^*)^2+(v_i\Delta t^*)^2+(\bar{w}_i\Delta t^*)^2} \qquad (4.12)$$

Finally, by comparing equations 4.4 and 4.11 it is observed that, formally, they are the same, i.e. the advective phenomenon represented by the original equation in the cartesian space is described by a similar equation in the transformed space (once the transformation is performed and 4.10 is considered) and, consequently, the same solution techniques can be used for solving both equations.

The method of characteristics is, given its properties, the natural choice when describing advective phenomena, its accuracy being higher than that of conventional Eulerian schemes (Baptista, 1987; Costa, 1991). A direct consequence of the properties of characteristic lines is that, for such problems as those described by equations 4.11, 4.9 and 4.10, and in order to obtain the concentration at a point $x^*=\chi$, $y^*=\zeta$, $\sigma=\xi$ and time $t^*=\tau+\Delta t$ it is only necessary to determine the concentration at point $x^*=\chi-u\Delta t$, $y^*=\zeta-v\Delta t$, $\sigma=\xi-\bar{w}\ \Delta t$, (i. e., reached along the characteristic) at time $t^*=\tau$ (as $\Delta t^*=\Delta t$). The backwards method of characteristics is a direct translation of this approach and consists of two steps:

(i) Backtracking the characteristic lines between time $(n+1)\Delta t$ and time $n\Delta t$, i.e. following backwards elementary fluid parcels or particles, whose positions at time $(n+1)\Delta t$ would coincide with the nodes of the computational grid, in order to locate their feet; mathematically, this corresponds to the integration of ordinary differential equations 4.9 and 4.10.

(ii) Determining the concentrations at the feet of the characteristic lines, through interpolation using the known nodal values at time $n\Delta t$, and transferring them to the heads of the characteristics.

The three dimensional algorithm developed for the backward method of characteristics and used by model SUSMUD3 requires velocity data at two generic time steps $(n+1)\Delta t$ and $n\Delta t$, at each node i, j, k, of the transformed domain, to progress the solution in time. For each node i, j, k, at time $(n+1)\Delta t$, an arbitrary particle is assumed to be located at the node and its characteristic line backtracked, starting with its velocity at that time, u^{n+1}_{ijk} , v^{n+1}_{ijk} , $\overline{w}^{n+1}_{ijk}$; the particle's velocity is updated through interpolation in space and time, every time the particle leaves a grid cell of dimensions Δx^*, Δy^*,$\Delta\sigma$. The backtracking procedure is stopped when the available time, Δt, has elapsed, or when the particle has reached a boundary plane. The concentration at the foot of the characteristic is determined through second degree polinomial interpolation, based on the conclusions of Baptista (1987) regarding the accuracy properties of several interpolation schemes for the method of characteristics.

In the first case (the foot of the characteristic is located within the domain, i.e. not at a boundary) the interpolation procedure consists of three successive sweeps (using concentration values at time $n\Delta t$):

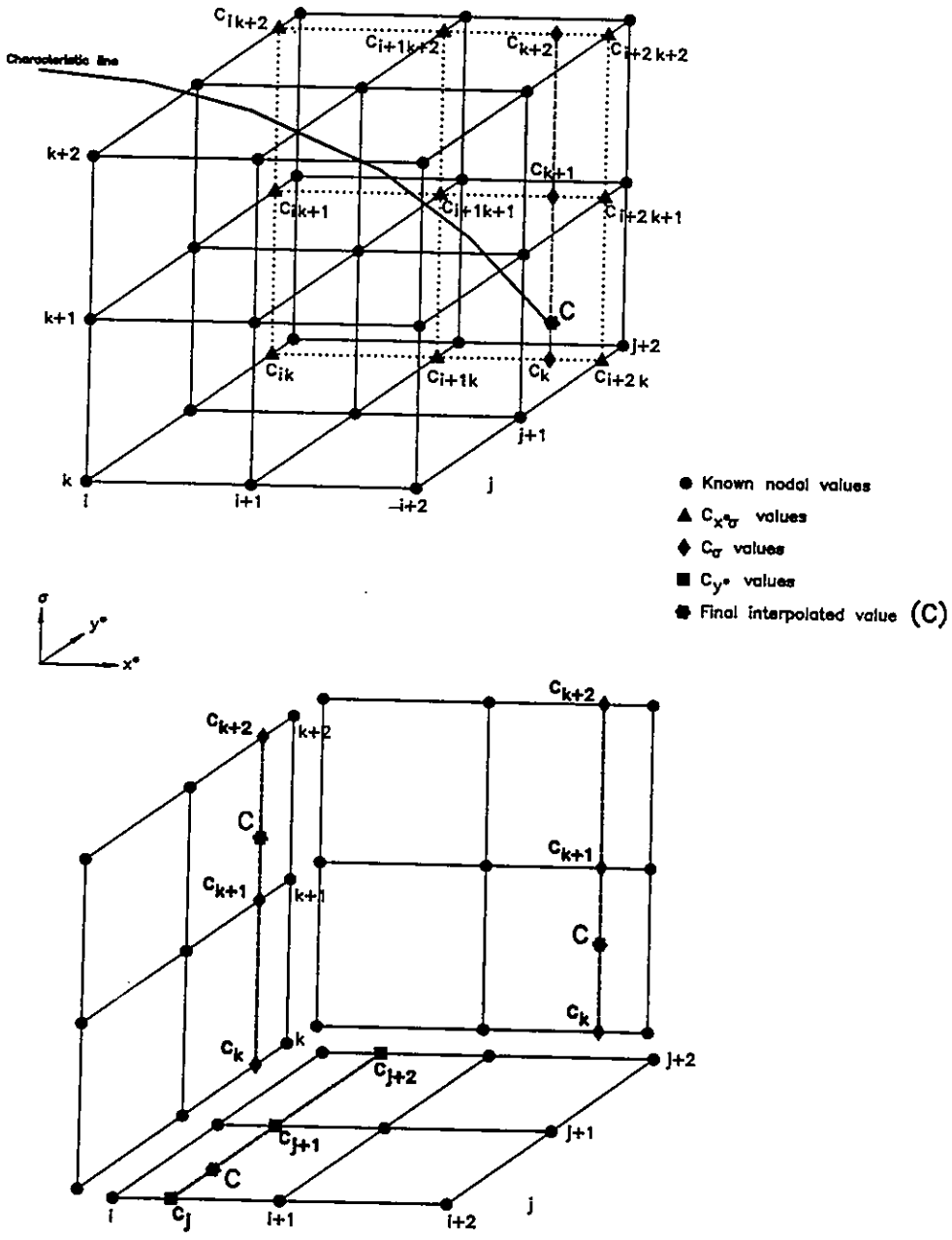

Figure 4.1 Illustration of 3D space and 2D plane interpolation procedure. The characteristic line, as computed by the model, is also sketched in the upper figure (note velocity updating in each cell).

(i) the first sweep involves 9 nodal values $C_{x^*y^*\sigma}$ in each of three planes of constant value of a variable, say σ, producing, through interpolation in a second direction, say y^*, 3 values $C_{x^*\sigma}$ per plane;

(ii) the second sweep is made in the x^* direction, in each one of the three constant σ planes, and produces one C_σ per plane;

(iii) the final sweep is made in the σ direction to produce the final interpolated C value at the foot of the characteristic (i.e. the C^* value at the head, at time $(n+1)\Delta t$).

In the second case (the foot of the characteristic is found at a boundary plane, at a time $n\Delta t<t<(n+1)\Delta t$), the concentration is found through bidimensional interpolation (two sweeps, only), of the nodal values in the boundary plane, at time step n, if the boundary is a solid or outflow one, or at time steps n and $n+1$, followed by time interpolation, if the boundary is an inflow one. The interpolation procedure and the shape of a characteristic line are sketched in figure 4.1.

4.3.3 The Vertical Step

The equation for the vertical step, which results from 3.40 and 4.1 is

$$\frac{\partial C}{\partial t^*} = \Gamma \frac{\partial}{\partial \sigma}\left[W_s C + \Gamma \varepsilon_v \frac{\partial C}{\partial \sigma}\right] \tag{4.13}$$

subject to boundary conditions:

$$N_\sigma\left[\sigma(z_b),t^*\right]=F_b=F_e-F_p \tag{3.41}$$

at the *bed*, where the *erosion* and *deposition* fluxes may represent exchanges with a cohesive bed or a fluid mud layer, and

$$N_\sigma\left[\sigma(\eta),t^*\right]=W_s C|_{\sigma(\eta)}+\Gamma\varepsilon_v\left.\frac{\partial C}{\partial\sigma}\right|_{\sigma(\eta)}=0 \tag{3.42}$$

at the free surface. The bed boundary condition can be rewritten by considering a re-entrainment coefficient (Nicholson and O'Connor, 1986), defined as

$$\begin{aligned} r&=\frac{\tau_b}{\tau_{cd}} && \tau_b<\tau_{cd} \\ r&=1 && \tau_b\geq\tau_{cd} \end{aligned} \tag{4.14}$$

which represents the fraction of sediment that, at a given time, could not withstand the near-bed hydrodynamic actions and did not deposit (τ_b and τ_{cd}, as defined in Chapter 2, are the mean bottom shear stress and a critical shear stress for deposition, respectively), and is related to Krone's probability of sediment deposition. Therefore, the deposition flux ($F_p=dm_d/dt$) can be expressed as:

$$F_p=\frac{dm_d}{dt}=(1-r)W_s C \tag{4.15}$$

Consequently, and since near the bed ($\sigma=\sigma(z_b)$) both the sediment that does not deposit and the eroded sediment have to be diffused to the upper layers

$$\varepsilon_v\left.\frac{\partial C}{\partial z}\right|_{z_b}=\Gamma\varepsilon_v\left.\frac{\partial C}{\partial\sigma}\right|_{\sigma(z_b)}=-\frac{dm_e}{dt}-rW_s C|_{\sigma(z_b)} \tag{4.16}$$

and, adding the settling flux to both sides, the bed boundary condition is transformed into

$$N_\sigma\left[\sigma(z_b),t^*\right]=\Gamma\varepsilon_v\frac{\partial C}{\partial\sigma}\bigg|_{\sigma(z_b)}+W_sC|_{\sigma(z_b)}=-\frac{dm_e}{dt}+(1-r)W_sC|_{\sigma(z_b)} \tag{4.17}$$

The finite difference equation resulting from 4.13 was obtained using a forward difference approximation for the time derivative and, in space, forward differences for the settling term (i.e. the gradient of the settling flux at a given grid point is computed using the concentration at that point and at the point above) and central differences for the diffusion term. An implicit method was used and, consequently, for a given point in a vertical, omitting indexes i, j for clarity:

$$\begin{aligned}
&\frac{\partial C}{\partial t^*}\bigg|_{\sigma=(k-1)\Delta\sigma}=\frac{C_{k+1}^{**}-C_k^*}{\Delta t^*}+O(\Delta t)\\
&\Gamma\frac{\partial}{\partial\sigma}(W_sC)|_{\sigma=(k-1)\Delta\sigma}=\Gamma_k\frac{W_{s_{k+1}}C_{k+1}^{**}-W_{s_k}C_k^{**}}{\Delta\sigma}+O(\Delta\sigma)\\
&\Gamma\frac{\partial}{\partial\sigma}\left(\Gamma\varepsilon_v\frac{\partial C}{\partial\sigma}\right)\bigg|_{\sigma=(k-1)\Delta\sigma}=\Gamma_k\left[\bar{\varepsilon}^v_{k+1/2}\frac{C_{k+1}^{**}-C_k^{**}}{\Delta\sigma^2}-\bar{\varepsilon}^v_{k-1/2}\frac{C_k^{**}-C_{k-1}^{**}}{\Delta\sigma^2}\right]+O(\Delta\sigma)^2
\end{aligned} \tag{4.18}$$

where

$$\bar{\varepsilon}^v_k=\varepsilon_{v_k}\Gamma_k=\varepsilon_v\Gamma|_{\sigma=(k-1)\Delta\sigma} \tag{4.19}$$

and both the diffusion coefficients and the settling velocities are computed using the latest known value of the concentration. Therefore, for points k in the water column (i.e. not located at the boundaries):

$$\begin{aligned}
&C_{k-1}^{n+1}\left[\Delta t\left(-\frac{\Gamma_k\bar{\varepsilon}^z_{k-1/2}}{\Delta\sigma^2}\right)\right]\\
&+C_k^{n+1}\left[1+\Delta t\left(\frac{\Gamma_k(\bar{\varepsilon}^z_{k+1/2}+\bar{\varepsilon}^z_{k-1/2})}{\Delta\sigma^2}+\frac{\Gamma_kW_{s_k}}{\Delta\sigma}\right)\right]\\
&+C_{k+1}^{n+1}\left[\Delta t\left(-\frac{\Gamma_k\bar{\varepsilon}^z_{k+1/2}}{\Delta\sigma^2}-\frac{\Gamma_kW_{s_{k+1/2}}}{\Delta\sigma}\right)\right]=C_k^n
\end{aligned} \tag{4.20a}$$

that is:

$$a_k C_{k-1}^{n+1} + b_k C_k^{n+1} + c_k C_{k+1}^{n+1} = C_k^n \tag{4.20b}$$

where a, b and c are the coefficients corresponding to the lower, main and upper diagonal of the matrix corresponding to the tridiagonal system of nk finite difference equations obtained for each vertical i, j. At the bottom ($k=1$) the coefficients are defined as:

$$\begin{aligned} &C_1^{n+1}\left[1+\Delta t\left(\frac{\Gamma_1 \bar{\varepsilon}_2^{\nu}}{\Delta\sigma^2}+\frac{\Gamma_1(1-r)W_{s_1}}{\Delta\sigma}\right)\right] \\ &+C_2^{n+1}\left[\Delta t\left(-\frac{\Gamma_1 \bar{\varepsilon}_2^{\nu}}{\Delta\sigma^2}-\frac{\Gamma_1 W_{s_2}}{\Delta\sigma}\right)\right]=C_k^n+\Delta t\frac{\Gamma_1}{\Delta\sigma}\frac{\partial m_e}{\partial t} \end{aligned} \tag{4.21a}$$

that is:

$$b_1 C_1^{n+1} + c_1 C_2^{n+1} = C_1^n + \Delta t \frac{\Gamma_1}{\Delta\sigma}\frac{\partial m_e}{\partial t} \tag{4.21b}$$

while at the free surface ($k=nk$) the following expression is obtained:

$$\begin{aligned} &C_{nk-1}^{n+1}\left[\Delta t\left(-\frac{\Gamma_{nk}\bar{\varepsilon}_{nk-1}^{\nu}}{\Delta\sigma^2}+\frac{\Gamma_{nk}W_{s_{nk-1}}}{\Delta\sigma}\right)\right] \\ &+C_{nk}^{n+1}\left[1+\Delta t\frac{\Gamma_k\bar{\varepsilon}_{k-1}^{\nu}}{\Delta\sigma^2}\right]=C_{nk}^n \end{aligned} \tag{4.22a}$$

that is:

$$a_{nk} C_{nk-1}^{n+1} + b_{nk} C_{nk}^{n+1} = C_{nk}^n \tag{4.22b}$$

The system of nk equations is solved using the Thomas algorithm (see, for example, Anderson et al., 1984). The numerical method used for solving the vertical step is consistent with the partial differential equation being solved and has a truncation error

of $O(\Delta t, \Delta\sigma)$. The method is also expected to be unconditionally stable (see Appendix D).

4.3.4 The Horizontal Diffusion Steps

The two horizontal diffusion steps in equation 3.40 are of the same type and were numerically treated using the same method. For example, the equation for the longitudinal diffusion step is:

$$\frac{\partial C}{\partial t^*} = \frac{1}{\eta + H}\frac{\partial}{\partial x^*}\left[(\eta + H)\,\varepsilon_h \frac{\partial C}{\partial x^*}\right] = \frac{1}{D}\frac{\partial}{\partial x^*}\left[D\,\varepsilon_h \frac{\partial C}{\partial x^*}\right] \tag{4.23}$$

where D is the total depth.

For the longitudinal diffusion step the domain was divided into x^*, σ planes (i.e. planes of constant y^*) and each plane was then swept longitudinally, row by row, using the unidimensional Barakat and Clark (1966) method. For the lateral difusion step a similar procedure was followed, after division of the domain in y^*, σ planes (i.e. of constant x^*).

The Barakat and Clark method is described as an alternate direction explicit method (Anderson et al., 1984) and consists of two steps followed by averaging. Applying the method in the x^* direction, for example, with y^* and σ constant: in the first step the

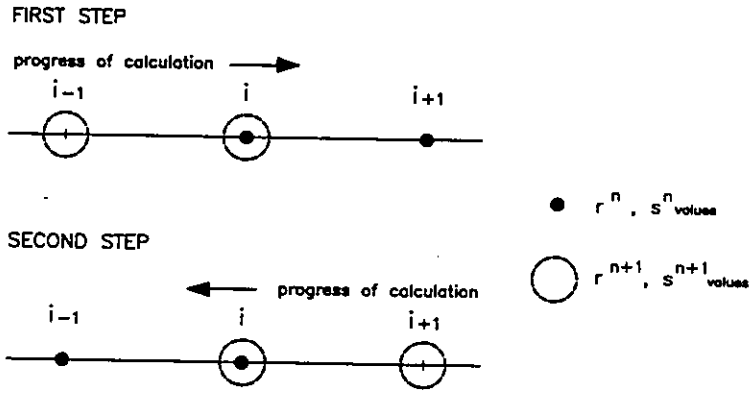

Figure 4.2 Computational molecule for the unidimensional Barakat and Clark method.

solution is propagated from the boundary nearest to the $x^*=x^*_{min}$ point in the domain, in the direction of increasing i (omitting j and k for clarity), using an already calculated or an inflow boundary value to the left (i-1) of the operating point (i) and the known value to the right (i+1) resulting from the previous time step (or, in this case, the previous partial step). The equation for the first step is (omitting superscript * in the longitudinal coordinate):

$$\frac{r_i^{n+1}-r_i^n}{\Delta t}=\frac{1}{D_i}\left[\frac{D_{i+1/2}\varepsilon^h_{i+1/2}}{\Delta x^2}(r_{i+1}^n-r_i^n)-\frac{D_{i-1/2}\varepsilon^h_{i-1/2}}{\Delta x^2}(r_i^{n+1}-r_{i-1}^{n+1})\right] \qquad (4.24)$$

where the r_i^n and r_{i+1}^n are, in fact, known C^{**} values (see 4.3), r_i^{n+1} is the intermediate value to be computed and r_{i-1}^{n+1} is an intermediate value already computed or an inflow boundary concentration. Combining terms, the following expression is obtained:

$$r_i^{n+1}=\left(\frac{1-\gamma}{1+\lambda}\right)r_i^n+\left(\frac{\gamma}{1+\lambda}\right)r_{i+1}^n+\left(\frac{\lambda}{1+\lambda}\right)r_{i-1}^{n+1} \qquad (4.25)$$

where

$$\lambda = \frac{D_{i-1/2}}{D_i}\ \frac{\Delta t \varepsilon_{i-1/2}^h}{\Delta x^2}$$
$$\gamma = \frac{D_{i+1/2}}{D_i}\ \frac{\Delta t \varepsilon_{i+1/2}^h}{\Delta x^2} \qquad (4.26)$$

In the second step the solution is propagated from the boundary nearest to the $x^*=x^*_{max}$ point in the domain in the direction of decreasing i, this time using an already calculated or an inflow boundary value to the right ($i+1$) of the operating point (i) and the known value to the left ($i-1$) resulting from the previous partial step. The equation for the second step is:

$$\frac{s_i^{n+1}-s_i^n}{\Delta t} = \frac{1}{D_i}\left[\frac{D_{i+1/2}\varepsilon_{i+1/2}^h}{\Delta x^2}(s_{i+1}^{n+1}-s_i^{n+1}) - \frac{D_{i-1/2}\varepsilon_{i-1/2}^h}{\Delta x^2}(s_i^n - s_{i-1}^n)\right] \qquad (4.27)$$

where, again, the s_i^n and s_{i-1}^n are known C^{**} values, s_i^{n+1} is the intermediate value to be computed and s_{i+1}^{n+1} is an intermediate value already computed or an inflow boundary concentration. Combining terms as in the first step:

$$s_i^{n+1} = \left(\frac{1-\lambda}{1+\gamma}\right)s_i^n + \left(\frac{\gamma}{1+\gamma}\right)s_{i+1}^{n+1} + \left(\frac{\lambda}{1+\gamma}\right)s_{i-1}^n \qquad (4.28)$$

where λ and γ were defined in 4.26. The concentration after the longitudinal diffusion partial step is then obtained, through averaging, as:

$$C_i^{***} = \frac{r_i^{n+1} + s_i^{n+1}}{2} \qquad (4.29)$$

The boundary conditions used in the horizontal diffusion step were:

$$\varepsilon_h \frac{\partial C}{\partial x^*}\Big|_{sbx^*} = 0 \qquad (4.30)$$

at outflow and solid boundaries, respectively, and

$$C(x_{ib}^*, y_{ib}^*, \sigma_{ib}, t^*) = C_{ib}(x_{ib}^*, y_{ib}^*, \sigma_{ib}, t^*) \tag{3.44}$$

at inflow boundaries. In the second case the boundary condition is automatically included in the calculations by making:

$$C_i^{***} = r_i^{n+1} = s_i^{n+1} = C_{ib}^{n+1} \tag{4.31}$$

for the boundary points. In the first case (no flux boundary at point i) two cases can happen.

(i) Flow domain develops to the right of point i (i.e. point $i+1$ belongs to the domain)

Considering that $\partial C/\partial x^*|_{i-1/2}=0$, the right-hand side of 4.23 is approximated as:

$$\frac{1}{D}\frac{\partial}{\partial x^*}\left[D\varepsilon_h\frac{\partial C}{\partial x^*}\right] \approx \varepsilon_h\frac{C_{i+1}-C_i}{\Delta x^2} \tag{4.32}$$

and therefore:

$$\frac{\partial C}{\partial t^*} - \frac{1}{D}\frac{\partial}{\partial x^*}\left[D\varepsilon_h\frac{\partial C}{\partial x^*}\right]_i \approx \frac{C_i^{n+1}-C_i^n}{\Delta t} - \frac{\varepsilon_h}{\Delta x^2}(C_{i+1}-C_i) = 0 \tag{4.33}$$

where the time levels of concentrations in the space derivatives will be specified in the two steps. Expanding, it is possible to obtain for the first step:

$$r_i^{n+1} = (1-\lambda)r_i^n + \lambda r_{i+1}^n \tag{4.34}$$

where

$$\lambda = \frac{\Delta t \varepsilon_i^h}{\Delta x^2} \tag{4.35}$$

For the second step a similar expression is obtained (with λ as defined in 4.35) as:

$$s_i^{n+1} = \left(\frac{1}{1+\lambda}\right) s_i^n + \left(\frac{\lambda}{1+\lambda}\right) s_{i+1}^{n+1} \tag{4.36}$$

(ii) Flow domain develops to the left of point i (i.e. point $i-1$ belongs to the domain)

Similarly to case (i) and considering that $\partial C/\partial x^*|_{i+1/2}=0$, the expression for the first step is:

$$r_i^{n+1} = \left(\frac{\lambda}{1+\lambda}\right) r_{i-1}^{n+1} + \left(\frac{1}{1+\lambda}\right) r_i^n \tag{4.37}$$

and for the second step:

$$s_i^{n+1} = \lambda s_{i-1}^n + (1-\lambda) s_i^n \tag{4.38}$$

where λ was defined in 4.35.

The Barakat and Clark method is consistent with the diffusion step equation being solved, is unconditionally stable and has a truncation error of $O(\Delta t^2, \Delta x^2)$ because the lower order error terms resulting from the two steps cancel in the averaging (see Appendix D).

4.4 Tests of Model Steps

4.4.1 General

The three-dimensional suspended cohesive sediment transport model SUSMUD3 was developed in FORTRAN 77 using three different computers: two Digital Equipment Corporation machines (VAX 11-780 running a VAX-11 FORTRAN compiler under a VMS operating system and a VAXstationII/GPX running a VAX FORTRAN compiler under a MicroVMS operating system) and a PC (with a 486DX2/66 processor, running a MS-FORTRAN compiler under a MS-DOS operating system). The need to use several computers was due to the end of operation of VAX services at the National Laboratory for Civil Engineering (LNEC) in Lisbon, Portugal, where the model was developed. A flowchart of the model is presented as Appendix E.

The set of routines which composes model SUSMUD3 was tested at two levels. In a first level, all routines were separately tested, in a comprehensive way for individual performance using known test results. In a second level, the routines included in computational modules were tested as a group against known analytical solutions or field data. The computational modules which were tested correspond closely to the different model steps; these are:

(i) the tridimensional advection module, which solves the advection step in the model;

(ii) two horizontal diffusion modules of similar structure, the first for solving longitudinal diffusion and the second for solving lateral diffusion;

(iii) two vertical modules, the first solving directly the vertical step, and the second solving a version of the vertical step which is derived from the vertical one dimensional transport equation.

In the following sections the test cases used for each of the above modules are presented together with the corresponding results.

4.4.2 The Advection Step

The advection module was tested against a bi-dimensional case in the x^*, y^* plane but the results are representative of conditions in the other planes(x^*, σ and y^*, σ) since the computer code is entirely similar, as confirmed during first level testing. Due to the nature of the code a three-dimensional grid had to be used and, therefore, the test conditions were repeated in each one of the horizontal planes of the grid. As a consequence, some small losses in accuracy can be expected, due to the need to carry out additional vertical interpolations.

A square domain (in plan) with $L_x=L_y=2400\ m$, was discretized with $\Delta x=\Delta y=50\ m$. The initial condition in the domain was a two dimensional gaussian distribution of unit height in the form (figure 4.3):

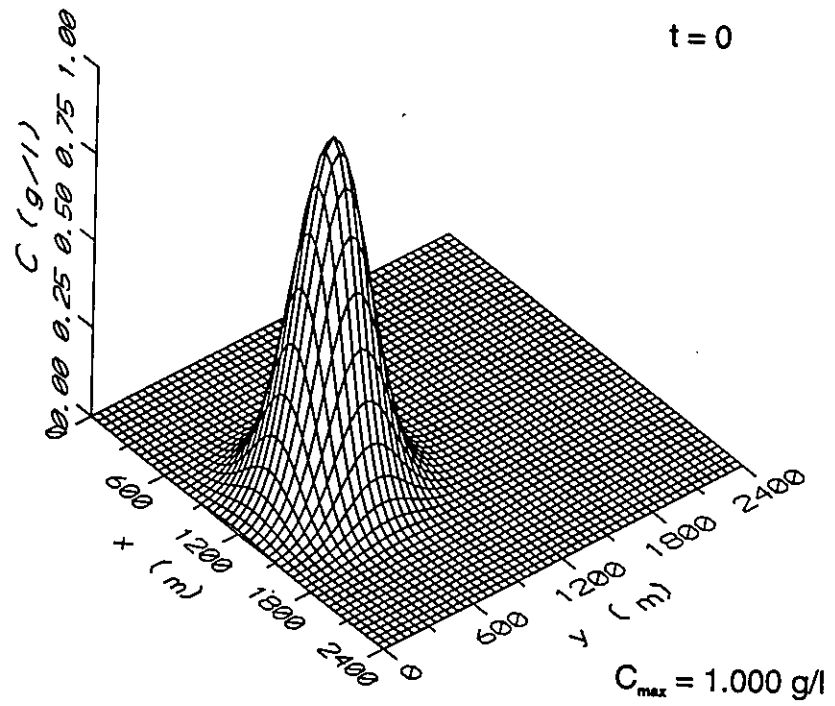

Figure 4.3 Initial condition for advection test case.

$$C_0(x^*,y^*)=\exp\left[-\frac{(x^*-x_0^*)^2}{2s_x^2}-\frac{(y^*-y_0^*)^2}{2s_y^2}\right] \tag{4.39}$$

with standard deviations $s_x = s_y = 4\Delta x$ and centered at $x_0^*=L_x/2$, $y_0^*=L_y/4$.

The advection of the gaussian distribution was studied in a clockwise rotating velocity field, in which the flow velocities at each point are proportional to the distance of the point to the center of the domain $x_c^*=L_x/2$, $y_c^*=L_y/2$:

$$\begin{aligned} u &= -\Omega(y-y_c^*) \\ v &= \Omega(x-x_c^*) \end{aligned} \tag{4.40}$$

a full revolution taking place in 120 time steps of $\Delta t=100$ s (i.e. $\Omega = -2\pi/T = -2\pi/(120\,\Delta t)$) and with boundary condition (for $t>0$):

$$C_{ib}(x^*, y^*, t) = 0 \tag{4.41}$$

where subscript *ib* denotes points at the horizontal edges of the domain, where the concentrations are already very small. The computed concentration distributions after *T/4*, *T/2*, *3T/4* and *T* are presented as figures 4.4, 4.5, 4.6 and 4.7. Agreement between the final result of the simulation and the initial condition, which should have been recovered through the solid body rotation, is good. The peak of the distribution, after a full revolution has a magnitude of 91.4% of the original value and only small negative values are found at the back of the distribution. This was mainly due to the nature of the interpolation method that was used. In terms of mass conservation the numerical method was found to cause a loss of mass of 0.22% per time step. The overall shape of the concentration distribution was well preserved but the peak of the computed distribution was not located at $x_0^*=L_x/2$, $y_0^*=L_y/4$, as in the initial distribution. This was mainly due to inacuracies in the back-tracking of the particles. Cross sections of the initial distribution and of the computed distribution for $t=T$ naturally reflect those inaccuracies. Cross-sections along planes parallel to the x axis are presented in figures 4.8, 4.9 and 4.10, while similar cross sections, along planes parallel to the y axis, are presented in figures 4.11, 4.12 and 4.13. Nevertheless, it is expected that the method is much more accurate than that used by Nicholson and O'Connor (1986) in which the end points of the trajectories were determined through a simple backward projection with no updating of the initial nodal velocity.

As an indication of the relative performance of several numerical methods for advective simulations it should be mentioned that Costa (1991) compared the output

of different schemes using the test case described above, but with a grid having twice the spacing, i.e. $\Delta x=\Delta y=100\ m$. The numerical methods which were used in the tests and the value of the concentration distribution peak, after one full revolution ($t=T$), are shown in table 4.1. From such results the bad performance of all Eulerian methods is apparent, a result which is confirmed by the very poor simulation of the shape of the distribution by such methods (see Costa, 1991, for details). The forward method of characteristics used by Costa (1991), on the contrary, produced good results, both in terms of the peak value and of the shape.

Table 4.1

Peak Values in Advection Test-Case Using Several Methods (After Costa, 1991)

Method	Peak Value of Distribution (t=T)
Forward Method of Characteristics	0.90
Upwind Scheme	0.10
Central Differences Scheme	0.69
QUICK Scheme	0.64

4.4.3 The Vertical Step

The vertical step was tested in two different ways. In the first, the vertical module was used to simulate two simple situations, a depositional one and an erosional one, for which an analytical solution is available (Dobbins, 1943). In the second, a modified version of the vertical module, a 1D model solving the one dimensional vertical

transport equation, was used to simulate a field situation using concentration profiles obtained by Kirby (1986) in the Severn estuary.

The Dobbins analytical solution was derived using concepts related to coarse sediment transport and expresses the evolution in time between two equilibrium concentration profiles (i.e. those for which the rate at which sediment is picked up from the bed equals the rate of deposition).

Equilibrium concentration profiles have the generic form

$$C = Ke^{-\left(\frac{W_s z}{\varepsilon_v}\right)} \tag{4.42}$$

where K is the concentration at the origin of the vertical coordinate z (i.e. at the top of the bed material, z growing upward), W_s and ε_v are the settling velocity and the vertical diffusion coefficient, respectively. For constant settling velocities and diffusion coefficients, the Dobbins analytical solution, expressing the time evolution between two equilibrium profiles for which $K=C_0$ (initial condition) and $K=A$, respectively, has the form:

$$C = Ae^{-\left(\frac{W_s z}{\varepsilon_v}\right)} + (C_0 - A)e^{-\left(\frac{W_s z}{2\varepsilon_v}\right)} \sum_{n=1}^{\infty} F_n \tag{4.43}$$

where:

$$F_n = \frac{2\alpha_n^2 W_s e^{-\left(\alpha_n^2 \varepsilon_v + \frac{W_s^2}{4\varepsilon_v}\right)t} Y_n}{\left(\alpha_n^2 \varepsilon_v + \frac{W_s^2}{4\varepsilon_v}\right)\left[\left(\alpha_n^2 \varepsilon_v + \frac{W_s^2}{4\varepsilon_v}\right)H + \frac{W_s}{\varepsilon_v}\right]} \tag{4.44}$$

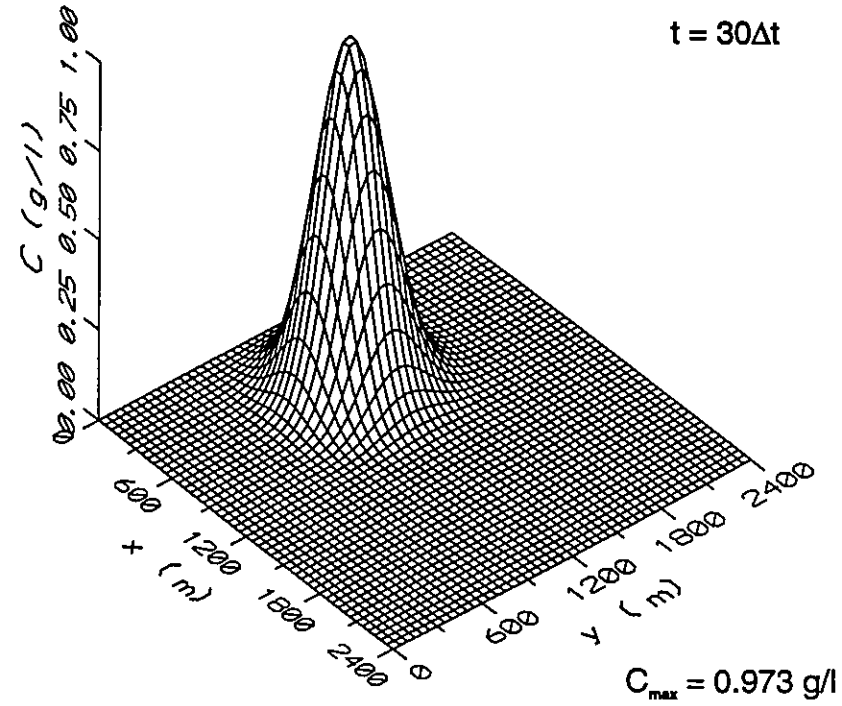

Figure 4.4 Simulated concentration distribution for advection test case (*t=T/4*).

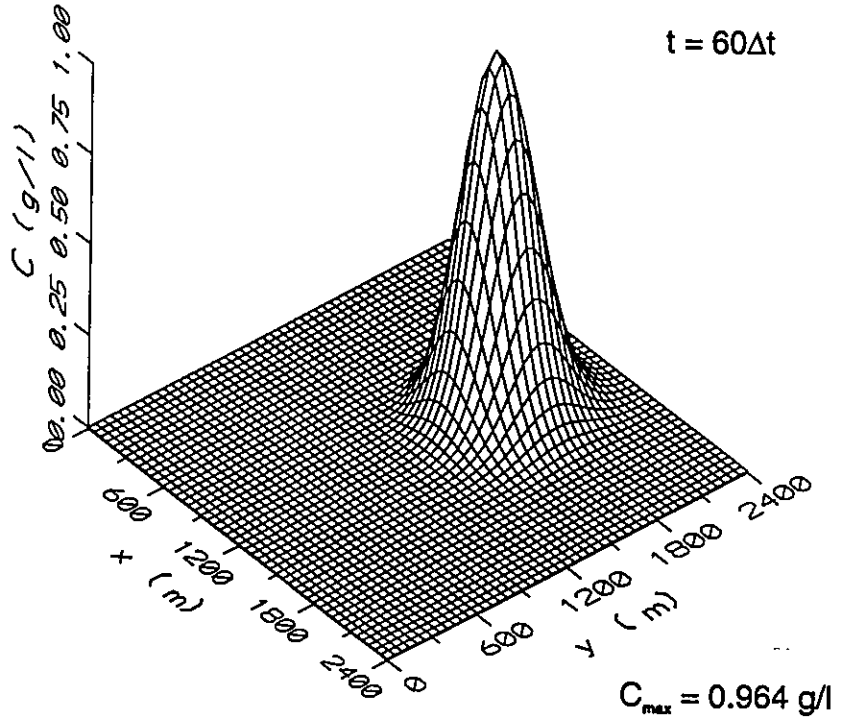

Figure 4.5 Simulated concentration distribution for advection test case (*t=T/2*).

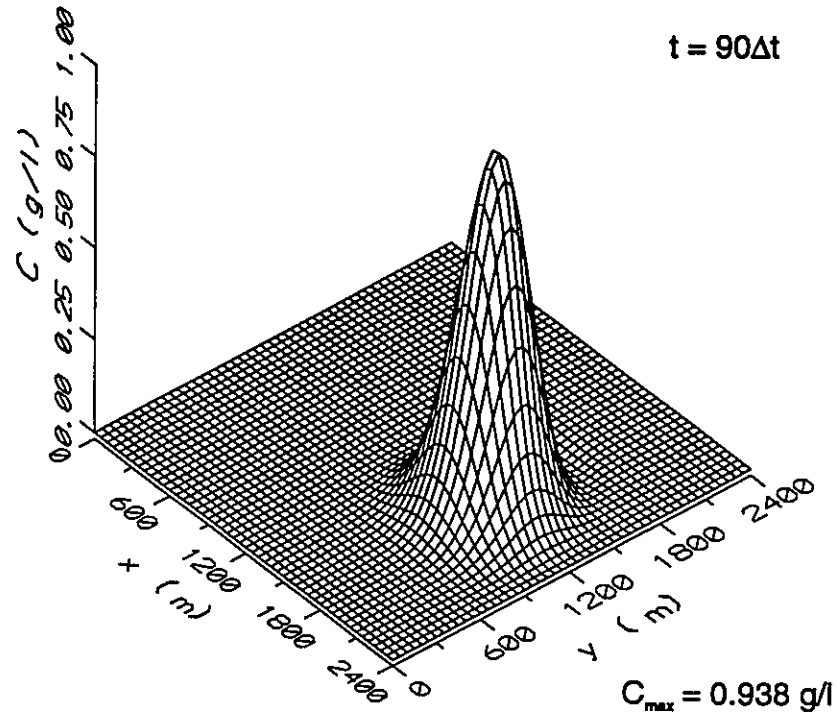

Figure 4.6 Simulated concentration distribution for advection test case (*t=3T/4*).

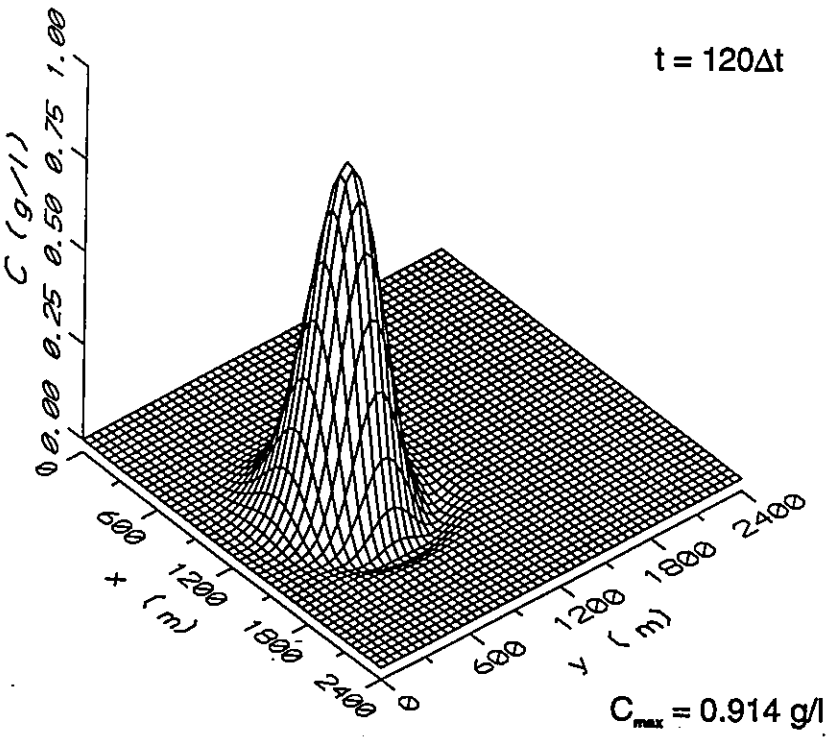

Figure 4.7 Simulated concentration distribution for advection test case (*t=T*).

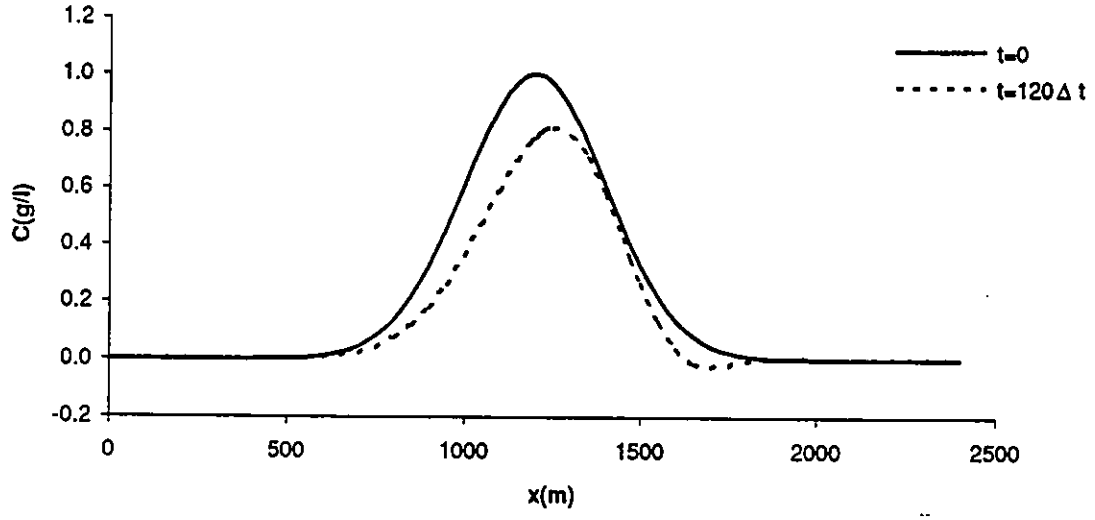

Figure 4.8 Cross-section, parallel to the x axis (y=*600m*) of the initial and simulated concentration distributions for advection test case (t=T).

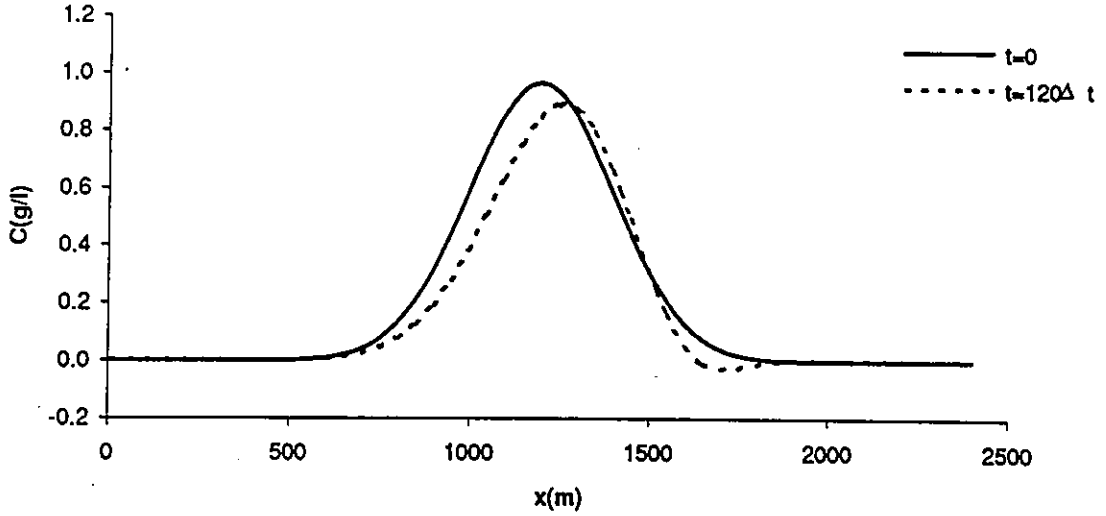

Figure 4.9 Cross-section, parallel to the x axis (y=*650m*) of the initial and simulated concentration distributions for advection test case (t=T) .

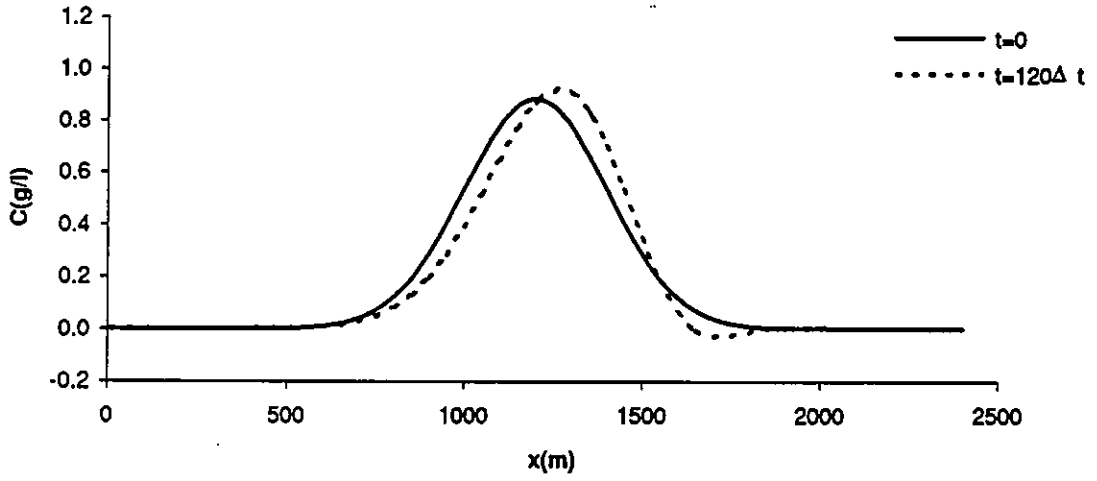

Figure 4.10 Cross-section parallel to the x axis (y=*700m*) of the initial and simulated concentration distributions for advection test case (t=T).

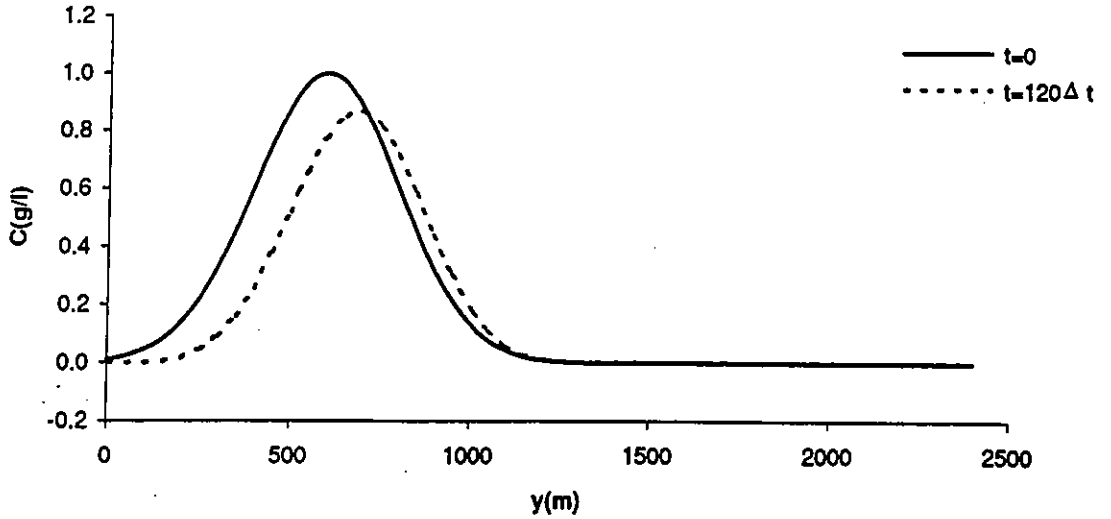

Figure 4.11 Cross-section parallel to the y axis (x=*1200m*) of the initial and simulated concentration distributions for advection test case (t=T).

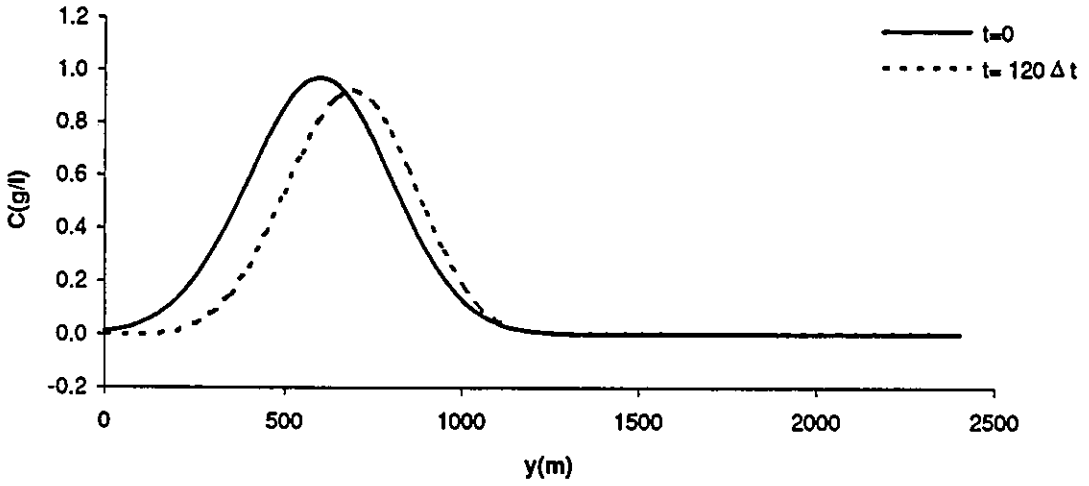

Figure 4.12 Cross-section parallel to the *y* axis (***x=1250m***) of the initial and simulated concentration distributions for advection test case (***t=T***).

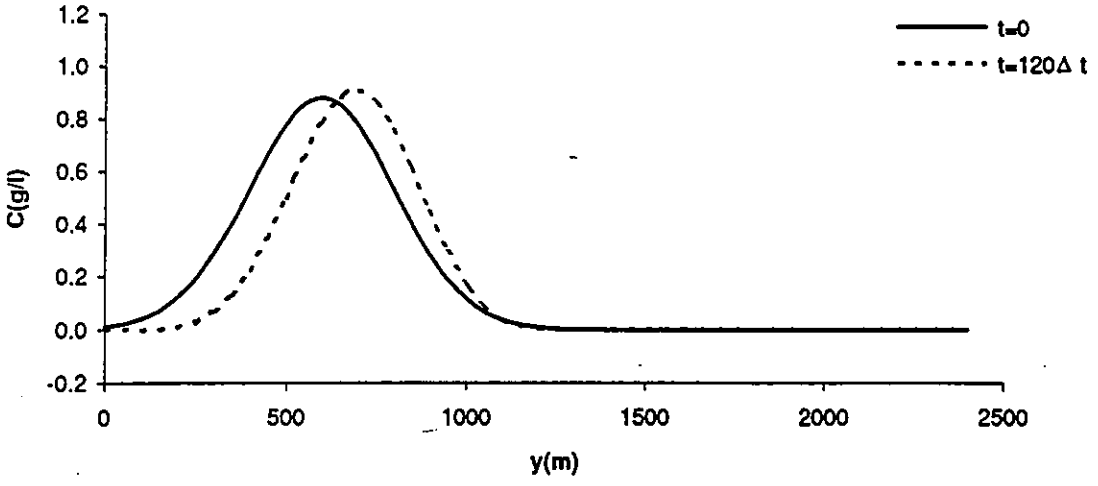

Figure 4.13 Cross-section parallel to the *y* axis (***x=1300m***) of the initial and simulated concentration distributions for advection test case (***t=T***).

and

$$Y_n = \cos(\alpha_n z) + \frac{W_s}{2\varepsilon_v \alpha_n}\sin(\alpha_n z) \tag{4.45}$$

In the above equations H is the water depth, as before, and the α_n are the real positive roots of the following equation

$$2\cot(H\alpha) = \frac{H\alpha}{\frac{W_s H}{2\varepsilon_v}} - \frac{\frac{W_s H}{2\varepsilon_v}}{H\alpha} \tag{4.46}$$

Boundary conditions used for the derivation of the Dobbins solution are a no net flux condition at the free surface, as in 3.10, and a condition corresponding to the existence of equilibrium profiles, at the bottom:

$$\varepsilon_v \left(\frac{\partial C}{\partial z}\right)\Big|_{z=0} + W_s C|_{z=0} = 0 \tag{4.47}$$

Dobbins checked his analytical solution against simple laboratory tests using lucite (a resin) as sediment. The physical parameters of his first test, i.e. $H=0.416\ m$, $W_s=2.46\times10^{-3}\ m/s$ and $\varepsilon_v=W_s\ /3\ m^2/s$, were used and 30 terms in the summation in equation 4.43 were considered, in order to compute the analytical solution for two cases:

i) A deposition case, with $C_0=1\ kg/m^3$ and $A=0\ kg/m^3$, closely corresponding to Dobbin's first example.

ii) An erosion case, with $C_0=0.15\ kg/m^3$ and $A=1\ kg/m^3$.

The results corresponding to the time evolution of the concentration profile for the deposition case are presented in figure 4.14, while the final profile corresponding to the erosion case is presented in figure 4.15. In this last case only the final profile is presented, since the numerical module does not assume intermediate equilibrium profiles, as happens with the analytical solution. The simulation results are good, as the output of the numerical module virtually coincides with the analytical solution in both cases.

For the second test a one-dimensional vertical transport equation in the transformed domain was used, in the form

$$\frac{\partial C}{\partial t^*} = \Gamma \frac{\partial}{\partial \sigma}\left[W_s C + \Gamma \varepsilon_v \frac{\partial C}{\partial \sigma}\right] + T\left(\frac{\partial C}{\partial \sigma}\right) \qquad (4.48)$$

This equation is obtained from the cartesian version of the same equation (see, for example, Ross, 1988), through the coordinate transformation described in the previous sections. Equation 4.48 differs from the vertical step in 4.13 only through the last term on the right-hand side and is solved using boundary conditions 3.42 and 4.17 and an appropriate initial condition (concentration profile at $t=t_0$).

The vertical one-dimensional model was applied, using the parameters for flow and sediment and the schematic hydrodynamics data (sinusoidal variations of water level and of the depth averaged velocities) described by Ross (1988), to the simulation of vertical concentration profiles in the Severn estuary (Kirby, 1986). A detailed description of the simulation is found in Costa (1994). In figure 4.16 the initial condition, the measured profiles (two profiles, measured at five minute intervals for

each case) and the results of the model simulation are presented. Good agreeement is found between the simulated profiles and the measured data, particularly if it is considered that the latter are also influenced by horizontal phenomena which cannot be reproduced by the vertical model.

4.4.4 The Horizontal Diffusion Steps

The two horizontal diffusion modules were tested against the same one-dimensional analytical solution, since both are one-dimensional versions of the original Barakat and Clark numerical scheme applied to successive rows or columns in the x^*,σ or y^*,σ planes.

The instantaneous point source release of a given mass (per unit area) m at $x_{01}^*=L/2$ of a laterally and vertically well mixed channel with no flow, closed at both ends, was simulated. For the computations $L=8m$, $m=1000\ g/m^2$ and a constant longitudinal diffusion coefficient $\varepsilon_x=0.25\ m^2/s$ were arbitrarily chosen.

In order to simulate zero diffusion fluxes at the closed ends of the channel four virtual sources of the same magnitude were placed at $x_{02}^*=-3L/2$, $x_{03}^*=-L/2$, $x_{04}^*=3L/2$ and $x_{05}^*=5L/2$ in order to compute the analytical solution as (Harleman, 1988):

$$C(x^*,t^*)=\sum_{i=1}^{5}\frac{m_i}{(4\pi t^*)^{1/2}\varepsilon_x^{1/2}}\exp-\left[\frac{(x^*-x^*_{0_i})^2}{4\pi\varepsilon_x}\right] \qquad (4.49)$$

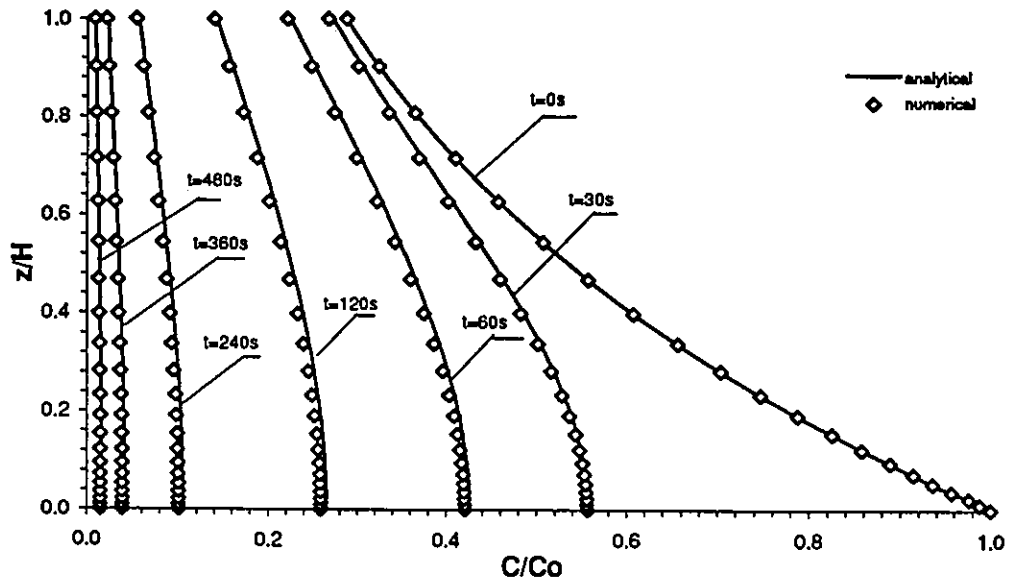

Figure 4.14 Analytical solution and computed concentrations for deposition test case.

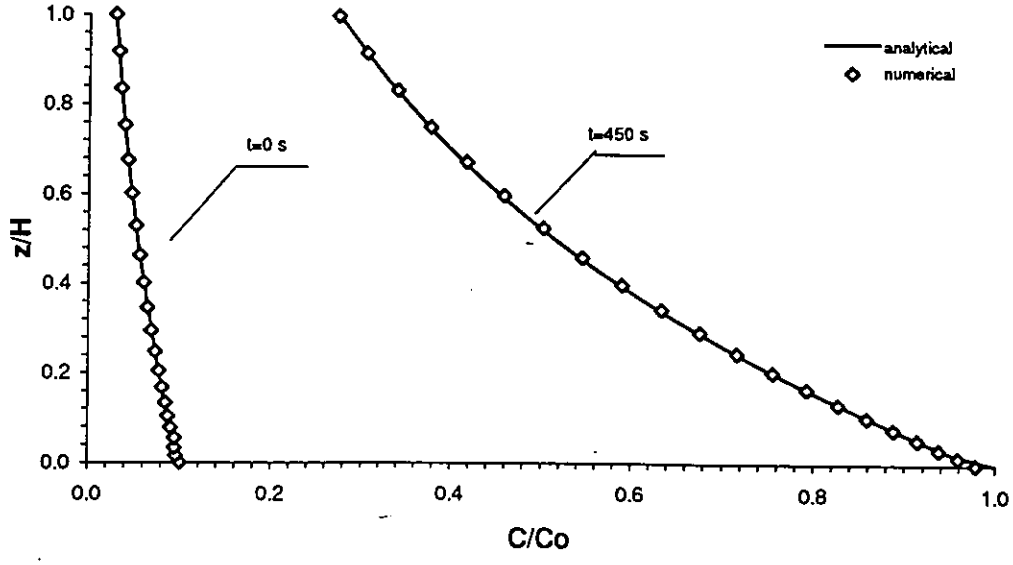

Figure 4.15 Analytical solution and computed concentrations for erosion test case.

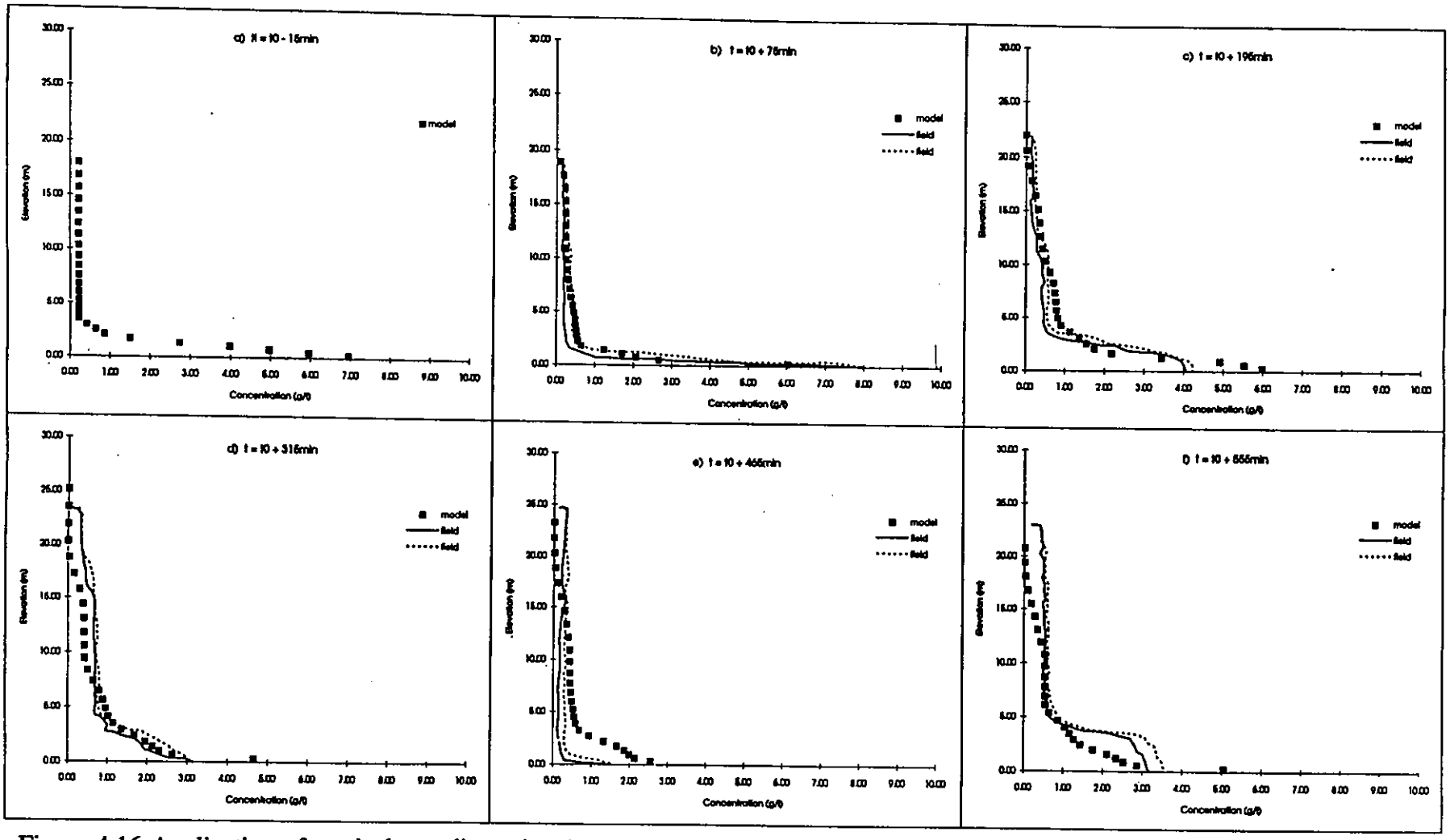

Figure 4.16 Application of vertical one-dimensional model to the simulation of concentration profile evolution in the Severn Estuary (t_0 is low water slack): initial condition (a), field data and computed profiles (b) to (f).

The horizontal diffusion modules were run taking the computed analytical solution at ***t=1 s*** as the initial condition (figure 4.16) with time steps ***Δt=0.1 s*** and ***Δt=0.01 s***.

Plots of concentration as a function of position along the channel for times ***t=5 s***, ***t=10 s***, ***t=20 s*** and ***t=30 s*** (figures 4.17 to 4.20) show that the Barakat and Clark method is well suited to simulate diffusive phenomena, as computations carried out with both time steps closely agree with the time evolution of the analytical solution. As

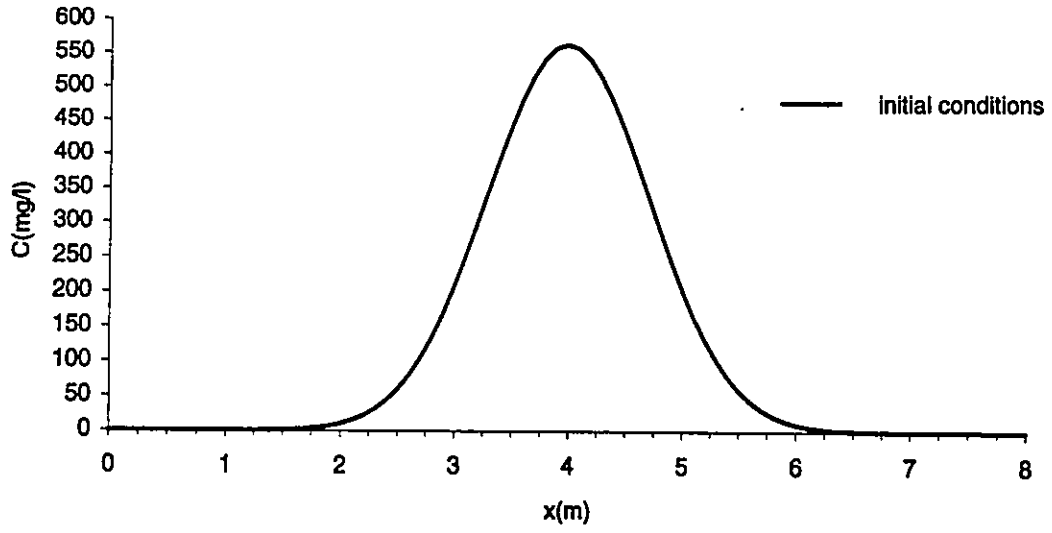

Figure 4.17 Initial condition for horizontal diffusion test case.

expected, better results are obtained with the smallest time step (***Δt=0.01 s***) and, in fact, such curves can hardly be distinguished from the analytical solution curves in figures 4.17 to 4.20.

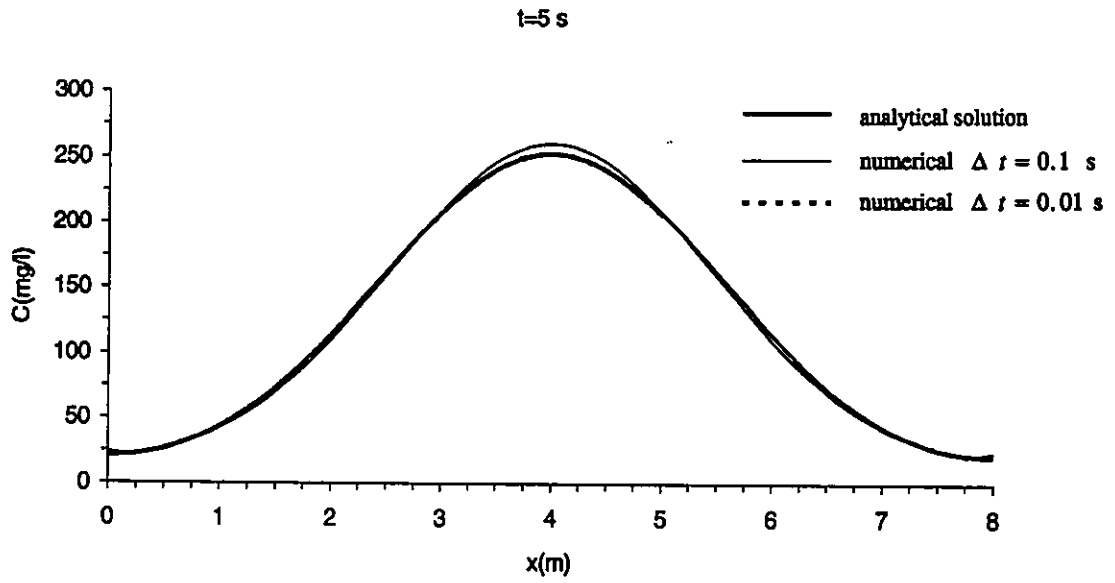

Figure 4.18 Analytical solution and computed concentrations for horizontal diffusion test case (*t=5 s*).

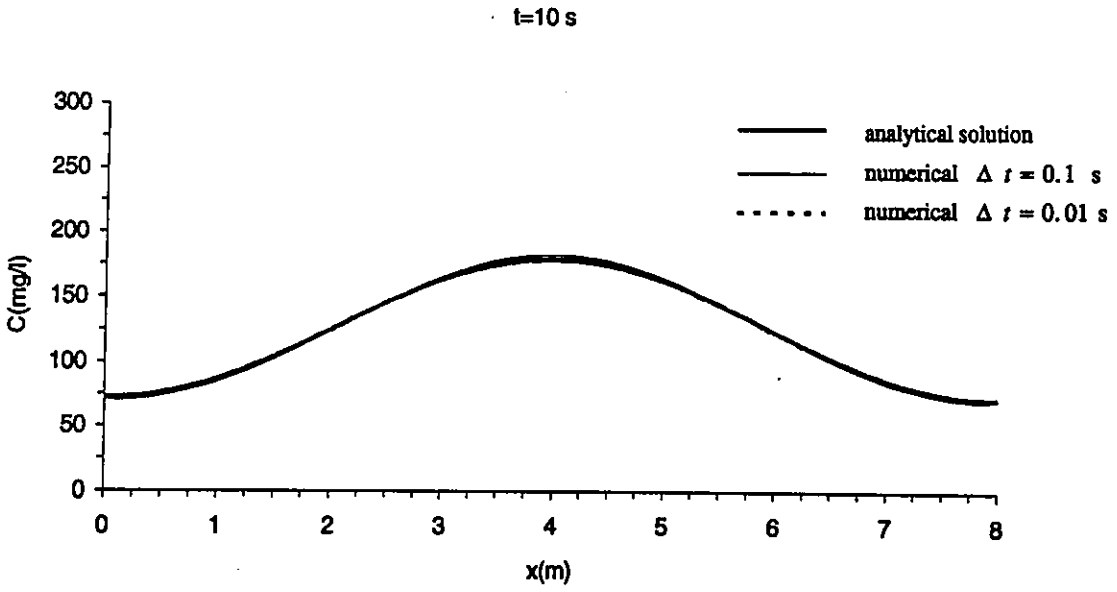

Figure 4.19 Analytical solution and computed concentrations for horizontal diffusion test case (*t=10 s*).

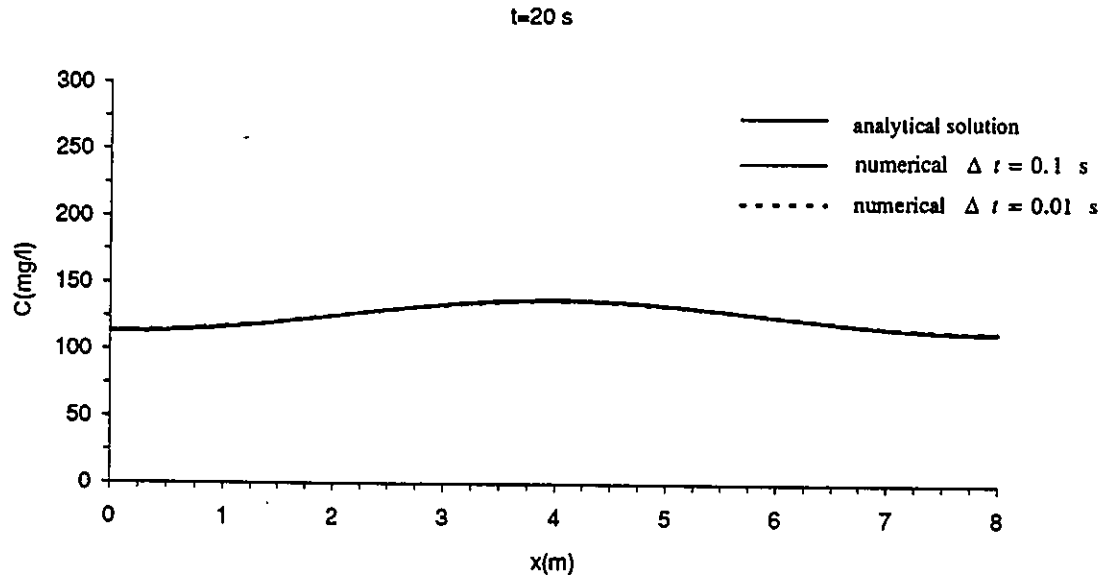

Figure 4.20 Analytical solution and computed concentration for horizontal diffusion test case (*t=20 s*).

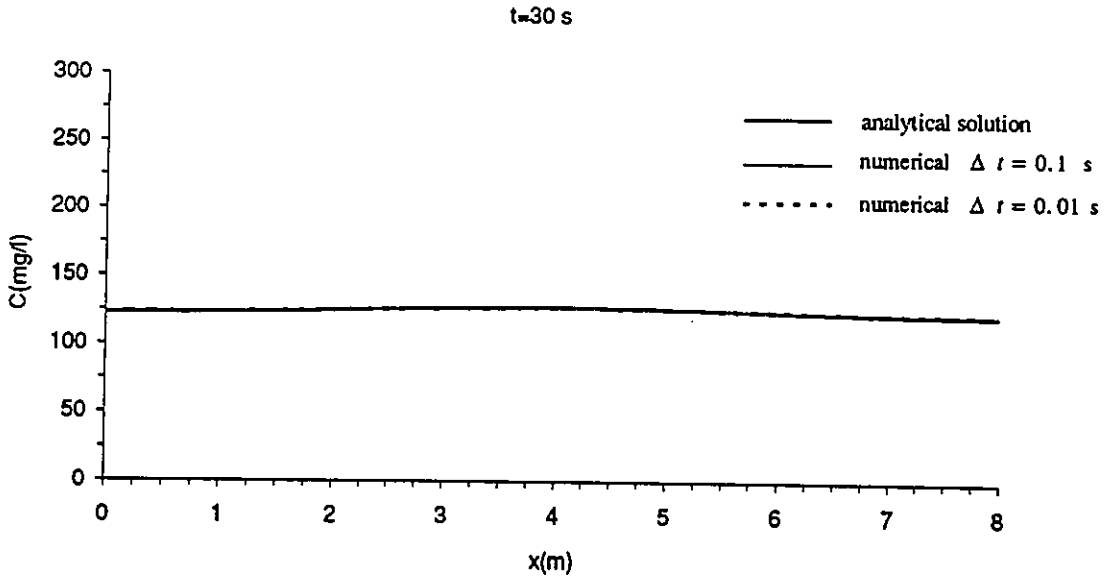

Figure 4.21 Analytical solution and computed concentration for horizontal diffusion test case (*t=30 s*).

4.5 Summary

In this chapter the development of a three-dimensional transport model for suspended cohesive sediment (SUSMUD3) in a computational domain was presented, using the formulation derived in Chapter 3. Time-splitting, the strategy adopted for numerically solving the transport equation was presented, together with the numerical methods used to solve each one of the transport components. Tests performed with the computational modules used in the model are described in detail and showed good agreement with the reference test cases. An application of model SUSMUD3 to an estuarine channel is presented in Chapter 5.

CHAPTER 5
THREE-DIMENSIONAL MODELLING OF FINE SUSPENDED SEDIMENT TRANSPORT IN THE MERSEY NARROWS

5.1 Introduction

In this chapter an application of the three-dimensional transport model for fine sediment described in Chapter 3 (SUSMUD3) is presented. The model was applied to the simulation of suspended fine sediment transport in the Mersey Narrows, in a winter spring tide situation, which, as noted by Halliwell and O'Connor (1974), produces ideal conditions for maximum movement of fine sediment in the estuary.

The Mersey estuary is one of the best studied estuaries in the world. A significant number of scientific papers have described its features and documented their evolution in more than one hundred years, as a result of both major civil engineering works in the estuary and of natural causes; such papers, even if published decades ago, provide valuable background information which does not exist for most estuarine systems. Furthermore, the Mersey estuary was chosen due to the availability of recent field and laboratory data and modelling results, most of which were promoted by the Mersey Barrage Company (MBC) within the framework of the feasibility studies for the construction of a tidal barrage in the estuary. The Narrows, in particular, was chosen as the simulation domain due to both its geometric regularity and to the fact that most of the available field data were collected in that region of the estuary.

In order to globally characterise the estuary, a brief description of the Mersey is presented in Section 5.2, based on the work of Cashin (1949), Price and Kendrick (1963), Agar and McDowell (1971), Bowden and Gilligan (1971) and Halliwell and O'Connor (1974). Data obtained by the same authors or compiled from earlier sources on the tide, flow, salt and sediment regimes of the Mersey and on the nature of the bed is also summarised and, despite the time elapsed until present, allows an useful overview, to be interpreted in the light of more recent studies. Section 5.3 contains recent information, obtained from reports either directly produced by MBC or its contractors, in particular, Hydraulics Research Ltd. (HR). Application of model SUSMUD3 to the Mersey Narrows, using as input the process modeling parameters previously described and, whenever necessary, three dimensional hydrodynamics and fine sediment modelling results by HR, is described in Section 5.4. Finally, the conclusions resulting from the application of model SUSMUD3 are summarised in Section 5.5.

5.2 A Brief Description of the Mersey Estuary

The estuary of the River Mersey is located on the NW coast of England, between the estuaries of the Ribble and of the Dee and separates Lancashire, to the North, from the Wirral peninsula in Cheshire, to the South (figure 5.1). The most important urban centre on its banks, Liverpool, developed into a major city mainly during the industrial revolution period, due to the proximity of its port facilities to the most important inland industrial areas, located around Manchester, and to to its convenience as a point

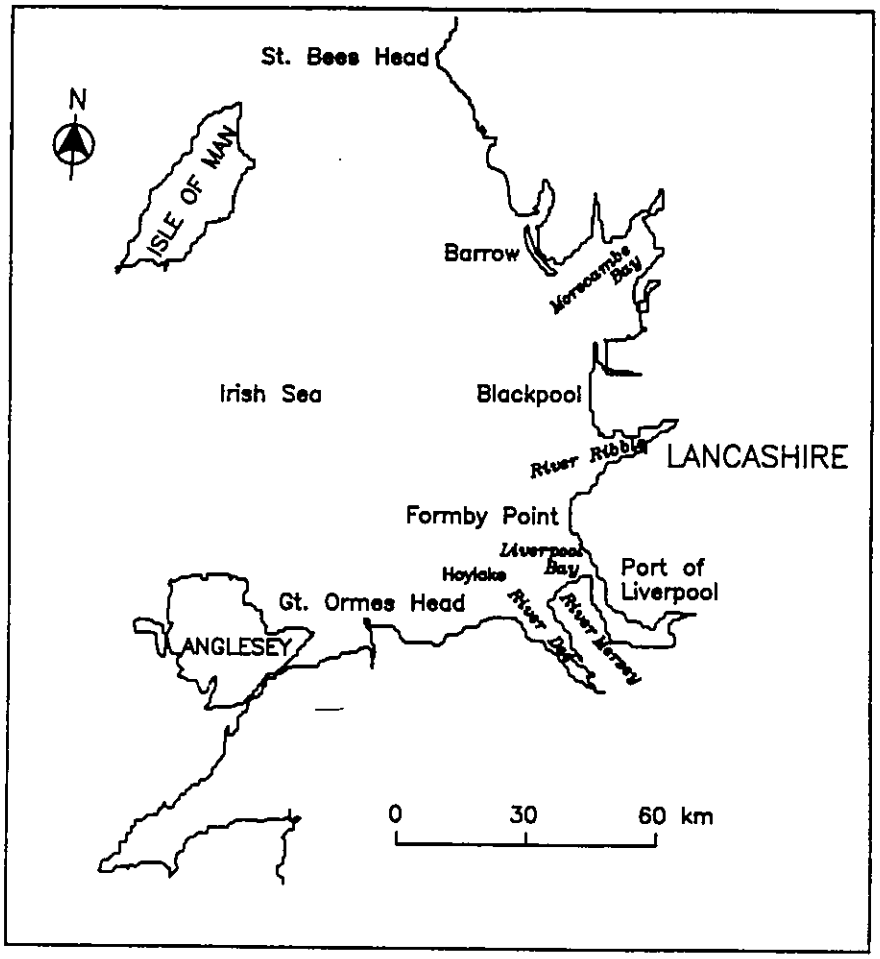

Figure 5.1 Location map of the Mersey Estuary (adapted from Agar and McDowell, 1971).

of departure for trans-Atlantic travel. Success of the Port of Liverpool, relative to other ports, was due to the large tidal range at its mouth which ensured enough water depth at high water, while also producing strong scouring currents in the main navigation channels. The large tidal range, however, also forced the construction of an expensive system of locks and basins for access to the main docks. Besides Liverpool other major dock systems have developed in the estuary, at Birkenhead, Garston, Bromborough and Manchester (through the Manchester Ship Canal, connecting

Eastham to Salford) while smaller ports are also found at Runcorn, Widnes and Warrington (figure 5.3).

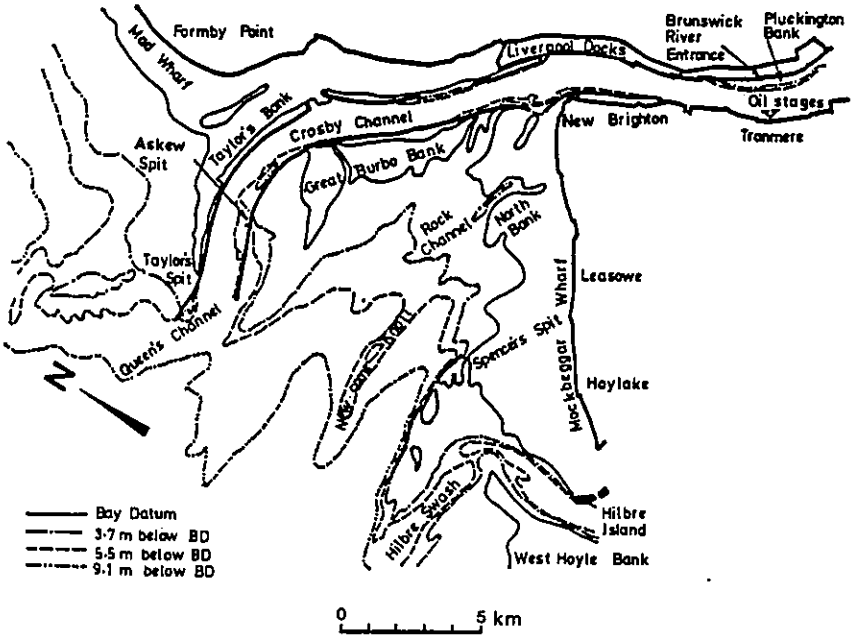

Figure 5.2 Liverpool Bay map (1969) showing the training banks (adapted from Agar and McDowell, 1971).

The Mersey estuary drains into Liverpool Bay (also known as the Lower or Outer Estuary) which is a shallow zone of about 180 km^2, containing large areas of sand banks which are exposed at low water (figure 5.2). Ships bound for the port facilities in the estuary cross the bay through the main navigation channel (comprising Queens Channel and Crosby Channel, connected by a bend at Askew Spit). The channel was initially maintained by dredging but, due to lateral channel movement, it was eventually trained, between 1909-1957, through tipped stone walls over a distance of about 14.5 km. Construction of training banks, while reducing the amount of dredging necessary in the channel itself, was found to produce major changes in the

hydrodynamic patterns of the Bay, which were responsible for bringing more sand to the mouth of the Mersey and, ultimately, due to the estuary's gravitational circulation, to the Upper Basin.

The Mersey Narrows and the Upper Basin form the Upper Estuary (figure 5.3). The Narrows is a straight deep channel, connecting Liverpool Bay to the Upper Basin, approximately 9.5 km long, from the mouth (New Brighton) to Dingle. It is about 1500 m wide at New Brighton, decreasing to a width of about 750 m at its narrowest part (Liverpool Landing Stage), which has depths of up to 18 m at low water spring tides. The channel's width increases again to about 2150 m at Dingle. The Upper Basin is a large, shallow, tidal basin, about 90 km^2 in area, which dries out almost entirely at low water. It has a length of about 42 km from Dingle to Howley weir, Warrington, and a maximum width of 5500 m. The low water channel in the Upper Basin meanders through areas of sand and mud, constantly changing its course, before flowing into either Garston or Eastham channels, which, together with the Middle Deep channel form the channel system of the lower zone. The Middle Deep is a flood channel while Garston and Eastham are ebb channels, a feature which still influences net flow distribution in some landward sections of the Narrows. The capacity of the Upper Mersey Estuary, between Rock Light and Runcorn, defined as the volume between the bed of the estuary and the highest level reached at all points by a particular high spring tide, decreased about 10% from 1861 to 1961, as a result of changes in erosion/deposition patterns arising from the construction of works and dredging.

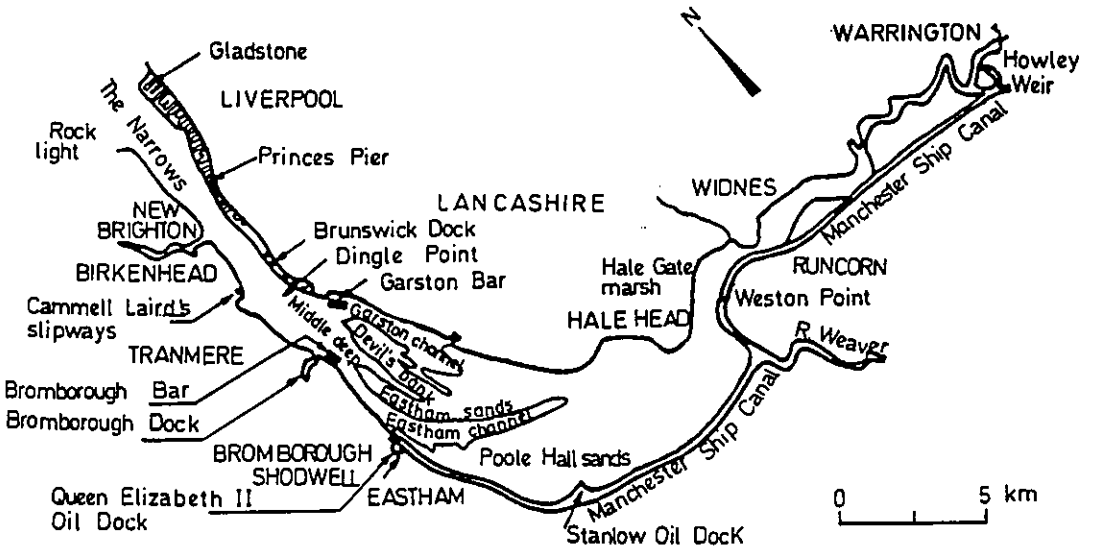

Figure 5.3 Upper Estuary of the Mersey (adapted from Price and Kendrick, 1963).

The estimated daily input of fresh water to the Mersey estuary from rivers and rainfall (carried either by sewers or directly falling over the estuary and the Manchester Ship Canal) is estimated at about 4.6×10^6 m^3, of which 52.1% correspond to the river Mersey and to its tributaries (Water Pollution Research Laboratory, 1938, cited by Price and Kendrick, 1963). More recent data indicates that freshwater discharges averaged over periods of 10 days vary between 24 m^3/s to 250 m^3/s with a median of about 80 m^3/s (Bowden and Gilligan, 1971).

Water levels in the Mersey estuary are usually measured relative to Liverpool Bay Datum (LBD) which is 4.43 m below Ordnance Datum (Newlyn) and approximately corresponds to the low water level of a 9 m tide at Liverpool. The mean water level in the estuary is 4.67 m above LBD. Tidal heights and ranges in the Mersey are given in table 5.1, while a diagram of tides at Princes Pier, Liverpool, is shown in figure 5.4.

Table 5.1
Tidal Heights and Ranges in the Mersey Estuary
Levels in m above LBD - Adapted from Price and Kendrick (1963)

Section	Mean Springs			Mean			Mean Neaps		
	HW	LW	Range	HW	LW	Range	HW	LW	Range
Gladstone Dock	8.75	0.55	8.20	7.83	1.46	6.37	6.98	2.35	4.63
Princes Pier	8.84	0.46	8.38	7.92	1.40	6.52	7.01	2.32	4.69
Eastham	9.14	0.27	8.87	8.17	1.31	6.86	7.28	2.26	5.02
Widnes	9.54	5.03	4.51	8.50	4.88	3.62	7.50	4.75	2.75
Fidler's Ferry	9.78	6.92	2.86	8.69	6.86	1.83	7.59	6.80	0.79
Warrington	10.03	7.92*	2.11*	8.84	7.65*	1.19*	7.53	7.35*	0.18*

* not absolutely reliable

The volumes of water entering and leaving the Upper Estuary in each tide (tidal prisms) are 535×10^6 m^3 at spring tides and 190×10^6 m^3 at neap tides (Cashin, 1949). Halliwell and O'Connor (1974) also indicate a value of similar magnitude, of 430×10^6 m^3, for the tidal prism of a spring tide having a high water level of 8.53 m at the Gladstone section.

In the Mersey Narrows, the estuary's gravitational circulation is well developed (Price and Kendrick, 1963) with a residual landward current in the lower layers (transporting sand, near the bed) and a residual seaward current in the upper layers. Nodal points, defined as those for which there is no net drift of water near the bed, usually coincide with bars, where mobile bed material tends to deposit. Three bars are found in the Mersey, namely at the seaward ends of the Garston and Eastham channels and at the end of the trained channel in Liverpool Bay. A further bar exists at the mouth of the Narrows (New Brigton bar) due to the interaction between the residual plan circulation generated by the trained channel and the gravitational circulation in the vicinity of the mouth.

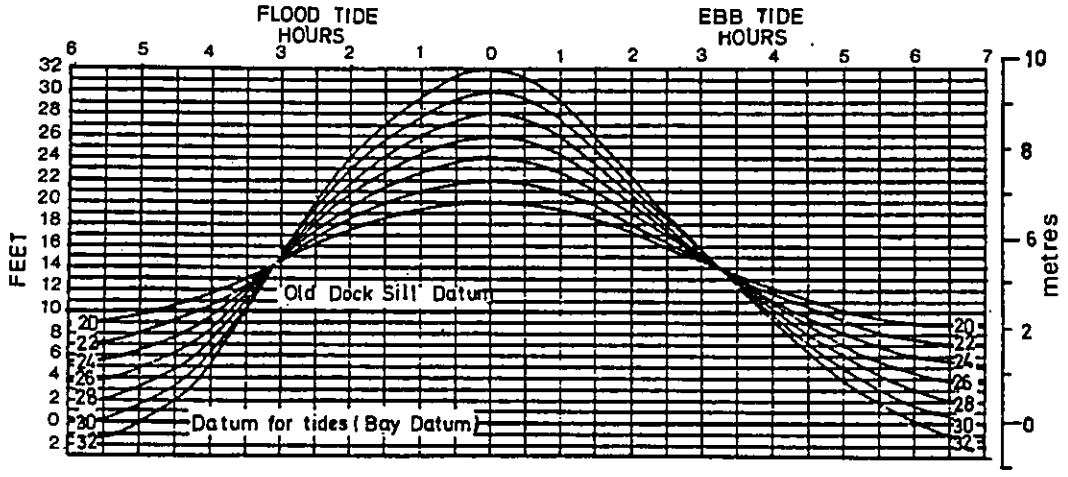

Figure 5.4 Diagram of tides at Princes Pier, Liverpool (adapted from Cashin, 1949). Note: figures in the curves are tidal ranges in feet.

The surface salinity distribution measured almost simultaneously along the estuary is shown in figure 5.5. Tidally-averaged salinity differences between the bottom and the surface are usually small and measured values at the Egremont section of the Narrows on 9 tides were observed to vary between 0.36 and 4.14 g/l, with an average of 1.8

g/l (Bowden and Gilligan, 1971). Salinity differences of 2 g/l between the bottom and the surface are also reported by Price and Kendrick (1963). Conditions in the Narrows are considered as fairly representative of those in the central portion of a partially-mixed coastal plain estuary (Bowden and Gilligan, 1971).

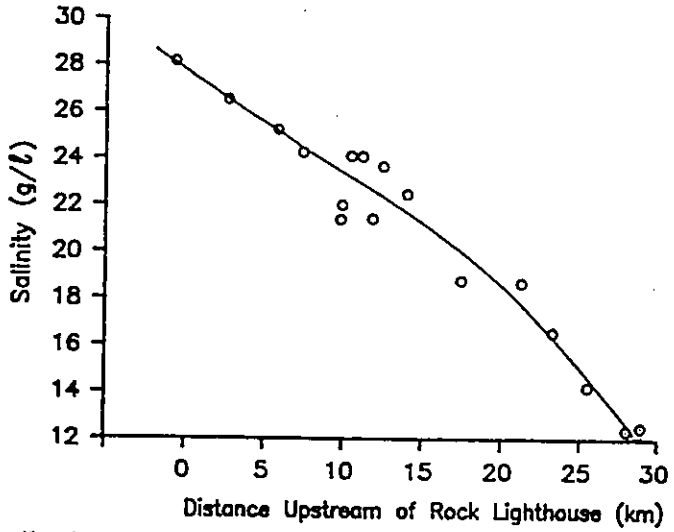

Figure 5.5 Distribution of surface salinity along the Mersey estuary, 6 hours after High Water (adapted from Bowden and Gilligan, 1971).

A concise description of the nature of the bed and the maximum tidal velocities in Liverpool Bay and the Upper Estuary is shown in figures 5.6 and 5.7, respectively, (Water Pollution Research Laboratory, 1938, cited by Cashin, 1949). Detailed information on the geology and sediment dynamics of the eastern Irish Sea and of Liverpool Bay and the Mersey estuary can be found in Sly (1966).

It can be seen from figures 5.6 and 5.7 that, at the time such figures were produced, muddy or clayey sediment occurred over small areas of Liverpool Bay and, more extensively, in the Upper Basin, being almost entirely absent from the Narrows. According to Halliwell and O'Connor (1974) the majority of the silt in suspension is

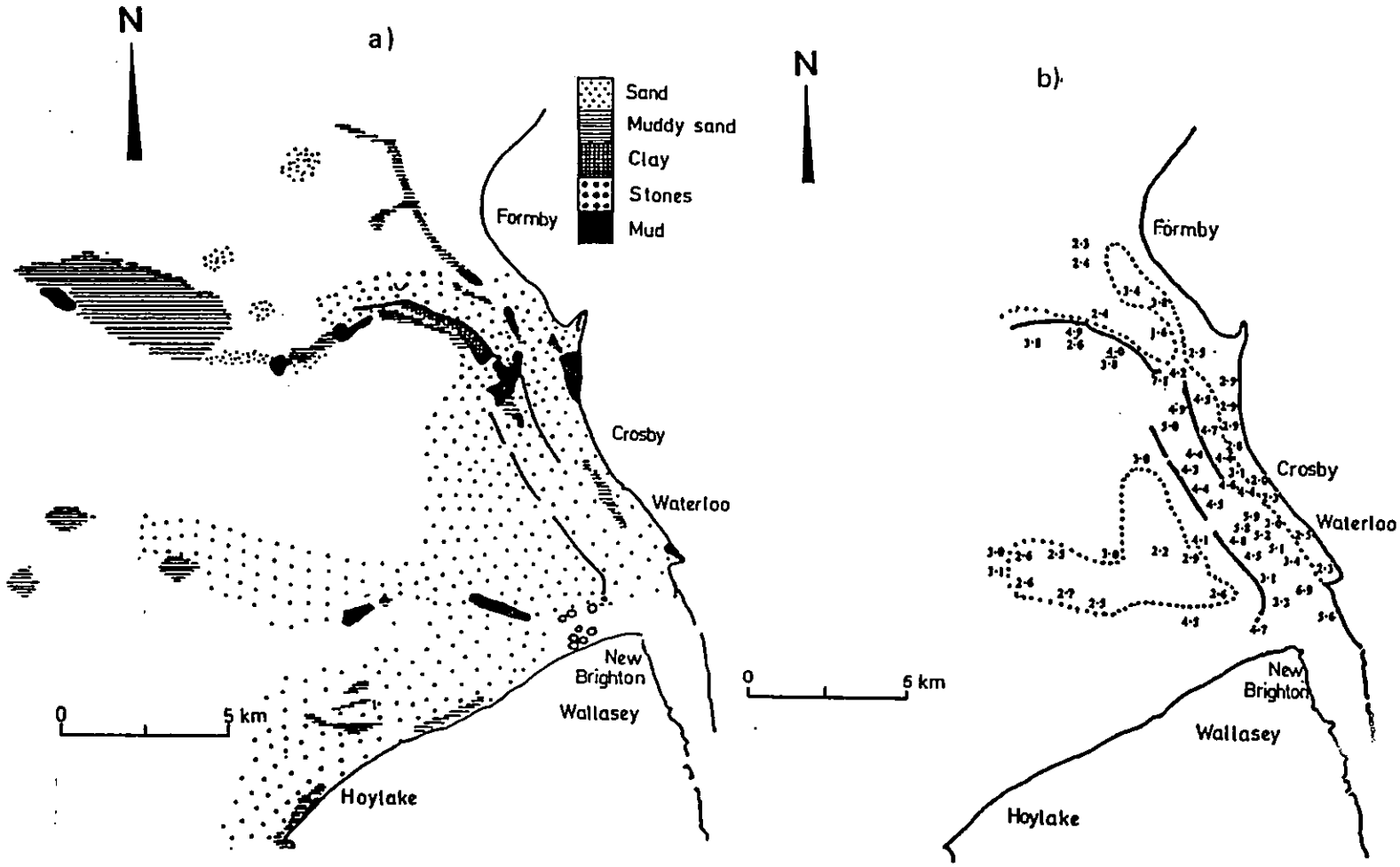

Figure 5.6 Nature of the bed (a) and maximum stream velocities in ft/sec (b) in Liverpool Bay (adapted from Cashin, 1949).

picked up from the area around the Middle Deeps and the Tranmere/Brunswick section and is spread out in a tongue by the ebb tide along the Narrows, towards Rock Light/Gladstone and the Crosby Channel. Silt is brought into suspension again by the flood tide and carried back into the Upper Estuary and, therefore, follows an oscillating pattern, some of it settling at slack water near dock entrances or shoaling the docks, as a result of water exchanges with the estuary during levelling periods. This pattern of fine sediment dynamics is also supported by data of the Water Pollution Research Laboratory (1938), who confirmed, through physico-chemical analyses, that suspended sediment and material forming the mud banks in the Upper Basin were of the same nature.

The long-term sources for new mud entering the Upper Estuary were also investigated by the Water Pollution Research Laboratory (1938). Although river and sewage discharges and erosion of shores and marshes in the estuary and in Liverpool Bay might be expected to contribute to sediment inflow into the estuary, analyses of sediment composition and of the volumes available from such sources indicate that their importance should be minor. The main source of new mud in the Mersey was found to be the bed of Liverpool Bay and of the Irish Sea outside it. This was confirmed by the similar compositions of the mud fractions deposited in the Irish Sea, in the Bay and in the Upper Estuary. Mud is widespread on the west coast of Britain and covers large areas of the bed of the Irish Sea. A tongue of this mud appears to connect the Mersey estuary to a large area of mud extending northwards in shallow water to the Solway (Water Pollution Research Laboratory, 1938).

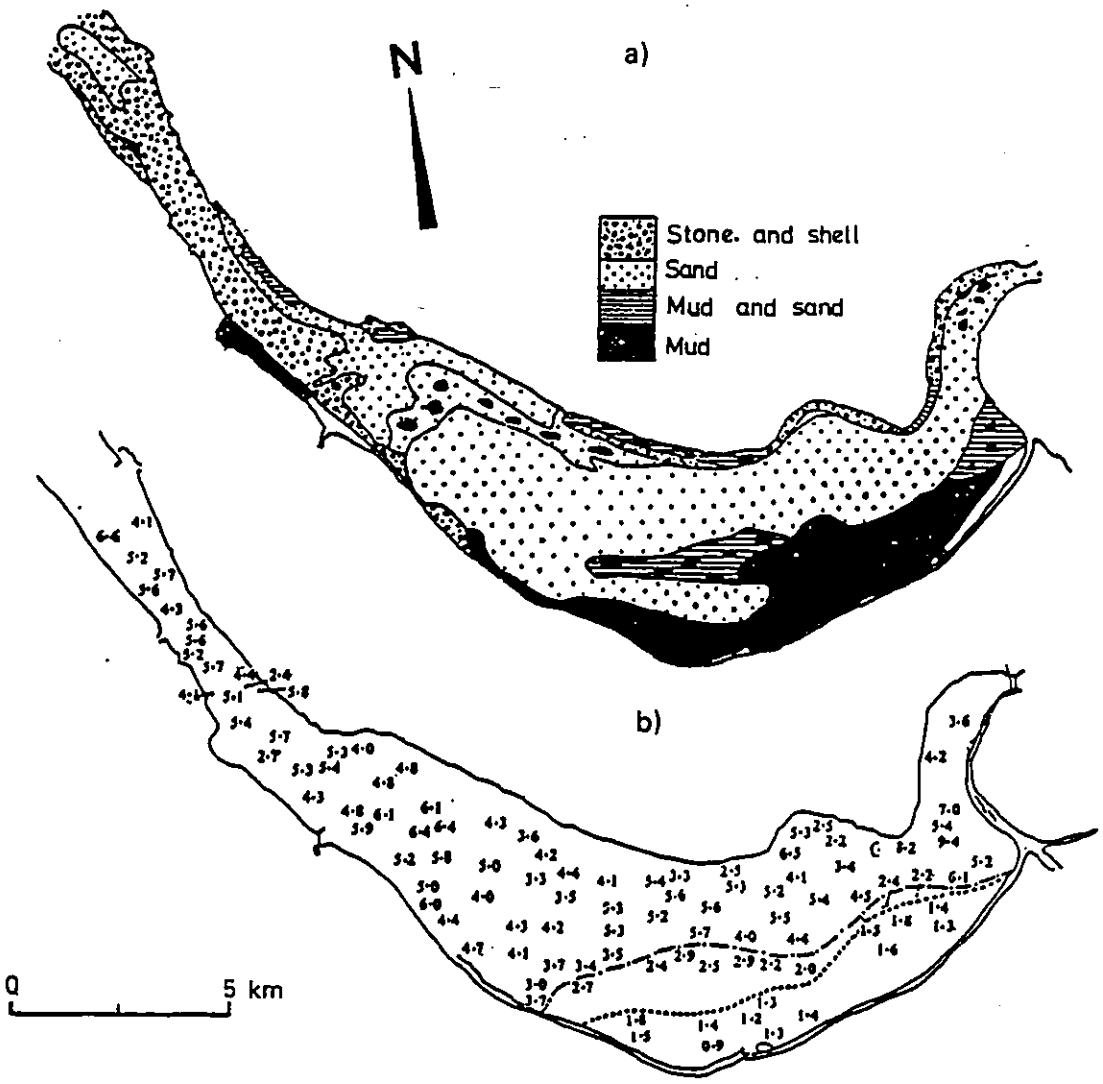

Figure 5.7 Nature of the bed (a) and maximum stream velocities in ft/s (b) in the Upper Estuary (adapted from Cashin, 1949).

O'Connor (1987) studied the long term trends in the evolution of the Mersey and confirmed that the estuary is currently filling with sediment of seaward origin. Data compiled by the same author indicates that every year in the late 1960's, on average, some 6×10^6 m^3 of silt and clay and 1.9×10^6 m^3 of sand entered the estuary from the sea, of which only 1.3×10^6 m^3 contributed to the loss of capacity of the Upper Estuary, the rest being recirculated. Since only about 10% of the sediment retained in

the Upper Estuary correspond to the silt/clay fractions and the Narrows are generally clear of deposits (O'Connor, 1987) it can be expected that most fine sediment entering the estuary will join the mass of sediment already following the oscillatory pattern described by Halliwell and O'Connor(1974) in the Narrows and can be expected to reduce as dredging activities reduce.

5.3 Background Data For Model Application

In order to apply model SUSMUD3 to the simulation of suspended fine sediment transport in the Mersey Narrows it is necessary to summarise the field and laboratory data produced in recent times and, in particular, since 1980, which is of direct interest for mud process description and for comparison with model output. It should be mentioned, however, that recent data sources are generally consistent with the global description presented in the previous section.

A first aspect to be studied is related to the dynamics of sediment in the estuary and the nature of the bottom in the Mersey Narrows. Studies by Hydraulics Research on the hydraulic feasibility of the proposed Mersey barrage (HR, 1988) indicated, based on interpretation of recent data, that "the quantity of sand entering the estuary at present time (1988) was insignificant" and that emphasis should be on the examination of the movements of silt. The same study recognised a quasi-equilibrium between the silt flux leaving the estuary and that (slightly higher) entering it. Furthermore, it is mentioned that "there is little evidence of silt in the bed of the main channels" and

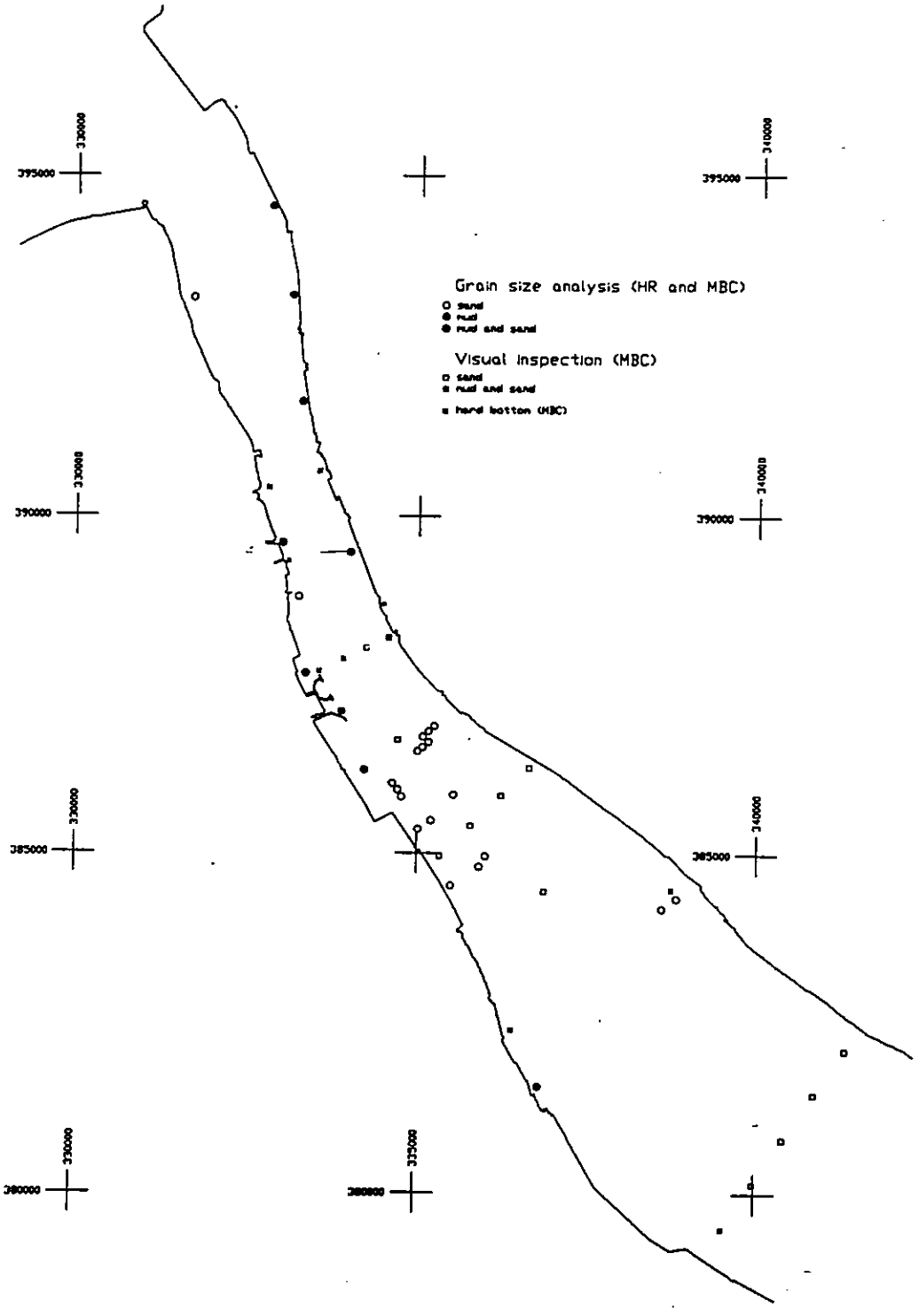

Figure 5.8 Nature of the bottom in the Mersey Narrows based on recent data collected by HR and MBC.

that "the small amount of deposition is confined to those areas of inter-tidal bank just covered by the respective tides".

Programmes of grab sampling were undertaken by HR in October 1989 (HR, 1989a; HR, 1990b) and by MBC in the Autumn of 1990 (Wilks, 1991). Samples collected by HR were characterised through grain size analysis while samples collected by MBC were characterised through visual inspection or grain size analysis. The nature of the bed in the Narrows, based on the information resulting from the studies by HR and MBC is presented in figure 5.8. It can be concluded from the figure that mud is only found in restricted areas in the banks (either in consolidated or in unconsolidated condition) while most of the bottom is sandy. Characterisation of the nature of the bottom as hard bottom may be interpreted as indicating either rock or very consolidated mud. These studies are in agreement with the conclusions of previous authors who describe the bed of the Narrows as, generally, sandy. Therefore the assumption can be made, for the Narrows area, that fine sediment moving landward and seaward, following the oscillatory pattern described by Halliwell and O'Connor (1974), does only briefly deposit around slack water before being re-entrained again during the accelerating stages of the tidal cycle. Simple erosion/deposition formulations, without explicit consideration of consolidation phenomena, as typically used to describe low concentration environments, should, consequently, be an adequate modelling choice and were adopted in the application of SUSMUD3 to the Narrows.

Properties of Mersey sediments are described by HR (1989b). Sediment samples from Egremont (in the Wirral, approximately opposite Victoria Tower in Liverpool), Runcorn and Eastham were collected and tested in the laboratory. The first two sampling positions were located in muddy patches within predominantly sandy areas and sediment collected there cannot be considered as representative of Mersey muds, as confirmed by the tests. Eastham sediment showed about 80% by weight of fine sediment (silt and clay) and was considered by HR as representative of recently deposited Mersey mud. Erosion tests were conducted with consolidated (1.7 to 8 days) Eastham mud in HR's annular flume (in which only the lid rotates). Tests produced a typical value for the erosion parameter of equation 2.35, taken as independent of depth, α_e***=0.0005 $m^{-1}s$***. Parameters for the shear strength versus dry density relationship of equation 2.44 were found to be ζ_1***=0.013*** and δ_1***=0.7*** (see figure 2.8). The critical shear stress for erosion is determined from this relationship as ***0.2 Pa***, by assuming a bed formation dry density of ***50 kgm^{-3}*** (see also HR, 1990a). The above values for the erosion parameter and for the critical shear stress for erosion were adopted in the application of SUSMUD3 to the Narrows.

A value for the critical shear stress for deposition was obtained by HR (1990a) as τ_{cd}***=0.08 Pa*** in the process of validation of a deposition algorithm using field data from Eastham. A slightly higher τ_{cd}***=0.1 Pa*** was used as input for SUSMUD3. The median settling velocity formulation used in the same study was in the form $W_{s,50}$***= 0.005 C*** and is plotted, for comparison purposes only, as a dotted line in figure 5.9.

Median settling velocities of silt in the flocculation settling range, using Owen tube data, were also obtained during the 1989 field measurements (HR, 1990b) and are plotted in figure 5.9. Although data points in the hindered settling range are not available for the Mersey it can be assumed that such data from the Severn (Thorn, 1981) are generally representative of conditions found in estuaries of the west coast of the UK (see figure 5.9). Assuming C_2=*0.8 g/l*, curve fitting produces k_1=1.557×10^{-2}, n_1= *2.087*, W_{s0}=$1.018\times10^{-2} ms^{-1}$ and, for n_2=*5.0*, k_2= 1.006×10^{-2}, in equations 2.8 and 2.9. Settling velocity curves computed with those parameters are also plotted in figure 5.9. Finally assuming C_1=*0.05 g/l*, and that the settling velocity in the free settling range is constant and equal to that computed for the flocculation range for the same concentration one obtains W_{s1}=$3.0\times10^{-5} ms^{-1}$. All these settling parameters were used in the application of SUSMUD3 to the Narrows.

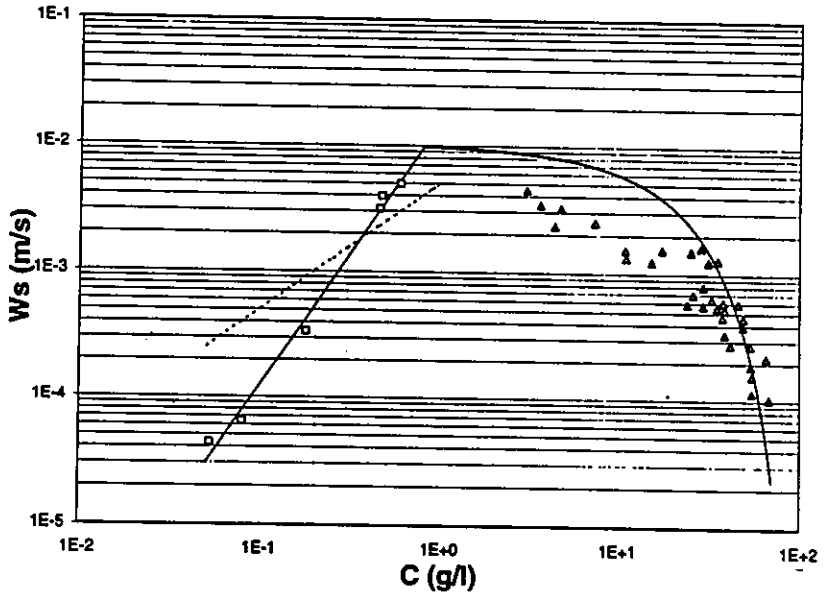

Figure 5.9 Settling velocity curves for the flocculation and hindered settling ranges based on data by HR (1990b) and Thorn (1981). See text and figure 2.5 for parameter definition.

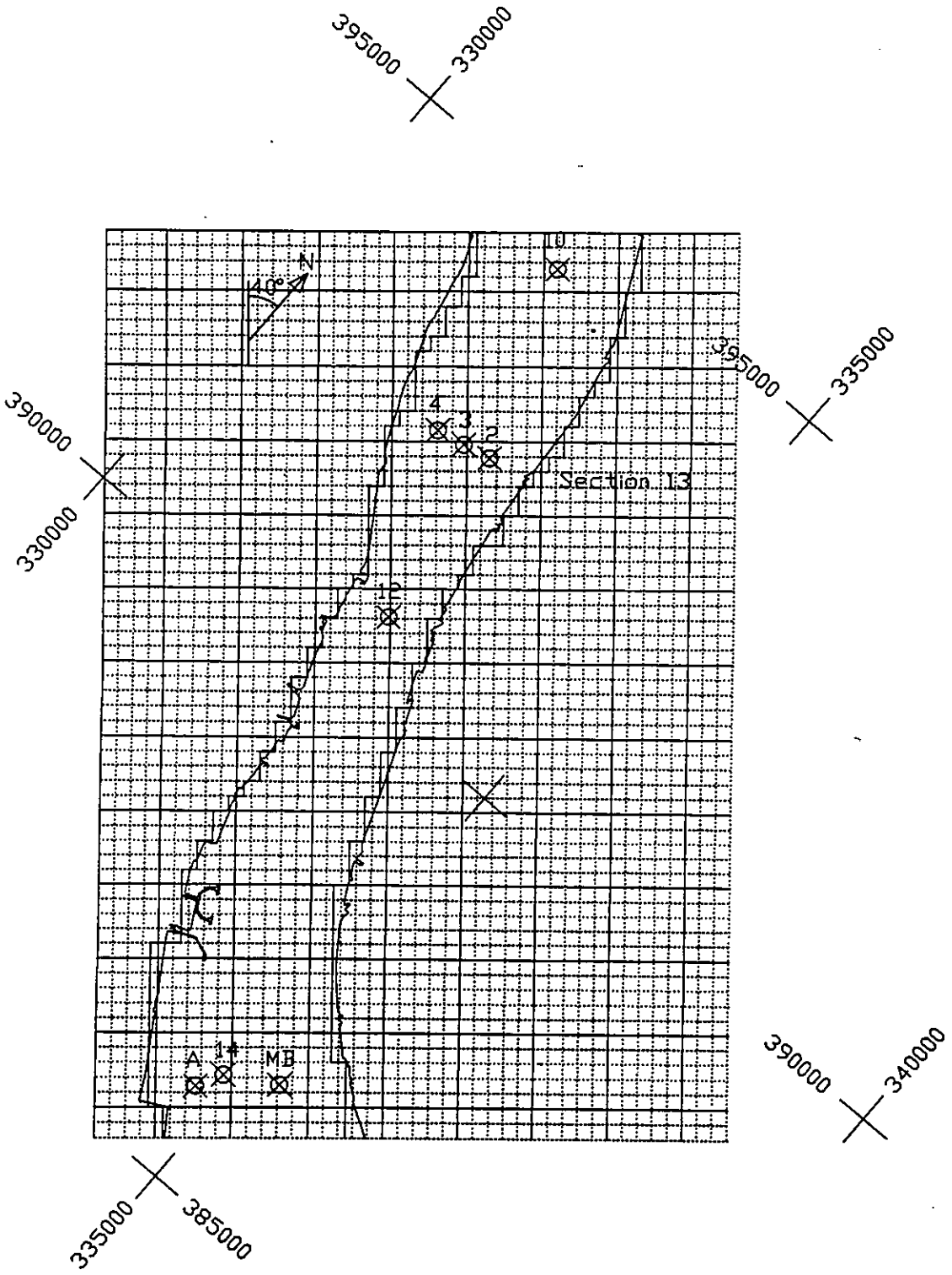

Figure 5.10 Plan view of the grid used by model SUSMUD3 and measurement positions for the field studies described in the text.

Numerous field measurement campaigns have been carried out in the Mersey by HR and MBC during studies for the Water Research Centre (WRC) and the successive stages of the feasibility studies for the construction of the Mersey Tidal Barrage. Some of those studies have produced data on sediment concentrations under a variety of conditions but since, as mentioned before, spring tides are considered to produce the best conditions for maximum sediment transport, measurements made in intermediate or neap tide conditions will not be considered in the present work. Furthermore, since model SUSMUD3 is three-dimensional, it is considered that data allowing the description of the vertical structure of the concentration field is the most adequate and, therefore, such data will be preferred to results presented in depth or section-averaged form. Measurement positions corresponding to the field studies described below are shown in figure 5.10.

Suspended solids concentrations were measured at positions 2, 3 and 4 of section 13 in the Narrows (in the Egremont zone). Concentrations, at points located 1 m below the surface and 1 m above the bed in such positions, were obtained at regular intervals during several tidal cycles. Data measured in intermediate and spring tides in March, 1982, September, 1982 and September 1983 is described in HR (1982a), HR (1982b) and HR (1983), respectively, and plotted in figures 5.38 to 5.43.

Suspended sediment concentration measurements at three positions located near the proposed barrage line were carried out in 1991 but only one position (Station A) was occupied during a spring tide (HR, 1991). Nevertheless a large number of discretely

sampled concentration profiles (divided into several size classes) were obtained at Station A during a full tidal cycle (see figures 5.47 to 5.49 for depth-normalised plots of the fine fraction, of size less than 63 μm). Data obtained during the campaign indicated that the flood and ebb transports of both coarse and fine sediment are finely balanced and very sensitive to the tidal range. Furthermore the sediment in movement across the barrage line during neap tides (the only ones for which more than one position was measured) was predominantly fine. These data confirm, once more, the conclusions of Halliwell and O'Connor (1974).

Vertical profiles of salinity, temperature and turbidity were measured, through rapid drop profiling, at seven positions during a spring tide on 23 November 1991 (HR, 1992a). Three of the stations measured, Points 10, 12 and 14, were located in the Narrows, at the centre of sections located at the mouth, between Liverpool and Birkenhead and at Barrage Line 3, respectively. The depth-normalised continuous profiles obtained during these studies are plotted in figures 5.44 to 5.46.

Continuous point monitoring of silt concentrations was also carried out between June 1990 and May 1992 in shore based stations at Prince's Pier, Eastham and Runcorn and, later, at Garston, at depths 0.6 m from the bottom. In such stations the silt transducers were attached to large concrete blocks, which were suspected of significantly influencing the recorded suspended concentrations (Carter, 1992). An environmental monitoring buoy (MB in figure 5.10) equipped with a turbidity transducer, 1 m below the surface, was also deployed, causing less disturbance in the

values obtained, at the approximate line of the proposed barrage, 2100 m east of the Dingle navigation buoy. A curve resulting from averaging the concentrations measured during spring tides (in ppm Formazin, assumed equivalent to ppm silt) was produced (Carter, 1992) and is presented in figure 5.50.

5.4 Model Application

Model SUSMUD3 was run for the tidal conditions used by HR in their 3D mathematical modelling studies of tidal flows and sedimentation in the Mersey (HR, 1992b) which had a tidal range of 8.4 m at Princes Pier and is comparable, in terms of levels, to the spring tide of July 23, 1990. Ebb and flood durations were 391 and 354 minutes, respectively. SUSMUD3 was run in a non-interactive way, i.e. the computed concentration field did not influence the velocity field during its calculation, a reasonable assumption for low to intermediate concentration environments. The model was therefore run using the 3D (by layers) horizontal velocity (i.e. depth averaged horizontal velocities in each layer) and bottom shear stress fields, previously produced by model TIDEFLOW3D from HR, and boundary conditions (in terms of concentrations), at the appropriate inflow sections, produced by the same model.

Calibration data for TIDEFLOW3D in terms of tidal levels, velocities, residual velocities and salinities is found in HR (1992b) and was considered by HR to be satisfactory (see, for example, figures 5.13 to 5.15). This model, like the field

observations reported by Price and Kendrick (1963) and Bowden and Gilligan (1971), did not indicate a significant amount of vertical saline stratification and, therefore, salinity effects were only indirectly (i.e., through their effect on the velocity field computed by TIDEFLOW3D) taken into account by model SUSMUD3.

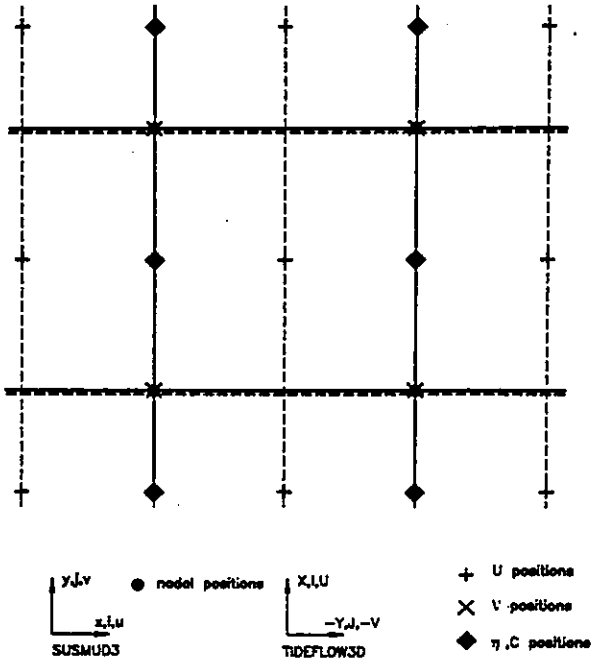

Figure 5.11 Grids used by models SUSMUD3 and TIDEFLOW3D.

The bathymetry of the finite difference grid used by SUSMUD3, with $\Delta x=\Delta y=150\ m$, was based on that provided by HR, which resulted from the bathymetry of a previous model having a 75 m grid size with corrections resulting from 1991 surveys. A view of the bathymetry of the Narrows, as used by HR's model which reproduced a much larger zone, from Liverpool Bay to Howley Weir, is presented in figure 5.12 For computational simplicity the tidal flats which represent a small area of the Narrows, were artificially taken as being at Chart Datum level (CD=-4.93 OD(N)) in the present application, while maintaining the total water discharge over the depth.

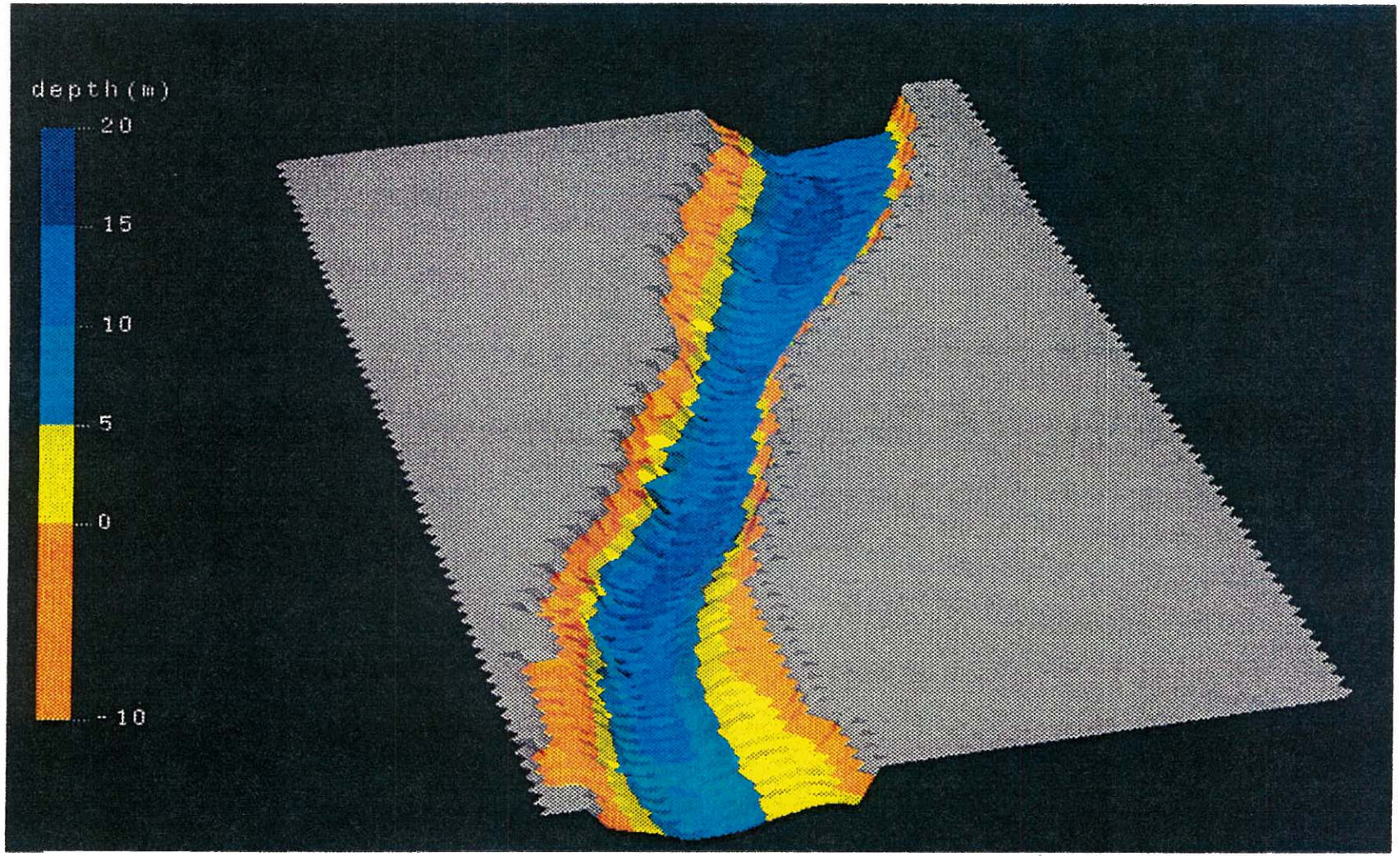

Figure 5.12 Channel depths in the Mersey Narrows relative to Chart Datum (CD = - 4.93 m OD(N)).

The grid used by model SUSMUD3 is node-based, (i.e. all values are defined at the same nodal positions) as opposed to the staggered grid used by HR's TIDEFLOW3D (see figure 5.11). Horizontally, the grid for SUSMUD3 was built on the positions

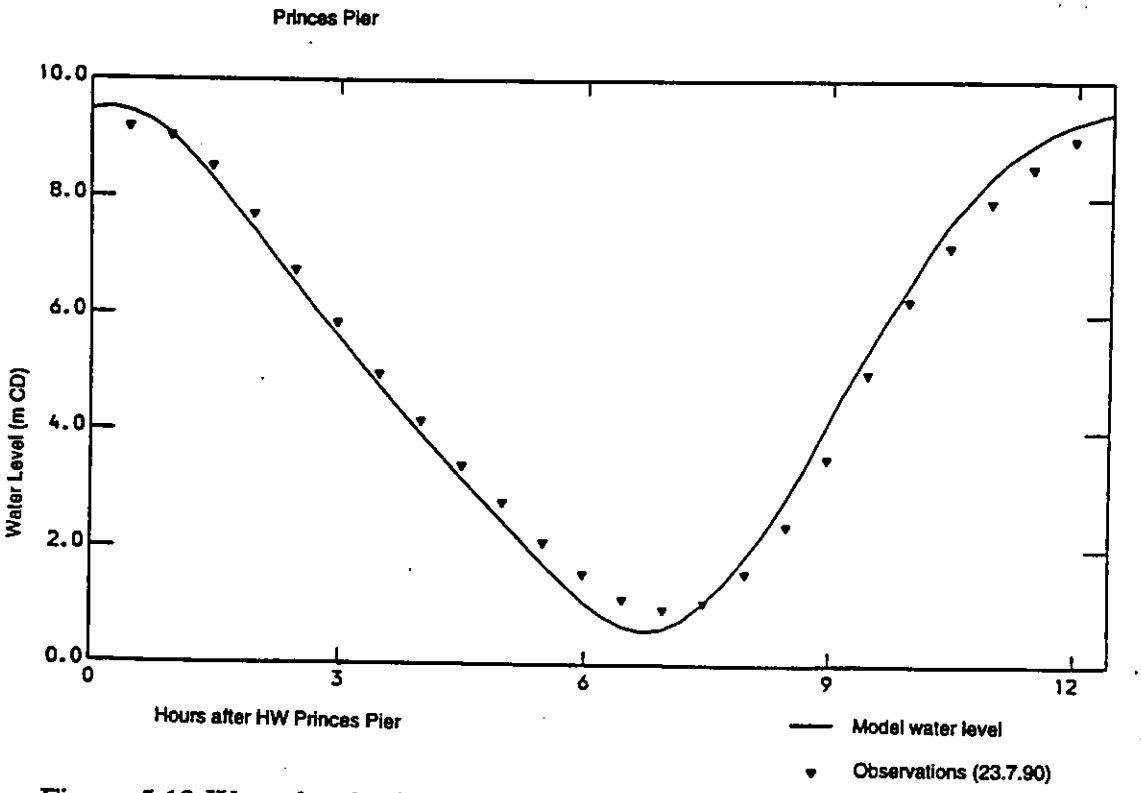

Figure 5.13 Water levels simulated by TIDEFLOW3D and field observations (23.07.90) at Princes Pier (adapted from HR, 1992b).

where the y velocity values were computed in the HR grid and horizontal interpolations of the water levels, x velocities and, at inflow boundaries, concentrations were carried out in order to define their respective values at the new grid positions. The grid used for running SUSMUD3 in the Narrows had 62x40 nodes (in the x and y directions, respectively). Furthermore, TIDEFLOW3D was set up with a maximum of 8 horizontal layers of unequal thicknesses and, in order to transform the layer-averaged velocities produced by this model into those required at the 21 vertical nodal positions used by SUSMUD3 for the Mersey Narrows, vertical interpolation was

performed, as well. In both the horizontal and vertical interpolation procedures the discharges in the original layers were calculated and conservation of the total discharge was imposed around each interpolation vertical. This aspect was particularly important in areas of the domain where the number of layers at the x velocity calculation positions was not the same, due to changing depths, to that at the y velocity interpolation position. Furthermore, as happens in TIDEFLOW3D, a logarithmic velocity profile was assumed in the bottom layer of each profile. Vertical velocities, needed by SUSMUD3 but not available from TIDEFLOW3D, were calculated in the cartesian domain by imposing a surface vertical velocity equal to the time rate of the free-surface variation and linearly interpolating to a zero value at the bottom. This simple approach was found to produce better results than mass conservation calculations based on the horizontal velocities, due to local inaccuracies resulting from the interpolation procedure of the latter. The time step used for running SUSMUD3 was, similarly to that used for HR's model, $\Delta t=894.24\ s$.

In all tests SUSMUD3 was set up to simulate a repeating tidal cycle, with t_0 corresponding to HW at Princes Pier. A uniform initial concentration of 0.15 g/l (consistent with the boundary values at HW) and the boundary conditions resulting from TIDEFLOW3D were used. The pattern of sediment transport was found to reach a state of dynamic equilibrium after 5 tides, sooner than TIDEFLOW3D under similar circumstances, possibly due to the smaller area involved in the simulation.

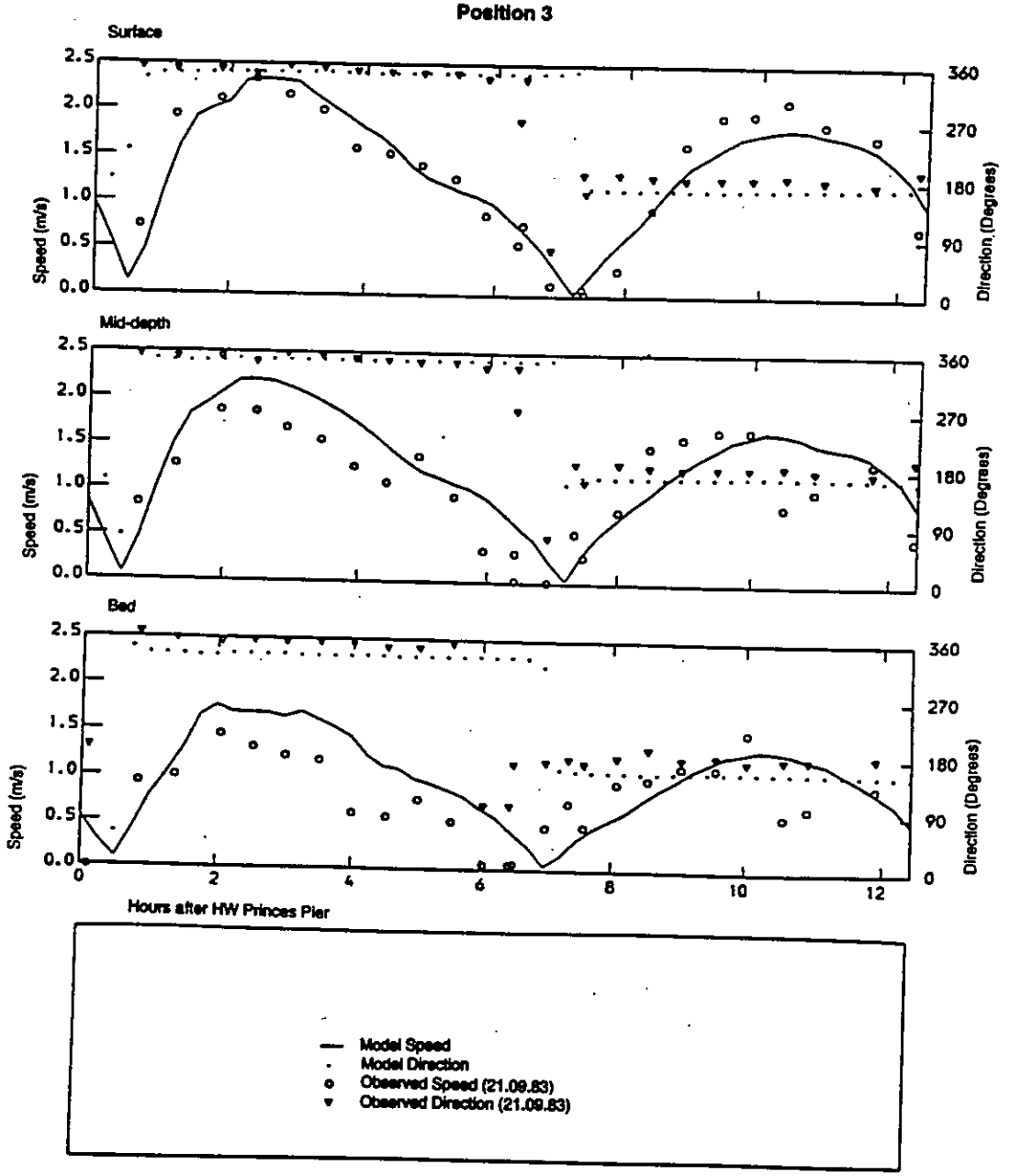

Figure 5.14 Velocities simulated by model TIDEFLOW3D and observed velocities (21.09.83) at Position 3 of Section 13 in the Narrows (adapted from HR, 1992b).

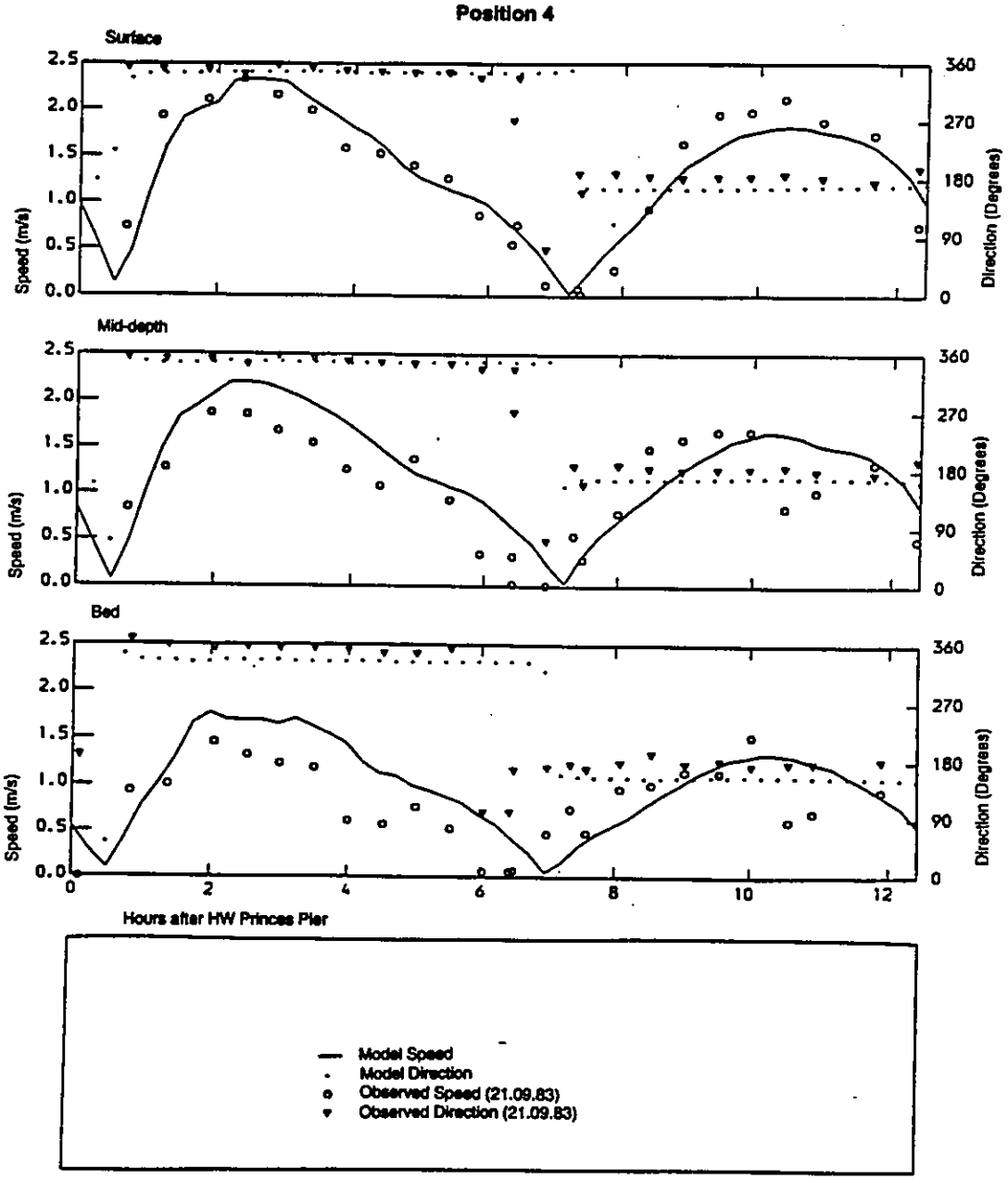

Figure 5.15 Velocities simulated by model TIDEFLOW3D and observed velocities (21.09.83) at Position 4 of Section 13 in the Narrows (adapted from HR, 1992b).

The final conditions of the initial run, both in terms of suspended sediment and of freshly deposited sediment were used as initial conditions of the final run of each test, encompassing a single tidal cycle.

A series of preliminary runs were carried out to check model sensitivity to variations in process defining parameters and to identify possible improvements in the computational structure. In these tests vertical diffusion coefficients were computed using the Smith and Kirby (1989) formulation, described by equations 2.23 to 2.27. In this case coefficient ε_0 was kept constant during the tidal cycle. Sensitivity tests indicated that a value of ***0.14 m^2/s***, proposed by the same authors, was adequate. Stability parameters used were α=*5.0* and β=*1.5*. Horizontal diffusion coefficients were set at ***10 m^2/s***, as in HR's model, and this value was adopted in all remaining runs, given the lack of sensitivity of the model to changes in these parameters. During the preliminary series of tests it was observed that the tidal variability of the settling velocities resulting from the range of concentrations found in the domain was small. Therefore, the generalised decrease in concentrations in the upper layers of the water column (and the corresponding increase in the lower layers) typically found in estuaries before slack water and confirmed by the Mersey field data, was not adequately reproduced by the model output.

A first attempt at improving this aspect was through the use of a unity probability of deposition, as suggested by Sandford and Halka (1993), allowing simultaneous erosion and deposition. This approach, however, did not produce significantly different results.

A second attempt was carried out through changes in certain process defining parameters. The critical shear stresses for deposition and erosion were slightly increased, to ***0.2*** and ***0.3 Pa***, respectively, allowing deposition to take place for a longer period. In the absence of a model allowing changes in the magnitude of the settling velocities during the tidal cycle, as a result of the decrease in floc breakup in the vicinity of slack water, as commonly observed in field situations, it was also decided to enhance such velocities through their multiplication by an empirical function. The function which was adopted had the form

$$F(\tau_b) = 1 + (10^{m_1} - 1)\left[1 - \left(\frac{\tau_b}{m_2 \tau_{ce}}\right)^{m_3}\right] \qquad \tau_b < m_2 \tau_{ce} \qquad (5.1)$$

$$F(\tau_b) = 1 \qquad \tau_b \geq m_2 \tau_{ce}$$

which indirectly translates the above effect, in the absence of a finer representation of floc aggregation and breakup in the turbulent velocity field. Parameters m_1, m_2 and m_3 were assigned values of *1*, *4* and *2*, respectively, leading to a tenfold increase of the settling velocity in the vicinity of slack water.

The use of function 5.1 and of the revised critical shear stresses allowed a much better representation of the depositional sequences near slack water and was adopted in the following runs. Furthermore, and given the large variations in the input shear stress between two consecutive time steps (separated by, approximately 15 minutes), giving rise to large inaccuracies in the computed erosion/deposition fluxes, it was decided to split the vertical calculation into a succession of 12 partial calculations. The bottom

shear stress for each one of the partial calculations resulted from linear interpolation between the input shear stress values.

Following the preliminary tests a reference case was computed using the process model formulations and the corrections already described. Diffusion formulations and parameters remained the same relative to the preliminary runs. The results of the reference simulation are shown in figures 5.18 to 5.37, where a vertical distortion factor of 50 was used for better visualisation. The figures correspond to time steps separated by, approximately, 75 minutes and should be analysed in conjunction with the bottom shear stress distributions, in particular around slack water, as shown in figures 5.16 (LW slack) and 5.17 (HW slack), plotted at Δt intervals. It should be noted, relatively to figure 5.16 that a conventional value τ_b=*0.2 Pa* (i.e. non-erosion/deposition conditions) has been assigned to dry areas near both banks.

It is observed from the shear stress distributions that depositional conditions do not occur simultaneously in the whole domain and that such conditions seem to prevail for longer periods at the innermost area of the Narrows, close to the barrage line. It is also observed from the figures that the time step of, approximately, 15 minutes which was used in the hydrodynamics calculations is, apparently, too large. In fact the shear stress evolution near slack water seems to be rather fast and in certain areas in the central zone of the domain (and, particularly, around HW slack) depositional conditions are not detected.

In the series of figures 5.18 to 5.37, and in very general terms, the first four sets of two figures can be described as representing ebb conditions, the fifth and sixth encompass a LW slack condition (see also figure 5.16), the following three represent flood conditions and the last set corresponds, approximately, to HW slack. In this sequence, figures at the bottom of each page show the vertical structure of the concentration field (including the imposed boundary condition), through mapping in seven equally-spaced cross-sections. Figures at the top of each page show the surface concentration distribution and that at the outflow section (i.e. the view is taken from the seaward end of the domain in the first five figures and from the landward end in the remaining). It should be noted that the concentration distributions at the inflow boundaries result from the calculations of TIDEFLOW3D and present a rather different vertical structure than that produced by SUSMUD3 in the inner domain. Therefore, the results produced by the latter in the immediate vicinity of the inflow boundaries should be analysed carefully. The inflow section in figures 5.18 to 5.27 is that of the barrage line, while in figures 5.28 to 5.37 it corresponds to that at the mouth of the Narrows.

It is observed from figures 5.18 to 5.37 that the model was able to reproduce the expected global features of a suspended fine sediment concentration field under tidal action. A vertical concentration structure in the water column which is typical of fine sediment suspensions and, in particular, the increased stratification associated with depositional conditions near slack water are well represented. Pickup of sediment from

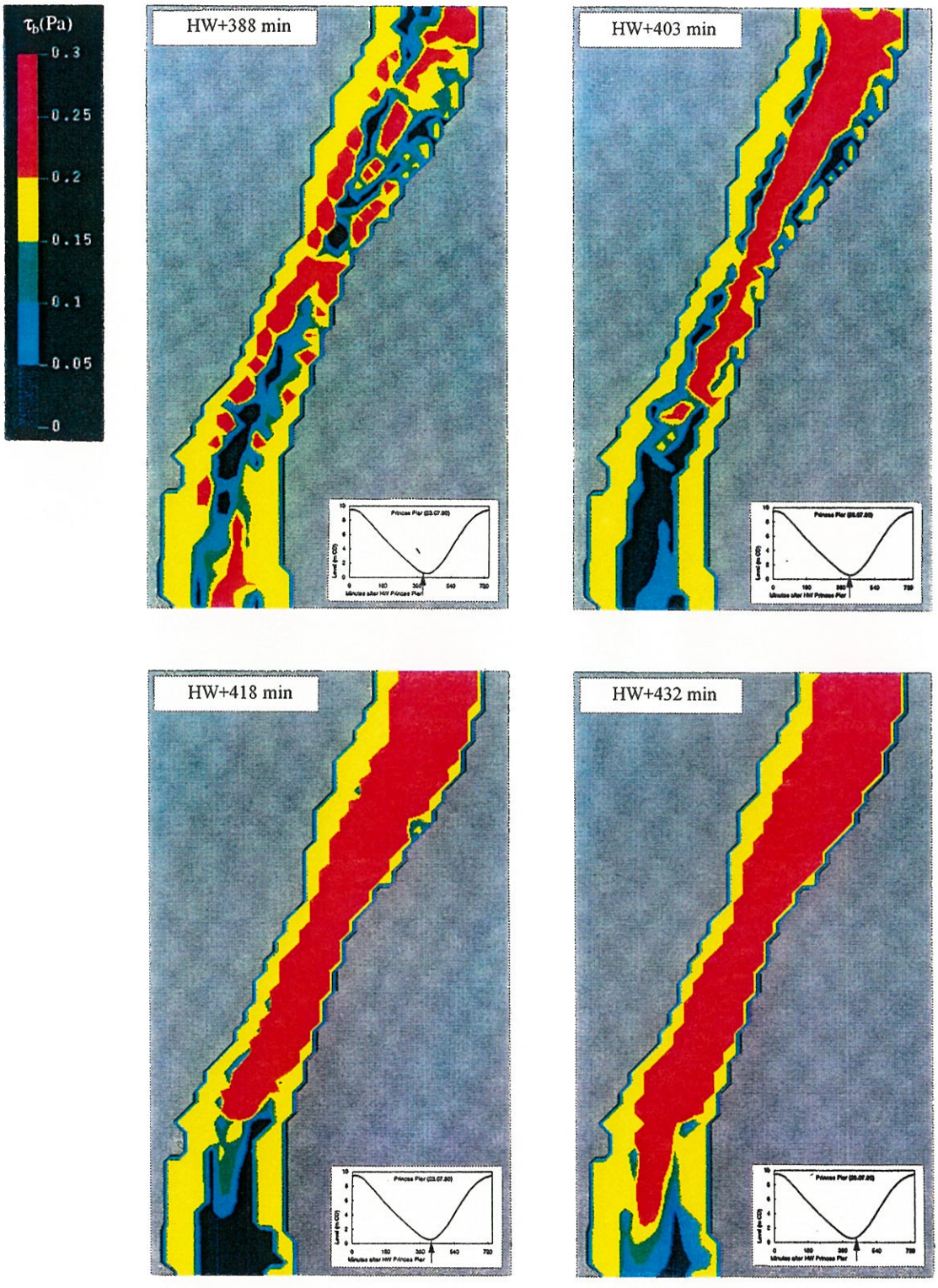

Figure 5.16 Bottom shear stress distribution around LW slack.

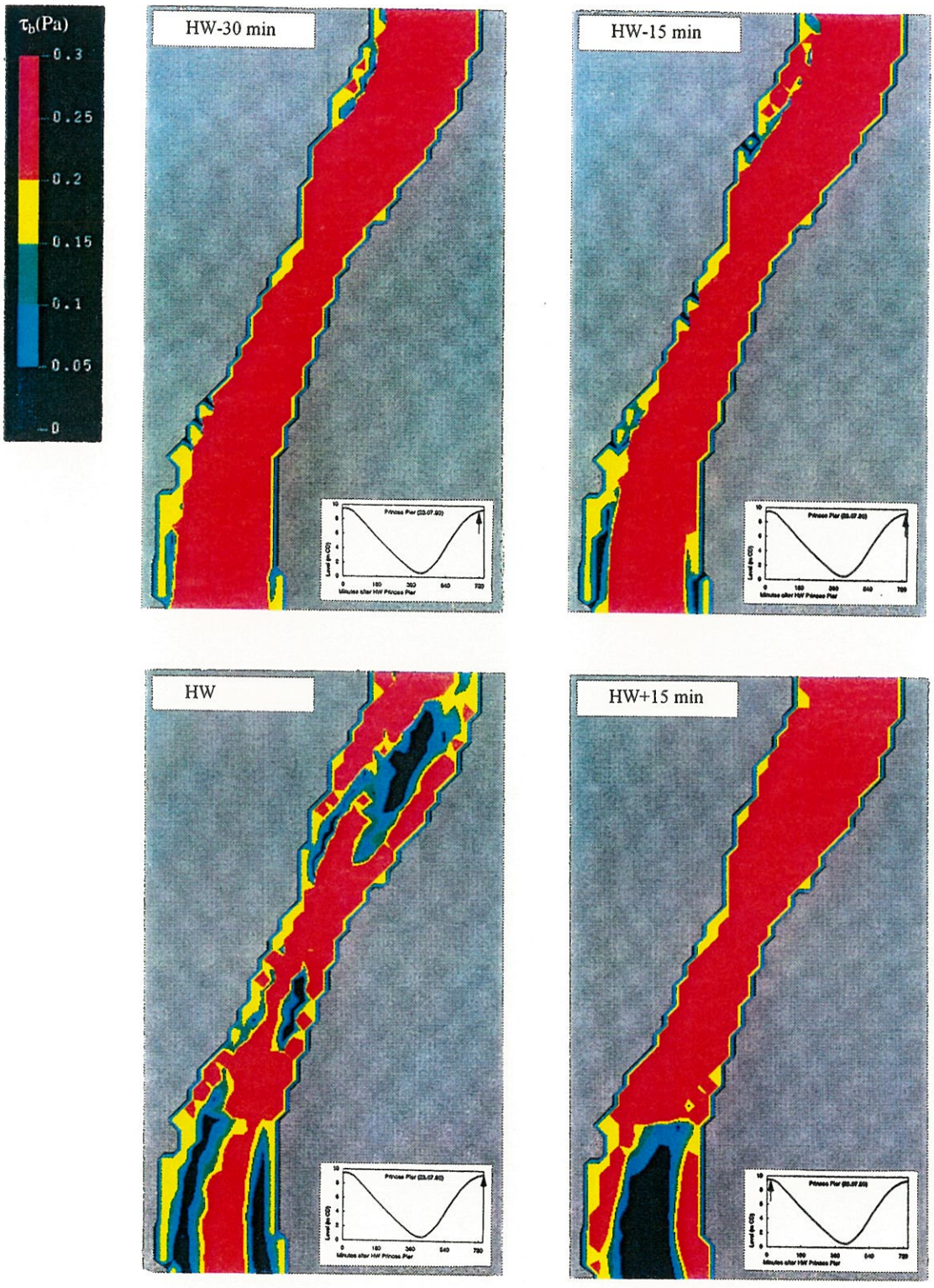

Figure 5.17 Bottom shear stress distribution around HW slack.

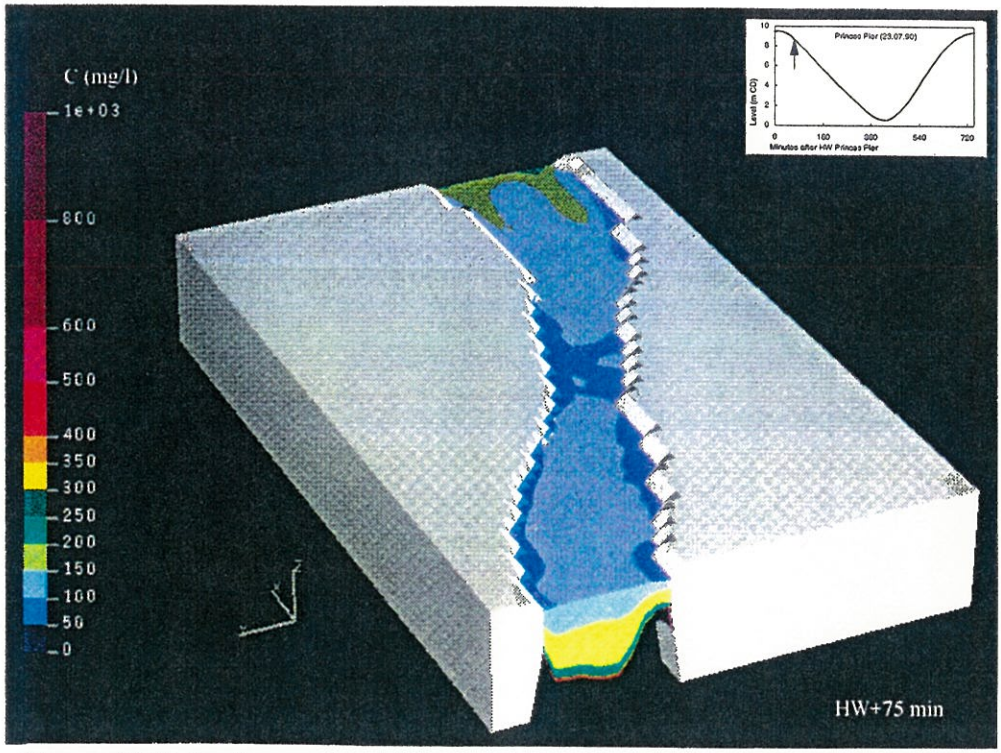

Figure 5.18 Surface and outflow section concentration distribution in the Narrows (HW+75 min).

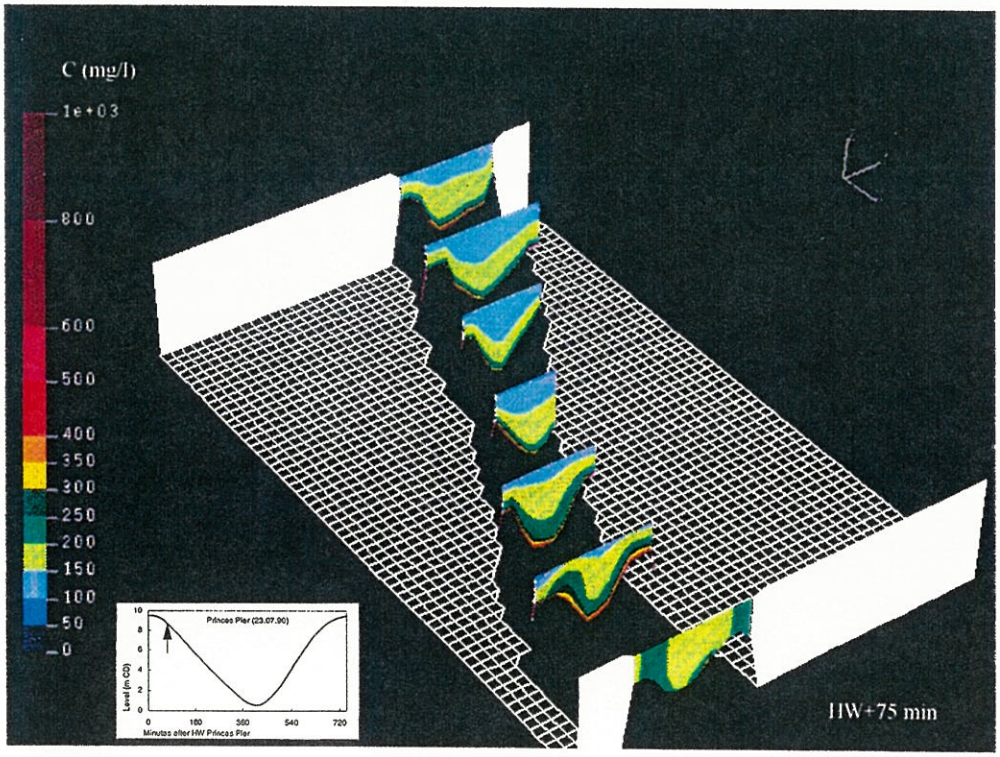

Figure 5.19 Vertical concentration structure in the Narrows (HW+75 min).

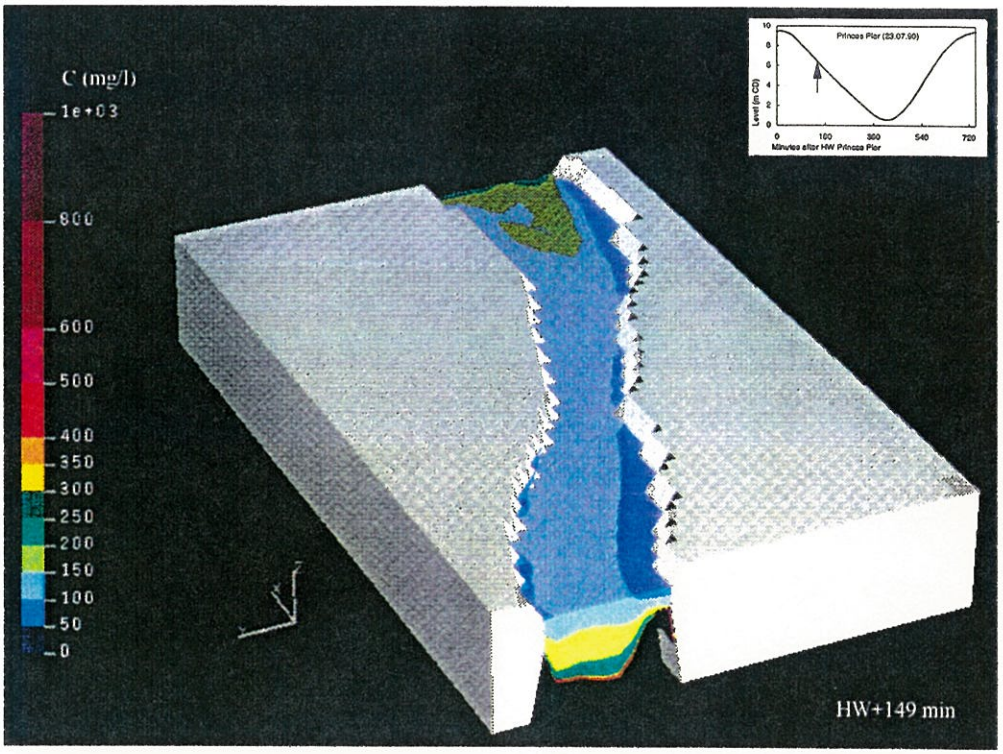

Figure 5.20 Surface and outflow section concentration distribution in the Narrows (HW+149 min).

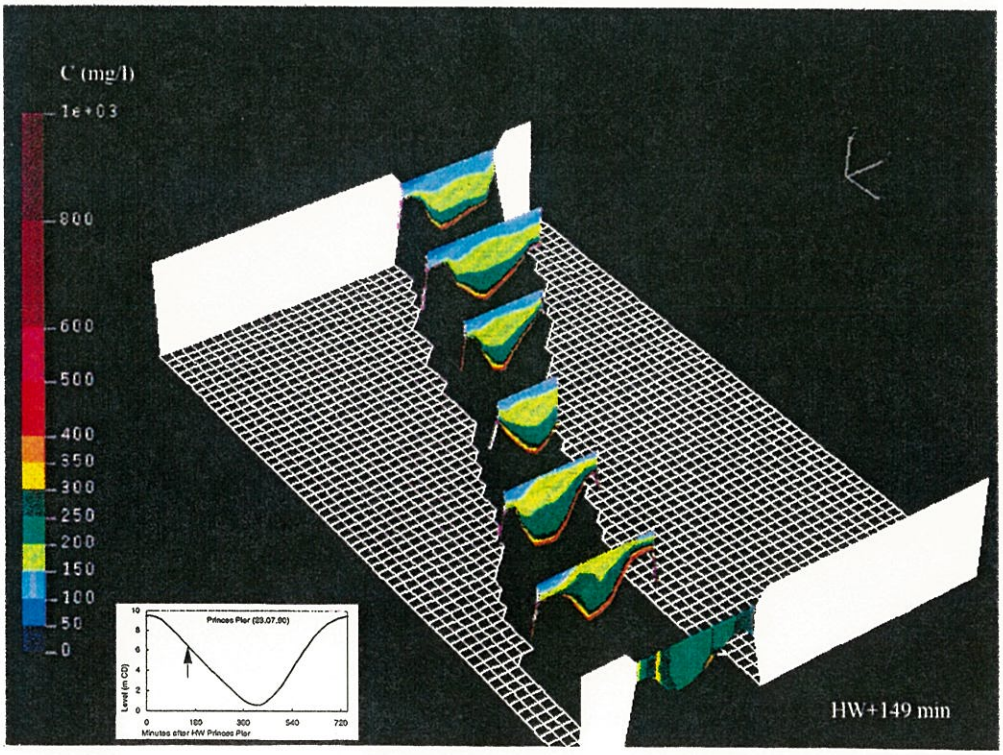

Figure 5.21 Vertical concentration structure in the Narrows (HW+149 min).

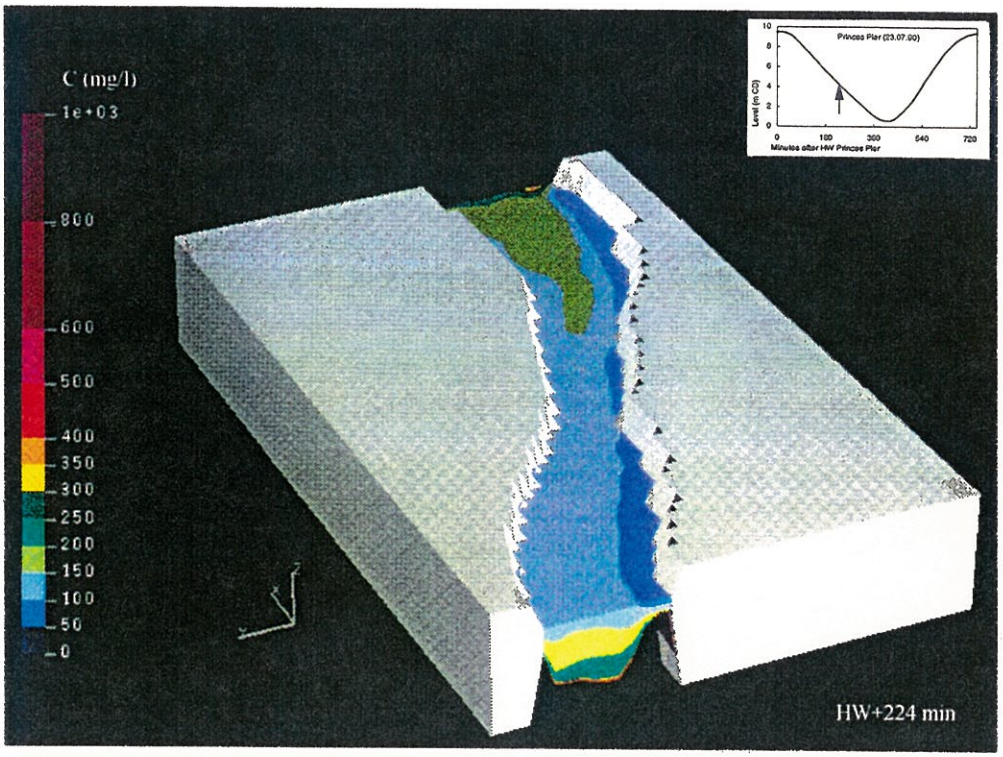

Figure 5.22 Surface and outflow section concentration distribution in the Narrows (HW+224 min).

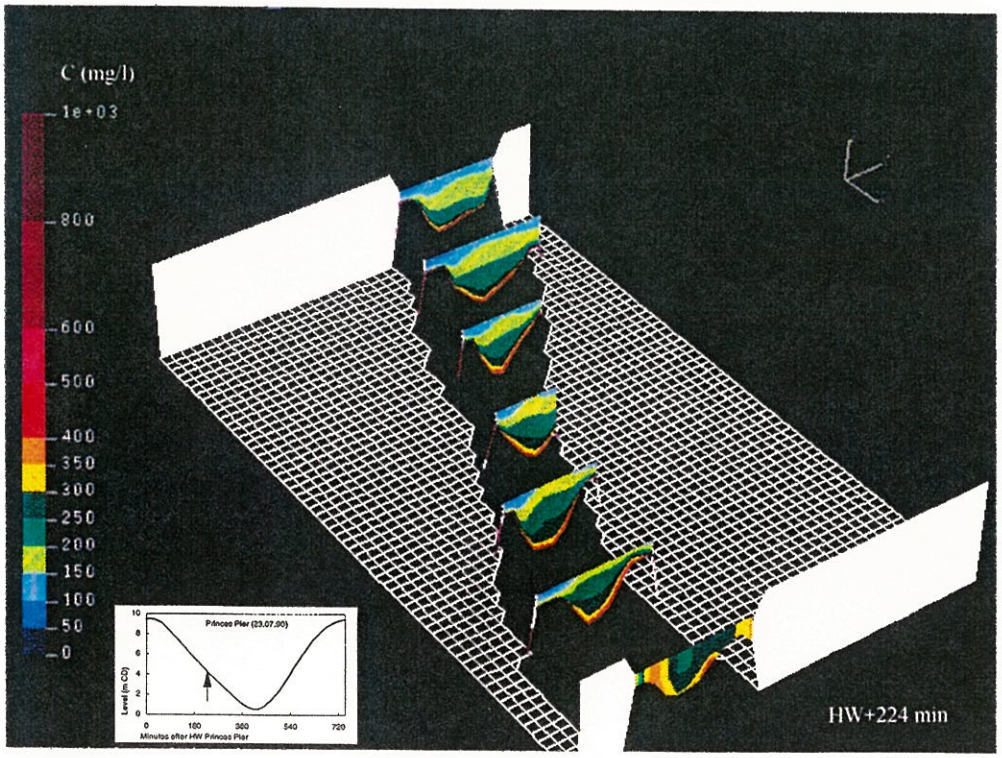

Figure 5.23 Vertical concentration structure in the Narrows (HW+224 min).

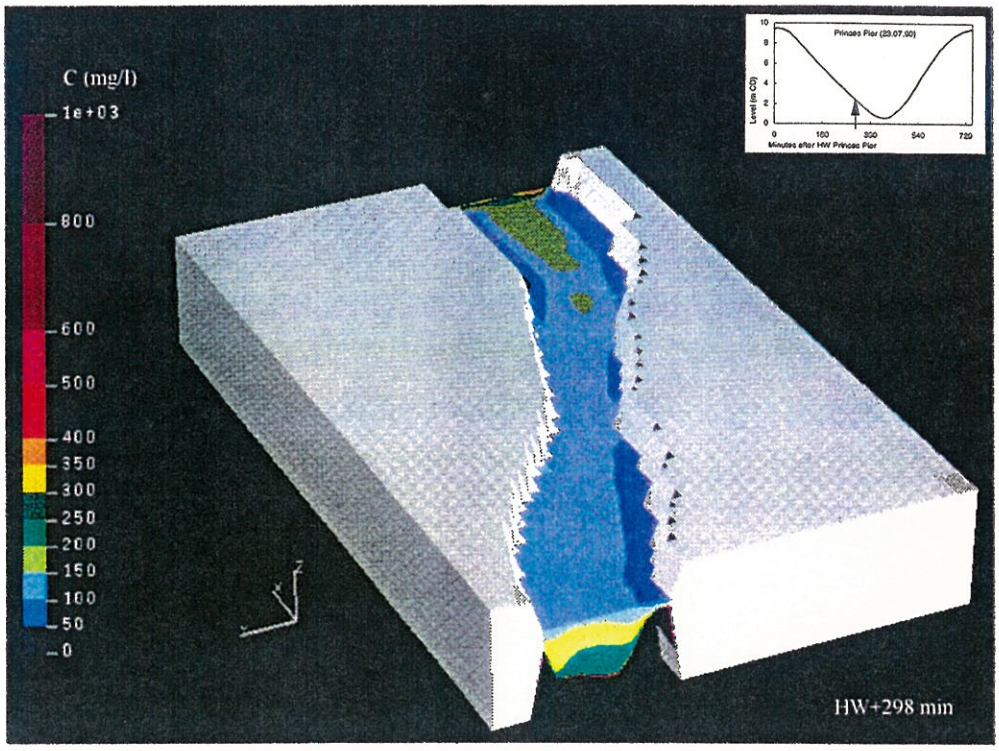

Figure 5.24 Surface and outflow section concentration distribution in the Narrows (HW+298 min).

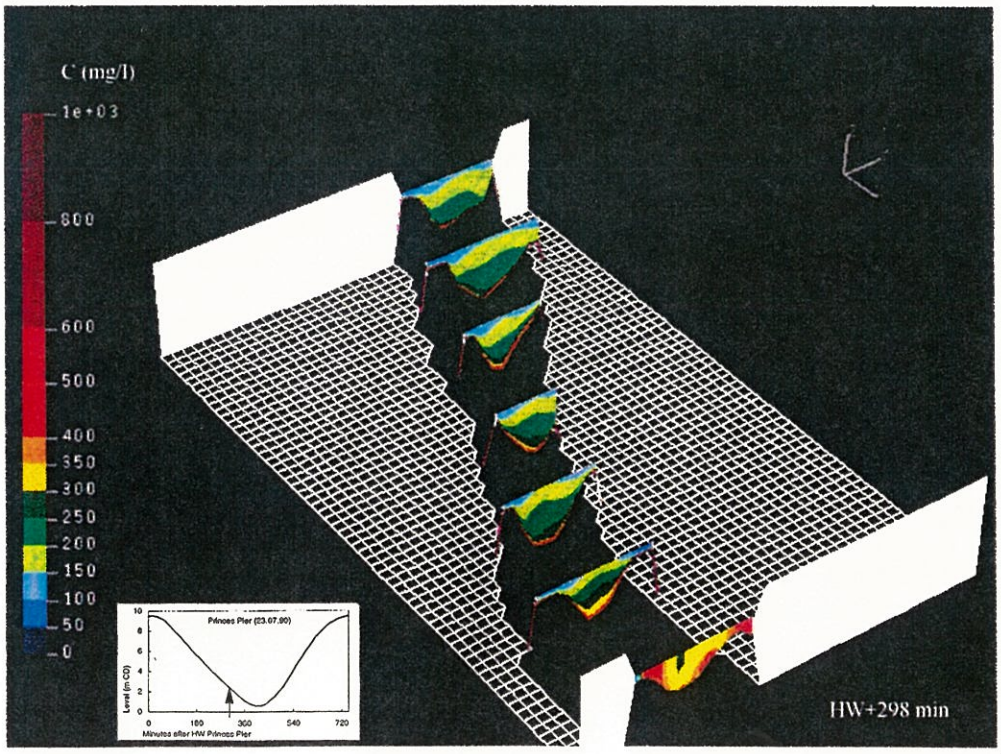

Figure 5.25 Vertical concentration structure in the Narrows (HW+298 min).

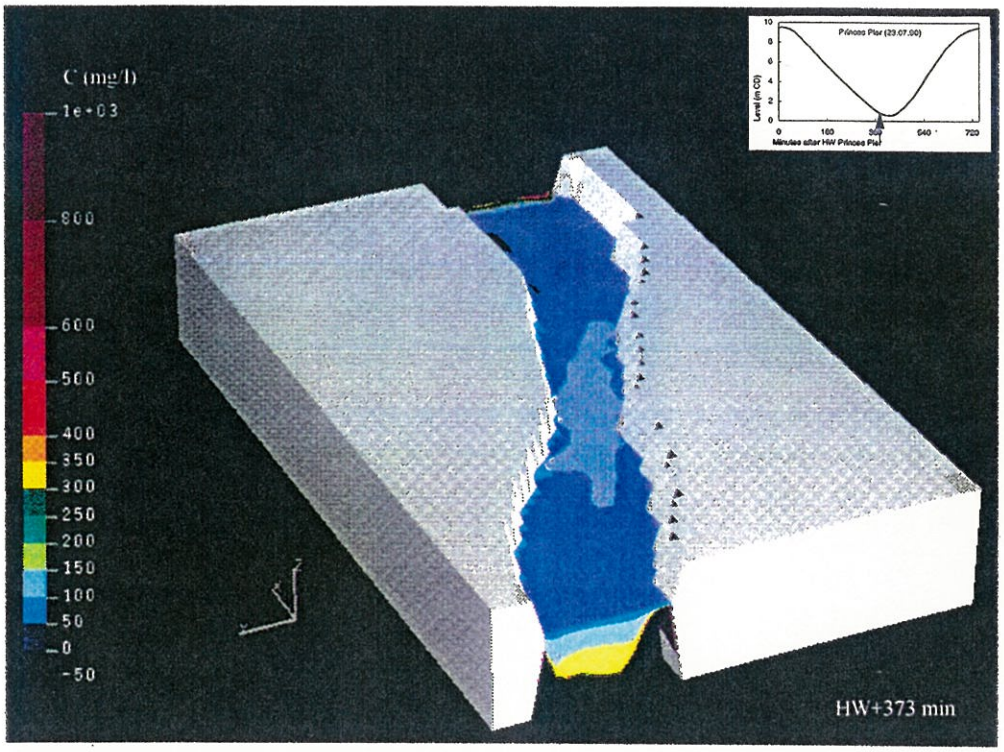

Figure 5.26 Surface and outflow section concentration distribution in the Narrows (HW+373 min).

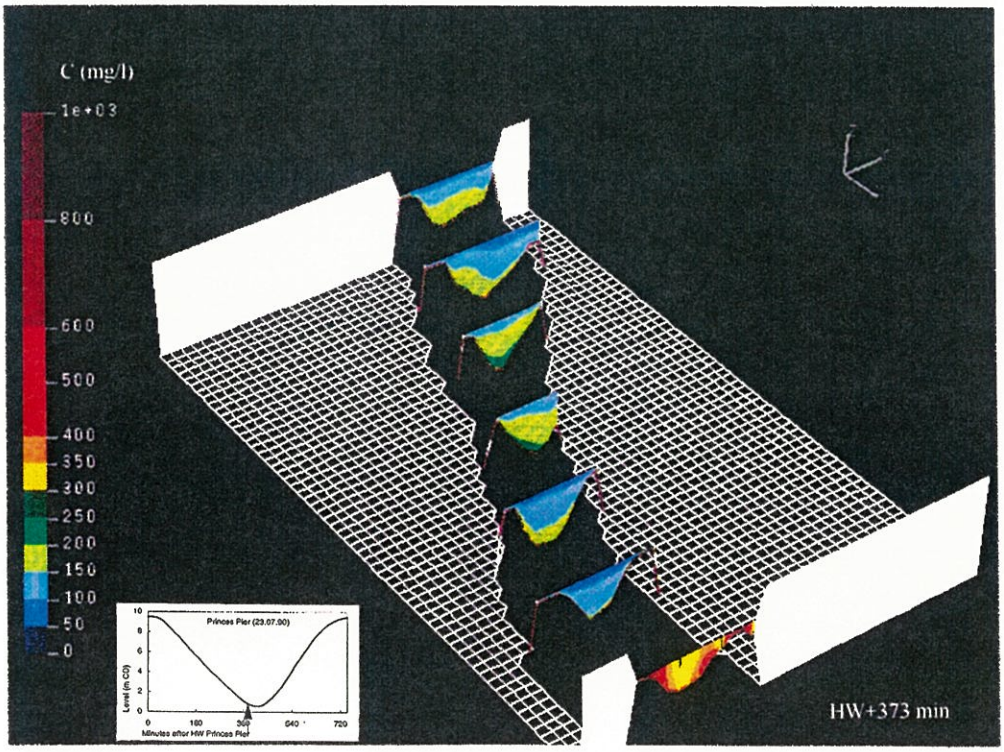

Figure 5.27 Vertical concentration structure in the Narrows (HW+373 min).

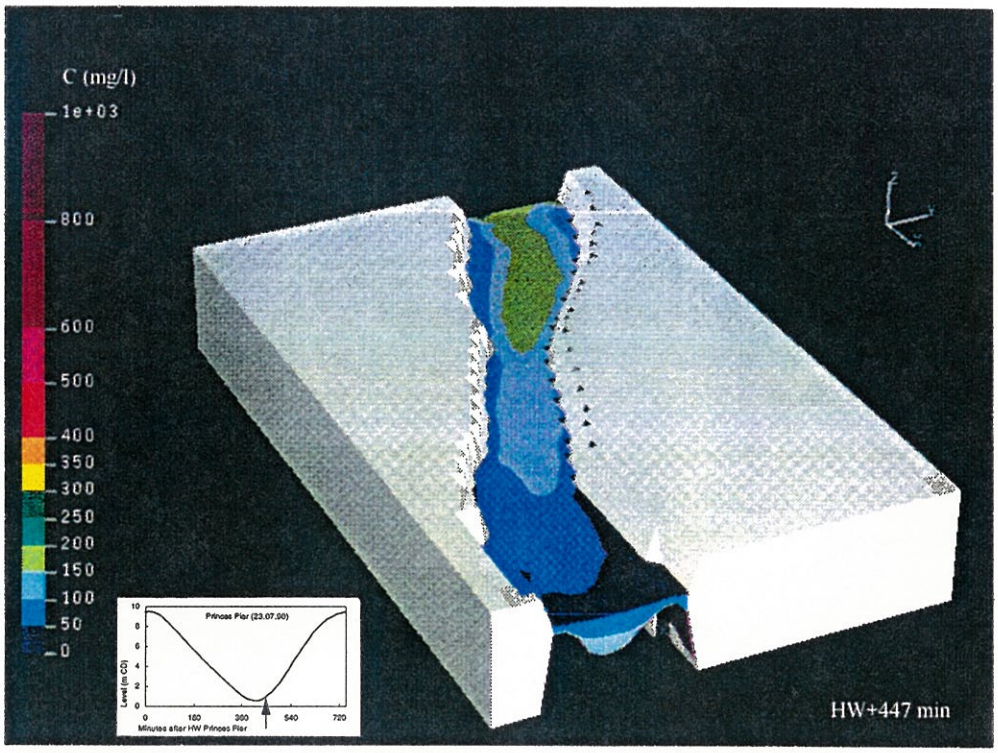

Figure 5.28 Surface and outflow section concentration distribution in the Narrows (HW+447 min).

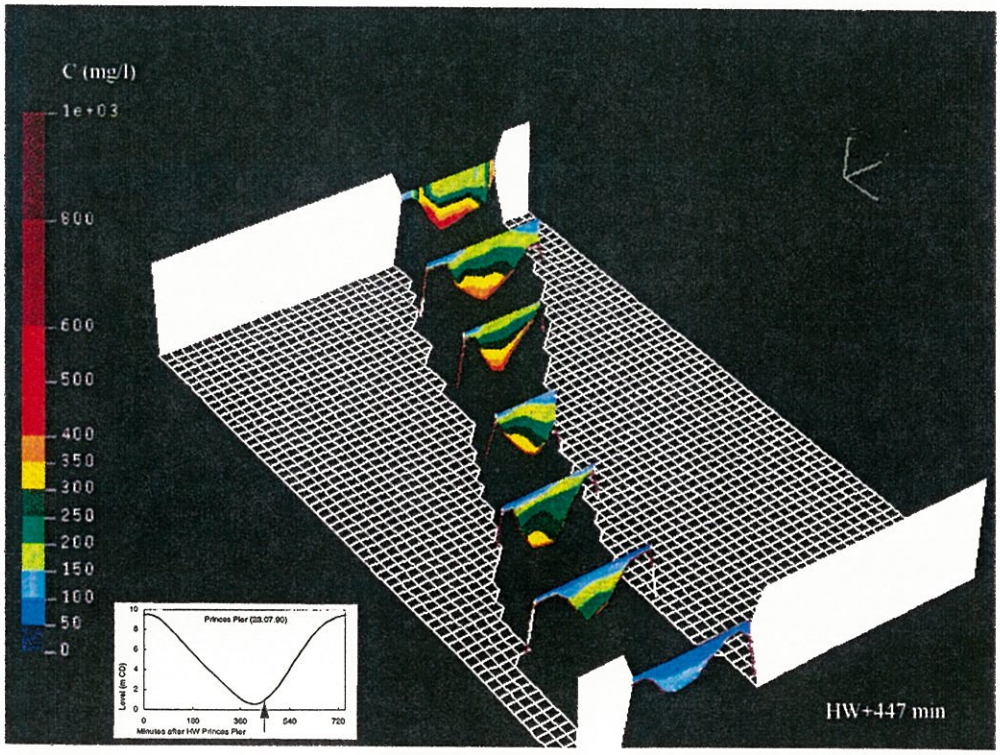

Figure 5.29 Vertical concentration structure in the Narrows (HW+447 min).

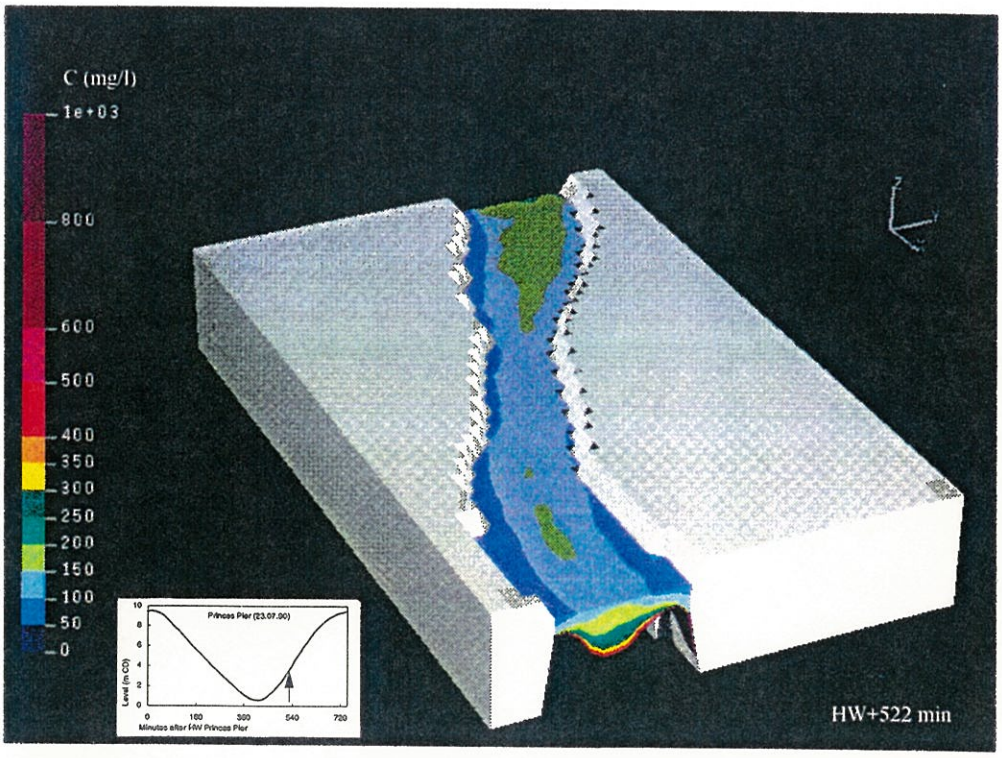

Figure 5.30 Surface and outflow section concentration distribution in the Narrows (HW+522 min).

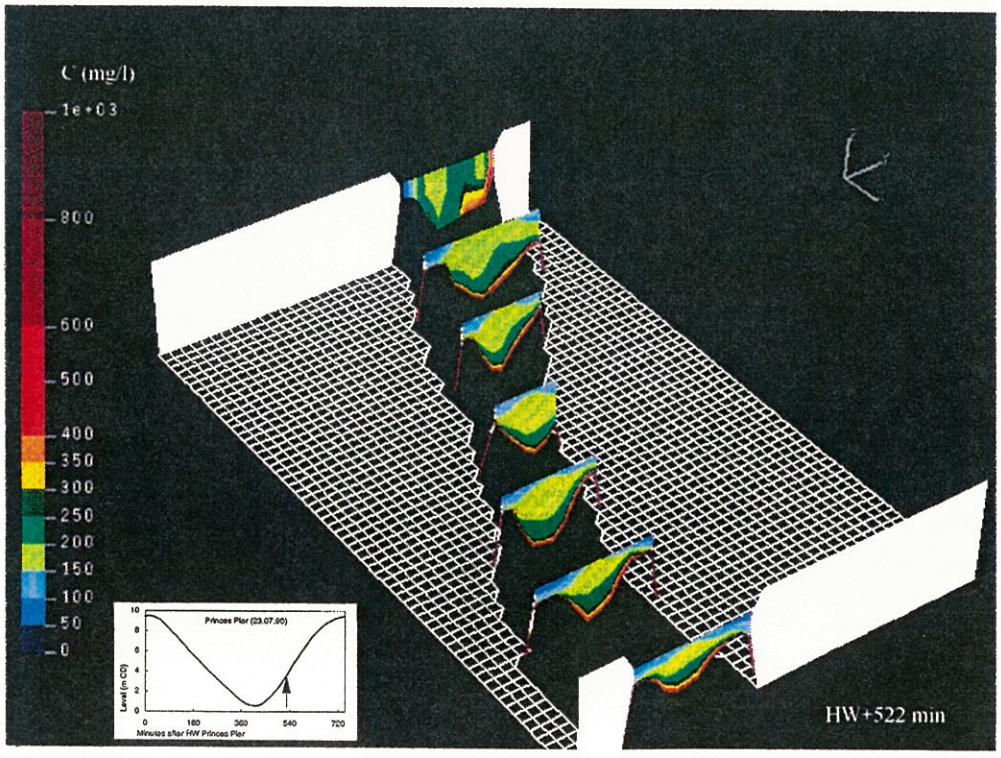

Figure 5.31 Vertical concentration structure in the Narrows (HW+522 min).

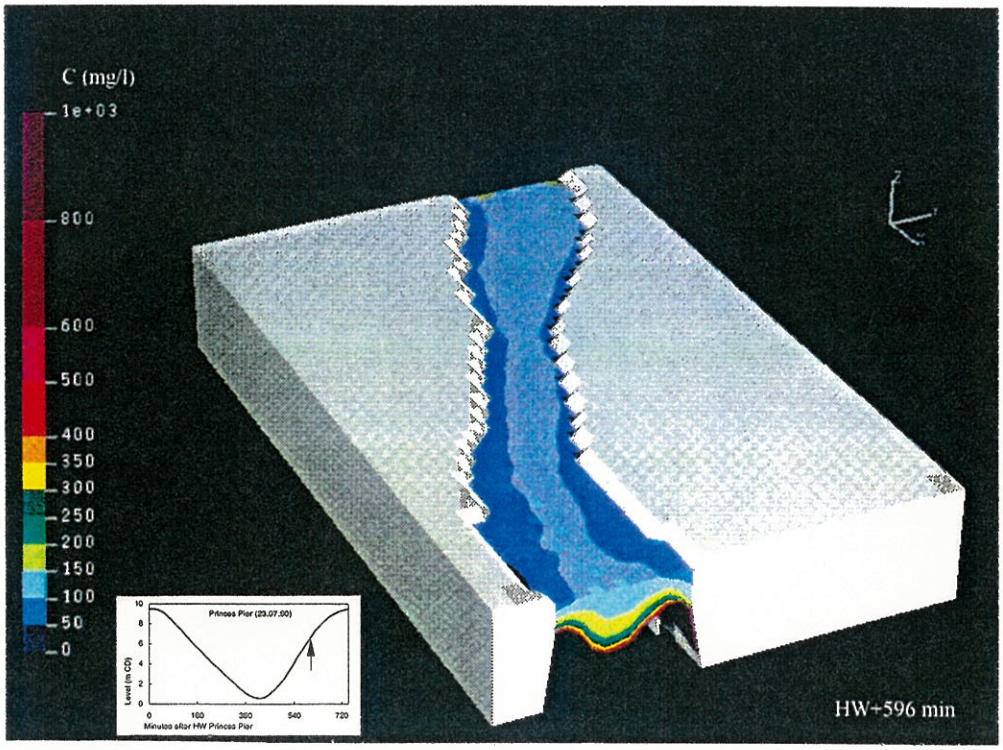

Figure 5.32 Surface and outflow section concentration distribution in the Narrows (HW+596 min).

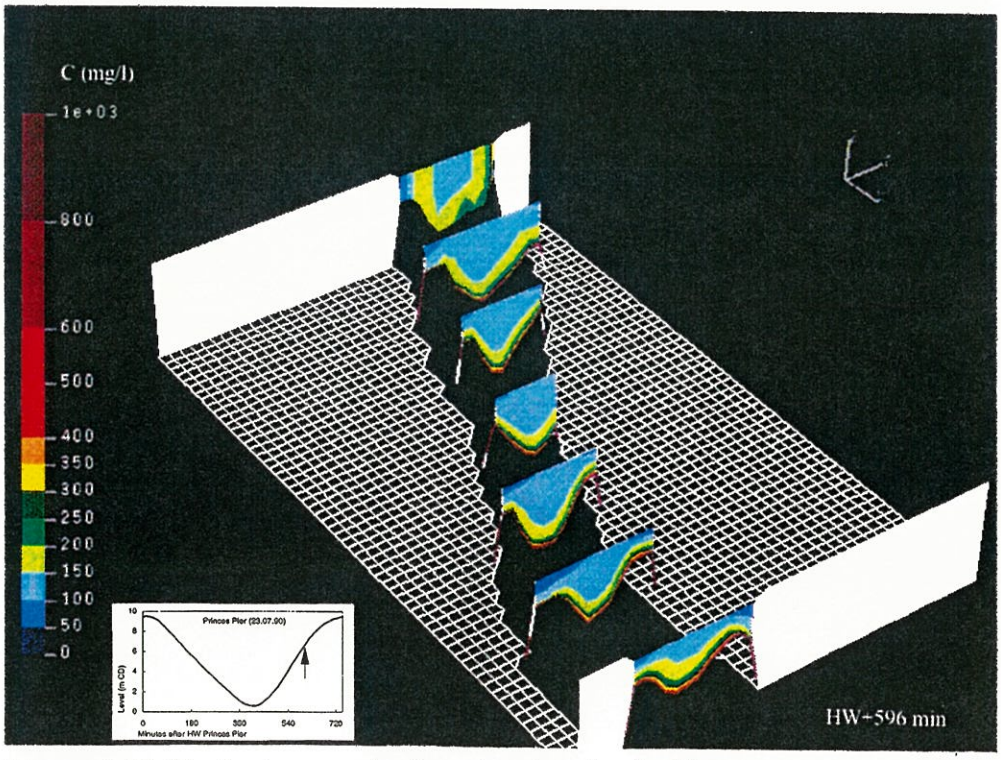

Figure 5.33 Vertical concentration structure in the Narrows (HW+596 min).

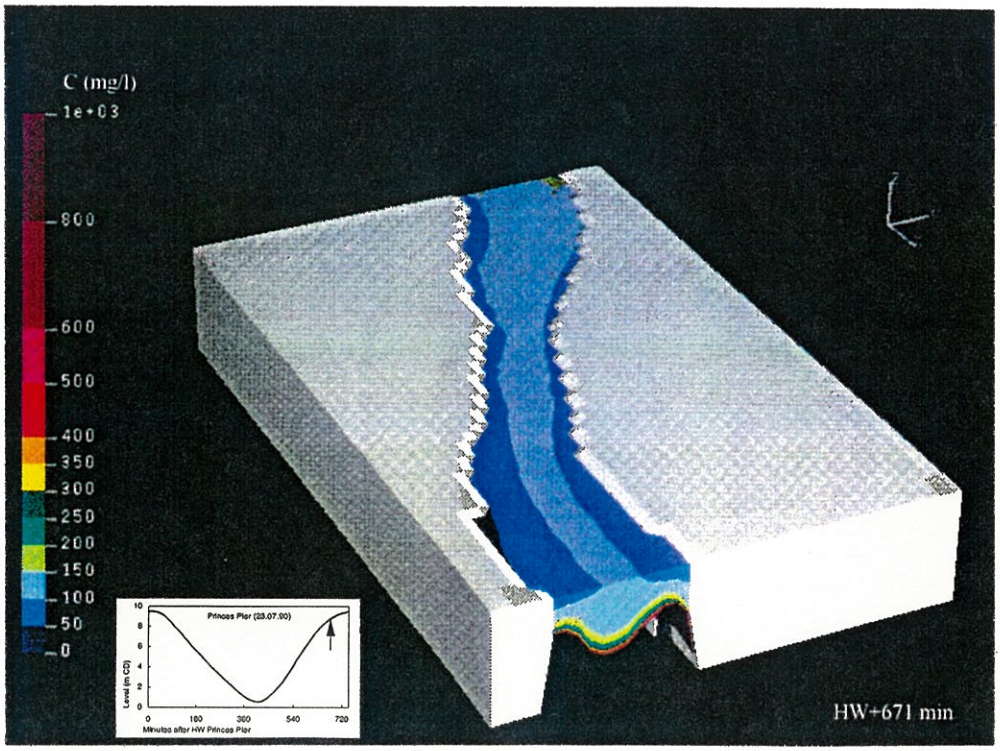

Figure 5.34 Surface and outflow section concentration distribution in the Narrows (HW+671 min).

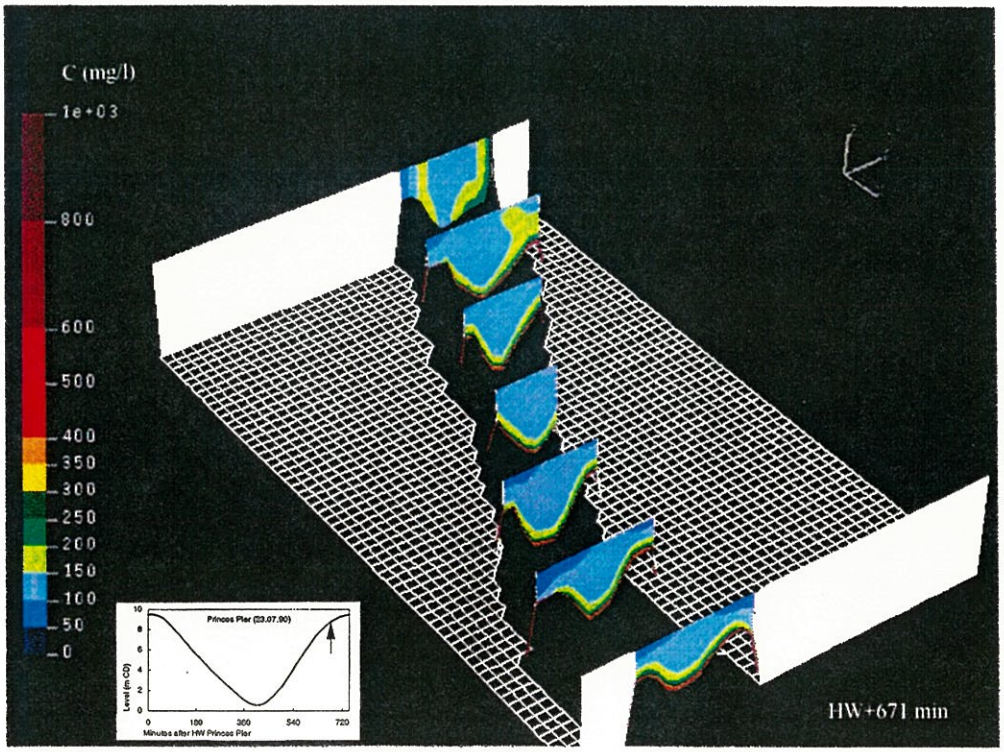

Figure 5.35 Vertical concentration structure in the Narrows (HW+671 min).

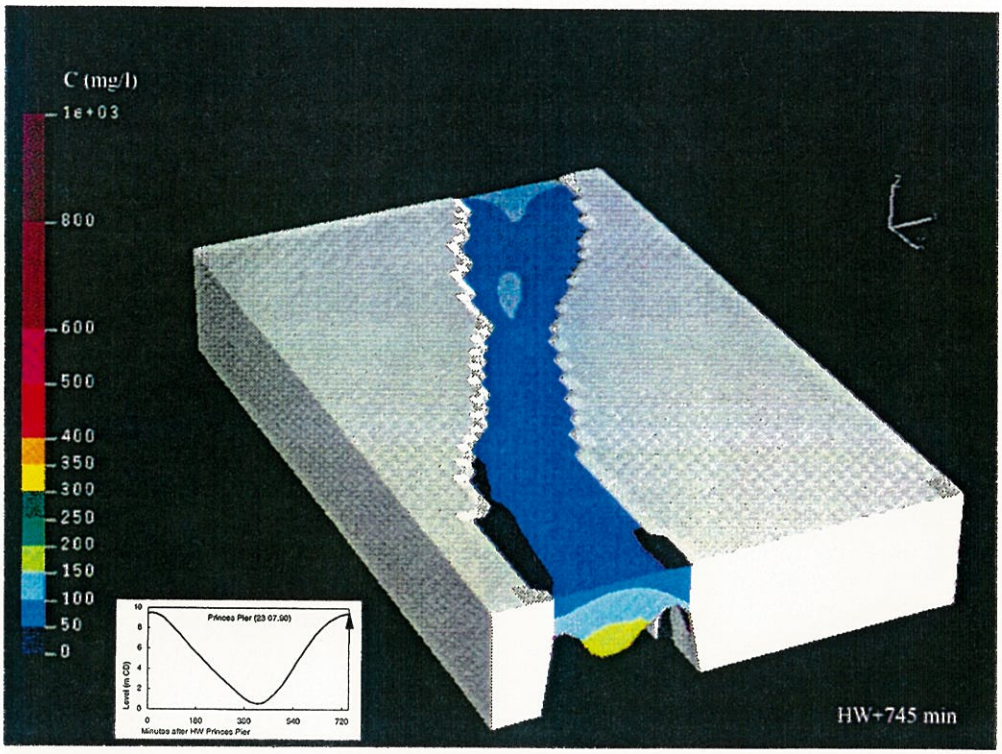

Figure 5.36 Surface and outflow section concentration distribution in the Narrows (HW+745 min).

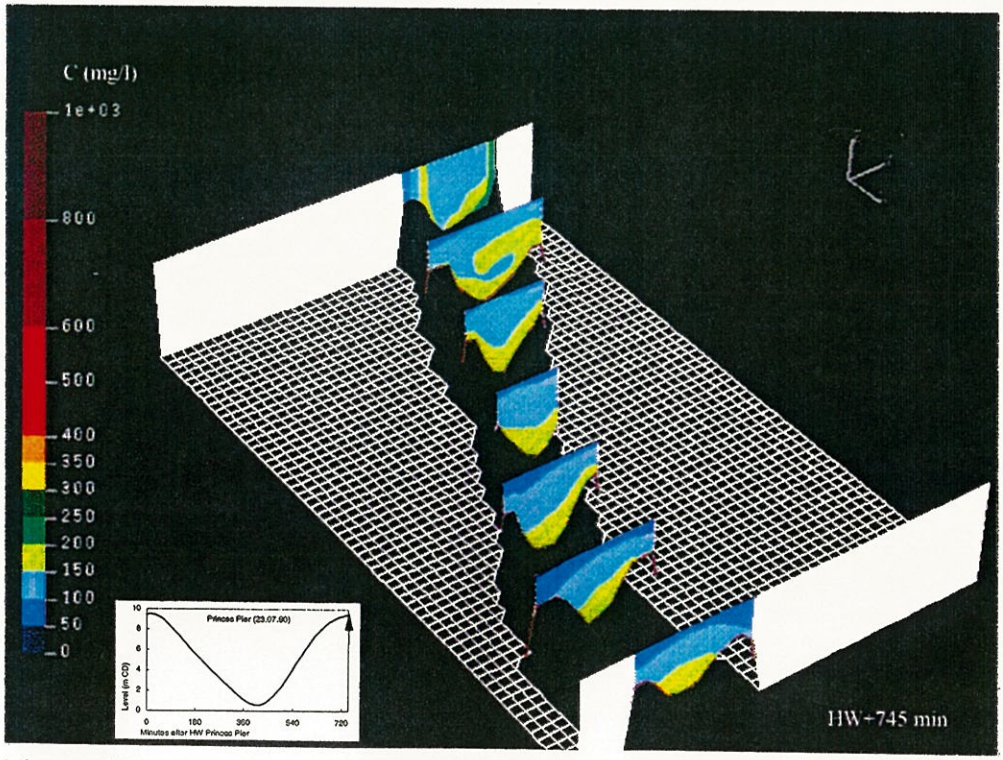

Figure 5.37 Vertical concentration structure in the Narrows (HW+745 min).

the bottom after slack water and its re-entrainment to upper layers of the water column are also well documented in the accelerating stages of both the ebb and the flood.

The inflow of turbid water from the Upper Basin into the Narrows, during the ebb, apparently in agreement with the oscillating pattern of sediment movement already described, is observed in the figures. Higher concentrations found near the banks (in the continuation of the Eastham and Garston channels) at the beginning of the ebb, are also apparent from the figures. The increase in concentration in the upper layers, during the accelerating stages of the ebb is followed by a drop in their values, as seen by the sediment distribution at the surface. Around LW slack most sediment is found in thin near-bed layers showing high concentrations. Pick-up of recently deposited sediment together with increased sediment concentrations in the incoming flow characterise the beginning of the flood while, at later stages, lower concentrations are found. Increasingly stratified conditions are, again, found when HW slack is approached.

In order to allow a more detailed evaluation of the model and, in particular, of the vertical structure of the computed concentrations, output was compared with field data from selected points.

Data from Section 13 (from Egremont, in the Wirral, to Sandon Dock, near Victoria Tower, in Liverpool) was used to compare two formulations for the vertical diffusion coefficients, all other parameters remaining the same relative to the reference

simulation. Case A was computed using the Smith and Kirby (1989) formulation with ε_0=*0.14 m²/s* as before. In Case B, coefficient ε_0 was replaced by ε_z defined as a function of the depth-averaged horizontal velocity and total water depth, as in equation 2.28. Values used were ε_0=*0.025 m²/s* and ε_1=*0.00125*, as recommended for the Mersey by Bowden and Hamilton (1975). In both cases the stability parameters had the same values as before (α=*5.0* and β=*1.5*).

As described in Section 5.3, data is available for near-bottom and near-surface points of positions 2, 3 and 4 at Section 13, during intermediate and spring tides of ranges 8.9 m, 7.8 m and 6.9 m at Gladstone Dock, corresponding to tides of March 9, 1982, September 16, 1982 and September 21, 1983, respectively. Of the three positions only the one at the centre of the section (Position 3) has data from all three occasions. Position 2 has data from the last two tides while at Position 4 data was only obtained during part of the second tide. Values obtained are plotted in figures 5.38 to 5.43 where the concentrations are the measured values (without any correction as a function of the tidal range) and the abscissas (times of measurement) were normalised, in terms of the ebb and flood times of the simulated tide (July 23, 1990).

Despite possible measurement inaccuracies and the large scatter observed in the data, trends can be estimated from the field measurements and compared with model simulations. In general terms it is observed that curves produced by the model at the near bed positions show better agreement with the field trends than those produced near the surface.

At near-surface positions the model was not able to reproduce the time variability of concentration and, in particular, the low turbidity levels observed in the field at Positions 2 and 3, during the two last tides, for about two hours around slack water. However, field measurements during the first tide at Position 3, seem to indicate a lower degree of variability and model simulations are in better agreement with them. A similar situation is found near the surface at Position 4, despite the small number of data points available.

At the near-bed positions, and despite the large scatter observed in the field data, reasonable agreement is obtained, in both magnitude and time evolution of the concentrations, although the sharp variations around slack water, which are found in the field, are still not reproduced by the model.

From the figures it is also observed that Case B shows a slightly better agreement with the field trends than Case A. A time-dependent formulation may, therefore, be preferred to a vertical mass diffusivity formulation using coefficients which are constant in time, although major improvements in accuracy are still not obatined. Results from the simulations seem to indicate that increasingly complex turbulence closure models are necessary if more realistic simulations are to be carried out. Furthermore, the need for better data sets, which will be necessary to validate system models using such turbulence closures, is also evident, as the scatter of points in figures 5.38 to 5.43 only allows a semi-quantitative model evaluation.

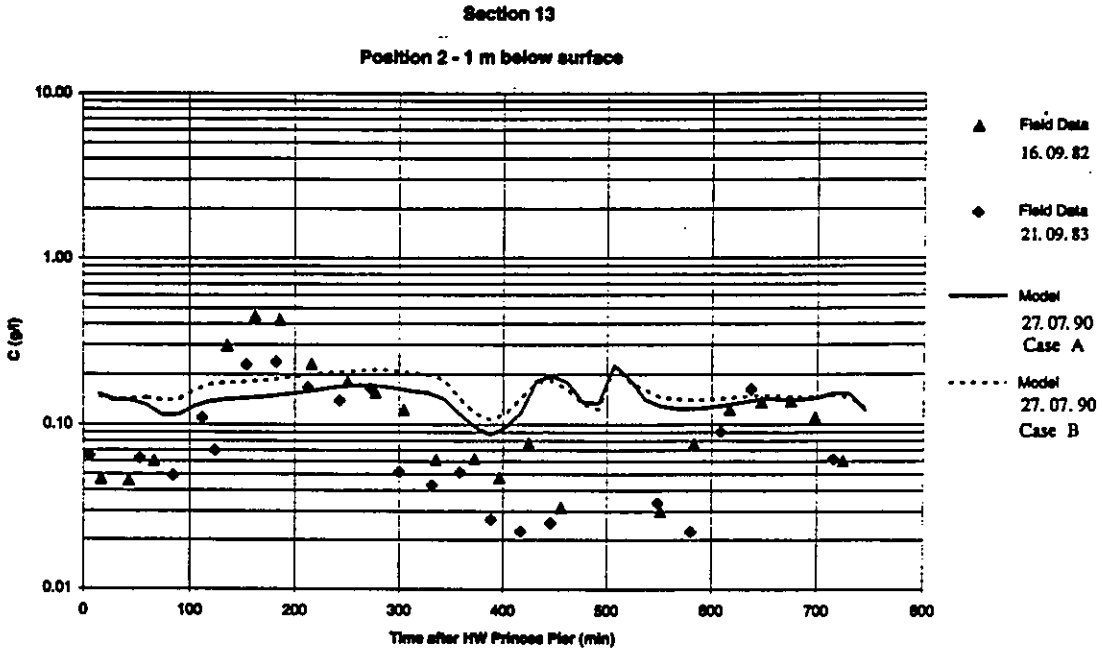

Figure 5.38 Near-surface field data and model simulations at Position 2 in Section 13 of the Narrows.

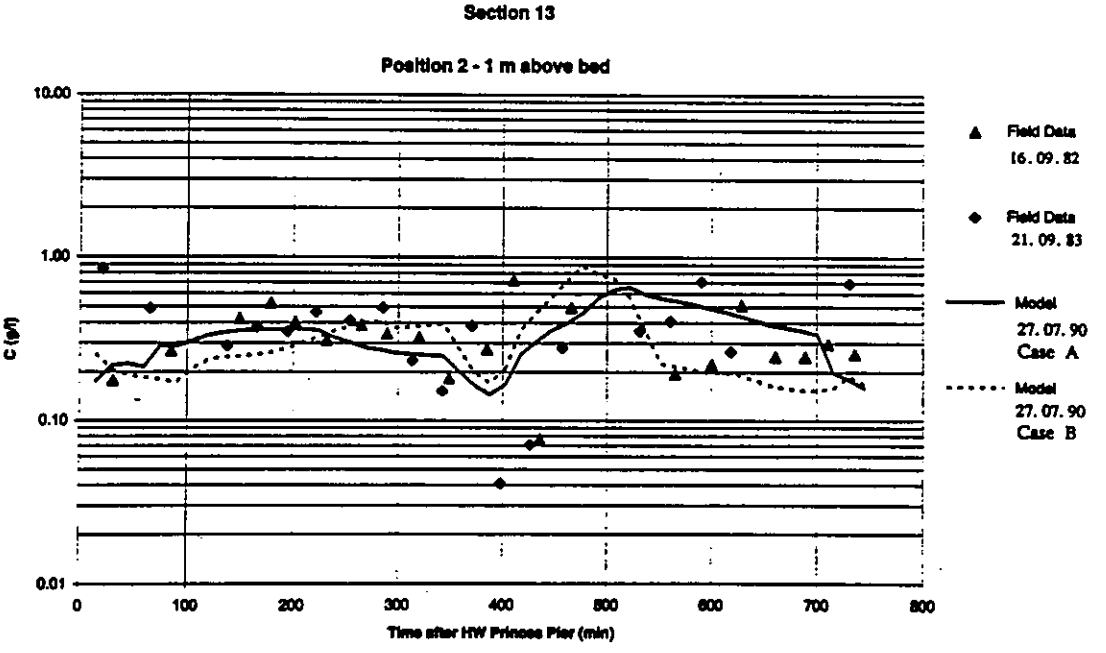

Figure 5.39 Near-bed field data and model simulations at Position 2 in Section 13 of the Narrows.

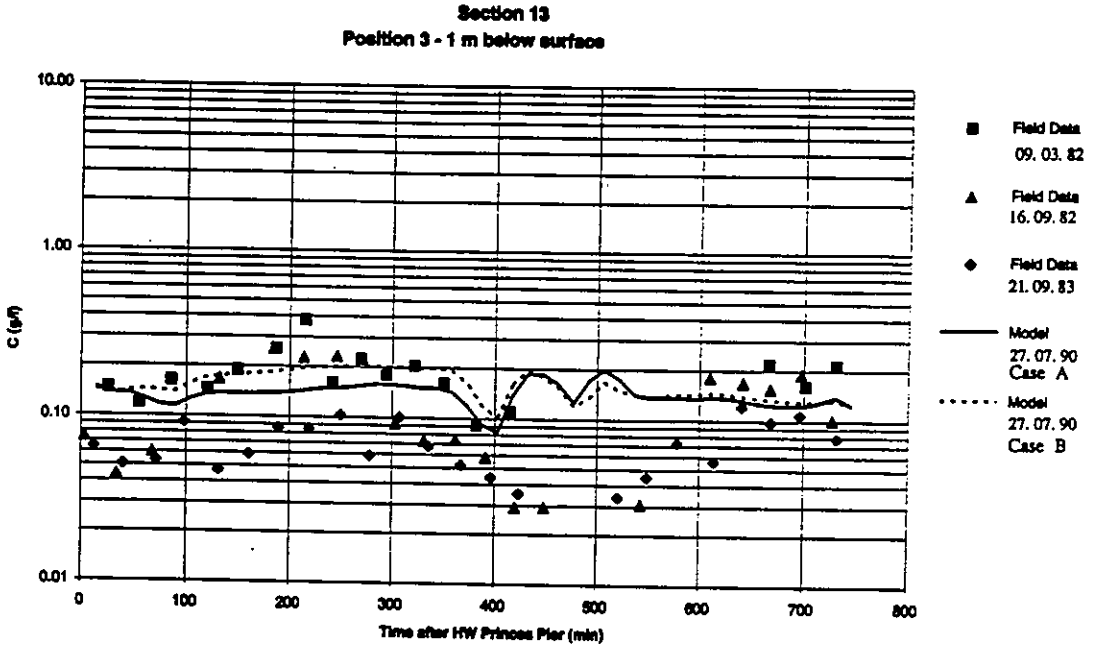

Figure 5.40 Near-surface field data and model simulations at Position 3 in Section 13 of the Narrows.

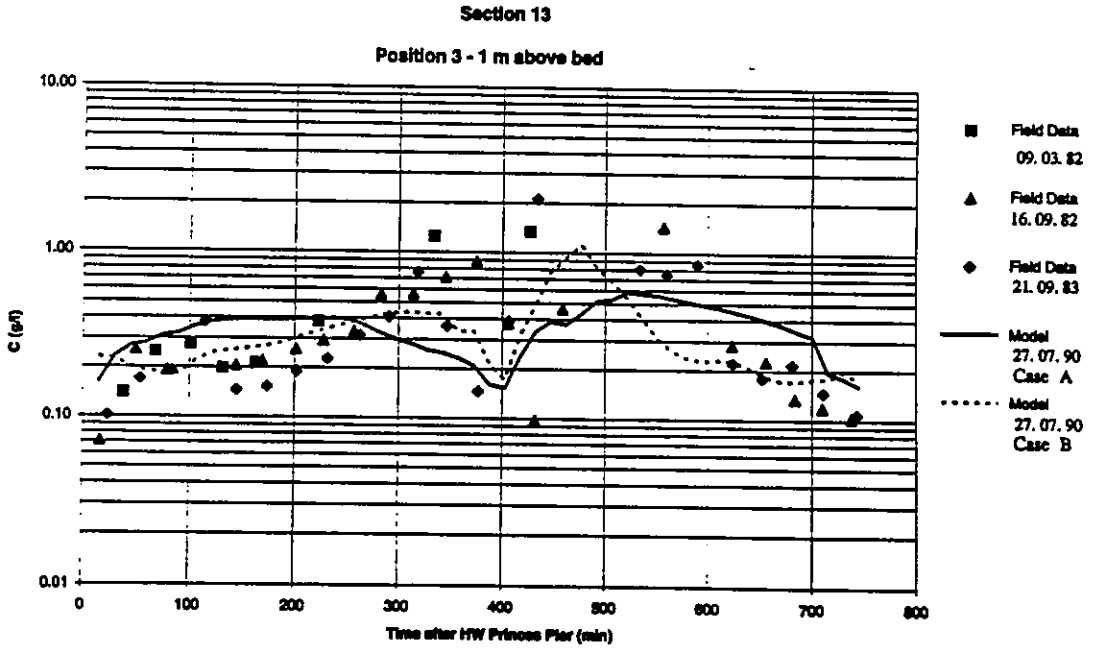

Figure 5.41 Near-bed field data and model simulations at Position 3 in Section 13 of the Narrows.

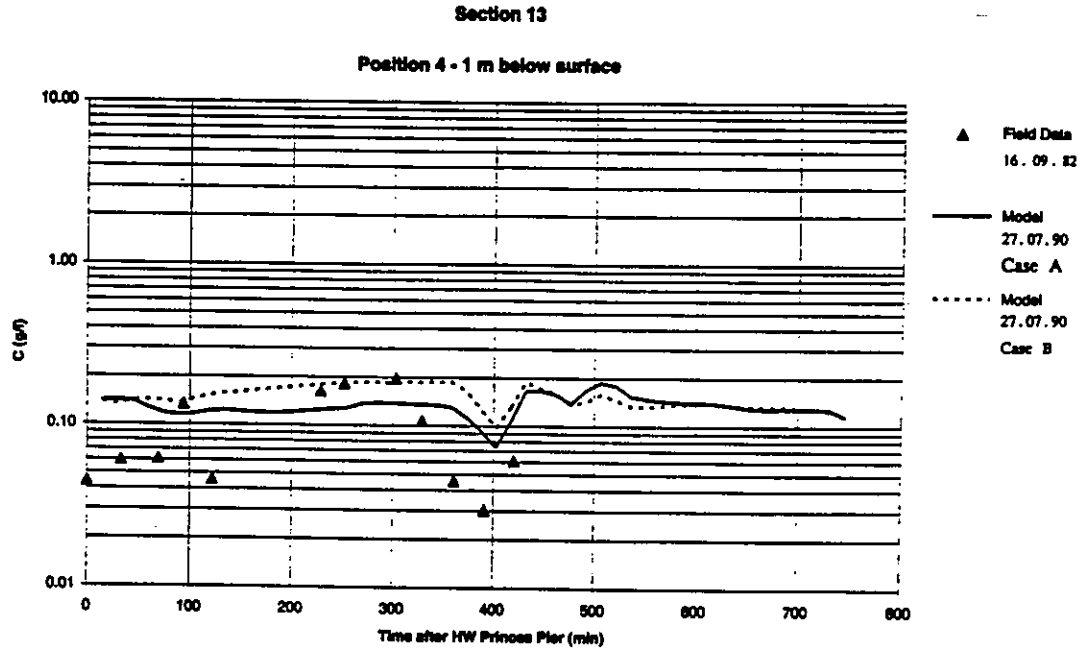

Figure 5.42 Near-surface field data and model simulations at Position 4 in Section 13 of the Narrows.

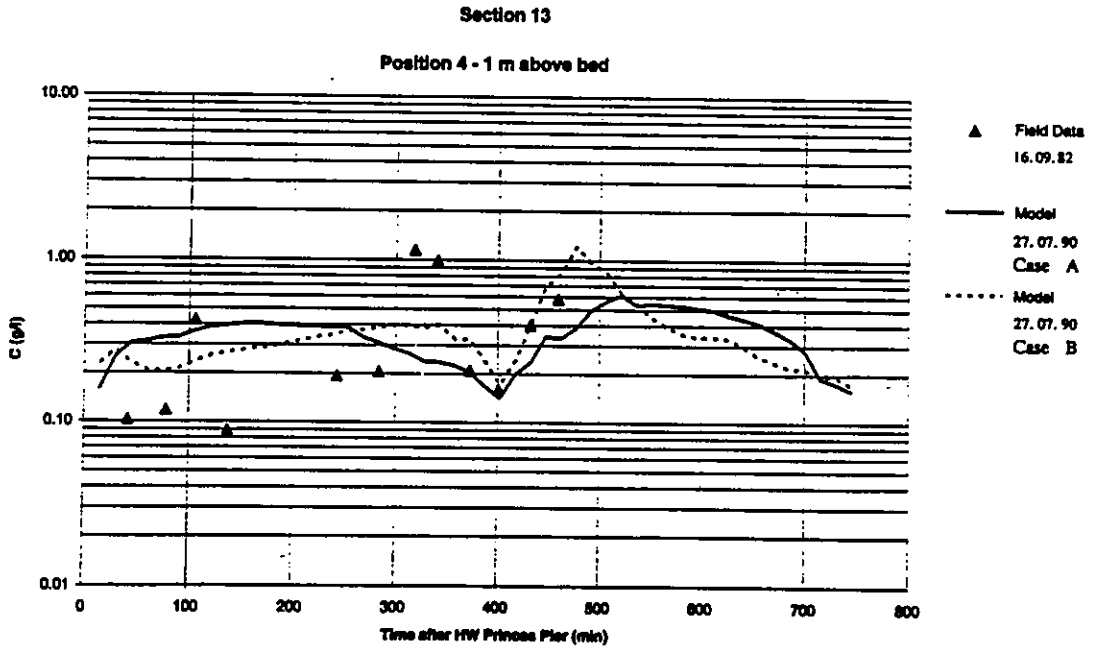

Figure 5.43 Near-bed field data and model simulations at Position 4 in Section 13 of the Narrows.

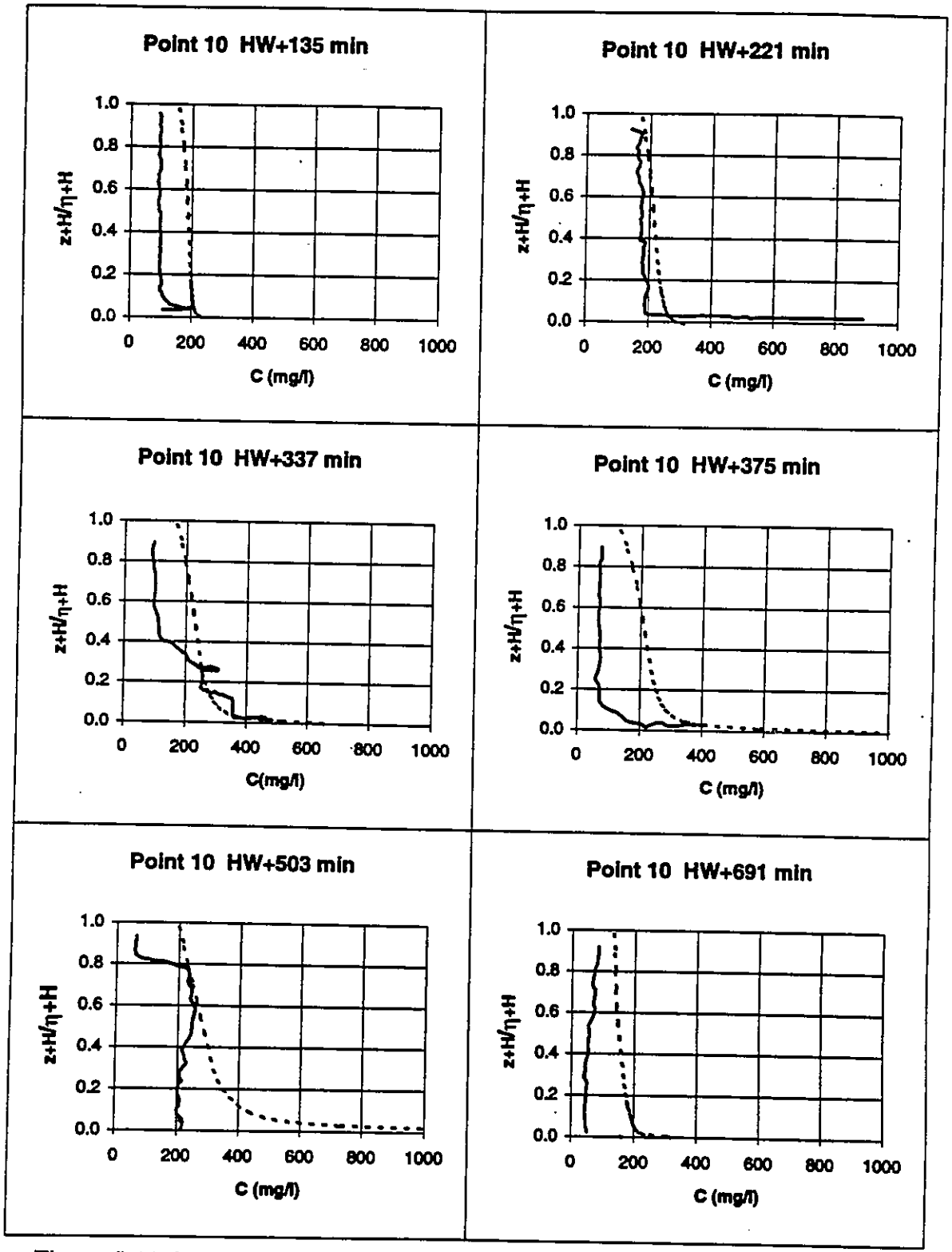

Figure 5.44 Continuous field profiles (full lines - 23.11.91) and model simulated profiles (dotted lines - 27.07.90) at Point 10 in the Mersey Narrows.

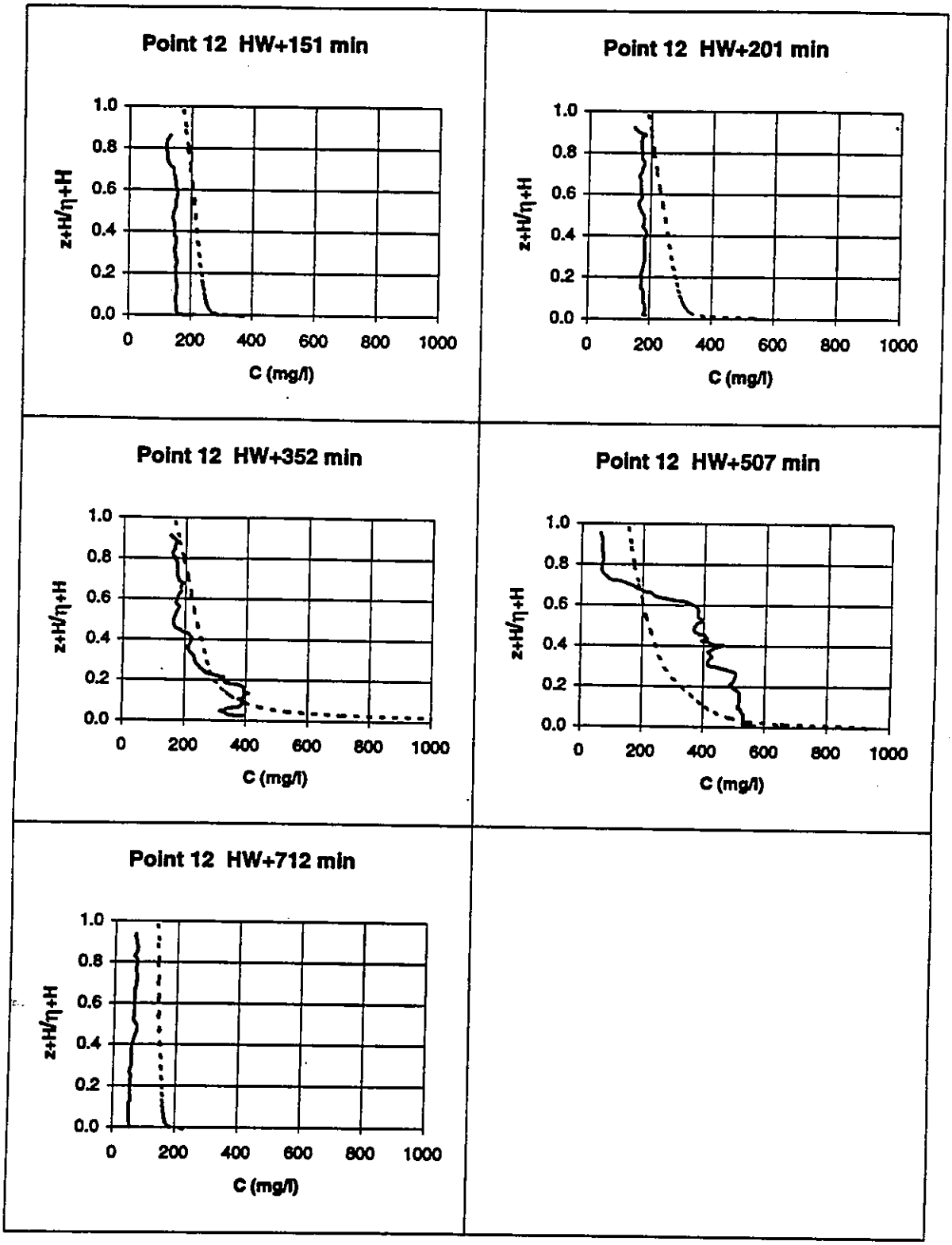

Figure 5.45 Continuous field profiles (full lines - 23.11.91) and model simulated profiles (dotted lines - 27.07.90) at Point 12 in the Mersey Narrows.

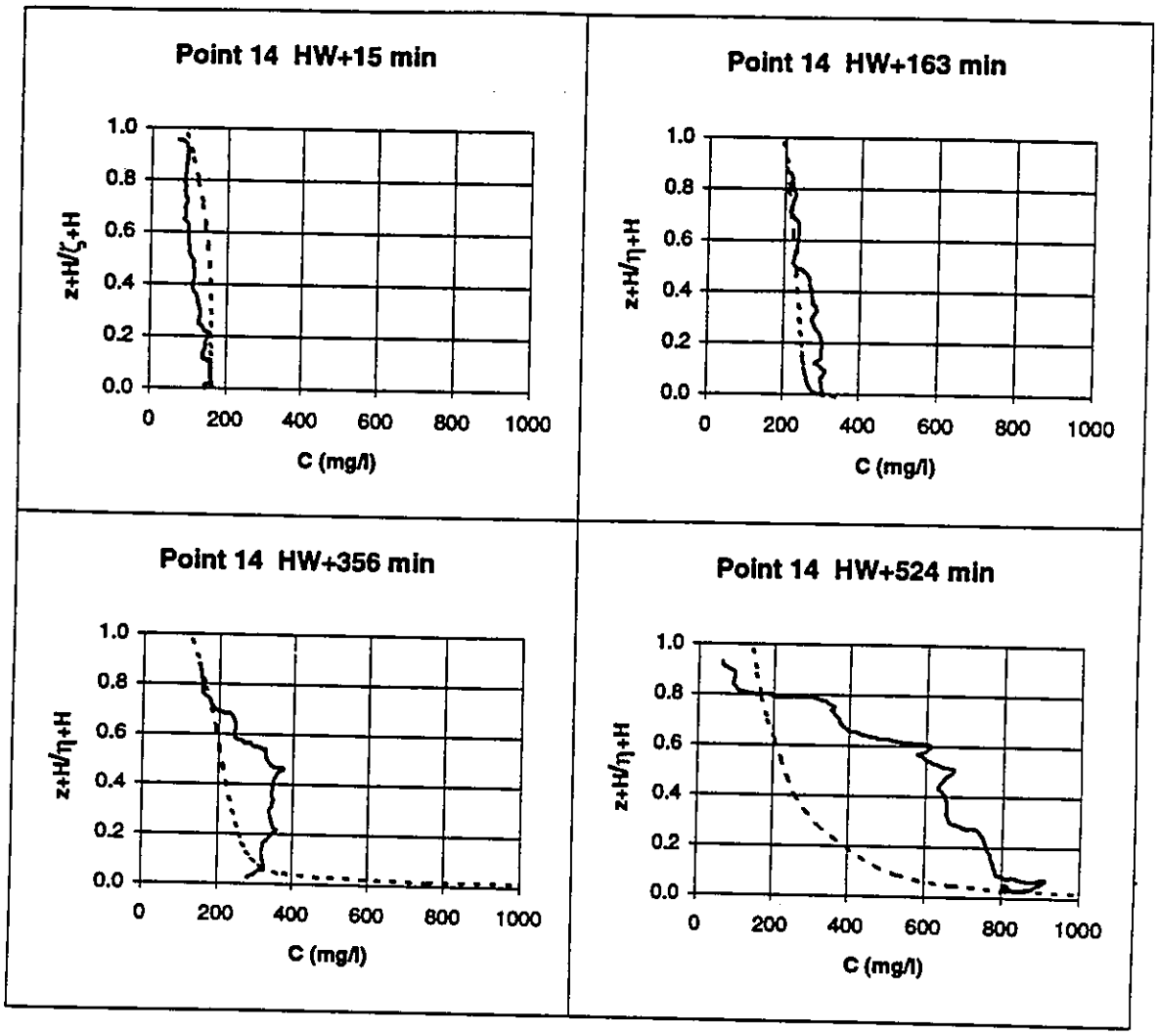

Figure 5.46 Continuous field profiles (full lines - 23.11.91) and model simulated profiles (dotted lines - 27.07.90) at Point 14 in the Mersey Narrows.

The vertical structure of the computed concentration field (reference case) was further investigated through the use of the continuous profiles obtained at Points 10, 12 and 14 during the spring tide of range 8.6 m at Princes Pier on November 23, 1991 (see figures 5.44 to 5.46). Measurement times were, again, normalised relative to those of the July 23, 1990, tide. Depths are also presented in normalised form, due to differences between the natural depths and those resulting from the model grid.

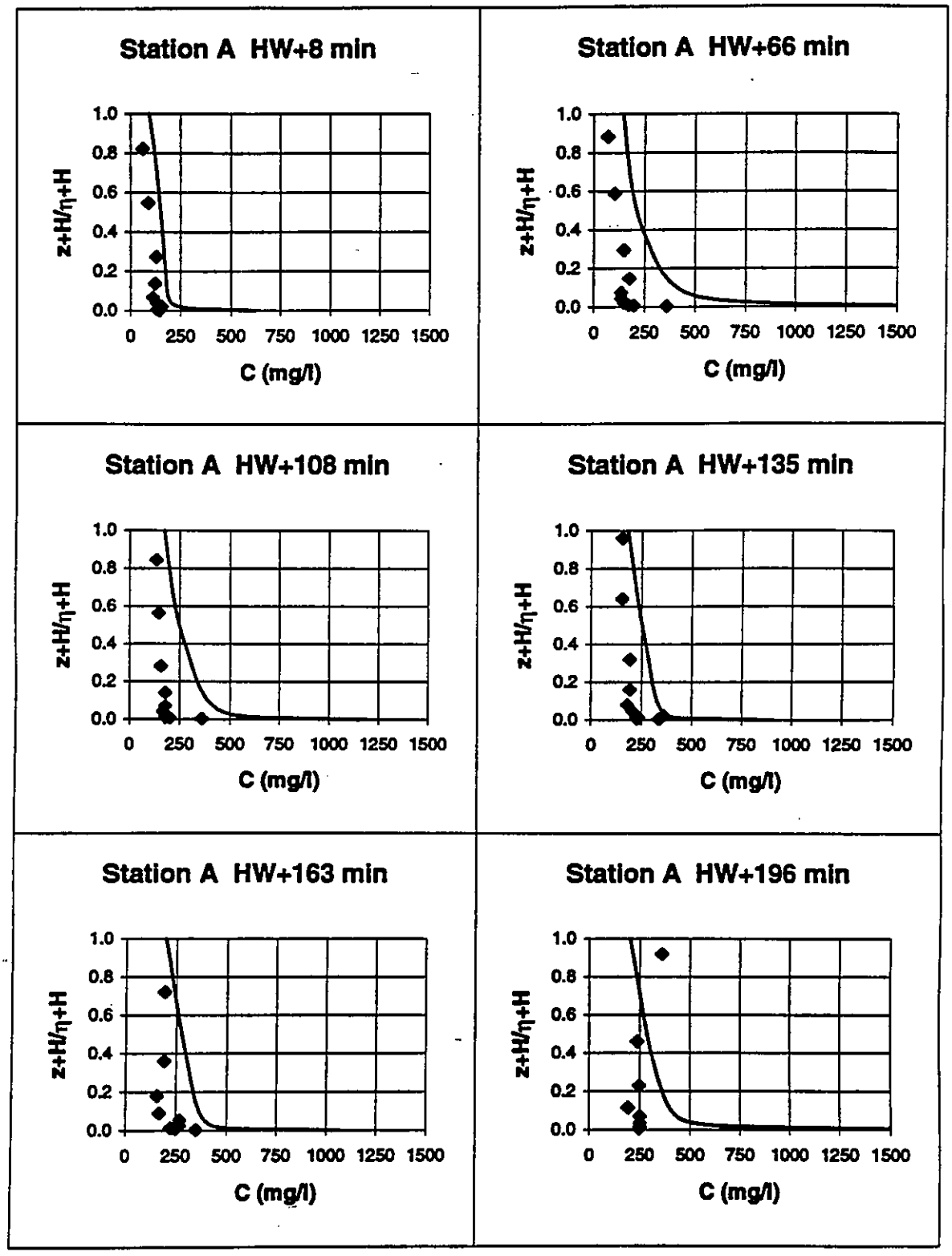

Figure 5.47 Discrete field profiles (02.07.90) and model simulated profiles (full lines - 27.07.90) at Station A in the Mersey Narrows.

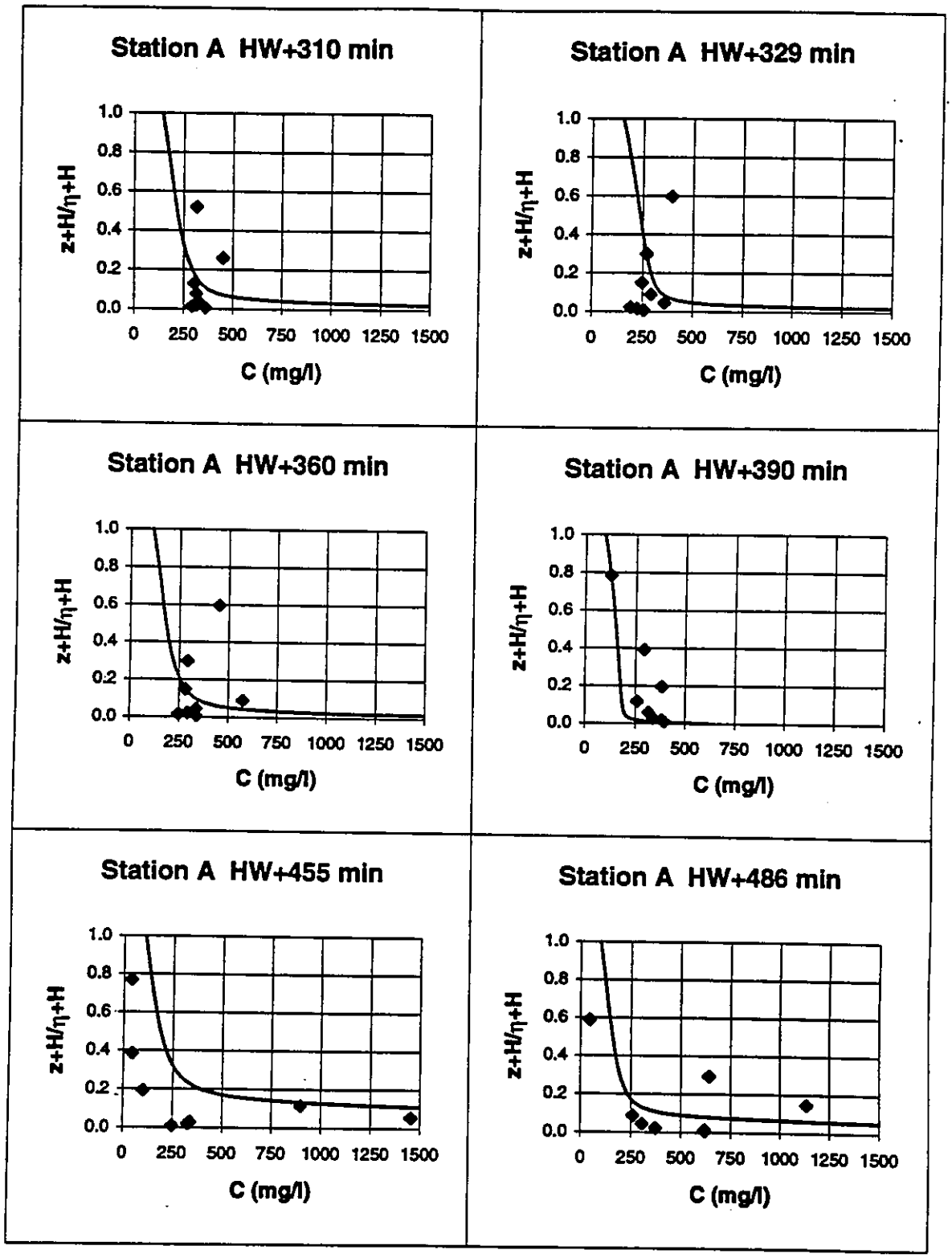

Figure 5.48 Discrete field profiles (02.07.90) and model simulated profiles (full lines - 27.07.90) at Station A in the Mersey Narrows.

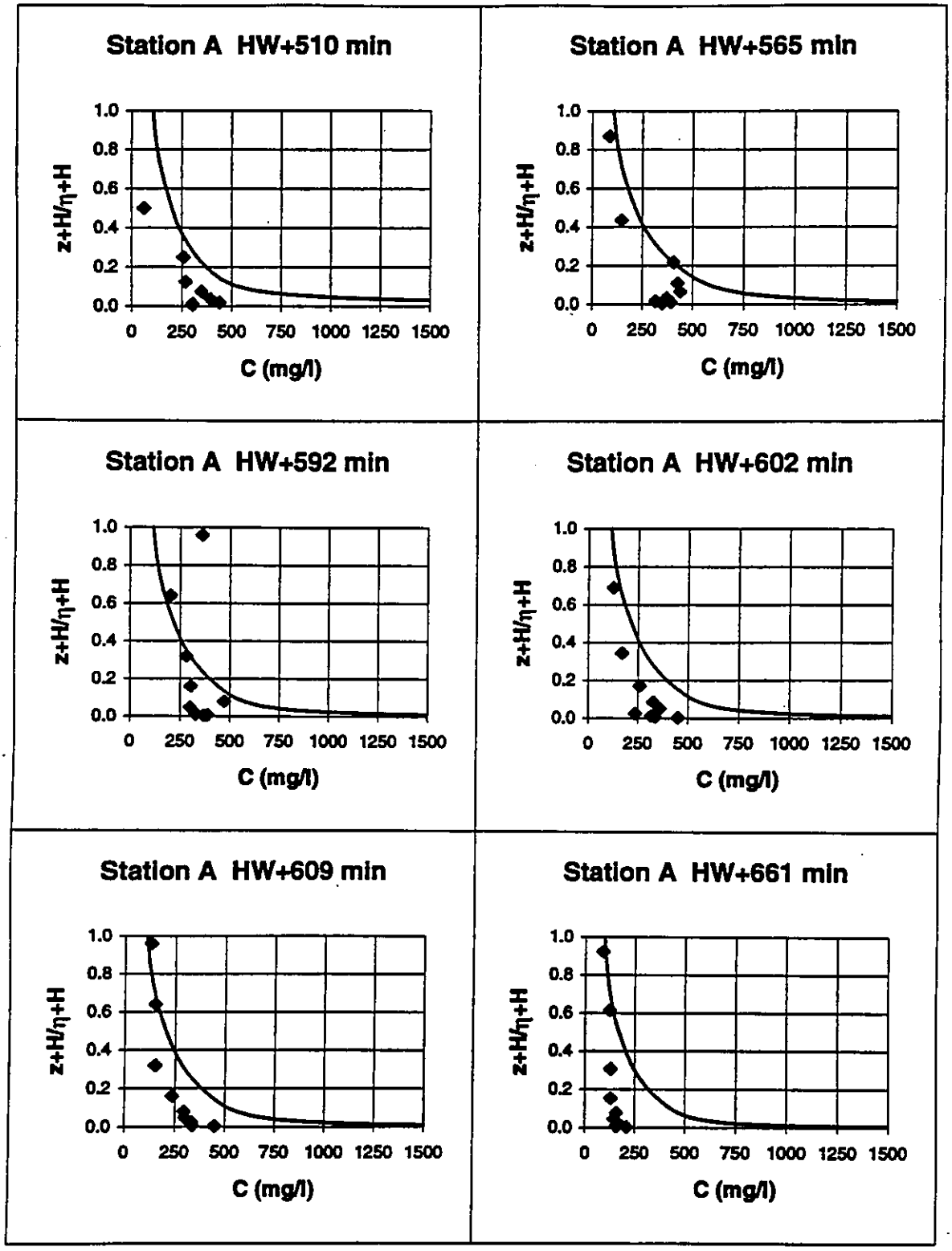

Figure 5.49 Discrete field profiles (02.07.90) and model simulated profiles (full lines - 27.07.90) at Station A in the Mersey Narrows.

The model is found to simulate reasonably well the concentration magnitudes and the general trends of most field profiles. High near-bed concentrations produced by the model cannot be adequately evaluated, given the difficulty in obtaining measurements close to the bottom (as confirmed by the elevations of the lowermost points in most profiles). Nevertheless the shape of some of the field profiles seems to indicate that high concentrations should be expected near the bed, if adequate measurement techniques are used in future studies. An obvious difference between model and field data is related to the fine details of the vertical concentration structure which are not simulated by the model. In fact, the simulation of lutocline formation can hardly be expected for the range of concentrations found in the Mersey (mostly in the flocculation settling range), given the process models adopted for settling and vertical diffusion. The need for improved descriptions of such processes, possibly including mutual interaction, is, again, apparent.

A second comparison was carried out using results from the reference case and the discretely sampled profiles at Station A near the proposed barrage line during the spring tide of range 8.4 m in November 2, 1990. The suspended concentrations of the fine fraction (diameters from 0 to 63 μm) are shown in time and depth normalised form in figures 5.47 to 5.49. Again, and although some field points seem inconsistent, the magnitude and general trends of the data are reasonably represented. Despite the lack of near bed resolution of the field measurements, it is confirmed that high concentrations can be expected in the Mersey Narrows at certain stages of the tide.

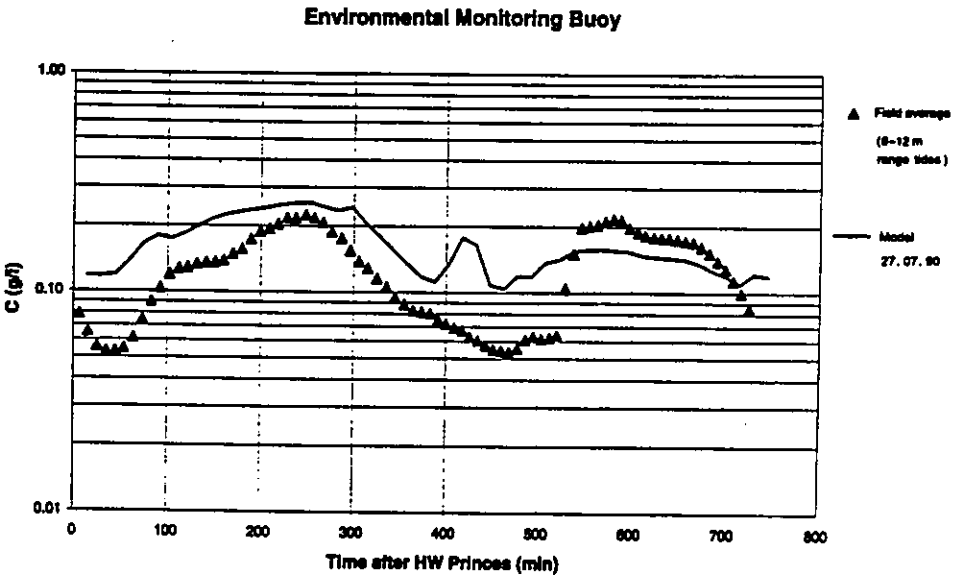

Figure 5.50 Model computed versus averaged concentrations over several spring tides at the Environmental Monitoring Buoy.

Finally, the near-surface concentrations computed for the reference case in the vicinity of the Environmental Monitoring Buoy were compared with the values, averaged over several spring tides, of the observed concentration represented in time-normalised form (figure 5.50). Although a direct comparison should be attempted with caution, due to the different nature of both data sets, it is observed that, during most of the tidal cycle, the model simulation corresponds reasonably well to the trend of the field averaged data, with the exception of near-slack water periods, as mentioned in previous comparisons.

5.5 Summary and Conclusions

Model SUSMUD3 was run for a spring tide condition in the Mersey Narrows using process modelling and sediment characterisation data provided by HR and MBC. The model was applied in a decoupled way, using hydrodynamic information and sediment concentration boundary conditions resulting from a previous run of model TIDEFLOW3D of HR for the same estuary.

Model operation and the values of some process defining parameters were improved during a series of preliminary runs. Changes introduced at that stage were imposed by the need to simulate near-slack deposition/erosion sequences and, once again, stressed the need to improve modelling and parameterisation of vertical transport processes.

Model simulations performed with a reference set of parameters were consistent with the results of the numerous studies carried out in the past in the Mersey estuary and reproduced well the expected global features of a fine suspended sediment concentration field under tidal action. In particular, vertical stratification in the water column, settling/deposition and erosion/re-entrainment sequences around slack water were observed. In order to allow a more detailed evaluation, model output was compared with field data from selected points and verticals, for which results from previous studies, carried out under different tidal ranges, were available.

Within the limitations of existing data sets and, in particular, their non-synoptic and local nature and the lack of near-bed resolution, the vertical structure of the computed concentration field was evaluated. The performance of the model was tested with two different formulations for the vertical mass diffusivities and it was possible to confirm that a time-dependent formulation may produce better results than a formulation using coefficients which are constant in time. It was also recognised, through comparison between computed and measured profiles, that, while the model was able to correctly simulate the magnitude of the concentrations measured in the field and, in general, the trends found in the vertical profiles, it was not possible to reproduce the finer structural details which are apparent in the field data. High near-bed concentrations detected in some of the field profiles were reproduced by the model but only improved data sets will allow a more complete characterisation of this phenomenon.

Evaluation of the results obtained, therefore, suggests that further improvements in the model and in the way it was applied should be attempted. Such improvements and, in particular, more complex formulations for the vertical settling and diffusive mass fluxes are expected to produce a finer description of the vertical concentration structure found in estuarine environments. It seems, therefore, that, in order to improve the performance of model SUSMUD3 for engineering applications in low to medium concentration environments, a number of steps need to be considered.

a) Using the model in a completely interactive way, with a fully 3D hydrodynamics driver (i.e. computing also vertical velocities) and a salt transport model.

b) Carrying out a detailed calibration study of the hydrodynamic field for each application case and, in particular, in connection with the bottom shear stresses which control erosion and deposition. The choice of an upper value of the time step for the numerical simulations, based on the evolution of the bottom shear stress near slack water should be considered.

c) Introducing in the coupled models more sophisticated turbulence closures, in conjunction with an improved description (i.e. as a function of turbulence parameters) of the aggregation/breakup dynamics of flocs and of their respective settling velocities. This approach does not necessarily imply, in a first stage, the development of a multiple size class approach (see, for example, Le Hir et al., 1993; Malcherek et al., 1995).

d) Carrying out tests with the vertical component of the model or with the simple vertical one dimensional model described in Chapter 4, in order to further investigate the vertical structure of concentration profiles and improve the simulation of vertical fluxes. It is possible, as indicated by runs of the vertical 1D model, that an upper value of the time step is also imposed by the need to simulate the time evolution of the finer structural details of the profile.

Again, testing of the above modifications would require improved field and laboratory data sets to be obtained, a difficult requirement, particularly in connection with the vertical dynamics of fine sediment. In fact, the nature and quality of such sets for validation purposes seems to be the critical issue for modelling progress at the present time. The costs of developing and running more complex codes should also be considered and carefully weighed in terms of the accuracy requirements for each application.

Nevertheless, and despite the difficulties and limitations related to the type of application which was carried out, it was possible to confirm that three-dimensional single sediment class models, using appropriate process model parameters, determined either in the field or through careful laboratory experiments, and considering fine near-bed discretisations are an extremely useful tool for a wide range of applications. Such models represent, in terms of vertical resolution and modelling of exchanges with the bed, a considerable improvement relative to classical 2DH models and, given current computing capabilities, are also an inexpensive tool to be used for engineering purposes and overall studies of estuarine systems.

CHAPTER 6
MODELLING OF TRANSPORT IN NEAR-BED HIGH CONCENTRATION LAYERS

6.1 Introduction and Objectives

Although the existence of near-bed high concentration sediment layers in estuaries has been known for decades (see, for example, Kirby, 1989), the extent of their importance in the dynamics of turbidity maxima, in the siltation of navigation channels, locks and port basins, in the transport of pollutants by sediments and in altering the conditions for the development of benthic fauna and flora has only recently been fully recognised. The Bingham plastic rheologic behaviour often attributed to high concentration cohesive suspensions (see figure 6.1), which implies that, for typical estuarine boundary layer shear velocities, such suspensions cannot flow, has induced a rather restrictive description of their behaviour, as noted by Kirby (1989). In fact, those ideas may suggest that dense suspensions can locally adjust on slopes but couldn't be expected to move along the bottom and, consequently, can only influence vertical sediment dynamics rather than have a significant advective contribution.

The development of new types of field equipment in the early seventies allowed important features to be recognized and, in particular, the mobility of dense layers and their discontinuous nature in space. Furthermore, horizontal velocities of similar magnitude but, in certain cases, different circulation patterns, relative to those of the

low concentation suspensions above, were detected in the dense layers. The need to correctly simulate the creation, evolution and destruction of the latter immediately became apparent from these field tests, not only to correctly model sediment dynamics in the low concentration layers (modification of the classically assumed exchange mechanisms with the cohesive bed is needed) but also to enable the description of advective sediment transport in the high concentration layers themselves.

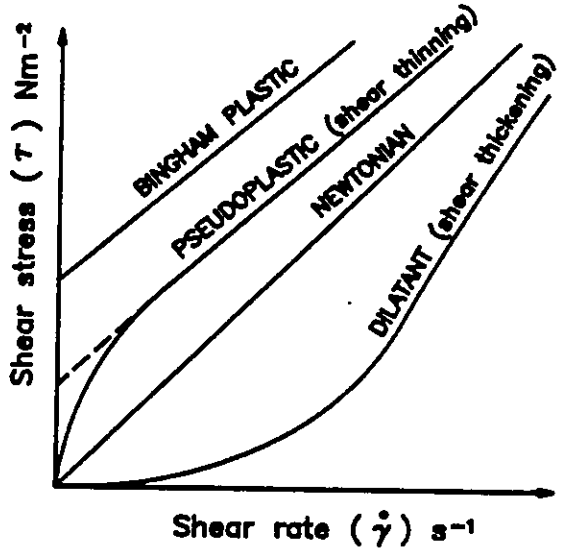

Figure 6.1 Idealised equilibrium shear stress/shear rate curves for typical materials (adapted from Kirby and Parker, 1977).

The key factors for the generation of high concentration layers due to natural causes are generally considered to be fine sediment availability and adequate energy levels in a given environment. Often the formation of such layers has been explained through intense flocculation and rapid deposition during slack water periods or through fluidisation of settled deposits during storm events. Anthropogenic activities, like dredging and disposal of cohesive sediments, can also cause the generation of high concentration layers, since bed disturbances by moving dragheads, dredger hopper

overflows and dumping at disposal sites can release large amounts of fine material into the water column.

In this chapter a depth-averaged mathematical formulation for describing the dynamics of near-bed high concentration suspension layers is developed (see Section 6.3). The formulation is derived for mobile thin to medium thickness layers, i.e. those which do not present a significant vertical structure or large vertical variations in either density or horizontal velocity. These layers are assumed to be dominant in most estuaries, as very thick, structured layers have only been described in a limited number of environments. However, and contrary to existing depth-averaged formulations which assume a constant density value in high concentration layers (see, for example, Odd and Cooper, 1988), the formulation derived in this chapter allows for time, longitudinal and lateral variations of the bulk density, as indicated by recent field studies (HR, 1990c; HR, 1991b).

The physical evidence leading to the development of the mathematical formulation is also presented in this chapter. The main findings concerning the global dynamics of high concentration layers, resulting from field studies, and the basic assumptions derived from them are presented in Section 6.2, while the mass exchange processes of interest for the creation, evolution and destruction of such layers are described in Section 6.4. Details of a pilot numerical model, which was developed to test the proposed formulation, are presented in Section 6.5. This model is intended, ultimately, to produce an improved bed boundary condition for the transport models used to

describe the dynamics of low concentration suspensions (see figure 2.3 for a schematic description) in those cases where near-bed high concentration suspensions exist. Application of the pilot model to simulate a laboratory experiment is described in Section 6.6. Finally, a summary of the main conclusions derived from this chapter is presented in Section 6.7.

6.2 General Aspects of the Problem

6.2.1 Basic Concepts

One of the main problems found when modelling cohesive sediment dynamics in estuaries is related to the transition between the low concentration suspensions found in the upper layers of the water column and the structured bed. Field evidence shows this transition, whose features largely depend on the amount and nature of the available sediment and on the energy of the estuarine environment, to happen through a broad grading of water-sediment mixtures which can qualitatively be divided into sub-zones of *muddy water*, *watery mud* and *firm mud substrate* (Kirby, 1989). Such sub-zones can more adequately be described as (see figure 2.3):

(i) *low concentration mobile suspension layers* (usually occurring over most of the water column), which consist of fluid-supported, relatively disperse, assemblages of particles having both horizontal and vertical components of movement;

(ii) *high concentration near-bed suspension layers*, which consist of fluid-supported but relatively dense assemblages of particles, showing vertical mobility: these suspensions can be either horizontally mobile or stationary;

(iii) *cohesive bed layers*, which correspond to dense assemblages of particles in which a solid particle framework has formed, part of the total stress being carried by this structure (effective stress) and the remaining by the fluid (pore pressure).

Based on empirical knowledge it would seem that, in order to separate the two last layers, the characterisation of the cohesive bed would present no difficulties. In fact, the definition and location of the *hard bed*, a fundamental piece of information for modelling sediment movement, building maritime structures and ship manoeuvering, is a rather difficult task and has been discussed in several papers (see Parker, 1986 and Parker, 1989, for example). Since a single criterion, of general applicability, is not available until present, the *bed* has been defined in a number of ways. Definitions can be grouped under *hydrodynamic*, *methodological* or *operational* headings, depending on whether the zero velocity (or movement) level, the nature of the instrument or method used in the measurement of the depth or the requirements associated to a given activity (navigation, for instance) are chosen as the most relevant criterion (Parker, 1989).

The cohesive bed structure is time dependent and its evolution is a consequence of self-weight consolidation and of fluid stress loading. Changes in the structure may drastically alter the volume occupied by a given mass of sediment and are accompanied by concurrent changes in bed properties, which are thought to give rise to resistance to erosion (Parker, 1989). The development, from a dense suspension, of a three dimensional space-filling framework, which indicates the development of a bed, is strongly influenced by the volume occupied by a given mass of sediment and is also a consequence of the previous shear history and sedimentation rate (Sills and Elder, 1986). However, the non-uniqueness of the mass to volume transform for cohesive sediments suggests that an appropriate parameter for defining the presence of a cohesive bed is, in fact, related to the detection of a continuous sediment structure (Parker, 1989). The development of a structure could, then, be characterised either through the detection of the development of effective stresses (which are small and not directly measurable) or through a critical solids volume fraction (volume of solids divided by the total volume). The value of this critical solids volume fraction, defining the so called *gel point*, is, again, strongly dependent on material parameters, such as interparticle forces, particle size and shape (Toorman, 1992).

Regarding high concentration suspensions, it should be mentioned that, despite their obvious importance, they had not been extensively detected until recently, and, indeed, have only been well described in a limited number of estuaries, where the thickness of the layers (up to several meters) made it difficult to ignore them. However, it is possible that, basic physical processes being the same in all estuaries, such

suspensions exist in most fine sediment environments. Odd and Rodger (1986), for example, pointed out that observations in many estuaries have indicated siltation rates which cannot be accounted for solely by considering the transport of suspended mud and can only be explained by the movement of thin layers of high concentration suspensions.

In certain cases, due to limited sediment supplies or inadequate energy conditions, high concentration layers are probably too thin to be detected, given the vertical resolution of conventional field techniques. While such layers may be too small to noticeably influence overall estuarine sediment dynamics (probably the reason why, in the past, classical erosion/deposition concepts have successfully been applied in system modelling) their influence on local phenomena, otherwise unaccountable for, has also been hypothesised. This is the case, for example, of rapid siltation phenomena in lock entrances, docks and navigation channels in many ports in the world.

Observations have recently been made in the Firth of Forth at Grangemouth (1989), using an oscilloscope and an echo sounder, capable of measuring bed levels to an accuracy of better than 0.1 mm (HR, 1990d). The field results showed that:

(i) the bed level, usually identifyable as a strong echo, was, at times, indistinct, the transition to the overlying suspension taking place over 1 or 2 cm;

(ii) on one occasion during the observation period a phenomenon was detected that seemed to correspond to the flow of a very thin (5 mm) mud layer down a steep bank.

These features seem all the more relevant as Grangemouth cannot be classified as a particularly high turbidity environment.

A widely used qualitative expression to describe high concentration suspensions is *fluid mud*, which will be used in this text for simplicity. Hydrographic surveyors apply it to stationary high concentration layers detectable by echo-sounders while the engineering concept is broader, encompassing mobile layers as well (Kirby, 1989). The latter concept will be adopted hereafter (see also figure 2.3). Fluid mud is defined by Odd and Cooper (1988) as a dense suspension containing a concentration of mud flocs which is high enough to significantly change the physical properties of the mud/water mixture compared to those of clear water, at the same salinity and temperature. Toorman (1992) defines fluid mud as a high concentration cohesive sediment suspension with a sediment volume fraction above the gel point, i.e. in a range corresponding to a bed whose structure was just broken, with only minor changes in concentration. The former definition, less restrictive, will be adopted in the present work, given the field evidence described in Section 6.2.2.

In terms of the concentration range for fluid mud, Odd and Cooper (1988) indicate values of 60 to 120 g/l but, more typically, a value of about 75 g/l. Toorman (1992)

considers that, below a concentration of 50 g/l the sediment/water mixture is just *dirty water* and behaves in an almost Newtonian way, as water, in agreement with Odd and Rodger (1986): at higher concentrations the mixture would become non-Newtonian and increasingly slurry-like. The problem can be stated in broader terms, i.e. can fluid mud be uniquely characterised in terms of concentration and, if that is the case, what are the upper and lower concentration limits which can be used to distinguish fluid mud from the cohesive bed below and the low concentration suspension above?

Regarding a possible concentration lower limit, values ranging from 3.5 g/l to 10 g/l are cited by Kirby (1989) and Toorman (1992), on grounds of the concentration at which hindered settling effects are first observed. As shown by field curves of settling velocity versus concentration, obtained in different environments, there is a clear dependence of W_s (and, of much higher importance, as noted by Ross and Mehta, 1989, of the settling flux) on the type of sediment and on the local hydrodynamics under which flocs are formed and, consequently, it is not surprising that a single, concentration-based, lower limit, in connection with hindered settling, is not found.

Furthermore, and besides the dependence of the critical solids volume fraction on sediment properties, mud can behave as a dense suspension, instead of as a soil, at very similar densities (see Section 6.4.4), fluidisation or liquefaction of the soil being sufficient (Toorman, 1992). Therefore, as happens with a possible lower limit, an upper limit cannot be adequately defined in terms of a given concentration. The sediment volume fraction at the gel point indicated by Toorman (1992), based on

consolidation experiments, had a value of approximately 0.05 for Scheldt mud, while Parker (1989) indicates for Zeebrugge mud a value of approximately 0.07 (133 g/l and 186 g/l, respectively, in terms of mass concentration, if a value of 2650 kg/m^3 is adopted for the solids density). Both values of this critical sediment volume fraction agree well with the range of values found in the literature (as discussed by Toorman, 1992).

The non-uniqueness of concentration-based limits, as a consequence of sediment properties and local hydrodynamics, suggests that concentration alone is not a sufficient parameter for defining fluid mud and should be supplemented by other physically-based criteria. The concept of a lutocline layer (a zone of rapid change in the gradient of the concentration profile) separating zones of near constant concentration may provide an additional criterion. In fact fluid mud is separated from the low concentration suspension above by a lutocline which, as already mentioned, seems to be related to the onset of hindrance in settling fluxes and from the cohesive bed below by the lutocline corresponding to the development of a solid particle structure (Ross and Mehta,1989).

Acoustic techniques are commonly used to detect interfaces in water/sediment suspensions, as sound waves are reflected at discontinuities between two media (Urick, 1983). High frequency waves used in such studies are reflected due to acoustic impedance (density dominated) gradients between layers but such reflections are also influenced by the roughness of the interfaces (Urick, 1983) and do not relate to

specific density values. Higher frequency systems detect much smaller density changes and thus less well consolidated suspensions (Parker and Kirby, 1982) and, consequently, double frequency echo-sounders are commonly used in the field. The lower frequency (usually about 30 kHz) is used to detect the more solid cohesive bed, while the higher frequency (usually about 200 kHz) is also reflected at the fluid mud/low concentration suspension interface.

6.2.2 Field Evidence

In order to build a framework for studying fluid mud, so that a mathematical description is possible, it is important to summarize the main features, supported by field observations, related to the production, movement and destruction of fluid mud layers. These features can be found in papers by Kirby (1989 and 1992), Kirby and Parker (1977) and Parker and Kirby (1982) and describe observations in the Severn estuary and in the Maas estuary, a tributary of the Rhine.

The Severn is a large and exposed estuary with predominantly erosional shores, with very high tidal range and large spring-neap differences, having small river discharges and being well mixed with respect to salinity and temperature. The Maas is a narrow, canalised and sheltered estuary with banks stabilised by training works and overdeepened through continuous dredging. It generally shows low turbidity, with a relatively low tidal range and is highly stratified with respect to salinity and temperature. The fine sediment regimes of estuaries as different as the Severn and the

Rhine can also be contrasted. In the Severn the regime is dominated by tides and perturbed by episodic storm events while in the Rhine it is strongly influenced by its gravitational circulation but dominated by storms.

Further field data have recently been obtained by Hydraulics Research (HR, 1990c; HR, 1991b) in a straight and canalised reach of the Parrett estuary, a branch of the Severn where a significant fluid mud layer develops over the slack water period. The measurements were carried out during spring tides and allowed the vertical structure of the layers to be investigated.

Mechanisms leading to the formation of fluid mud in the Severn and in the Maas seem to be different. In the deep channels of the Severn at spring tides, an initially homogeneous vertical concentration profile (at maximum ebb or flood) develops a discontinuity caused by settling, high in the water column. This discontinuity progressively drops and, by slack water time, separates a low concentration layer from a 2 to 3 m thick near-bed high concentration (perhaps higher than 20 g/l) layer. At this time the lower layer becomes stationary for a short period before being re-entrained and destroyed by the accelerating flow. A typical sequence of turbidity profiles measured in a channel of the Severn is shown in figure 6.2. A similar phenomenon occurs during neap tides but, due to lack of energy to completely re-entrain the fluid mud layers, these can persist for several intermediate tides of the neap-spring cycle. In the Parrett, as happens in the Severn channels, thick layers of fluid mud also form after the slack water period, showing average concentration values ranging from 20

g/l, when forming, to over 70 g/l. In the Maas, a fluid mud layer was detected entering the estuary after a major storm event in the North Sea, possibly resulting from wave fluidisation of settled deposits.

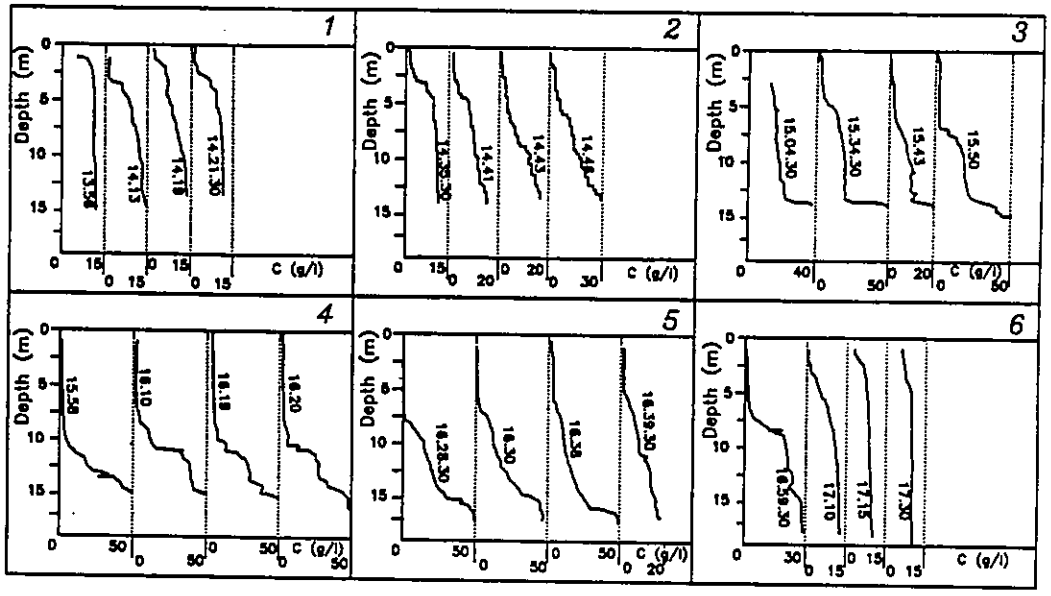

Figure 6.2 Typical time series of vertical turbidity profiles in the Severn Estuary (adapted from Kirby and Parker, 1977). Labels on curves are measurement times (hr.min.sec).

Mobility of fluid mud layers was not an expected feature until developments in field instrumentation allowed fluid mud movements to be detected. In the Severn, dense fluid mud layers, formed during neap tides and persisting during the following tides, separated from the above suspension by stable lutoclines, are tidally advected without vertical mixing, possibly even eroding the bed. The repeated movement of high concentration layers during late stages of a sequence of neap tides causes them, possibly through bottom friction and the development of an incipient internal structure, to be longitudinally divided into smaller pieces (nucleation process). The movement,

at this stage, takes place under the form of *slugs* or *pulses*, prior to stagnation to form localised stationary suspension pools. On the succeeding neap to spring tide transition most of the longitudinally segregated layers are eroded and remixed up into the low concentration layers again. A similar advective situation was found in the Maas where a dense suspension was locally detected at a measuring station, moving at the bed against the tidal flow. The dense layer (undetected at other stations) which, eventually, stopped flowing past the measuring point had the form of a narrow *ribbon* of sediment, comparable to the features found in the Severn. In the Parrett, fluid mud was observed to form and flow seaward while the water above was still flowing in the opposite direction. A general feature was that its upper layers were found to flow at velocities, at least, similar to those of the water above. A significant aspect of the dynamics of fluid mud layers seems, consequently, to be that their movement can be partly or totally decoupled from the movement in the overlying water column.

The movement of fluid mud layers in the Severn and in the Maas seemed to end abruptly, in a process that could take only a few seconds, leading to what is described as the *freezing* of the moving *pulses*, although this was not confirmed in the Parrett. Observations in the lattermost estuary seem to indicate that no movement of the fluid mud layers is observed when the concentration exceeds 90 g/l and, in certain cases, lower sub-layers were observed to stop, start dewatering and consolidate while the upper sub-layers were still flowing. Typical velocity and concentration profiles in the Parrett are shown in figures 6.3 and 6.4 in which, in the latter case, the upper sub-layers of the fluid mud can be seen to flow at higher velocities than the overlying

water. An unexpected feature of mobile fluid mud behaviour in the same estuary was the existence of a significant seaward longitudinal slope of the fluid mud-water interface (instead of an interface almost parallel to the water surface), although local effects may have significantly contributed to it.

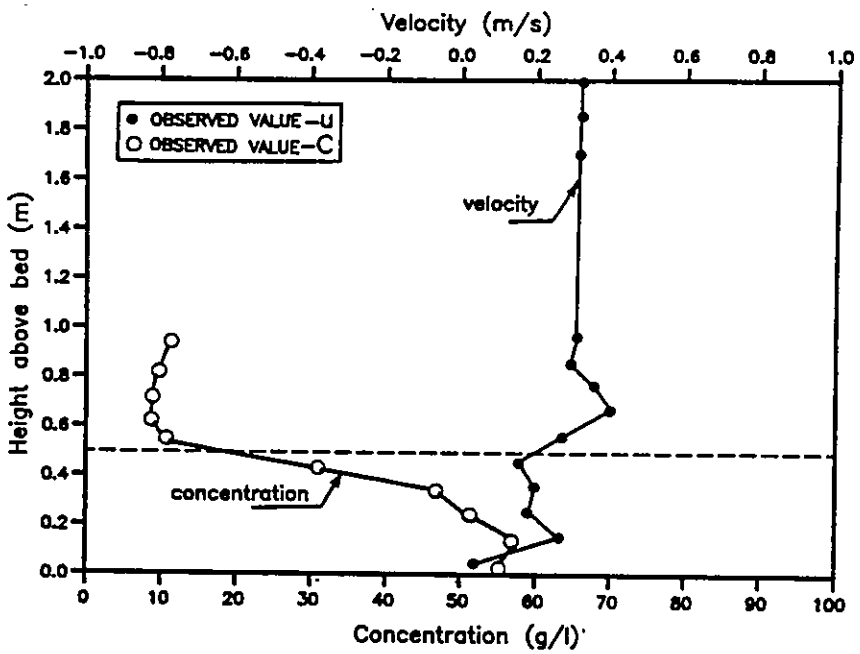

Figure 6.3 Typical concentration and velocity profiles for a fluid mud layer in the Parrett estuary (adapted from HR, 1991b).

Once arrested, internal re-arrangement of the layers and increased density allows them to be detected with echo-sounders. The upper surfaces of stationary layers seem to vary from horizontal to mildly sloping while, internally, multilayering (parallel to the interface rather than the bed) has been observed. In the Maas, the stationary suspensions seem to consolidate towards a settled bed due to lack of natural re-entrainment while in the Severn the layers are destroyed through *erosion* and the sediment is re-entrained into upper zones of the water column in the accelerating flow stages of spring tides or in the neap to spring transition.

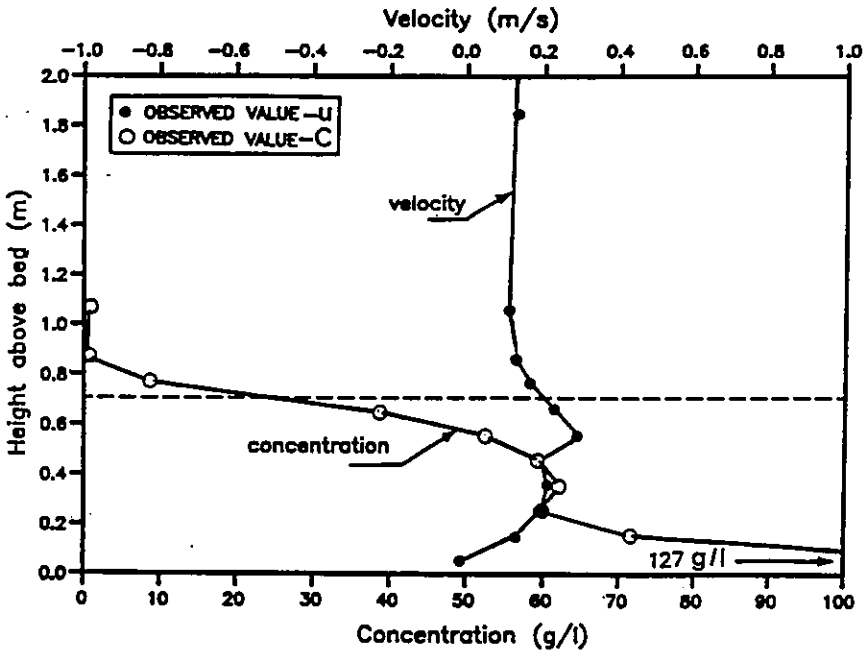

Figure 6.4 Concentration and velocity profiles for a fluid mud layer in the Parrett, showing high velocities in the upper sub-layers (adapted from HR, 1991b).

Summarising, fluid mud may form, under natural conditions, either through rapid vertical deposition from dispersed suspensions, under low energy conditions at rates high enough to prevent immediate dewatering, or through fluidisation of settled deposits during storm events. Once formed, fluid mud layers are able to flow horizontally over the bed, generally in the form of sediment *ribbons*, without vertical mixing and showing partial or total decoupling from the water flow above, eventually splitting up into individual slugs. In certain cases mobile fluid mud layers stop abruptly, although contradictory evidence exists about this phenomenon. Arrested layers can undergo internal structural re-arrangement, and disappear either through

consolidation to produce settled beds or through *erosion* and sediment re-entrainment into the water column.

6.2.3 General Assumptions

Based on the field evidence presented in Section 6.2.2 a number of assumptions will be used to develop a mathematical formulation for the dynamics of thin to medium thickness mobile fluid mud layers (see figure 6.5 for variable definition). Such layers are defined as those which do not present a significant vertical structure or large vertical variations, in either density or horizontal velocity, and are expected to have a range of thicknesses up to tens of centimeters. The assumptions are:

a) Assumption on the low concentration suspension (*clear water*) layers

CW1 The low concentration suspension above the fluid mud can be described as a single layer of incompressible fluid, vertically homogeneous and whose density dependence on salinity and temperature variations can be neglected.

b) Assumptions on the fluid mud layers

FM1 Fluid mud layers are comparatively thin and vertically homogeneous, i.e. a depth-averaged approach is possible (as in Odd and Cooper, 1988); however, the bulk density in such layers can vary in both time and space.

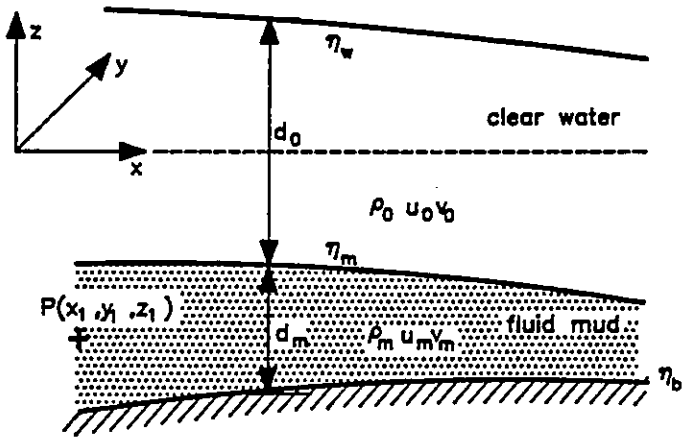

Figure 6.5 Definition of axes and symbols for depth-averaged formulation of fluid mud movement.

FM2 Fluid mud is composed of water and incompressible *grains* (flocs of a single order of aggregation, for simplicity), of known density. The ratio of volumes occupied by the liquid and *solid* (floc) phases is given by a void ratio, e_m, defined as an extension of the same concept for saturated soils, in which the voids are completely filled with water. This voids ratio is defined as:

$$e_m = \frac{V_w}{V_f} = \frac{\rho_f - \rho_m}{\rho_m - \rho_w} \tag{6.1}$$

where V and ρ represent volume and density and subscripts f, w and m denote the flocculated solids phase, the liquid phase and fluid mud, respectively.

FM3 The flow of fluid mud can be decoupled from that of the low concentration suspension above, whose effect is only exerted through pressure gradients and shear stress at the interface and through mass exchanges.

FM4 Fluid mud shows no lower value of the shear strength below which no motion is detected (i.e. it can be assumed Newtonian), although a value of concentration above which no motion takes place seems to exist; the viscosity of fluid mud is significantly higher than that of water (HR, 1991b).

c) Assumption on the cohesive *bed*[1]

CB1 The cohesive bed is a saturated soil for which a void ratio, e_b (subscript b denoting a bed layer), is defined in terms of the flocculated material as:

$$e_b = \frac{V_w}{V_f} = \frac{\rho_f - \rho_b}{\rho_b - \rho_w} \tag{6.2}$$

where symbols have a similar definition to those in equation 6.1.

d) Assumption on the mass exchanges between layers

EX1 Fluid mud exchanges mass with the low concentration suspension above through:

- *settling* at the upper interface which is, basically, composed of a flocs flux but, in the process, also causes some water to be trapped into the fluid mud layer;

[1] The concept of cohesive bed is taken, in this case, in a broad sense, encompassing, without loss of generality, stationary fluid mud layers (as apparently formed during laboratory experiments) as well.

entrainment, in which globules of the high density suspension, in volume proportions given by the fluid mud void ratio, are thrown into the upper layer (solids and water fluxes);

water expulsion from the fluid mud layer to the clear water layer, as a result of internal floc settling and re-arrangement of particles.

EX2 Fluid mud exchanges mass with the cohesive bed (solids and water fluxes) through *bed formation* and *liquefaction* or *fluidisation* fluxes in water/floc proportions which are given by the void ratio of the cohesive bed.

6.3 Derivation of a System of Equations for the Movement of Fluid Mud

6.3.1 General Aspects

Considering the basic assumptions previously described, a set of four unknowns, d_m (fluid mud layer thickness), u_m and v_m (depth-averaged velocities of the fluid mud, in the x and y directions, respectively) and ρ_m (depth averaged bulk density of the fluid mud layer) is adopted to describe the viscous flow of thin to medium thickness fluid mud layers under the assumptions described in Section 6.2.3. In this section a system of four partial differential equations allowing the four unknowns to be computed will be presented: to the classical continuity, x and y momentum equations, a fourth equation, describing the time evolution of the bulk density, is added; the assumptions

described in 6.2.3 which support some steps in the derivations are indicated in brackets when deriving the equations.

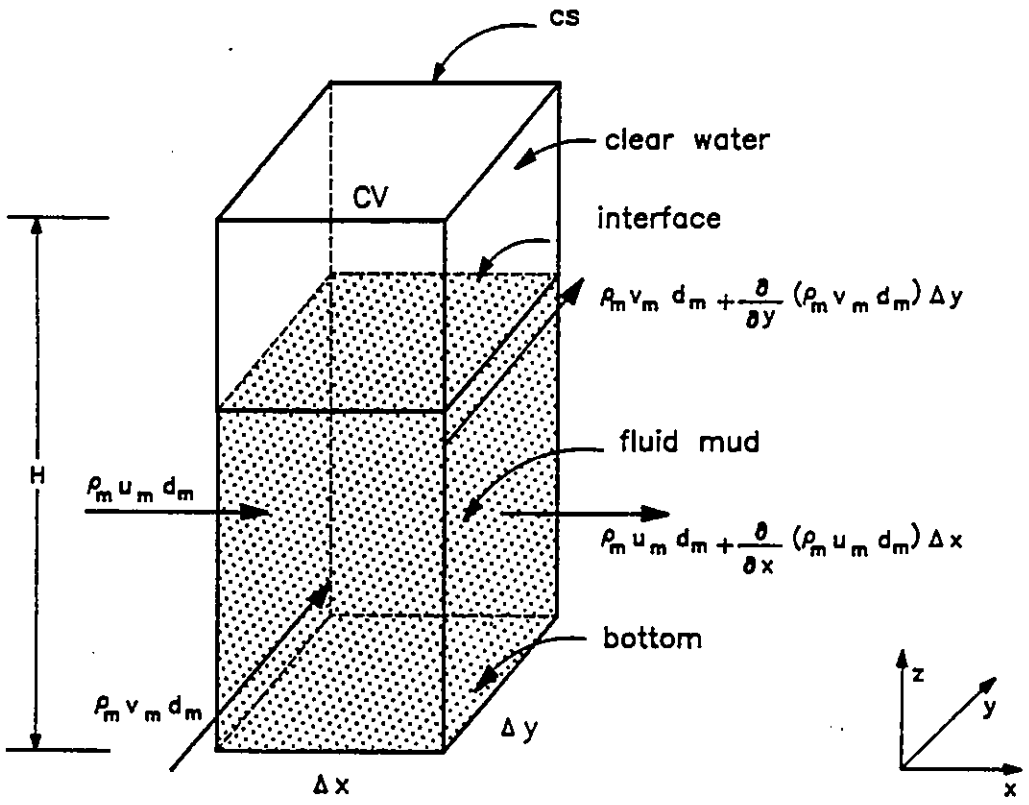

Figure 6.6 Definitions of control volume, control surface and fluxes used in the derivation of the continuity equation.

6.3.2 Continuity Equation

In order to derive the continuity equation for fluid mud layers it is useful to consider a control volume (**CV**), bounded by a control surface (**CS**), of horizontal dimensions Δx, Δy and fixed height H, such that it is always much greater than the thickness of

the fluid mud layer d_m (see figure 6.6 for symbol definition). The density of the low concentration suspension is given by:

$$\rho_0=\rho_w+\left(\frac{\rho_s-\rho_w}{\rho_s}\right)C \tag{6.3}$$

where C is the mass concentration and subscript 0 denotes variables in the upper layer. For continuity purposes it will be assumed that the effect of (small) sediment concentrations in the upper layer is negligible on the density of the layer. It will also be assumed that the effects of salinity or temperature variations on the density of salt water can be neglected and, furthermore, that it is incompressible (assumption CW1); consequently:

$$\frac{d\rho_0}{dt}=0 \tag{6.4}$$

Given the previous assumptions, which also imply that spatial variations of clear water density are negligible, and considering the definition of the material derivative one obtains

$$\frac{\partial\rho_0}{\partial t}=0 \tag{6.5}$$

Since the movements of both layers are assumed to be completely decoupled (assumption FM3) it may be considered, without loss of generality, that $u_0=v_0=0$. Consider now the Reynolds Transport Theorem for a fixed, non-deforming control volume, in the form:

$$\frac{d}{dt}B_{sys}=\frac{d}{dt}\iiint_{CV} b\rho dV+\int_{CSout}\int b\rho v_n dA-\int_{CSinp}\int b\rho v_n dA \qquad (6.6)$$

where B is an extensive property or parameter (e.g. mass, energy, momentum) of a system[1], b the corresponding intensive parameter (amount of B per unit mass) and v_n is the component of the velocity vector normal to the area elements of the control surface. The theorem states that the rate of change of an arbitrary extensive parameter of a system which instantaneously coincides with a control volume CV equals the rate of change of the extensive parameter within the CV as the fluid flows through it plus the net flow rate of the parameter across the entire control surface CS (White, 1979). Taking mass as the extensive parameter, the intensive parameter becomes unity and, consequently,

$$\frac{d}{dt}m_{sys}=\iiint_{CV}\frac{\partial}{\partial t}\rho dV+\int_{CSout}\int \rho v_n dA-\int_{CSinp}\int \rho v_n dA \qquad (6.7)$$

where the first term on the right-hand side has been re-written since, for the fixed control volume, the volume elements do not vary. The left-hand side of the equation is zero, since the total mass doesn't change in a system. The volume integral can be computed as:

$$\begin{aligned}\iiint_{CV}\frac{\partial}{\partial t}\rho dV&=\frac{\partial}{\partial t}(\rho_m A_h d_m)+\frac{\partial}{\partial t}[\rho_0 A_h(H-d_m)]\\&=A_h d_m\frac{\partial \rho_m}{\partial t}+A_h\rho_m\frac{\partial d_m}{\partial t}+A_h(H-d_m)\frac{\partial \rho_0}{\partial t}-A_h\rho_0\frac{\partial d_m}{\partial t}\end{aligned} \qquad (6.8)$$

[1] A system is defined as an arbitrary quantity of mass of fixed identity (White, 1979).

where the third term in the second line is zero due to the time rate of density change in the low concentration suspension and the horizontal area is $A_h=\Delta x\Delta y$. The integrals of the mass fluxes out of the control volume CV, through control surfaces CS perpendicular to the x and y directions are, respectively:

$$\begin{matrix}\rho_m u_m A_x+\dfrac{\partial \rho_m u_m A_x}{\partial x}\Delta x \\ \rho_m v_m A_y+\dfrac{\partial \rho_m v_m A_y}{\partial y}\Delta y\end{matrix} \qquad (6.9)$$

where $A_x=d_m\Delta y$ and $A_y=d_m\Delta x$, while the integrals of the mass fluxes into the control volume CV, through control surfaces CS perpendicular to the same axes are:

$$\begin{matrix}\rho_m u_m A_x \\ \rho_m v_m A_y\end{matrix} \qquad (6.10)$$

The fluxes leaving and entering the control volume in the z direction are:

$$\begin{matrix}\rho_0 A_h\dfrac{\partial d_m}{\partial t} \\ -A_h\dfrac{dm}{dt}\end{matrix} \qquad (6.11)$$

which correspond, respectively, to clear water leaving (or entering) the volume due to incompressibility and dependence of d_m on time and to added (or removed) mass due to fluxes at the interfaces. In the last expression $m=m_f+m_w$ (flocculated solids and water) is a mass per unit area. Collecting terms and dividing by $\Delta x\Delta y$:

$$d_m\frac{\partial \rho_m}{\partial t}+\rho_m\frac{\partial d_m}{\partial t}-\rho_0\frac{\partial d_m}{\partial t}+\frac{\partial \rho_m u_m d_m}{\partial x}+\frac{\partial \rho_m v_m d_m}{\partial y}+\rho_0\frac{\partial d_m}{\partial t}-\frac{dm}{dt}=0 \qquad (6.12)$$

Cancelling and grouping terms, the following equation is obtained:

$$\frac{\partial \rho_m d_m}{\partial t}+\frac{\partial \rho_m u_m d_m}{\partial x}+\frac{\partial \rho_m v_m d_m}{\partial y}=\frac{dm}{dt} \qquad (6.13)$$

If the products of the longitudinal and lateral variations of the bulk density by their corresponding velocities are considered to be much smaller than its time variation:

$$u_m\frac{\partial \rho_m}{\partial x}<\frac{\partial \rho_m}{\partial t} \qquad v_m\frac{\partial \rho_m}{\partial y}<\frac{\partial \rho_m}{\partial t} \qquad (6.14)$$

Dividing by ρ_m and re-arranging, the following equation is obtained:

$$\frac{\partial d_m}{\partial t}+\frac{\partial u_m d_m}{\partial x}+\frac{\partial v_m d_m}{\partial y}+\frac{d_m}{\rho_m}\frac{\partial \rho_m}{\partial t}=\frac{1}{\rho_m}\frac{dm}{dt} \qquad (6.15)$$

which is similar to the continuity equation used by Odd and Cooper (1988), but allows for bulk density variation in time.

6.3.3 Momentum Equations

In order to derive the depth-averaged x momentum equation the Navier-Stokes equation in the x direction is considered, in the conservative form:

$$\frac{\partial \rho u}{\partial t}+\frac{\partial \rho u^2}{\partial x}+\frac{\partial \rho vu}{\partial y}+\frac{\partial \rho wu}{\partial z}=\rho F_x+\frac{\partial \sigma_{xx}}{\partial x}+\frac{\partial \sigma_{yx}}{\partial y}+\frac{\partial \sigma_{zx}}{\partial z} \qquad (6.16)$$

where F_x is the x component of the body forces and the σ_{ix} $(i=x,y,z)$ are the viscous stresses in the same direction (see figure 6.5 for symbol definition).

Equation 6.16 can be rewritten, by specifying the body force and the pressure term and by grouping the remaining of the stress terms acting in vertical planes into a term T_v as:

$$\frac{\partial \rho u}{\partial t}+\frac{\partial \rho u^2}{\partial x}+\frac{\partial \rho vu}{\partial y}+\frac{\partial \rho wu}{\partial z}=\rho fv-\frac{\partial p}{\partial x}+T_v+\frac{\partial \tau_{zx}}{\partial z} \qquad (6.17)$$

where f is the Coriolis parameter and p is the pressure. In order to average the terms in the equation over the depth of the fluid mud layer it is useful to consider the product of three generic variables α,β,δ decomposed into their depth averaged parts and their deviations from the average along the depth, in the form $\alpha=a+a'$, $\beta=b+b'$ and $\delta=d+d'$. Depth-averaging is denoted by $\langle\rangle$ and defined as:

$$\langle\alpha\rangle=\frac{1}{\eta_m-\eta_b}\int_{\eta_b}^{\eta_m}\alpha dz \qquad (6.18)$$

While depth-averaging of some of the terms in the product is straightforward as, for example:

$$\begin{aligned}\langle abd\rangle &= abd\\ \langle (ab)d'\rangle &= 0\end{aligned} \qquad (6.19)$$

some of the remaining terms are non-zero, although their evaluation would only be possible if $a'(z)$, $b'(z)$, $d'(z)$ were known; for example:

$$\langle (a'b')d \rangle \neq 0$$
$$\langle a'b'd' \rangle \neq 0 \qquad (6.20)$$

Such terms depend on vertical gradients and are commonly considered in the depth-averaging process of the momentum equations as residuals. They are either neglected (if gradients are small) or modelled as dispersive terms.

In order to obtain the depth-averaged version of the horizontal momentum equations, it is necessary to consider that in a two layered system the pressure at a point **P** (see figure 6.5) with vertical coordinate z_l in the fluid mud layer is (assuming, as usual, a hydrostatic pressure distribution):

$$p = p_a + g\rho_0(\eta_w - \eta_m) + g\rho_m(\eta_m - z_l) \qquad (6.21)$$

where p_a is the atmospheric pressure and the remaining symbols are also defined in figure 6.5.

The pressure term in the equation takes the form:

$$\frac{\partial p}{\partial x} = \frac{\partial}{\partial x}[g\rho_0(\eta_w - \eta_m)] + \frac{\partial}{\partial x}[g\rho_m(\eta_m - z)] =$$
$$= \frac{\partial}{\partial x}[g\rho_0(\eta_w - \eta_m)] + g\frac{\partial \rho_m}{\partial x}(\eta_m - z) + g\rho_m\frac{\partial}{\partial x}(\eta_m - z) \qquad (6.22)$$

Depth-averaging over the fluid mud layer:

$$\left\langle -\frac{\partial p}{\partial x} \right\rangle = -g\frac{\partial}{\partial x}[\rho_0(\eta_w - \eta_m)] - \frac{g}{2}\frac{\partial \rho_m}{\partial x}(\eta_m - \eta_b) - g\rho_m\frac{\partial \eta_m}{\partial x} \qquad (6.23)$$

Performing the same operation on the left-hand side terms of equation 6.17 and considering that:

$$\eta_m - \eta_b = d_m \tag{6.24}$$

$$U = \int_{\eta_b}^{\eta_m} u\,dz \tag{6.25}$$

$$u = \bar{u} + u' = \frac{U}{d_m} + u' \tag{6.26}$$

the following terms (where the R_i are depth-averaging residuals) are obtained:

$$\left\langle \frac{\partial \rho u}{\partial t} \right\rangle = \frac{1}{d_m}\frac{\partial}{\partial t}(\bar{\rho}\bar{u}d_m) + \frac{1}{d_m}\left[-\rho u|_{\eta_m}\frac{\partial \eta_m}{\partial t}\right] + R_t \tag{6.27}$$

$$\left\langle \frac{\partial \rho uu}{\partial x} \right\rangle = \frac{1}{d_m}\frac{\partial}{\partial x}(\bar{\rho}\bar{u}^2 d_m) + \frac{1}{d_m}\left[-\rho u^2|_{\eta_m}\frac{\partial \eta_m}{\partial x}\right] + R_x \tag{6.28}$$

$$\left\langle \frac{\partial \rho uv}{\partial y} \right\rangle = \frac{1}{d_m}\frac{\partial}{\partial y}(\bar{\rho}\bar{u}\bar{v}d_m) + \frac{1}{d_m}\left[-\rho uv|_{\eta_m}\frac{\partial \eta_m}{\partial y}\right] + R_y \tag{6.29}$$

$$\left\langle \frac{\partial \rho uw}{\partial z} \right\rangle = \frac{1}{d_m}\left[\rho uw|_{\eta_m} - \rho uw|_{\eta_b}\right] = \frac{[\rho uw|_{\eta_m}]}{d_m} \tag{6.30}$$

Collecting the terms within square brackets on the right-hand sides of equations 6.27 to 6.30 it is observed that:

$$\frac{1}{d_m}\left(-\rho u|_{\eta_m}\right)\left[\frac{\partial \eta_m}{\partial t}+u|_{\eta_m}\frac{\partial \eta_m}{\partial x}+v|_{\eta_m}\frac{\partial \eta_m}{\partial y}-w|_{\eta_m}\right]=0 \tag{6.31}$$

since:

$$w|_{\eta_m}=\frac{d\eta_m}{dt}=\frac{\partial \eta_m}{\partial t}+u|_{\eta_m}\frac{\partial \eta_m}{\partial x}+v|_{\eta_m}\frac{\partial \eta_m}{\partial y} \tag{6.32}$$

is the surface boundary condition at $z=\eta_m$.

Collecting and re-arranging the terms on the right-hand side in equations 6.27 to 6.30 which are not enclosed in brackets (with the exception of the residuals):

$$\begin{aligned}&\frac{1}{d_m}\left[\frac{\partial}{\partial t}(\bar{\rho}\bar{u}d_m)+\frac{\partial}{\partial x}(\bar{\rho}\bar{u}^2d_m)+\frac{\partial}{\partial y}(\bar{\rho}\bar{u}\bar{v}d_m)\right]\\&=\frac{\bar{u}}{d_m}\left(\frac{\partial \bar{\rho}d_m}{\partial t}+\frac{\partial \bar{\rho}\bar{u}d_m}{\partial x}+\frac{\partial \bar{\rho}\bar{v}d_m}{\partial y}\right)+\bar{\rho}\left(\frac{\partial \bar{u}}{\partial t}+\bar{u}\frac{\partial \bar{u}}{\partial x}+\bar{v}\frac{\partial \bar{v}}{\partial y}\right)\end{aligned} \tag{6.33}$$

Depth averaging the remaining right-hand side terms in equation 6.17:

$$\langle \rho f v\rangle=\bar{\rho}f\bar{v}+R_c \tag{6.34}$$

$$\left\langle\frac{\partial \tau_{zx}}{\partial z}\right\rangle=\frac{1}{d_m}(\tau_{ix}-\tau_{bx}) \tag{6.35}$$

$$\langle T_v\rangle=R_v \tag{6.36}$$

R_t and R_c are expected to be small and will be neglected. Also, if it assumed that the remaining residuals can be modelled as diffusive terms, in the form:

$$R_v - R_x - R_y = \bar{\rho}\frac{\partial}{\partial x}\left(\varepsilon_{xx}\frac{\partial \bar{u}}{\partial x}\right) + \bar{\rho}\frac{\partial}{\partial y}\left(\varepsilon_{xy}\frac{\partial \bar{u}}{\partial y}\right) \tag{6.37}$$

where ε_{xx} and ε_{xy} are dispersion coefficients and making

$$u_m = \bar{u} \tag{6.38}$$

$$v_m = \bar{v} \tag{6.39}$$

$$\rho_m = \bar{\rho} \tag{6.40}$$

noting, from continuity, that:

$$\frac{\partial}{\partial t}(\rho_m d_m) + \frac{\partial}{\partial x}(\rho_m u_m d_m) + \frac{\partial}{\partial y}(\rho_m v_m d_m) = \frac{dm}{dt} \tag{6.41}$$

and dividing by ρ_m , the x momentum equation finally becomes:

$$\begin{aligned}\frac{\partial u_m}{\partial t} + u_m\frac{\partial u_m}{\partial x} + v_m\frac{\partial u_m}{\partial y} + \frac{u_m}{\rho_m d_m}\frac{dm}{dt} &= fv_m - \frac{g}{\rho_m}\frac{\partial}{\partial x}\rho_0(\eta_w - \eta_m) \\ -\frac{1}{2}\frac{g}{\rho_m}\frac{\partial \rho_m}{\partial x}(\eta_m - \eta_b) - g\frac{\partial \eta_m}{\partial x} &+ \frac{1}{\rho_m d_m}(\tau_{ix} - \tau_{bx}) \\ +\frac{\partial}{\partial x}\left(\varepsilon_{xx}\frac{\partial u_m}{\partial x}\right) + \frac{\partial}{\partial y}\left(\varepsilon_{xy}\frac{\partial u_m}{\partial y}\right)\end{aligned} \tag{6.42}$$

Similarly the y momentum equation is:

$$\frac{\partial v_m}{\partial t}+u_m\frac{\partial v_m}{\partial x}+v_m\frac{\partial v_m}{\partial y}+\frac{v_m}{\rho_m d_m}\frac{dm}{dt}=-fu_m-\frac{g}{\rho_m}\frac{\partial}{\partial y}\rho_0(\eta_w-\eta_m)$$
$$-\frac{1}{2}\frac{g}{\rho_m}\frac{\partial \rho_m}{\partial y}(\eta_m-\eta_b)-g\frac{\partial \eta_m}{\partial y}+\frac{1}{\rho_m d_m}(\tau_{iy}-\tau_{by}) \qquad (6.43)$$
$$+\frac{\partial}{\partial x}\left(\varepsilon_{yx}\frac{\partial v_m}{\partial x}\right)+\frac{\partial}{\partial y}\left(\varepsilon_{yy}\frac{\partial v_m}{\partial y}\right)$$

It should be noted that the above equations were derived for the case of viscous fluid mud flow. For turbulent flows the usual averaging process of the variables in time (over a timescale larger than that of turbulent fluctuations) would produce, formally, similar equations but in which the coefficients in the diffusive terms should have a much higher magnitude, in order to simulate turbulent diffusion. Symbols in the equation would, in that case, also denote time-averaged quantities.

6.3.4 Bulk Density Equation

In order to derive an equation for bulk density it is necessary to consider the phenomena leading to changes of the solids (i.e. flocs) and water masses and volumes in the fluid mud layers (assumption FM2).

Consider the block diagram of a fluid mud layer (figure 6.7), of unit area and of thickness d_m, in which all the flocs and water have been separated and *compressed*,

occupying layers of thickness d_f and d_w. The bulk density of the fluid mud layer (ρ_m) is defined as:

$$\rho_m = \frac{\rho_w V_w + \rho_f V_f}{V} = \frac{\rho_w d_w + \rho_f d_f}{d_m} \tag{6.44}$$

where V, d and ρ denote volume, thickness and density and subscripts m, f and w denote fluid mud, flocs and water, respectively. Bulk density variation in time is described as:

$$\begin{aligned} \frac{d\rho_m}{dt} &= \frac{d}{dt}\left(\frac{\rho_w d_w}{d_m}\right) + \frac{d}{dt}\left(\frac{\rho_f d_f}{d_m}\right) = \\ &= \frac{\rho_w}{d_m}\frac{d}{dt}d_w + \frac{\rho_f}{d_m}\frac{d}{dt}d_f - (\rho_w d_w + \rho_f d_f)\left(\frac{1}{d_m^2}\right)\frac{d}{dt}(d_w + d_f) = \\ &= \left(\frac{\rho_w - \rho_m}{d_m}\right)\frac{d}{dt}d_w + \left(\frac{\rho_f - \rho_m}{d_m}\right)\frac{d}{dt}d_f \end{aligned} \tag{6.45}$$

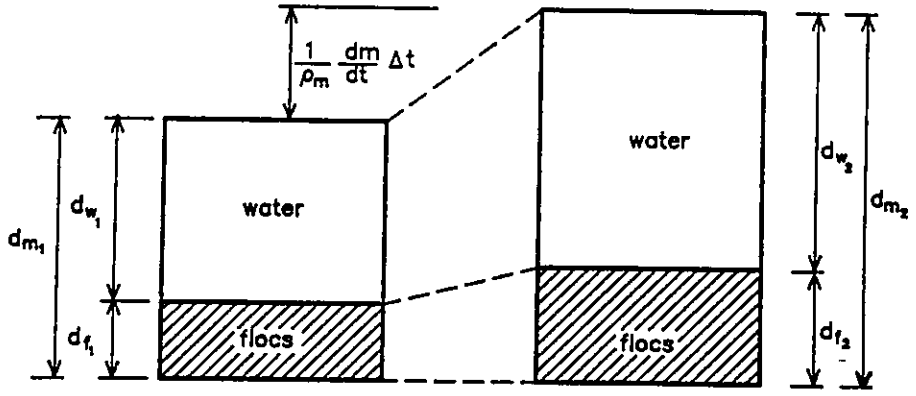

Figure 6.7 Block diagram representation and evolution of a fluid mud layer.

The variations in the water and solids thicknesses in the fluid mud layer are due to (assumption EX1):

(i) loss of water through the upper interface, due to internal re-arrangement of the flocs within the layer;

(ii) loss of water and flocs to the bed through dewatering of lower sublayers (leading to bed formation) and to the low concentration layer through entrainment;

(iii) gain of water and flocs from the bed through erosion and from the low concentration layer through settling.

The gains and losses of water and flocs are considered through their contributions to the water and floc fluxes dm_w/dt and dm_f/dt, to be specified in Section 6.4. Consequently:

$$\frac{d\rho_m}{dt}=\left(\frac{\rho_w-\rho_m}{d_m}\right)\frac{1}{\rho_w}\frac{dm_w}{dt}+\left(\frac{\rho_f-\rho_m}{d_m}\right)\frac{1}{\rho_f}\frac{dm_f}{dt} \qquad (6.46)$$

or, expanding the material derivative,

$$\frac{\partial\rho_m}{\partial t}+u_m\frac{\partial\rho_m}{\partial x}+v_m\frac{\partial\rho_m}{\partial y}=\left(\frac{\rho_w-\rho_m}{d_m}\right)\frac{1}{\rho_w}\frac{dm_w}{dt}+\left(\frac{\rho_f-\rho_m}{d_m}\right)\frac{1}{\rho_f}\frac{dm_f}{dt} \qquad (6.47)$$

which represents the bulk density variation in the layer, as a function of the water and floc fluxes.

6.4 Process Modelling of Interface Exchanges

6.4.1 General

In order to model fluid mud formation, evolution and destruction according to the formulation described in the previous section it is necessary to characterise the physical processes occurring at the interfaces between the fluid mud layers and the low concentration suspensions above and between the same layers and the cohesive beds below. Although substantial efforts are still needed to improve knowledge in this area, namely regarding the processes taking place at the lower interface, some basic information has already been obtained by several researchers (Odd and Cooper, 1988; Srinivas and Mehta, 1989; Mehta and Srinivas, 1993). In figure 2.3 a sketch of the physical processes of interest was presented while a summary of such processes and of their respective formulations is found in the following subsections.

6.4.2 Entrainment

The physical process leading to mass removal from fluid mud layers by turbulent shear (entrainment) has been recognised to be different from those leading to mass removal from a settled bed showing a structured solids matrix (surface erosion or mass erosion, the latter following bed liquefaction, fluidisation or bed failure). In estuaries, after slack water, rapid flow reversal causes the top layer of (fluid) mud, not sufficiently dewatered to form a cohesive bed, to be entrained by turbulent flow in a

similar manner to the entrainment of a layer of salt water underneath flowing fresh water (Mehta and Srinivas, 1993). Laboratory studies by the same authors showed that, conversely, if the newly placed mud was not subjected to shear flow, typically within about an hour, the mud gained sufficient strength by dewatering and, presumably, by gelling[1], to preclude interface deformation and instability and, ultimately, mixing by the flow. Particulate removal then occurred by individual floc breakup at the (soft) bed surface (Mehta and Srinivas, 1993), i.e. according to classical surface erosion mechanisms described in Chapter 2. A comparison between the erosion rates corresponding to both phenomena can be found in figure 6.8, where the expression for soft beds used in the comparison is equation 2.33 (Parchure and Mehta, 1985).

A general description of salt water entrainment by an upper layer of fresh water flowing at higher velocity can be found in Dyer (1973). When shear becomes sufficiently intense, the interface between layers becomes disturbed by waves, which grow higher with increasing shear. Eventually the waves break and globules of the lower, denser, layer are ejected from the wave crests into the lighter fluid above, in a strictly one way process. This characterisation of the phenomenon generally matches the description of the same phenomena observed by Mehta and Srinivas (1993) for the

[1] Clay dispersions are classified as colloidal solutions or *sols* (if the dimensions of the clay particles are small and they do not settle within a reasonable time) or suspensions (when the particles are large and settle rapidly). A *gel* is a moderately concentrated *sol* to which an electrolyte has been added, causing the particles to form a single structure, which extends throughout the available volume and shows some rigidity and elasticity (van Olphen, 1963).

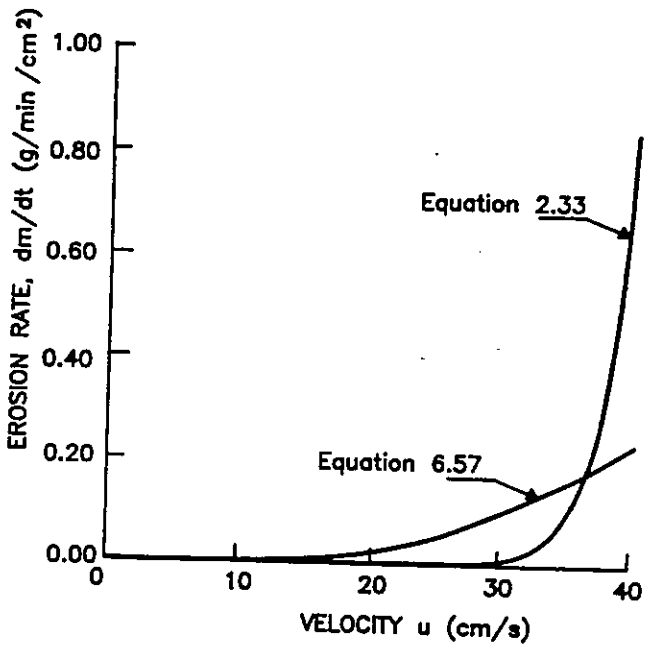

Figure 6.8 Comparison of erosion rates for soft beds computed with equation 2.33 with the entrainment rates predicted by equation 6.57 (u is a depth-averaged velocity). Adapted from Srinivas (1989).

case of fluid mud and overlying low concentration layers, in a race-track type flume. However, the latter authors were able to give a more detailed description of the phenomenon for the case of their experimental conditions. At low Richardson numbers (defined below), $Ri<5$, the authors found that entrainment appeared to be turbulence dominated, with a rather diffuse and highly irregular interface. As Ri increased above 5 the interface became better defined and convoluted with large, irregular, undulations, entrainment being dominated by wave breaking, while interspersed, solitary type waves (which seemed to decay without breaking) were also observed. The frequency and amplitude of the disturbances decreased with increasing Ri and, as it increased above 10, the disturbances could be seen to grow slightly in amplitude, sharpen into non-linear crests and disappear suddenly, as the *roller-action* of eddies sheared off the crests. For values of Ri beyond 20, the intensity of entrainment appeared to taper off

rapidly with increasing Richardson number. Differences between the entrainment of salt water and cohesive sediment are also noted by Mehta and Srinivas (1993). These are related to the effects of particle settling, cohesion and viscosity of the lower layer, although quantitative information about the effects of such parameters is scarce. It is concluded by the same authors that mud and salt are entrained at similar rates for low Richardson numbers but that, for increasing ***Ri*** (i.e. greater than about 10), mud entrainment rates decrease rapidly relative to those of salt (see figure 6.10).

The entrainment flux has traditionally been described in the models of Hydraulics Research, by analogy to salt entrainment from a saline wedge (Odd and Cooper, 1988; Roberts, 1992) as:

$$\left.\frac{dm_s}{dt}\right|_e = V_e C_m \qquad Ri_B < Ri_c$$
$$\left.\frac{dm_s}{dt}\right|_e = 0 \qquad Ri_B \geq Ri_c \tag{6.48}$$

where V_e (m/s) is an entrainment velocity given by:

$$V_e = \frac{0.1\,\Delta U}{(1+63\,Ri_B^2)^{3/4}} = E(Ri_B)\,\Delta U \tag{6.49}$$

In this expression $E(Ri_B)$ is the entrainment coefficient (see figure 6.9) and:

$$\Delta U = [(u_0 - u_m)^2 + (v_0 - v_m)^2]^{1/2} \tag{6.50}$$

In expressions 6.48 to 6.50, C_m is the fluid mud mass concentration, u and v the horizontal depth-averaged velocities (subscripts m and 0 denoting fluid mud and clear water, respectively); Ri_B is the bulk Richardson number, defined as:

$$Ri_B=\frac{\Delta\rho g d_m}{\rho_0(\Delta U)^2} \tag{6.51}$$

where $\Delta\rho=\rho_m-\rho_0$ is the density difference or *density jump* between the fluid mud layer and the clear water layer above ($\Delta\rho=0.62\ C_m$, assuming that the solids particles have a density $\rho_s=2650\ kg/m^3$) and d_m the thickness of the fluid mud layer. According to the above formulation, entrainment can only occur at sufficiently low values of Ri_B, as the critical value of the bulk Richardson number is $Ri_c=10$, based on experimental work (Roberts, 1992). A plot of the entrainment coefficient versus the Richardson number is presented in figure 6.9 for salt, with two additional points obtained for mud.

Srinivas and Mehta (1989) performed a first series of experiments in their race-track flume, simulating entrainment from an immobile fluid mud layer by a moving water layer using kaolinite and bentonite as sediments. Defining a Richardson number as:

$$Ri=\frac{d_0\Delta b}{u_0^2} \tag{6.52}$$

where d_0 is the depth of the low concentration (clear water) layer, u_0 the mean velocity of the same layer and Δb the interfacial buoyancy step. Buoyancy or reduced gravity is defined as:

$$b=g\frac{\rho_1-\rho_r}{\rho_r} \tag{6.53}$$

where ρ_1 and ρ_r are the density of a given fluid and a reference density, respectively. For the case of a fluid mud layer ρ_1 was taken as the density of fluid mud at the level

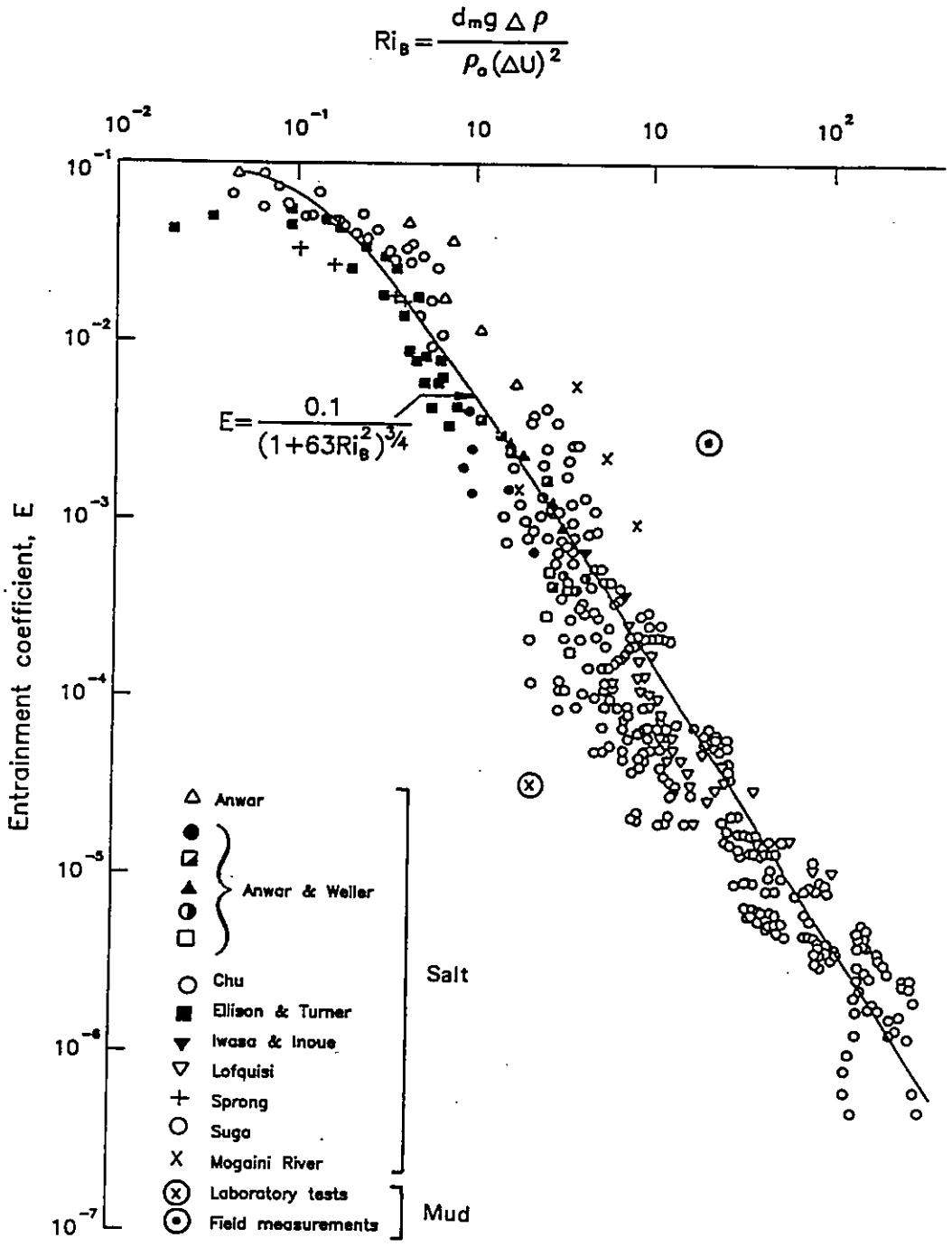

Figure 6.9 Entrainment function for the case of an arrested salt wedge, with point obtained for mud in laboratory tests and field measurements (adapted from HR, 1991c).

of the interface, ρ_m. Considering, as the same authors, that the reference density is that of the low concentration layer one obtains:

$$\Delta b = g\frac{\rho_m - \rho_0}{\rho_0} \tag{6.54}$$

Defining the buoyancy flux as:

$$q = \frac{g}{\rho_0}\frac{dm_s}{dt}\bigg|_{en} \tag{6.55}$$

where dm_s/dt is the entrained mass flux into the turbulent low concentration layer (dry mass of sediment per unit time and unit bed area) and the non dimensional-buoyancy flux Q (or non-dimensional entrainment rate E) as:

$$Q = \frac{q}{u_0 \Delta b} \tag{6.56}$$

the trend line obtained by the same authors, corresponding to a limited laboratory data set, was:

$$Q = \frac{FRi^{-0.9}}{(G^2 + Ri^2)^p} \tag{6.57}$$

with $F=0.27$, $G=20$ and $p=0.66$, which applied up to $Ri = 25$.

A second series of laboratory experiments was also undertaken by the same researchers (Mehta and Srinivas, 1993), using the same flume and three types of sediment: kaolinite, a kaolinite/volclay bentonite mixture and natural mud from a lake. Entrainment was observed to fall rapidly for Ri greater than 10 and the non-

dimensional entrainment rate E became almost independent of the Richardson number for Ri greater than about 15. The best fit resulting from the improved data set was now (see figure 6.10):

$$E=ARi^{-1}-DRi \tag{6.58}$$

where $A=0.0052$ and $D=0.000016$ (according to the same authors coefficient D reflects mud properties, i.e. settling and cohesion).

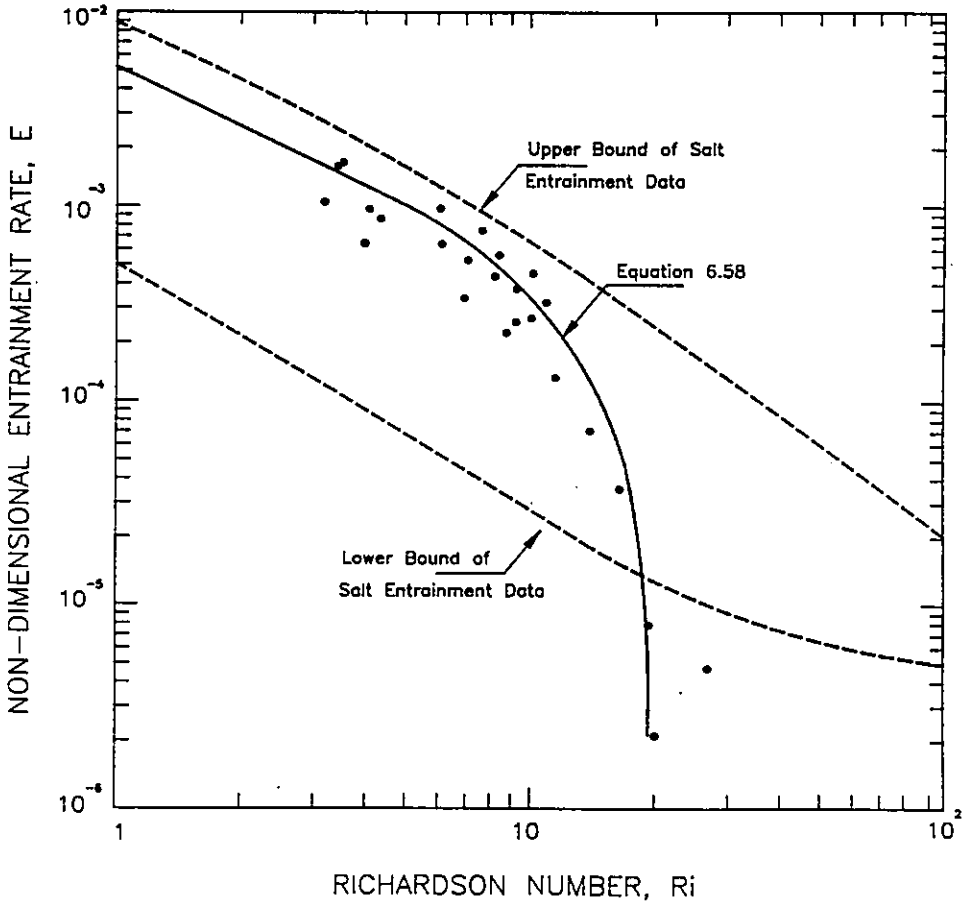

Figure 6.10 Non-dimensional entrainment rate versus Richardson number (adapted from Mehta and Srinivas, 1993).

6.4.3 Settling of Mud from Low Concentration Suspension

In many estuaries, particularly in high concentration environments, at times just prior to slack water, intense flocculation leads to hindered settling of sediment and, in the absence of fast dewatering, a fluid mud layer is formed. Settling of mud flocs continues while the rate of vertical turbulent exchange at the clear water/fluid mud interface is insufficient to keep the mud flocs in suspension or to entrain fluid mud globules from the layer. The vertical flux of solids settling into the fluid mud layer was defined by Odd and Cooper (1988), by analogy to deposition onto a settled bed (see equation 2.40), as:

$$\left.\frac{dm_s}{dt}\right|_s = W_s C_0 \left(1 - \frac{\tau_i}{\tau_{dm}}\right) \qquad \tau_i < \tau_{dm}$$
$$\left.\frac{dm_s}{dt}\right|_s = 0 \qquad \tau_i \geq \tau_{dm} \tag{6.59}$$

where C_0 is the sediment concentration at the bottom of the low concentration layer, τ_i is the shear stress at the fluid mud/low concentration suspension interface and τ_{dm} is the critical shear stress value for settling from the low concentration suspension. The latter was expected to be higher (τ_{dm}=*0.4Pa*) than the usual value (τ_{cd}=*0.1Pa*) for deposition onto a bed (Odd and Cooper, 1988). An alternative equation (HR, 1991c) is:

$$\left.\frac{dm_s}{dt}\right|_s = W_s C_0 \qquad \tau_i < \tau_{dm}$$
$$\left.\frac{dm_s}{dt}\right|_s = 0 \qquad \tau_i \geq \tau_{dm} \tag{6.60}$$

This alternative equation was found to produce results in better agreement with field data on the distribution of fluid mud pools and soft mud from the Severn estuary.

6.4.4 Bed Destruction and Erosion

Once formed, a cohesive bed can have its structure weakened and broken and the resulting entity will behave as a fluid again. Mechanisms leading to the generalised destruction of a bed are:

(i) *fluidisation*, which is caused by pore water flow, as a result of pressure gradients (through wave-induced oscillatory loading, for example);

(ii) *liquefaction*, which results from shear forces within the bed, leading to structural breakup;

(iii) *structural failure* along a given plane, due to oversteepening of the bed (caused, for example, by dredging or significant deposition) leading to the collapse of the layers above or *local detachment* of large portions of the bed.

Following structural break-up, cohesive material can be removed through erosive mechanisms in large masses (mass or bulk erosion). However, the most common erosive mechanism is particle by particle (or surface) erosion from a structured bed, in which separation of individual particles from the bed, under shear action, occurs (see Chapter 2).

A fluid mud layer moving over a cohesive bed at velocities high enough for the bottom shear stress to exceed the bed strength will erode it. Assuming a particle by particle removal, the erosion solids flux per unit area will be, by analogy to clear water erosion of a settled bed (see Section 2.5.2):

$$\left.\frac{dm_s}{dt}\right|_e = m_e\left(\frac{\tau_b - \tau_{ce}}{\tau_{ce}}\right) \qquad \tau_b > \tau_{ce}$$
$$\left.\frac{dm_s}{dt}\right|_e = 0 \qquad \tau_b \le \tau_{ce} \tag{6.61}$$

where m_e is an erosion constant, τ_b and τ_{ce} are the bed shear stress and the critical shear stress for erosion. Mass erosion mechanisms of cohesive beds were not considered in the present version of the formulation.

6.4.5 Bed Formation and Dewatering

Dewatering is caused by a reduction in the water content of a water/solids mixture. In the case of a fluid mud layer, internal rearrangement of the solids particles under gravity and cohesive forces leads, through a loss of water from the lower sublayers,

to the development of a solids matrix capable of bearing some of the applied load and thereby producing a cohesive bed. The water lost by these sublayers, which have now become part of the cohesive bed, remains within the fluid mud layer (i.e. passes up to higher sublayers).

In a similar way to the deposition of mud from a low concentration suspension to a bed, the formation of a solids matrix can only occur at low shear stresses, i.e. below a critical shear stress for bed formation, τ_{bf}. The rate of solids loss at the bottom of a fluid mud layer can be described in a similar way to settling and is modelled as (Roberts, 1992):

$$\left.\frac{dm_s}{dt}\right|_{bf} = V_{bf} C_m \qquad \tau_b < \tau_{bf}$$
$$\left.\frac{dm_s}{dt}\right|_{bf} = 0 \qquad \tau_b \geq \tau_{bf} \tag{6.62}$$

where V_{bf} (m/s) is a bed formation velocity and C_m is the fluid mud mass concentration.

Furthermore, it is hypothesised that the internal solids rearranging process in the fluid mud layer, which forces water to move upwards, will also lead to the expulsion of some of it through the low concentration/fluid mud interface, at a rate which is not necessarily the same as that for bed formation. The water flux resulting from this process will be given by:

$$\left.\frac{dm_w}{dt}\right|_i = V_i \rho_w \qquad (6.63)$$

where V_i is the upper interface lowering velocity due to loss of water from the layer. This process will be included in the interface flux formulation derived in the next subsection.

6.4.6 Fluxes at the Interfaces

The solids fluxes described in the previous subsections are, usually, obtained through filtering, drying and weighing of the dry masses of sediment contained in known volumes of suspension. Although no deflocculation operation usually takes place before the solids masses are evaluated it seems reasonable to assume that the floc structure is destroyed through filtering and drying and that only the solids content of the flocs is actually determined. Considering a single order of aggregation (assumption FM2) and that for a floc or aggregate a *floc void ratio* (ratio of the volume occupied by water, V_{wf}, to the volume occupied by solids, V_{sf}, within the floc) can be defined as:

$$e_f = \frac{V_{wf}}{V_{sf}} = \frac{\rho_s - \rho_f}{\rho_f - \rho_w} \qquad (6.64)$$

where ρ_s, ρ_w and ρ_f are the solids, water and floc densities, respectively. It can be written, in terms of volumes in a generic floc, i, that

$$V_{tf}^{i}=(1+e_f)V_{sf}^{i}=(1+e_f)\frac{M_{sf}^{i}}{\rho_s} \tag{6.65}$$

i.e. a floc with density ρ_f and solids mass M_{sf} occupies a total volume V_{tf} . The volume occupied by the total number of flocs, n, is, therefore:

$$\sum_{i=1}^{n} V_{tf}^{i}=\frac{(1+e_f)}{\rho_s}\sum_{i=1}^{n} M_{sf}^{i} \tag{6.66}$$

In terms of the rate of volume variation per unit time corresponding to a given solids flux, in flocculated condition, entering the fluid mud layer through a plan area $\Delta x\Delta y$:

$$\frac{dV_f}{dt}=\frac{d}{dt}\sum_{i=1}^{n} V_{tf}^{i}=\frac{(1+e_f)}{\rho_s}\frac{d}{dt}\sum_{i=1}^{n} M_{sf}^{i}=\frac{(1+e_f)}{\rho_s}\frac{dm_s}{dt}\Delta x\Delta y \tag{6.67}$$

and, in terms of the total floc flux per unit area (dm_f/dt):

$$\frac{dm_f}{dt}=\frac{\rho_f}{\Delta x\Delta y}\frac{dV_f}{dt}=\frac{\rho_f(1+e_f)}{\rho_s}\frac{dm_s}{dt} \tag{6.68}$$

Considering now that the settling flux is composed of flocs which trap some water between them, that there is some water expulsion through the upper interface, that the entrainment flux is composed of both flocs and water, in proportions given by the fluid mud void ratio e_m, and that both fluxes at the lower interface, bed formation and erosion, are composed of flocs and water in proportions given by the cohesive bed void ratio, e_b, the floc mass flux (mass of flocs per unit area per unit time) into the fluid mud layer will be given by:

$$\frac{dm_f}{dt}=\left[\left.\frac{dm_s}{dt}\right|_s+\left.\frac{dm_s}{dt}\right|_{er}-\left.\frac{dm_s}{dt}\right|_{en}-\left.\frac{dm_s}{dt}\right|_{bf}\right]\frac{(1+e_f)}{\rho_s}\rho_f \qquad (6.69)$$

where subscripts *s*, *er*, *en* and *bf* denote settling, erosion, entrainment and bed formation, respectively. The total water flux (mass of water per unit area per unit time) accompanying the floc flux into the fluid mud layer and leaving the layer through the upper interface is given by:

$$\frac{dm_w}{dt}=\left[\left.\frac{dm_s}{dt}\right|_s k_s e_m+\left.\frac{dm_s}{dt}\right|_{er} e_b-\left.\frac{dm_s}{dt}\right|_{en} e_m-\left.\frac{dm_s}{dt}\right|_{bf} e_b\right]\frac{(1+e_f)}{\rho_s}\rho_w-V_i\rho_w \qquad (6.70)$$

where coefficient k_s is related to the water which is trapped between the settling flocs, when entering the layer. Finally, the total mass flux into the fluid mud layer is given by:

$$\frac{dm}{dt}=\frac{dm_f}{dt}+\frac{dm_w}{dt} \qquad (6.71)$$

while the rate of change in bed thickness per unit time, assuming no immediate crushing of the flocs, is given by:

$$\frac{d\,d_b}{dt}=\left[\left.\frac{dm_s}{dt}\right|_{bf}-\left.\frac{dm_s}{dt}\right|_{er}\right]\frac{(1+e_f)(1+e_b)}{\rho_s} \qquad (6.72)$$

Equations 6.69 to 6.71 enable the time variation of the total, water and floc masses into the fluid mud layer to be computed (for use in equations 6.13, 6.42, 6.43 and 6.47) as a function of the upper interface lowering velocity and of the solids fluxes (defined in Sections 6.4.2 to 6.4.5) entering/leaving the layer through the interfaces

with the low concentration suspension, and the cohesive *bed* (immobile fluid mud or settled bed).

6.5 Development of a Pilot Numerical Model

6.5.1 General

In order to apply the formulation described in Section 6.3, a pilot numerical model (FLDMUD2) was developed which solved equations 6.13, 6.42, 6.43 and 6.47 using the interface fluxes defined in equations 6.69 to 6.71.

The pilot numerical model was, primarily, intended to test the suitability of the mathematical formulation derived in Section 6.3 for simulating the dynamics of fluid mud layers, given the process models described in Section 6.4 and their respective parameterisations. The identification of future research needs in the same topics, as a result of model application, was also intended. Previous formulations (see, for example, Odd and Cooper, 1988) do not take into account time and space variability of the bulk density in the fluid mud layer but results from recent field studies (HR, 1990c; HR,1991b) indicate that this variability should be included, as happens in model FLDMUD2. Development and testing of the model was also considered to be a necessary step towards the eventual development of an improved bed boundary condition for transport modelling in low concentration suspension layers, for those cases in which near-bed high concentration layers exist.

Given the nature of the model and the immediate purposes of its application it was decided to use in its development simple and well tested numerical methods. A staggered grid was adopted (see figure 6.11) in which the scalar quantities are calculated at the centre of the cells and the x and y velocities are calculated at their left and bottom faces, respectively. A split of the time step, similar to that used in the Alternating Direction Implicit (ADI) method, was chosen as the basic approach, following the technique used by Neves (1985) for the development of a depth-averaged hydrodynamics model, whose continuity and momentum equations are very similar to those of the present model. In the ADI method the time step is divided into two half-steps. In the first step, part of the equation to be solved (i.e. derivatives in one of the spatial dimensions) is calculated implicitly while the remaining terms (derivatives in the other dimension) are calculated explicitly. The converse operation

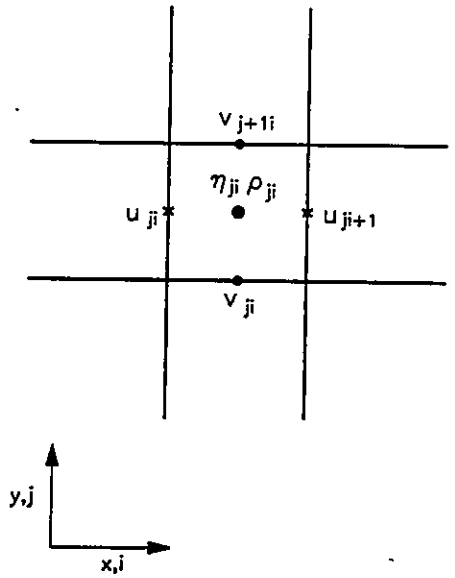

Figure 6.11 Computational grid used in the development of model FLDMUD2.

happens in the second half-time step. The ADI method is unconditionally stable and requires only the inversion of tridiagonal matrices.

In the current version of model FLDMUD2 the continuity and bulk density equations were both solved using the ADI technique. However, and for programming simplicity, the two momentum equations were solved explicitly in both half-steps. The choice of explicit methods introduces stability restrictions on the time discretisation but such restrictions are of minor importance for the simple test case simulated in Section 6.6. Modification of the current version to the full ADI scheme can easily be carried out in future versions of the code, as necessary.

The finite difference equations and process parameterisations used in the current version of model FLDMUD2 are described in the following subsections. In the model the x and y velocities are first calculated, using the appropriate momentum equations, followed by the calculation of the densities and depths, through the bulk density and continuity equations, respectively. A flowchart describing the computational structure of the code is presented in Appendix F. The model is run using an initial condition in terms of prescribed values of the velocities, densities and depths at all points, while, in terms of boundary conditions, levels or velocities are imposed at inflow/outflow boundaries, densities are imposed at inflow boundaries and zero fluxes, perpendicular to solid walls, are also imposed.

6.5.2 Continuity Equation

The ADI finite difference equation used to represent the continuity equation, at generic node i, j, in order to progress the solution in the first half-time step of the model (i.e. from time levels n to $n+1/2$) is:

$$\begin{aligned}
&\frac{(\rho_{ji} d_{ji})^{n+1/2} - (\rho_{ji} d_{ji})^{n}}{\Delta t/2} \\
&+\frac{1}{2\Delta x}\left[(\rho_{ji+1} d_{ji+1} + \rho_{ji} d_{ji}) u_{ji+1} - (\rho_{ji} d_{ji} + \rho_{ji-1} d_{ji-1}) u_{ji}\right]^{n+1/2} \\
&+\frac{1}{2\Delta y}\left[(\rho_{j+1i} d_{j+1i} + \rho_{ji} d_{ji}) v_{j+1i} - (\rho_{ji} d_{ji} + \rho_{j-1i} d_{j-1i}) v_{ji}\right]^{n} \\
&= \left.\frac{dm}{dt}\right|_{ji}^{n+1/2}
\end{aligned} \tag{6.73}$$

where Δx, Δy and Δt are the x, y, t discretisations, subscript m (denoting fluid mud properties) was omitted for conciseness and the remaining symbols were defined in equation 6.13 (separators between subscripts, i.e. $j+1,i$ have also been omitted for clarity). The corresponding equation for the second half-step is, with a similar notation:

$$\begin{aligned}
&\frac{(\rho_{ji} d_{ji})^{n+1} - (\rho_{ji} d_{ji})^{n+1/2}}{\Delta t/2} \\
&+\frac{1}{2\Delta x}\left[(\rho_{ji+1} d_{ji+1} + \rho_{ji} d_{ji}) u_{ji+1} - (\rho_{ji} d_{ji} + \rho_{ji-1} d_{ji-1}) u_{ji}\right]^{n+1/2} \\
&+\frac{1}{2\Delta y}\left[(\rho_{j+1i} d_{j+1i} + \rho_{ji} d_{ji}) v_{j+1i} - (\rho_{ji} d_{ji} + \rho_{j-1i} d_{j-1i}) v_{ji}\right]^{n+1} \\
&= \left.\frac{dm}{dt}\right|_{ji}^{n+1/2}
\end{aligned} \tag{6.74}$$

Both half-steps produce systems of equations leading to tri-diagonal matrices, which are solved using the Thomas algorithm (see, for example, Anderson et al., 1984). Each half-step (and the full time step) are second order accurate in space. The half-steps are first order accurate in time but the full step is also second order accurate (see, for example, Roache, 1972).

6.5.3 x Momentum Equation

The explicit finite difference equation used in the first half-step of the model, at node i, j, is:

$$\begin{aligned}
&\frac{u_{ji}^{n+1/2}-u_{ji}^{n}}{\Delta t/2}+u_{ji}^{n}\frac{u_{ji+1}^{n}-u_{ji-1}^{n}}{2\Delta x}+\bar{v}_{ji}^{n}\frac{u_{j+1i}^{n}-u_{j-1i}^{n}}{2\Delta y} \\
&\quad+\frac{u_{ji}^{n}}{2}\left(\frac{(dm/dt)_{ji}^{n}}{\rho_{ji}^{n}d_{ji}^{n}}-\frac{(dm/dt)_{ji-1}^{n}}{\rho_{ji-1}^{n}d_{ji-1}^{n}}\right)=f\bar{v}_{ji}^{n} \\
&\quad-\frac{2g[(\rho_0 d_0)_{ji}^{n}-(\rho_0 d_0)_{ji-1}^{n}]}{(\rho_{ji}^{n}+\rho_{ji-1}^{n})\Delta x}-\frac{g}{4}\frac{\rho_{ji}^{n}-\rho_{ji-1}^{n}}{\Delta x}\left(\frac{d_{ji}^{n}}{\rho_{ji}^{n}}+\frac{d_{ji-1}^{n}}{\rho_{ji-1}^{n}}\right) \\
&\quad-g\frac{\eta_{ji}^{n}-\eta_{ji-1}^{n}}{\Delta x}+\varepsilon_{xx}\frac{u_{ji+1}^{n}-2u_{ji}^{n}+u_{ji-1}^{n}}{\Delta x^2} \\
&\quad+\varepsilon_{xy}\frac{u_{j+1i}^{n}-2u_{ji}^{n}+u_{j-1i}^{n}}{\Delta y^2}+\frac{2\left[(\tau_{mx})_{ji}^{n}-(\tau_{bx})_{ji}^{n}\right]}{(\rho_{ji}^{n}d_{ji}^{n}+\rho_{ji-1}^{n}d_{ji-1}^{n})}
\end{aligned} \tag{6.75}$$

where, again, subscript m has been omitted, subscript 0 denotes the low concentration layer, f is the Coriolis parameter and, besides the symbols defined in equation 6.42:

$$\overline{v}_{ji}^{n}=\frac{(v_{ji}^{n}+v_{ji-1}^{n}+v_{j+1i-1}^{n}+v_{j+1i}^{n})}{4} \tag{6.76}$$

The equation for the second half-step is entirely similar and is simply obtained by replacing, in equation 6.75, ***n+1/2*** by ***n+1*** and ***n*** by ***n+1/2***, respectively. Both half-steps are first order accurate in time and second order accurate in space.

6.5.4 y Momentum Equation

The explicit finite difference equation used in the first half-step of the model, at node i, j, is:

$$\begin{aligned}
&\frac{v_{ji}^{n+1/2}-v_{ji}^{n}}{\Delta t/2}+\overline{u}_{ji}^{n}\frac{v_{ji+1}^{n}-v_{ji-1}^{n}}{2\Delta x}+v_{ji}^{n}\frac{v_{j+1i}^{n}-v_{j-1i}^{n}}{2\Delta y}\\
&\quad+\frac{v_{ji}^{n}}{2}\left(\frac{(dm/dt)_{ji}^{n}}{\rho_{ji}^{n}d_{ji}^{n}}-\frac{(dm/dt)_{j-1i}^{n}}{\rho_{j-1i}^{n}d_{j-1i}^{n}}\right)=-f\overline{u}_{ji}^{n}\\
&\quad-\frac{2g[(\rho_0 d_0)_{ji}^{n}-(\rho_0 d_0)_{j-1i}^{n}]}{(\rho_{ji}^{n}+\rho_{j-1i}^{n})\Delta y}-\frac{g}{4}\frac{\rho_{ji}^{n}-\rho_{j-1i}^{n}}{\Delta y}\left(\frac{d_{ji}^{n}}{\rho_{ji}^{n}}+\frac{d_{j-1i}^{n}}{\rho_{j-1i}^{n}}\right)\\
&\quad-g\frac{\eta_{ji}^{n}-\eta_{j-1i}^{n}}{\Delta y}+\varepsilon_{yx}\frac{v_{ji+1}^{n}-2v_{ji}^{n}+v_{ji-1}^{n}}{\Delta x^{2}}\\
&\quad+\varepsilon_{yy}\frac{v_{j+1i}^{n}-2v_{ji}^{n}+v_{j-1i}^{n}}{\Delta y^{2}}+\frac{2\left[(\tau_{my})_{ji}^{n}-(\tau_{by})_{ji}^{n}\right]}{(\rho_{ji}^{n}d_{ji}^{n}+\rho_{j-1i}^{n}d_{j-1i}^{n})}
\end{aligned} \tag{6.77}$$

with the same notation as for the x momentum equation, where, besides the symbols defined in equation 6.43:

$$\bar{u}_{ji}^{n}=\frac{(u_{ji}^{n}+u_{ji+1}^{n}+u_{j-1i}^{n}+u_{j-1i+1}^{n})}{4} \tag{6.78}$$

The equation for the second half-step is, again, entirely similar and is, again, simply obtained by replacing ***n+1/2*** by ***n+1*** and ***n*** by ***n+1/2***, respectively. The method is, again, first order accurate in time and second order accurate in space.

6.5.5 Bulk Density Equation

The ADI finite difference equation used to represent the bulk density equation, at node ***i, j***, in the first half-step of the model is:

$$\begin{aligned}\frac{\rho_{ji}^{n+1/2}-\rho_{ji}^{n}}{\Delta t/2}+\frac{1}{2\Delta x}\left[(\rho_{ji+1}+\rho_{ji})u_{ji+1}-(\rho_{ji}+\rho_{ji-1})u_{ji}\right]^{n+1/2}\\ +\frac{1}{2\Delta y}\left[(\rho_{j+1i}+\rho_{ji})v_{j+1i}-(\rho_{ji}+\rho_{j-1i})v_{ji}\right]^{n}=W_{ji}^{n+1/2}+F_{ji}^{n+1/2}\end{aligned} \tag{6.79}$$

where:

$$W=\frac{1}{\rho_w}\frac{dm_w}{dt}\left(\frac{\rho_w-\rho_m}{d_m}\right) \tag{6.80}$$

and:

$$F=\frac{1}{\rho_f}\frac{dm_f}{dt}\left(\frac{\rho_f-\rho_m}{d_m}\right) \tag{6.81}$$

The corresponding equation for the second half-step is:

$$\frac{\rho_{ji}^{n+1}-\rho_{ji}^{n+1/2}}{\Delta t/2}+\frac{1}{2\Delta x}\left[(\rho_{ji+1}+\rho_{ji})u_{ji+1}-(\rho_{ji}+\rho_{ji-1})u_{ji}\right]^{n+1/2}+$$
$$+\frac{1}{2\Delta y}\left[(\rho_{j+1i}+\rho_{ji})v_{j+1i}-(\rho_{ji}+\rho_{j-1i})v_{ji}\right]^{n+1}=W_{ji}^{n+1/2}+F_{ji}^{n+1/2} \quad (6.82)$$

Both half-steps produce systems of equations leading to tri-diagonal matrices, which are, again, solved using the Thomas algorithm. The method in each full time step is similar to that used to solve the continuity equation and is second order accurate in both time and space.

6.5.6 Model Parameterisation

The formulation for the individual fluxes at the interfaces are computed in the model through equations 6.55, 6.56 and 6.58, for the entrainment flux, equation 6.60 for the settling flux, equation 6.61 for the erosion flux, equation 6.62 for the bed formation

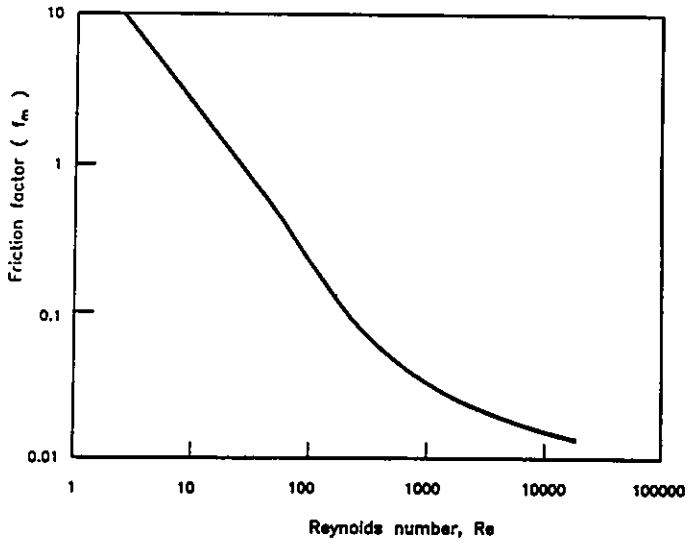

Figure 6.12 Friction factor f_m in the fluid mud layer as function of the Reynolds number (adapted from HR, 1991c).

flux and equation 6.63 for the water expulsion flux through the upper interface, while the floc, water and total fluxes are given by equations 6.69, 6.70 and 6.71, respectively.

Further to the description of the fluxes at the interfaces, definition of other variables is necessary. The shear stresses at the upper interface are defined as in Roberts (1992):

$$\tau_{ix}=\frac{f_0\rho_0}{8}\Delta u(\Delta u^2+\Delta v^2)^{1/2} \tag{6.83}$$

$$\tau_{iy}=\frac{f_0\rho_0}{8}\Delta v(\Delta u^2+\Delta v^2)^{1/2} \tag{6.84}$$

where f_0 is a friction factor ($f_0=0.008$, Odd and Cooper, 1988) and:

$$\Delta u=u_0-u_m \tag{6.85}$$

$$\Delta v=v_0-v_m \tag{6.86}$$

Similarly the shear stresses on the cohesive bed can be defined as:

$$\tau_{bx}=\frac{f_m\rho_m}{8}u_m(u_m^2+v_m^2)^{1/2} \tag{6.87}$$

$$\tau_{by}=\frac{f_m\rho_m}{8}v_m(u_m^2+v_m^2)^{1/2} \tag{6.88}$$

where the friction factor f_m is obtained, as a function of the Reynolds number, from figure 6.12. The bed shear stress definitions are based on a theoretical approach which treats the fluid mud layer as a smooth turbulent boundary layer in which the lower part would be a thick laminar sublayer in which viscous forces predominate.

The Reynolds number is defined as:

$$Re=\frac{(u_m^2+v_m^2)^{1/2}d_m}{\nu_m} \tag{6.89}$$

while fluid mud viscosity is taken as a function of concentration (Roberts, 1992) in the form:

$$\nu_m(C_m)=10^{-6}\exp(\gamma C_m) \tag{6.90}$$

where C_m is the mass concentration (dry density) in the fluid mud layer and:

$$\gamma=\frac{1}{C_R}\ln\left[\frac{\nu_m(C_R)}{10^{-6}}\right] \tag{6.91}$$

This formulation corresponds to the assumption that for $C=0$ the viscosity is that of water, while for a given $C=C_R$ the viscosity has a known value, $\nu_m\ (C_R\ )$, obtained from laboratory or field measurements.

6.6 Model Application

6.6.1 General Aspects

The numerous physical processes governing formation, growth and destruction of fluid mud layers are complex and, in terms of their global interactions, not completely understood. Also, as described in previous subsections, the field and laboratory evidence and process formulations available with respect to each one of these processes do not present the same degree of modelling usefulness and reliability.

Clearly, most physical processes require further investigation, even for relatively crude modelling purposes.

Given the currently available body of knowledge, simplifications are necessary, as noted by Kusuda et al. (1993). Studying the behaviour of fluid mud layers in an inclined bed, once formed from a quiescent suspension and allowed to flow, is a simple situation which permits the investigation of some fundamental aspects. In particular, the experiment illustrates rapid deposition during near-slack periods, commonly asociated with the formation of fluid mud layers. Laboratory experiments simulating such conditions were carried out by Ali and Georgiadis (1991) and Kusuda et al. (1993). The main findings of interest for model application resulting from such experiments are summarised in the next subsection. Data resulting from one of the experiments performed by Ali and Georgiadis (1991) was used to run the pilot numerical model and the results of the simulations are presented in Section 6.6.3.

6.6.2 Laboratory Results

Kusuda et al. (1993) used salt water and natural sediment from Kumamoto Port in Japan, of silty-clayey nature, for their tests. These were carried out in two flumes of lengths 2 and 1 m (both were 2 m high and 0.2 m wide), respectively, inside which inclined beds, of slopes up to 1:4, were installed. Mobile fluid mud, once formed through settling from suspensions which were pumped into the flumes (up to a depth of 1.7 m), flowed down the bed towards pits from which the sediment was gradually

withdrawn. Sampling pipes of small diameter were installed on the sides of the flumes and the volumes sampled from the moving layers were controlled, in order to avoid destruction of the layers. Layer thicknesses and floc velocities were determined from video records obtained using a close-up lens. Eight runs were carried out with different slopes and different initial concentrations.

Kusuda and co-workers distinguished during their experiments the formation of two layers, below the low concentration suspension:

(i) an upper, mobile, fluid mud layer, which increased in thickness for a few minutes after the beginning of each run, before approaching steady state in terms of thickness and movement;

(ii) a lower, stationary, fluid mud layer (rather than a fully developed bed, given the short duration of the experiments, of about 60 minutes), which developed after the mobile layer was fully formed; the former, to which the researchers attributed much lower effective stresses than would be expected in a cohesive bed, was also called the bed mud layer.

Apparent viscosity of the fluid mud was found to be 0.2 Pa.s, two orders of magnitude larger than that of water and the overall mobile fluid mud behaviour was that of a Newtonian fluid. According to the investigators, typical flow velocities of mobile fluid

mud were found to be around 1 mm/sec; concentrations in the mobile fluid mud layers had a tendency to increase as the initial concentrations increased.

The thicknesses of the stationary mud layers were uniform in space but showed an increase in time, at a constant rate, which also increased with smaller bed slopes and higher initial concentrations. Mobile fluid mud layers did not increase in thickness downstream and were found to be spatially uniform and temporally constant, *as long as the settling flux remained constant*; mobile layers showed thicknesses of 13 to 20 mm in all runs and became greatest for a slope of 1:10, regardless of the initial concentration of suspended solids. Such observations indicate that, as long as the concentration in the mobile layer is constant, the settling flux from the overlying water and the depositional flux to the bed mud are almost the same. Velocity and concentration profiles were also almost the same along the flume.

One of the figures (figure 8 in the original paper) in Kusuda et al. (1993) also seems to indicate that, after a stage of near constant value, the thickness of the moving layers may decrease in time, while, in space, a small rise from upstream to downstream may occur. Such aspects should be due a decrease in the settling flux and seem to confirm that settling should be the fundamental process controlling fluid mud dynamics.

Following initial SERC-funded exploratory work by O'Connor et al. (1991), Ali and Georgiadis (1991) investigated the dynamics of fluid mud using a perspex channel, 2.4 m long, 1.2 m deep and 0.15 wide, pivoted at the lower end, where a reservoir for

collecting the flowing mud was placed (see figure 6.13). A mechanical jack was attached at the other end thus allowing a horizontal or sloping bed to be produced. Slopes of 1:5, 1:10 and 1:20 were obtained and tested with saline water and mud from the Mersey estuary at initial concentrations of 3.2 g/l, 7 g/l, 10 g/l, 15.6 g/l and 30 g/l.

The experiments were carried out under similar conditions to those of Kusuda et al. (1993), i.e. sediment was allowed to settle from a quiescent suspension onto the sloping (or horizontal) bed. During the experiment four bands or layers were visually observed (except the third layer, in the case of the horizontal slope):

(i) a first layer, underneath the water surface, having a low concentration and containing mostly unflocculated particles;

(ii) a second layer, below the top one, where hindered settling and flocculation were observed; the top interface of this layer was horizontal and settled during the tests until reaching the bed layer while the bottom interface was parallel to the channel's bed;

(iii) a third layer (fluid mud), at the base of the previous one, formed by a dense suspension with interfaces parallel to the channel's bed; particles in this layer were settling but also moving downslope, while thicknesses and elevations from the bed were changing with time;

(iv) a fourth layer, termed settled bed by the investigators, but probably corresponding to stationary fluid mud (as in Kusuda et al., 1993) in the early stages of the tests; the thickness of this layer initially increased with time but, due to consolidation effects, decreased with increasing time towards the end of the tests .

The layers described by Ali and Geogiadis (1991) and those described by Kusuda et al. (1993) are, therefore, consistent but the former authors give a more detailed description of the low concentration suspension.

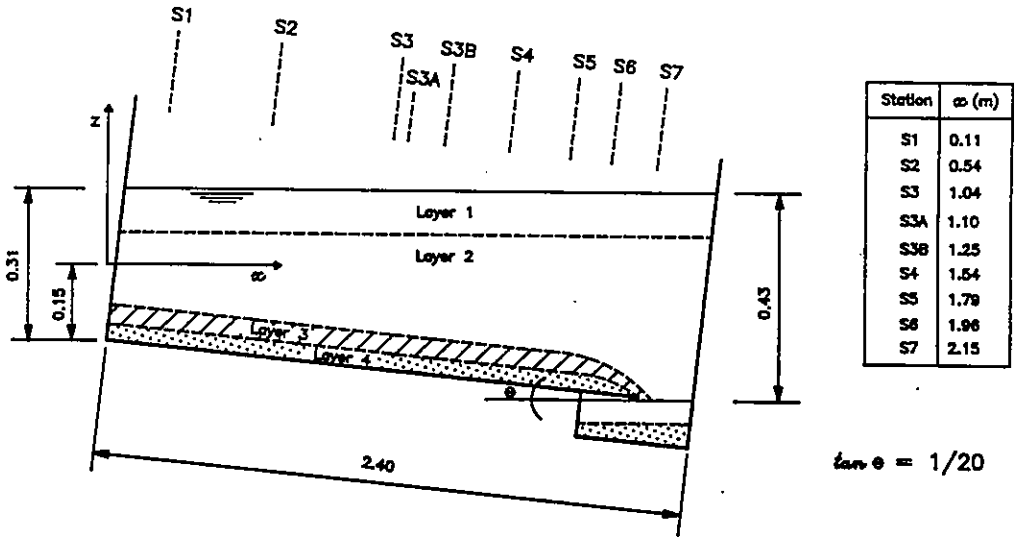

Figure 6.13 Sketch of the experimental set-up used by Ali and Georgiadis (1991).

Scales were placed on the side of the channel at various positions to measure water depths, stationary mud thicknesses and mobile fluid mud elevations and thicknesses. Bulk densities were obtained by taking samples through ports located at several

elevations of a single measuring section, an aspect which proved to be a severe limitation of the set-up for the intended modelling purposes. Average velocities of the fluid mud were determined by injecting Rhodamin B diluted in salt water into the layer and measuring the time taken by the dye to travel a given distance.

Results obtained at Station S3 regarding the characteristics of the stationary mud layer indicated that its thickness increased with time at a rate which increased with decreasing slope (as happened in the experiment of Kusuda et al. 1993). The thickness of the mobile fluid mud layer initially increased with time, reaching a maximum value, then decreased with a further increase in time. This seems to be related to the magnitude of the settling flux, which decreases after a certain time, due to lack of sediment in the upper layers. In most cases the thickness increased with the increase in slope for a given time. The average velocity of the mobile fluid mud layer decreased with time and, in most cases increased with increasing slope.

The variation of the bulk density at Station S3A was less defined. For an initial concentration of 30 g/l the bulk density reached a peak before decreasing with time (for all slopes) while for initial concentrations of 7 g/l and 15.6 g/l the density increased in time for slopes 1:5 and 1:10, while for slope 1:20 it reached a peak before decreasing. The initial increase of the bulk density, reaching a peak value before decreasing with time, seems consistent with the expected time evolution of the settling flux. However, due to the need to interpolate values between sampling ports, the investigators indicate that density values have to be taken with great caution.

6.6.3 Model Simulation of a Laboratory Experiment

One of the channel experiments carried out by Ali and Georgiadis was used to apply model FLDMUD2. Given the available data it was decided to use the results obtained for a slope of 1:20 (a typical upper value for natural estuarine bottoms) and an initial concentration of 30 g/l, for which a minimum, although not optimal, data set existed. A sketch of the geometry of the channel (of width 0.15 m) used in the experiment is presented in figure 6.13. Since the experiment corresponds, basically, to a one-dimensional situation, the x axis was oriented along the axis of the channel and lateral variability was neglected. In particular, the y momentum equation was not used (y velocities were set to zero). The orientation of the axes used in model application and the positions of the measurement stations along the channel are also indicated in figure 6.13.

The domain was discretised with $\Delta x=0.05\ m$ and a time step $\Delta t=0.5\ s$ was adopted due to the stability constraints resulting from the explicit numerical method used to solve the x momentum equation. In model application the densities of the layers were taken as horizontally uniform, at each time step, given the limited information available on concentrations and densities. This is expected to be a reasonable assumption, given the short length and width of the flume.

Initial conditions for the model run were taken at $t=2\ min$ in order to avoid the initial stages of sediment settling and formation of the mobile and stationary fluid mud

layers, which are difficult to simulate given the uncertainties associated with the determination of the settling flux. Based on the laboratory data set, linear variations, along the length of the channel, of the stationary mud thickness (d_b) and of the mobile fluid mud thickness (d_m), were imposed as initial conditions, in the form:

$$d_b^i(x) = 0.0035 + 0.0035(x - x_1)/(x_6 - x_1)$$
$$d_m^i(x) = 0.0040 + 0.0070(x - x_1)/(x_6 - x_1) \qquad (6.92)$$

where the thicknesses are obtained in metres and the x_j are the x coordinates of the j stations, which are indicated in figure 6.13. An uniform initial longitudinal velocity u_m=*0.003 m/s* was imposed, while the fluid mud layer bulk density, ρ_m, was assigned a value of *1052.6 kg/m*^{3}, as indicated by the laboratory data. In the immobile clear water layer both the x and y velocities were set to zero (as happened throughout the simulation), while the density of the same layer was assigned an initial value ρ_0=*1047.2 kg/m*^{3}, given the initial sediment concentration in the flume and the settling fluxes into the fluid mud layers from the beginning of the experiment, at *t=0*. These fluxes were computed using the updated concentrations in the upper layer for each calculation time (*0<t<2 min*) and the settling flux curve curve produced by Ali and Georgiadis (1991) and were assumed uniform along the length of the channel.

Stations S1 and S6 (see figure 6.13) were chosen as the inflow and outflow boundaries, respectively. The thickness and the bulk density of the fluid mud layer (d_m and ρ_m, respectively) were imposed at Station S1, while the x velocity (u_m) was imposed at Station S6. At Station S1 some extrapolation in time of d_m, at the beginning and at the end of the simulation period, was carried out, based on the

measured levels, but this allowed most of the channel length to be included in the computational domain. The alternative of using Station S2 as the upstream boundary, for example, would imply that a much shorter reach of the channel could be used for comparison with laboratory results. The layer thicknesses (in metres) at Station S1 and the velocities (in metres per second) at Station S6 were specified, based on the laboratory data as:

$$\begin{aligned} d_m^1(t) &= 0.004 - 0.002\,(t-t_0)/120 && t_0 < t \le 360s \\ d_m^1(t) &= 0.002 && 360s < t \le t_M \\ u_m^1(t) &= 0.005 - 0.002\,(t-t_0)/(t_M-t_0) \end{aligned} \qquad (6.93)$$

while the bulk density at Station 1 was imposed using the bulk density curve of figure 6.22 for the slope and initial concentration of the experiment.

The fluid mud viscosity for the reference concentration (see equation 6.91) used in the simulation was $\nu_m(C_R)=6.5\times10^{-4}\ m^2/s$, with $C_R = 75\ g/l$ (as in Roberts, 1992), much higher than that of water and in agreement with the value determined by Kusuda et al. (1993). Ali et al. (1994) used several methods for computing fluid mud friction factors and kinematic viscosities, using data from their race-track flume experiments and the Parrett estuary and confirmed that both the friction factor f_m and ν_m should have extremely high values. In particular, values of ν_m calculated with the Parrett data were in agreement with the value adopted in the runs of model FLDMUD2.

Other parameters used in the simulation were $V_t=0.2\times10^{-5}$ *m/s* in equation 6.63 (based on typical interface lowering velocities during consolidation experiments), $k_s=0.93$ in equation 6.70 and $V_{bf}=0.85W_s(C_m)$ in equation 6.62. These parameters were adjusted during model runs but will need to be studied in specific experiments, possibly leading to improved descriptions of the phenomena they describe in a crude way. The floc density was taken as 1300 *kg/m*^{3} while the solids and salt water densities were taken as *2650* and *1030* *kg/m*^{3}, respectively, the latter being estimated given the initial volume and sediment concentration in the flume.

One of the objectives of the simulation was to run the model for a total time encompassing and, if possible, exceeding the settling period, i.e. that time during which a significant amount of sediment was still available for settling from the upper layers. The model was, therefore, run for 8 minutes, from $t_0=120$ *s* to $t_M=600$ *s*, as the mobile fluid mud thickness apparently became negligibly small at Station S1 shortly after the end of the settling period.

The main problem found in using the available laboratory data set to test model FLDMUD2 resulted from difficulties in accurately computing the settling fluxes into the fluid mud layers which, as indicated by the experiments of Kusuda et al. (1993) and confirmed by those of Ali and Georgiadis (1991), are fundamental in determining the dynamics of such layers.

A first difficulty results from the fact that the settling flux versus concentration curve produced by Ali and Georgiadis (1991) was obtained through the use of a field settling velocity curve obtained in the Severn estuary. An indirect verification was carried out by Ali and Georgiadis by computing the approximate settling velocities from the laboratory data and those, according to the same authors, were *consistent* with those of the original field curve. However, it is unlikely that turbulence levels (and, therefore, floc aggregation and breakup conditions and the corresponding settling velocities) produced during mixing of the suspension in the laboratory can be directly related to those found under natural conditions in the Severn estuary. A simple laboratory settling column test, carried out with the same suspension used in the flume tests, would have produced more consistent results.

A second problem was that, due to the fact that concentrations were only directly measured at three ports (located 1, 3 and 5 cm above the bottom of the channel) and at a single station, Station 3A, the direct determination of the concentration at the bottom of the upper layer (and, therefore, of the settling flux) becomes extremely difficult.

It was, therefore, decided to obtain the settling fluxes from the curve produced by Ali and Georgiadis (1991) but to compute the concentration in the the upper layer, at each time step, as a result of the initial concentration and of mass losses to the fluid mud layers. The settling flux was observed to increase up to about 5 minutes and to

decrease afterwards, becoming very small after about 8 minutes, an evolution which is consistent with the measured thicknesses and densities of the fluid mud layer.

Due to the uncertainties associated with the determination of settling fluxes during the laboratory experiment, allowing mass exchanges at the upper interface to be accurately specified and the bulk density of the fluid mud layer to be computed, it was decided to test this part of the model indirectly. The bulk density curve measured in the laboratory (see figure 6.22) was used in the model to compute d_m and u_m, while these values and the computed settling fluxes were used, in a parallel computation, to determine the bulk density through equations 6.79 and 6.82.

The results of model simulations are presented in figures 6.14 to 6.18 for the thicknesses and depth-averaged velocities of the mobile fluid mud layer at Stations S2, S3, S3B, S4 and S5 and in figure 6.19 for the depth-averaged bulk density (also averaged over the area of the flume, as previously indicated).

For comparison purposes the thicknesses measured during the laboratory experiment of Ali and Georgiadis (1991) at Stations S2, S3, S3B, S4 and S6, for initial concentration C^i=*30 g/l* and slope *1:20* are shown in figure 6.20. Velocities measured at Station S3 for the same initial concentration and slopes *1:20*, *1:10* and *1:5* are shown in figure 6.21, while bulk densities measured at Station 3A for the same initial concentration and slopes are presented in figure 6.22. The measured bulk density

values at Station S3A for C^i=*30 g/l* and slope *1:20* (i.e. the simulated experiment) are also shown in figure 6.19 for comparison with the model output.

It is observed from the simulated thicknesses of the mobile fluid mud layer (figures 6.14 to 6.18) that their magnitudes show good correspondence with those measured in the laboratory (figure 6.20) at Stations S2, S3 and S3B while at Stations S4 and S5 they are higher, by a factor of about 3. However the time evolution of the simulated thicknesses at the latter stations shows a better correspondence with the laboratory trends. Simulated thicknesses reach a peak value, before decreasing with time, at all stations. The peak occurs later in the downstream direction and, at Stations S2, S3 and S3B, it occurs while the settling flux is still increasing. These features seem to indicate that, for the conditions of the simulation, loss of mass through longitudinal advection prevails over the gain due to settling at the upstream sections and that the advected mass accumulates in the downstream reaches of the flume, as indicated by the simulated thicknesses in Stations S4 and S5. This aspect also seems to be confirmed by the velocities simulated at Stations S2, S3 and S3A. These show values which are somewhat higher, relative to the measured laboratory velocities, and their trends in time only seem to match the latter after about 8 minutes. Conversely, at Stations S4 and S5 agreement between the simulated velocities and those obtained in the laboratory is good during most of the simulation period, regarding both their magnitude and their time evolution.

From figures 6.20 and 6.22 it can be concluded that, in the laboratory experiment, settling was the dominant factor, as indicated by the decrease in both the layer thicknessess and densities after about 8 minutes, in agreement with the observations of Kusuda et al. (1993). Ali et al. (1994) applied model FLUIDMUDFLOW-2D developed by HR Wallingford (see Odd and Cooper, 1988, for details) to the simulation of laboratory experiments carried out by Ali and Georgiadis (1991) in the setup of figure 6.13 and by Crapper and Ali (1994) in a race-track flume. These authors concluded from their simulations that the behaviour of the model was highly sensitive to the way in which settling was described, an aspect which is also expected to hold for model FLDMUD2.

In order to check the accuracy of the settling flux calculation, the bulk density resulting from the parallel computation carried out with equations 6.79 and 6.82 was also compared with that measured during the laboratory experiment (see figure 6.19). It is possible to conclude that, although the initial increase in density detected in the laboratory (up to about 4 minutes) is not reproduced by the model, both the magnitude and the general trend of the computed densities are in reasonable agreement with the measured data. This is an encouraging result, especially if the rather crude descriptions adopted for some of the interface mass exchange processes and the nature of the simple relationships between the masses and the volumes, which result from assuming a single order of floc aggregation, are considered. This result may also indicate that the computed settling fluxes were also in good agreement with those actually occurring during the laboratory experiment.

All the above conclusions seem to indicate that, despite being much higher than that of water, the viscosity reproduced in the model is still insufficient. This is in agreement with the findings of Ali et al. (1994).

Full confirmation of the present conclusions would, however, require that a more comprehensive laboratory data set is obtained, including detailed measurements of densities and velocities and a more accurate determination of the settling velocity curve. It is expected that such a data set would allow full testing of model FLDMUD2, although, as indicated before, some process modelling aspects also need improvement.

6.7 Summary

In this chapter a mathematical formulation aimed at describing the dynamics of thin to medium thickness mobile fluid mud layers was developed and tested. Such layers are defined as those having no significant vertical structure or large vertical variations in either density or horizontal velocity. They are also believed to be the most frequent case of high-concentration layers occurring in estuarine environments, as very thick layers have seldom been detected.

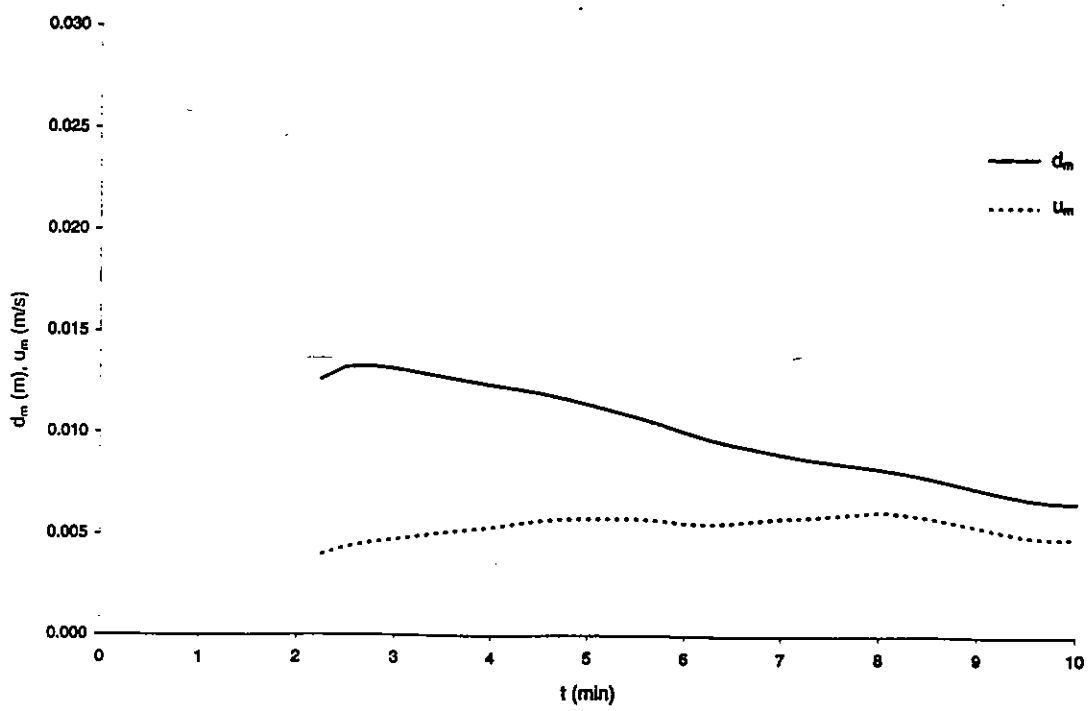

Figure 6.14 Computed mobile fluid mud thicknesses and velocities at Station S2.

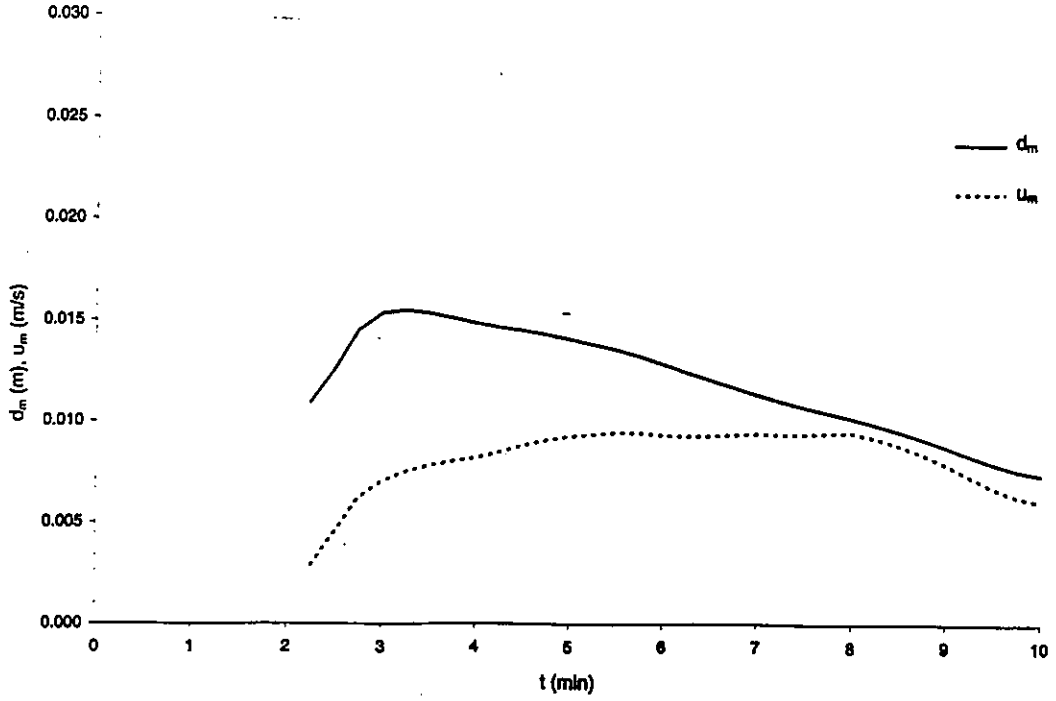

Figure 6.15 Computed mobile fluid mud thicknesses and velocities at Station S3.

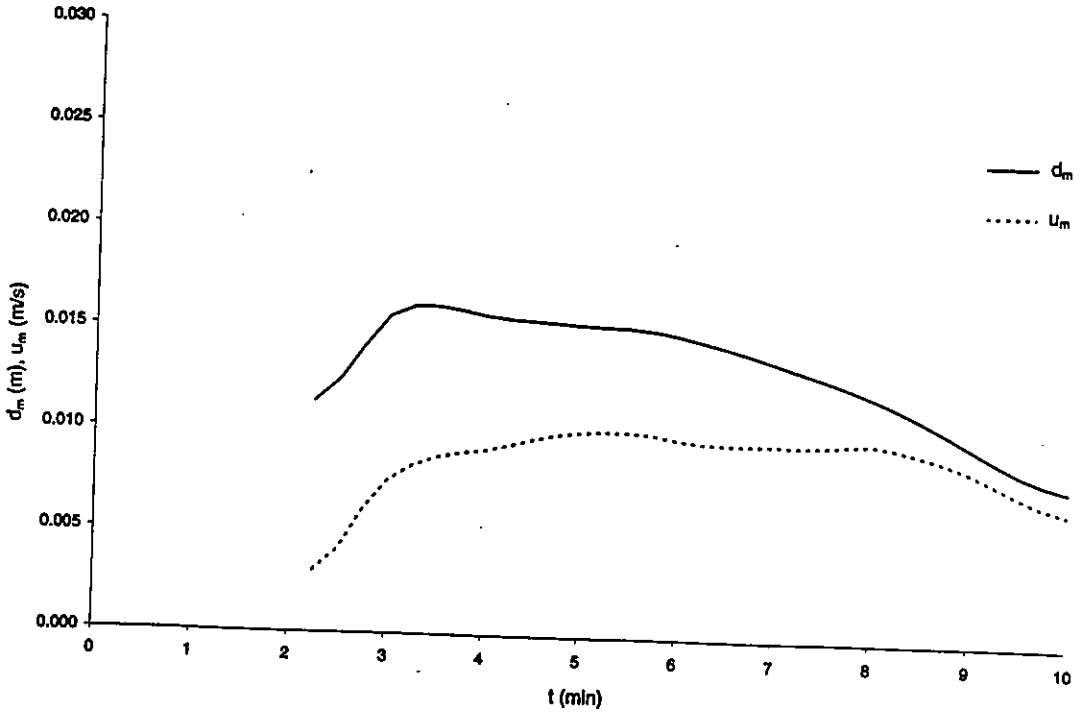

Figure 6.16 Computed mobile fluid mud thicknesses and velocities at Station S3B.

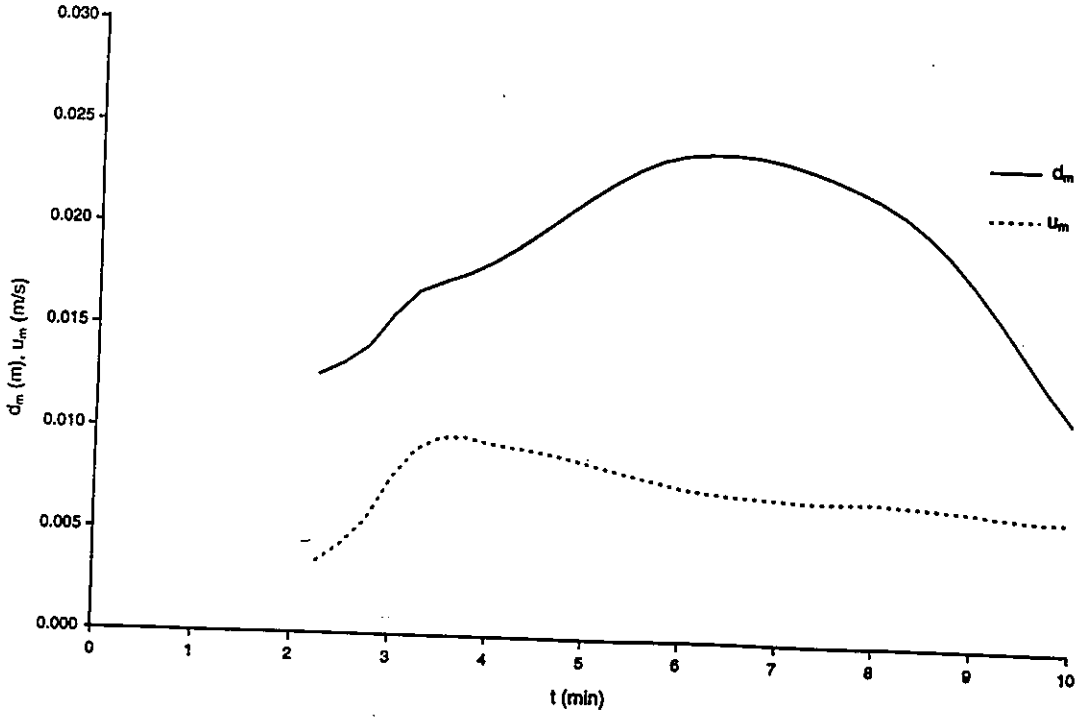

Figure 6.17 Computed mobile fluid mud thicknesses and velocities at Station S4.

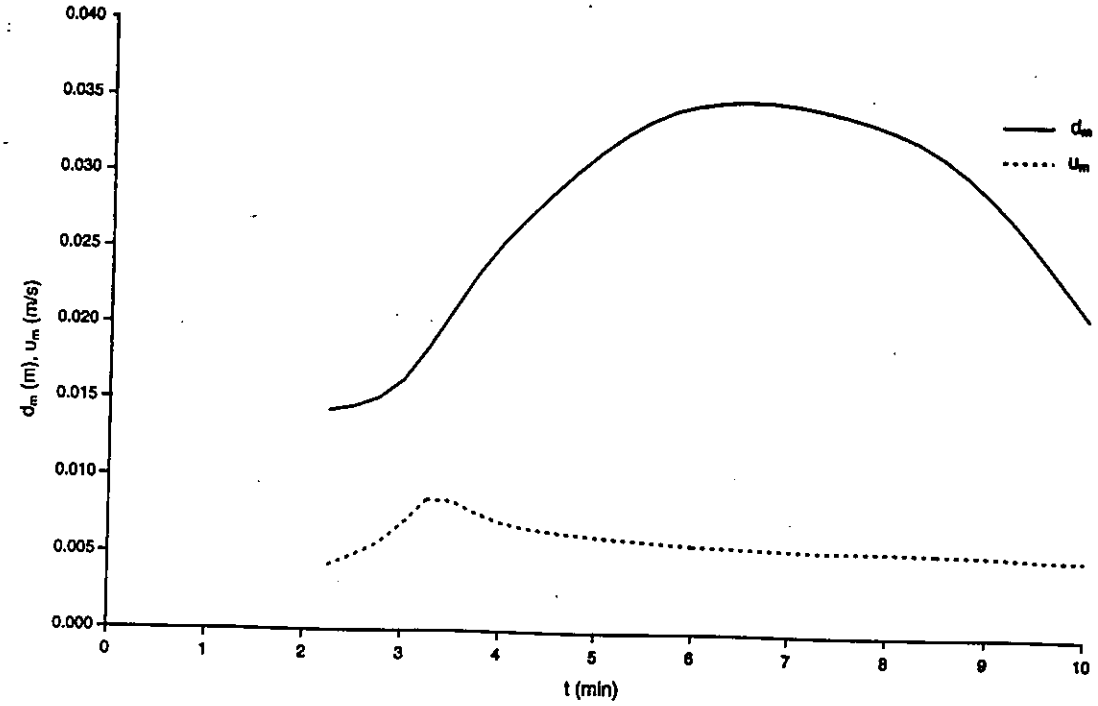

Figure 6.18 Computed mobile fluid mud thicknesses and velocities at Station S5.

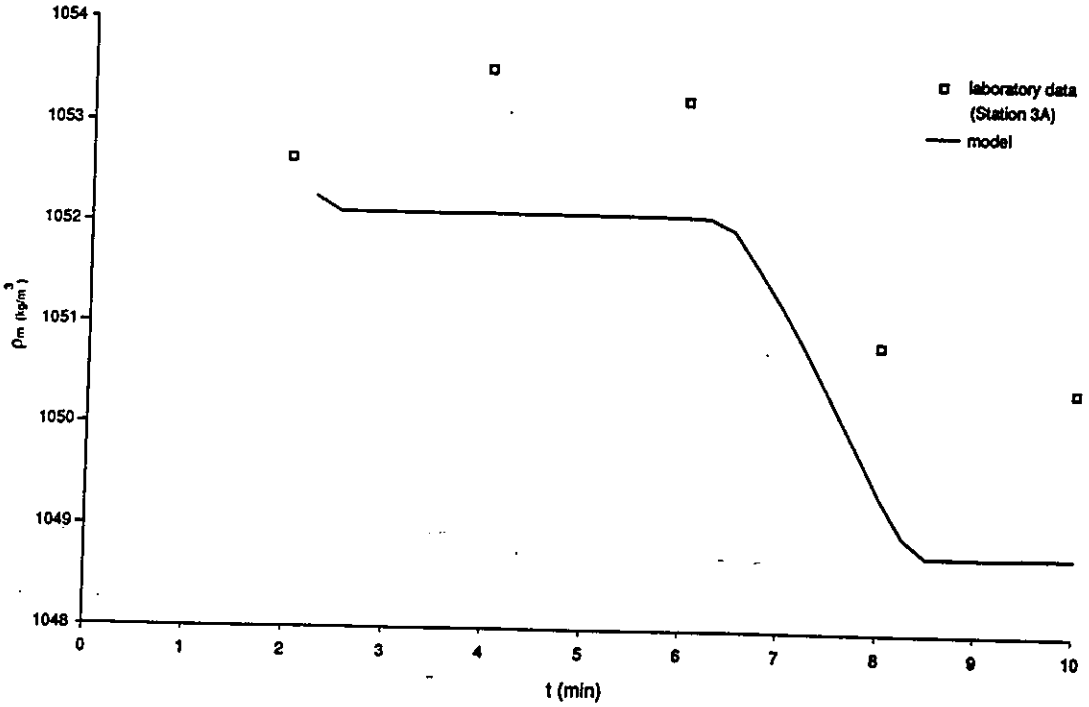

Figure 6.19 Computed mobile fluid mud bulk densities (averaged over the area of the flume) and laboratory-measured bulk densities (C^i=30 g/l , slope 1:20).

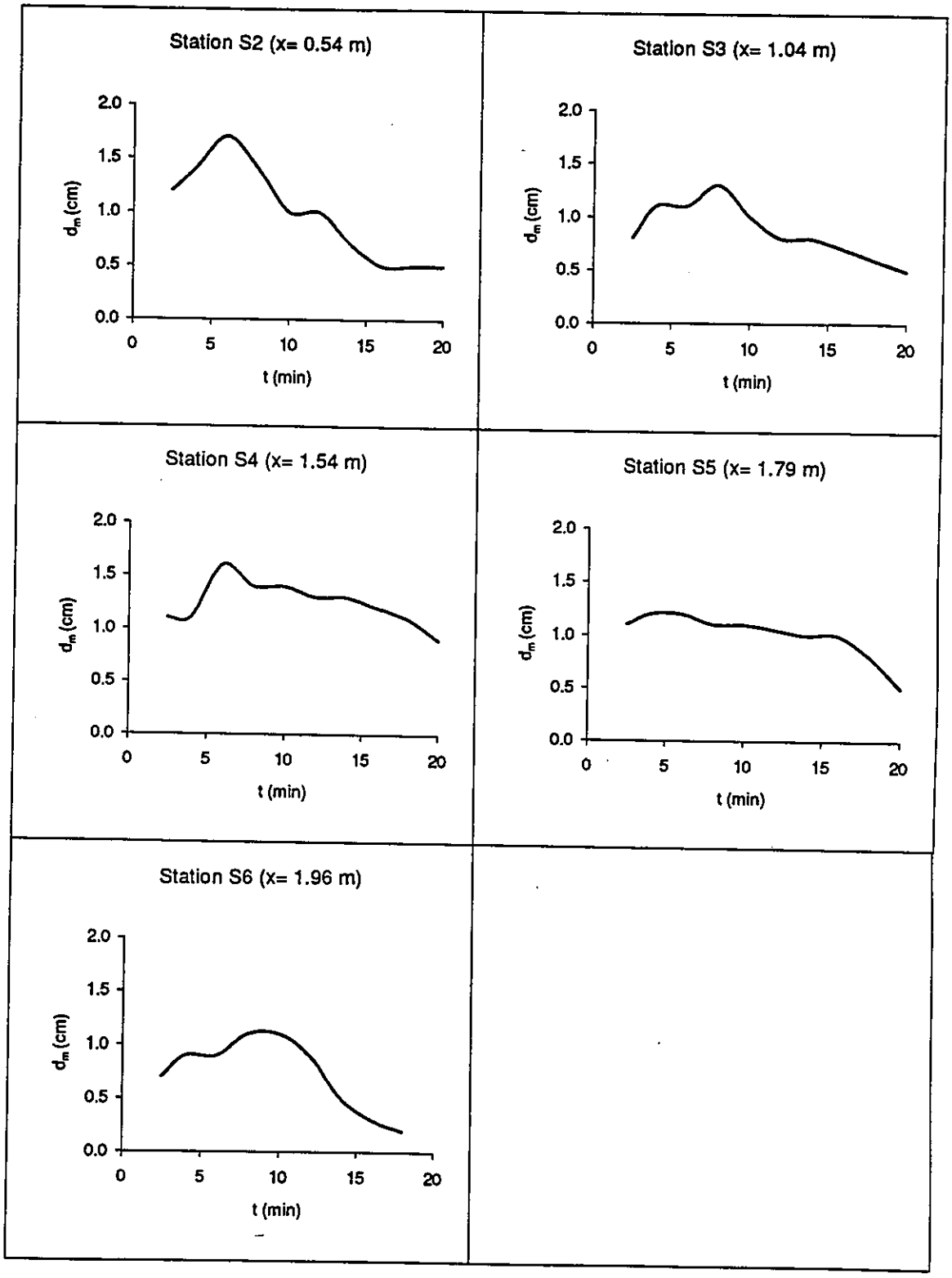

Figure 6.20 Laboratory-measured thicknesses of mobile fluid mud layers at several Stations for C^i =30 g/l and slope 1:20 (adapted from Ali and Georgiadis, 1991).

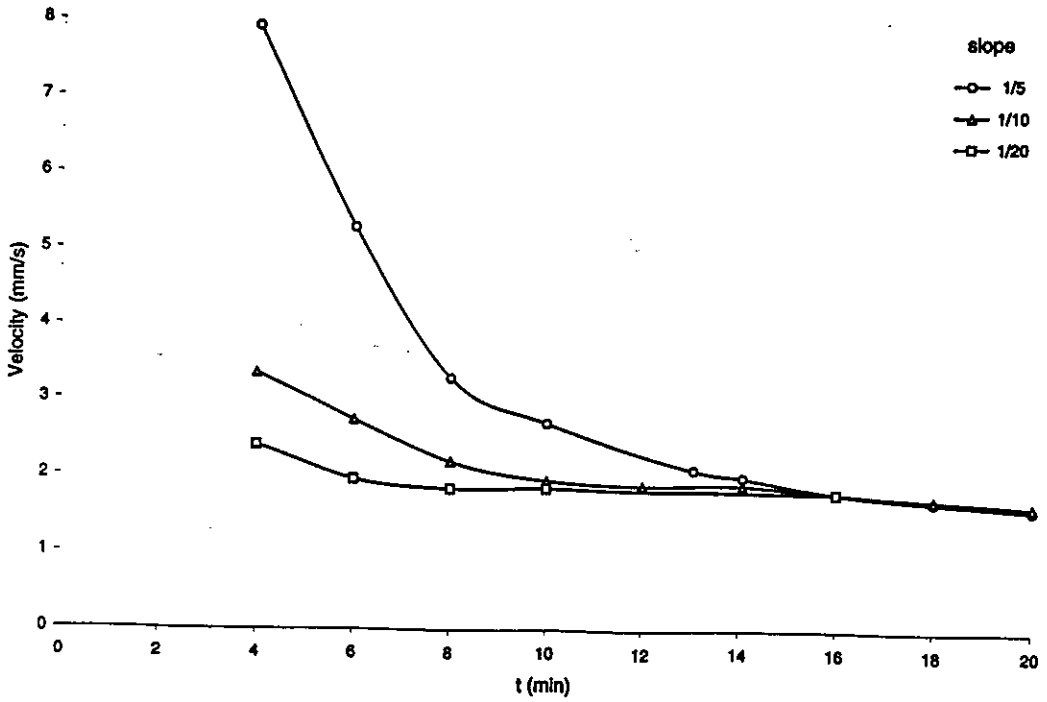

Figure 6.21 Laboratory-measured velocities of mobile fluid mud at Station S3 for C^i =30 g/l and slopes 1:5, 1:10 and 1:20 (adapted from Ali and Georgiadis, 1991).

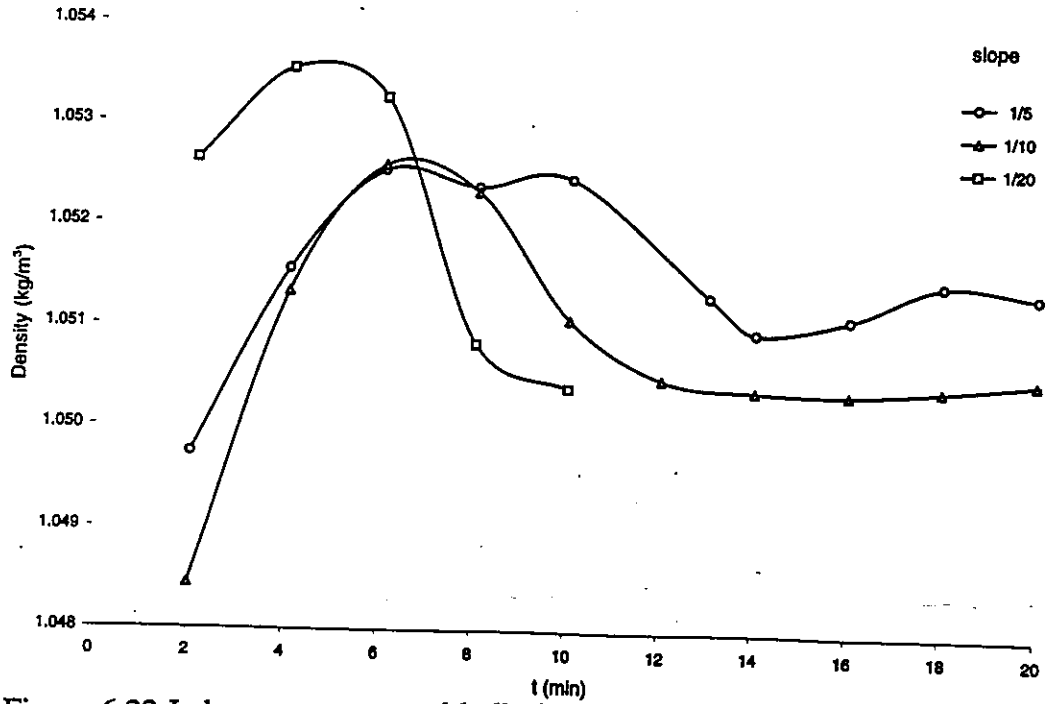

Figure 6.22 Laboratory-measured bulk densities of mobile fluid mud at Station S3A for C^i=30 g/l and slopes 1:5, 1:10 and 1:20 (adapted from Ali and Georgiadis, 1991).

The motivation for studying the dynamics of fluid mud layers in estuaries is twofold:

(i) the existence of fluid mud layers drastically changes both the magnitude of the mass fluxes through which low concentration suspensions exchange solids and water with the lower layers and the time intervals during which such exchanges take place;

(ii) the near-bed mass transport in high-concentration layers, which flow at velocities very similar to those of the low concentration suspensions above, is very significant.

Models describing the dynamics of fluid mud layers will, therefore, be useful both for producing improved bed boundary conditions for transport models in the water column (low concentration suspensions) and to describe the advective mass transport taking place in near-bed layers.

The most relevant features of fluid mud, derived from field studies were, therefore, reviewed in this chapter and allowed the development of a set of assumptions regarding the dynamics of thin to medium thickness mobile layers. Based on this set of assumptions a depth-averaged mathematical formulation was derived, which allows the calculation, not only of the thickness and velocities in the layers, but also of their densities.

The possibility of computing the bulk densities of high-concentration layers is considered to be particularly important as field measurements indicate that a characteristic bulk density value, assumed not to change in either space or time (as happens in existing formulations), leads to severe simplifications in the physics of the phenomenon being described. A fourth equation for computing the bulk density was, therefore, added to the classical continuity and x and y momentum equations and, in order to test the proposed formulation, a pilot numerical model (FLDMUD2) was developed.

In order to apply the system of equations derived in the present chapter it is also required that the mass exchanges, composed of water and solids (in flocculated condition), taking place with the low concentration layers, above, and the structured bed (or the stationary fluid mud layers), below, are specified. Although such fluxes result from a rather limited number of physical processes, the corresponding process models are far from presenting the same degree of reliability for system modelling purposes. Further investigation on such processes is, clearly, necessary. This aspect was found to be one of the most important limitations of the proposed formulation.

The pilot model was applied to the simulation of a simple laboratory experiment, namely the flow of fluid mud layers along an inclined bed, once formed from a quiescent suspension (Ali and Georgiadis, 1991). This experimental set-up is representative of rapid deposition conditions during near-slack periods and allows a number of relevant aspects to be studied.

Limitations of the available data set and, in particular, those regarding the determination of the settling fluxes and of the bulk densities, prevented full testing of the model. However, analysis of model output and its comparison with the laboratory results produced by the same authors and with the trends resulting from a similar experiment by Kusuda et al. (1993) allowed some conclusions to be drawn. Two main factors were identified which largely determine modelling results:

(i) the accurate simulation of the settling fluxes into the fluid mud layers, which is the key factor in determining the vertical dynamics (growth and decay) of the layers;

(ii) the accurate characterisation of fluid mud, in terms of its viscosity (apparently, higher than currently assumed) which largely determines the transport of fluid mud along the bed.

Finally it is recognised that, while modelling progress in the field of fluid mud dynamics should benefit from the existence of improved data sets it is also expected that the needs resulting from model development and application will contribute towards the design of new laboratory and field experiments. It is expected that concurrent improvements in both data sets and process modelling capabilities will allow gains of accuracy in fluid mud model simulations and their coupling with existing 3D transport models in the water column, therefore significantly increasing the capabilities of overall system models for cohesive sediment transport.

CHAPTER 7
SUMMARY, CONCLUSIONS AND RECOMMENDATIONS

7.1 Summary

In the present investigation mathematical formulations and numerical models, aimed at describing the dynamics of cohesive sediments in three dimensions, were developed. The adopted formulations incorporated recent process modelling results while the choice of numerical techniques resulted from their suitability to accurately describe each process. Models were developed considering the differences between cohesive sediment transport and the transport of either coarse sediment or dissolved constituents in tidal environments, which are mainly expressed through the vertical dynamics of muddy sediments. The need for practical tools, aimed at solving specific engineeering problems with adequate accuracy, was also a relevant criterion in model development.

Following the conclusions of the specialised panel on numerical modelling at the Estuarine Cohesive Sediment Workshop, held in 1991 (Mehta, 1991b), modelling improvements were sought in two main aspects:

(i) The development of a three-dimensional transport model for low to medium concentration suspensions (SUSMUD3), using process model descriptions classically associated with such suspensions but including a flexible vertical coordinate transformation. This transformation should, in the case of muddy sediments, allow grid refinement in those areas where concentration gradients

are larger, without requiring a uniformly fine vertical discretisation in the whole domain, an important aspect when considering three-dimensional modelling of large estuarine domains.

(ii) The development of a model describing the dynamics of near-bed high-concentration layers, also called fluid mud layers (FLDMUD2). The need to model fluid mud dynamics is twofold: mass exchanges specified at the lower boundary, in low concentration transport models, are changed in the presence of fluid mud; transport in fluid mud layers is very significant due to the occurrence of both high velocities and high sediment concentrations in such layers.

A description of the physical processes of interest for model SUSMUD3 is found in Chapter 2, while model formulation, development and application to a real estuarine channel are found in Chapters 3, 4 and 5, respectively. Specific conclusions resulting from model application are also described in the latter chapter. The relevant physics and process modelling aspects relative to model FLDMUD2 are found in Chapter 6. Formulation, development and application of FLDMUD2 to the simulation of a laboratory experiment are also described in Chapter 6, where the specific conclusions are summarised.

As noted by Teisson (1991, 1994) the critical aspect for engineering cohesive sediment modelling lies in the description and implementation, in terms of workable algorithms,

of cohesive sediment processes. This aspect was also confirmed during the formulation and application stages of the models developed during the present research, as process models required to describe low concentration suspensions are better known than those which are of interest to simulate fluid mud dynamics. Model SUSMUD3 can, consequently, be regarded as an application tool for real estuaries, while FLDMUD2 was mainly developed to test process models and model formulation. The latter is a depth-averaged formulation which includes, besides the classical continuity and x and y momentum equations, an equation describing bulk density evolution. This parameter, as indicated by recent field measurements, is not adequately described by a single value, as happens in existing models, and its time and space variability should be accounted for. Application of model FLDMUD2 indicated that further improvements on the physics it describes and improved data sets for further testing are still required. It is expected that, once this model is in fully operational condition, it will be possible to couple both models, therefore ensuring the applicability of the resulting modelling system to most environments where muddy sediments exist.

Drawing on the conclusions derived from the formulation, development and application of models SUSMUD3 and FLDMUD2 some overall conclusions and recommendations for system modelling practice of muddy sediments are presented in this chapter.

7.2 Conclusions and Recommendations

The dynamics of muddy sediments in estuaries is both a consequence of tidal hydrodynamics and a prerequisite for describing the fate of associated pollutants. Mud modelling is a fundamental link if a comprehensive description of estuarine systems is sought. However, current modelling practice shows that the degree of accuracy which can be expected from numerical modelling rapidly decreases from hydrodynamics to muddy sediment simulations and from these to the description of associated pollutant transport (Mehta, 1991b). Neglecting, as a first level approach, the complex and not fully understood interactions between mud and pollutants, a number of aspects deserve consideration, if sediment modelling (and, ultimately, overall modelling) is to be improved:

(i) Mud Transport in the Water Column as an Essentially 3D Phenomenon

As described in Chapter 3, reduction in the number of modelling dimensions has, usually, been due to limitations of the available computing resources, as flow and sediment transport patterns are, basically, three-dimensional. The application of model SUSMUD3 to the Mersey Narrows indicates that, for the adopted level of assumptions (namely, a single sediment class approach) and given currently available computing capabilities, 3D models are an economical tool to be used for short term engineering simulations and overall studies of estuarine systems. It seems, therefore, that the use of 2D or 1D models should be restricted to testing

improvements in process models and formulations. Also, given the importance of vertical phenomena, it is unlikely that depth-averaged approaches retain any advantages regarding short term modelling applications.

(ii) Mud Transport in the Water Column as a Consequence of Hydrodynamics

As noted by Teisson (1994) it is usual to run cohesive sediment transport models by previously running hydrodynamics models which produce the necessary advective velocity field. This decoupled approach was also followed in the application of model SUSMUD3 to the Mersey Narrows. However, a number of aspects require consideration (Teisson, 1994):

(a) cohesive particles are advected back and forth, over large distances during each tidal cicle and their residual displacement is highly dependent on the accuracy of the hydrodynamics calculation;

(b) the importance of the processes taking place over estuarine tidal flats on the overall dynamics of mud requires that wetting and drying of such areas is accurately reproduced in hydrodynamics models;

(c) in harbours and enclosed basins, gyres control deposition; however, their simulation using eddy viscosity concepts is strongly dependent on the

empirical values assigned to these coefficients: higher order turbulence closures should be used instead;

(d) process models for erosion and deposition are based on relationships between the bottom shear stress and threshold values; the former are determined from the flow field and errors in the velocity can induce significant changes on erosion/deposition patterns.

Application of model SUSMUD3 to the Mersey Narrows (Chapter 5) also indicated that:

(e) given the importance of correctly simulating settling/deposition and erosion/re-suspension sequences around slack water, the time step for hydrodynamics simulations should be determined as a consequence of the evolution of the bottom shear stresses in time and of the erosion/deposition thresholds;

(f) although vertical velocities may be negligibly small for other modelling purposes, it is observed that their magnitudes are very similar to those of the settling velocities of mud flocs and that, therefore, they should significantly influence vertical sediment dynamics; the accurate calculation of vertical velocities is fundamental for cohesive sediment modelling;

All the above justify that:

(A) cohesive sediment transport models should rely on the most accurate hydrodynamics models (Teisson, 1994);

(B) hydrodynamics and transport models (for sediment and salt) should be used in a completely coupled way;

(C) application conditions of the coupled model sets (i.e. time and space discretisations, turbulence closures) should be determined by the requirements arising from sediment transport modelling rather than by strictly hydrodynamics criteria.

(iii) Vertical Dynamics in the Water Column

Cohesive sediment transport is basically different from the transport of dissolved constituents due to settling and to mass exchanges with the *bed* (cohesive bed or fluid mud layers). The magnitude of the settling fluxes is a consequence of the physico-chemical properties of the sediment and of the characteristics of the turbulence field, which determine particle collision, aggregation and breakup. Sediment concentration, in turn, influences turbulence damping and inhibits vertical turbulent mass exchanges. Mass exchanges with the bed, classically described in

terms of erosion/deposition concepts become significantly different in the presence of fluid mud layers.

Application of model SUSMUD3 to the Mersey Narrows confirmed the importance of correctly reproducing the vertical component of cohesive sediment transport if overall accuracy is to be improved. The same study indicated the importance of introducing into coupled hydrodynamics/transport models more sophisticated turbulence closures, in conjunction with improved modelling of the settling fluxes, relative to classical formulations, if detailed simulations of the concentration field are to be carried out. Results of the same application confirmed that vertical grid refinement in near bed regions (where larger gradients are expected) should improve modelling accuracy, while avoiding excessive vertical discretisation.

Application of a vertical 1D model to test the vertical formulation of SUSMUD3 suggests that this type of models should be used to test improved process models of vertical phenomena and to investigate the structure of the concentration profile. It is possible, as indicated by runs of the 1D model, that an upper value of the time step is imposed by the need to simulate the time evolution of the finer structural details of the profile.

(iv) Transport in Near-bed High-concentration Layers

Development and testing of model FLDMUD2 allowed the identification of two fundamental factors in the dynamics of such layers: settling (and associated phenomena, leading to layer formation) and fluid mud viscosity. More research on basic physical processes is needed. Also, given that concentration alone does not seem to be a sufficient criterion for the identification of fluid mud, further research is also needed in order to define a practical modelling criterion, which will allow models describing transport in the water column and fluid mud models to be linked.

A crucial aspect in model application is the availability of adequate data sets and, in particular, their consistency. It is often necessary to apply models to study sites where some fundamental information is not available and certain parameters have to be estimated from the literature. Although sensitivity analysis can be carried out, it is unlikely, given the strong dependence of mud transport on sediment properties and local hydrodynamics, and the multiple and complex flow-sediment interactions that such applications may provide any meaningful insight into the performance of models or on the behaviour of the systems they intend to describe. Also, as indicated in Chapter 2, the development of more realistic but, also, much more complex formulations, for cohesive sediment modelling requires that suitable data sets are concurrently obtained. In the absence of such data sets, models may provide diagnostic

capabilities (a useful development by itself) but the quality of their contribution for solving engineering problems will scarcely have improved.

Finally, as noted by Teisson (1994), given the numerous limitations currently existing, cohesive sediment transport models should not be regarded as ready-to-use tools. The accuracy obtained in each application will largely depend on the quality and consistency of the available data set and on the expertise of the modeller. Present trends towards more complex formulations, allowing the description of a larger number of water-sediment-pollutant interactions, indicate that this situation should not be expected to change in the near future.

REFERENCES

Abbott, M.B., "An Introduction to the Method of Characteristics," American Elsevier, New York, USA, 1966.

Abraham, G., "Turbulence and Mixing in Stratified Tidal Flows," In: *Physical Processes in Estuaries*, W. van Leussen and J. Dronkers, eds., Springer-Verlag, Berlin, Germany, 1989.

Agar, M. and McDowell, D.M., "The Sea Approaches to the Port of Liverpool," *Proc. Inst.Civil Eng.*, 49, 1971, pp. 145-156.

Alexis, A., Bassoulet, P., Le Hir, P. and Teisson, C., "Consolidation of Soft Marine Soils: Unifying Theories, Numerical Modelling and In-situ Experiments," *Proc. XXIII Int. Conf. Coastal Eng.*, ASCE, Venice, Italy, 1992, pp. 2949-2961.

Ali, K.H.M., Crapper, M. and O'Connor, B.A., "Physical and Mathematical Modelling of Fluid Mud Transport," *II Int. Symp. Eurocoast - Littoral'94*, Lisbon, Portugal, 1994.

Ali, K.H.M. and Georgiadis, K., "Laminar Motion of Fluid Mud," *Proc. Inst.Civil Eng.*, Part 2, 91, 1991, pp. 795-821.

Anderson, D.A., Tannehill, J.C. and Pletcher, R.H., "Computational Fluid Mechanics and Heat Transfer," Hemisphere Publishing Corporation, New York, USA, 1984.

Ariathurai, R. and Krone, R.B., "Finite Element Model for Cohesive Sediment Transport," *J. Hyd. Division ASCE*, 102 (HY3), 1976, pp. 323-338.

Bain, A.J., "Erosion of Cohesive Muds," *MSc Thesis*, Department of Civil Engineering, University of Manchester, Manchester, UK, 1981.

Baptista, A.M., "Solution of Advection-Dominated Transport by Eulerian-Lagrangian Methods Using the Backwards Method of Characteristics," *PhD Dissertation*, Department of Civil Engineering, MIT, Cambridge, Massachusetts, USA, 1987.

Barakat, H.Z. and Clark, J.A., "On the Solution of the Diffusion Equation by Numerical Methods," *J. Heat Transfer ASME*, 87-88, 1966, pp. 421-427.

Berlamont, J., Ockenden, M., Toorman, E. and Winterwerp, J., "The Characterisation of Cohesive Sediment Properties," *Coastal Eng.*, 21, 1993, pp. 105-128.

Berlamont, J., van den Bosch, L. and Toorman, E., "Effective Stresses and Permeability in Consolidating Mud," *Proc. XXIII Int. Conf. Coastal Eng.*, ASCE, Venice, Italy, 1992, pp. 2962-2975.

Bowden, K.F. and Gilligan, R.M., "Characteristic Features of Estuarine Circulation as Represented in the Mersey Estuary," *Limnol. Oceanogr.*, 16, 1971, pp. 490-502.

Bowden, K.F. and Hamilton, P., "Some Experiments with a Numerical Model of Circulation and Mixing in a Tidal Estuary," *Estuarine Coastal Mar. Sci.*, 3, 1975, pp. 281-301.

Capitão, J.J.A., "A Two-Dimensional Hydrodynamic Model Using a Finite Volume Approach," *MSc Thesis*, Coastal and Oceanographic Engineering Department, University of Florida, Gainesville, Florida, USA, 1989.

Carter, S.E.F., "Mersey Barrage Company. Stage IIIA Feasibility Study. Hydraulics and Sedimentation Working Paper on Activity D Task 5(b) and 5(c). Continuous Silt Monitoring in the River Mersey. June 1990 to May 1992," *Report*, Mersey Barrage Company, Liverpool, UK, 1992.

Cashin, J.A., "Engineering Works for the Improvement of the Estuary of the Mersey," *J. Inst.Civil Eng.*, 32, 1949, pp. 296-367.

Costa, M.V., "A Three-Dimensional Eulerian-Lagrangian Method for Predicting Plume Dispersion in Natural Waters," *Memoire-DEA Européen en Modélisation de L'Environnement Marin*, Instituto Superior Técnico, Lisbon, Portugal, 1991.

Costa, R.G., "Flow-Fine Sediment Hysteresis in Sediment-Stratified Coastal Waters," *MSc Thesis*, Coastal and Oceanographic Engineering Department, University of Florida, Gainesville, Florida, USA, 1989.

Costa, R.G., "Numerical Modelling of the Vertical Dynamics of Cohesive Sediments in Estuarine Environments," *Proceedings of the Portuguese-French Seminar on Modelling in Maritime Hydraulics*, Civil Engineering Department, University of Coimbra, Coimbra, Portugal, 1994.

Costa, R.G. and Mehta, A.J., "Flow-Fine Sediment Hysteresis in Sediment-Stratified Coastal Waters," *Proc. XXII Int. Conf. Coastal Eng.*, ASCE, Delft, The Netherlands, 1990, pp. 2047-2060.

Crapper, M. and Ali, K.H.M., "A Laboratory Study of Cohesive Sediment Transport," *4th Nearshore and Estuarine Cohesive Sediment Transport Conference*, Wallingford, UK, 1994.

Dellersnijder, E., "Upwelling and Upsloping in Three-Dimensional Marine Models," *Appl. Math. Modelling*, 13, 1989, pp.462-467.

Dellersnijder, E. and Beckers, J.M., "On the Use of the σ-Coordinate System In Regions of Large Bathymetric Variations," *J. Mar. Systems*, 3, 1992, pp. 381-390.

DHI - Danish Hydraulic Institute and Water Quality Institute, "Newport Borough Council, River Usk Barrage, Sediment Transport Modelling," Vol. 2, *Report*, Danish Hydraulic Institute, Hørsholm, Denmark, 1990.

Dobbins, W. E., "Effect of Turbulence on Sedimentation," *Trans. ASCE*, 109, 1944, pp. 629-656.

Dyer, K.R., "Estuaries, a Physical Introduction," John Wiley and Sons, London, UK, 1973.

Eisma, D., "Flocculation and De-Flocculation of Suspended Matter in Estuaries," *Neth. J. Sea Res.*, 20 (2/3), 1986, pp. 183-199.

Farley, K.J. and Morel F.M.M., "Role of Coagulation in the Kinetics of Sedimentation," *Environ. Sci. Technol.*, 20 (2), 1986, pp. 187-195.

Feng, J., "Flow-Fine Sediment Hysteresis in Sediment-Stratified Coastal Waters. Appendix B: Data from Second Field Tower Deployment in Hangzhou Bay," *Report*, Coastal and Oceanographic Engineering Department, University of Florida, Gainesville, Florida, USA, 1990.

Gibson, R.E., Engelund, G.L. and Hussey, M.J.L., "The Theory of One-Dimensional Consolidation of Saturated Clays, I," *Geotechnique*, 17, 1967, pp. 261-273.

Gorsline, D.S., "A Review of Fine Grained Sediment Origins, Characteristics, Transport and Deposition," In: *Fine-Grained Sediments: Deep-Water Processes and Facies*, D.A.V. Stow and D.J.W. Piper, eds., Geological Society Special Publication N° 15, Blackwell, Oxford, UK, 1984.

Grimm, R.E., "Applied Clay Mineralogy," McGraw-Hill, New York, USA, 1962.

Halliwell A.R., " Discussion on The Sea Approaches to the Port of Liverpool, by Agar and Mc Dowell", *Proc. Inst.Civil Eng.*, 51, 1972, pp. 609-620.

Halliwell A.R. and O'Connor, B.A., "Quantifying Spoil Disposal Practices", *Proc. XIV Int. Coastal Engineering Conf.*, ASCE, Copenhagen, Denmark, 1974, pp. 2581-2600.

Harleman, D.R.F., "Transport Processes in Environmental Engineering. A Series of Notes to Accompany Lectures in 1.77 Water Quality Control," Ralph M. Parsons Laboratory, Department of Civil Engineering, MIT, Cambridge, Massachusetts, USA, 1988.

Hayter, E.J. and Pakala, C.V., "Transport of Inorganic Contaminants in Estuarial Waters," *J. Coastal Res.*, Special Issue N° 5, 1989, pp. 217-230.

HR, "The Mersey Estuary. Observations of Tidal Currents, Salinities and Suspended Solids Concentrations. WRC Pilot Study, March 1982," *Report N° EX 1054*, Hydraulics Research Ltd., Wallingford, UK, 1982a.

HR, "The Mersey Estuary. Observations of Tidal Currents, Salinities and Suspended Solids Concentrations During a Spring Tidal Cycle," *Report N° EX 1088*, Hydraulics Research Ltd., Wallingford, UK, 1982b.

HR, "The Mersey Estuary. Observations of Tidal Currents, Salinities and Suspended Solids Concentrations During a Spring Tidal Cycle," *Report N° EX 1171*, Hydraulics Research Ltd., Wallingford, UK, 1983.

HR, "Mersey Barrage. Report on Hydraulic Feasibility Studies. Part I. Text and Tables," *Report N° EX 1712*, Hydraulics Research Ltd., Wallingford, UK, 1988.

HR, "Mersey Barrage Feasibility Study. Stage II. Field Sediment Measurements, September 1989," *Report N° EX 2028*, Hydraulics Research Ltd., Wallingford, UK, 1989a.

HR, "Mersey Barrage Feasibility Study Phase II. Mud Properties," *Report N° EX 1988*, Hydraulics Research Ltd., Wallingford, UK, 1989b.

HR, "Estuarine Sediments Near-Bed Processes. Verification of a Deposition Algorithm in the Mersey Estuary," *Report N° SR 251*, Hydraulics Research Ltd., Wallingford, UK, 1990a.

HR, "Mersey Barrage Feasibility Study. Stage II. Field Sediment Measurements, September 1989," *Note on HR Report N° EX 2028*, Hydraulics Research Ltd., Wallingford, UK, 1990b.

HR, "Fluid Mud in Estuaries. Field Measurements 1989," *Report N° EX 2076*, Hydraulics Research Ltd., Wallingford, UK,1990c.

HR, "Grangemouth Fluid Mud Study. Field Investigation," *Report N° SR 224*, Hydraulics Research Ltd., Wallingford, UK,1990d.

HR, "Mersey Barrage. Feasibility Study - Stage II. Hydraulic and Sedimentation Study. Sand Flux Measurement," *Report N° EX 2225*, Hydraulics Research Ltd., Wallingford, UK, 1991a.

HR, "Fluid Mud in Estuaries. Analysis of Field Measurements Made in 1989," *Report N° EX 2164*, Hydraulics Research Ltd.,Wallingford, UK, 1991b.

HR, "Fluid Mud in Estuaries," *Report N° EX 2392*, Hydraulics Research Ltd.,Wallingford, UK, 1991c.

HR, "Mersey Barrage. Feasibility Study - Stage IIIA. Hydraulic and Sedimentation Studies. Vertical Profiles of Salinity, Temperature and Turbidity on 23 November 1991," *Report N° EX 2526*, Hydraulics Research Ltd., Wallingford, UK, 1992a.

HR, "3D Mathematical Modelling of Tidal Flows and Sedimentation," *Report N° EX 2615*, Hydraulics Research Ltd., Wallingford, UK, 1992b.

Hwang, K.N., "Erodibility of Fine Sediments in Wave-Dominated Environments," *MSc Thesis*, Coastal and Oceanographic Engineering Department, University of Florida, Gainesville, Florida, USA, 1989.

Kandiah, A., "Fundamental Aspects of Surface Erosion of Cohesive Soils," *PhD Dissertation*, University of California, Davis, California, USA, 1974.

Kirby, R., "Suspended Fine Cohesive Sediment in the Severn Estuary and Inner Bristol Channel, UK," *Report N° ETSU-STP-4042*, Ravensrodd Consultants Ltd., Taunton, Somerset, UK, 1986.

Kirby, R.R., "High Concentration Suspension (Fluid Mud) Layers in Estuaries," In: *Physical Processes in Estuaries*, Job Dronkers and Wim van Leussen eds., Springer-Verlag, Berlin, Germany, 1989.

Kirby, R.R., "Detection and Transport of High Concentration Suspensions," In: *Proc. Int. Conf. on the Pearl River Estuary in the Surrounding Area of Macao*, Laboratório de Engenharia Civil de Macau, Macao, 1992.

Kirby, R.R. and Parker, W.R., "The Physical Characteristics and Environmental Significance of Fine-Sediment Suspensions in Estuaries," In: *Estuaries, Geophysics and the Environment*, National Academy of Sciences, Washington DC, USA, 1977.

Krishnappan, B.G., "Modelling of Settling and Flocculation of Fine Sediments in Still Water," *Can. J. Civil Eng.*, 17 (5), 1990, pp. 763-770.

Krone, R.B., "Flume Studies of the Transport of Sediment in Estuarial Shoaling Processes. Final Report," *Report*, Hydraulic Engineering Laboratory and Sanitary Engineering Research Laboratory, University of California, Berkeley, California, USA, 1962.

Krone, R.B., "Aggregation of Suspended Particles in Estuaries," In: *Estuarine Transport Processes*, B.J. Kjerfe, ed., University of South Carolina Press, Columbia, South Carolina, USA, 1978.

Krone, R.B., "Sedimentation Revisited," In: *Nearshore and Estuarine Cohesive Sediment Transport*, A.J. Mehta, ed., Coastal and Estuarine Studies Series, 41, AGU, Washington DC, USA, 1993.

Kusuda, T., Umita, T., Koga, K., Futawatari, T. and Awaya, Y., "Erosional Process of Cohesive Sediments," *Wat. Sci. Tech.*, 17 (6/7), 1985, pp. 891-901.

Kusuda, T., Watanabe, R., Futawatari, T. and Yamanishi, H., "Fluid Mud Movement on an Inclined Bed," In: *Nearshore and Estuarine Cohesive Sediment Transport*, A.J. Mehta ed., Coastal and Estuarine Studies Series, 41, AGU, Washington DC, USA, 1993.

Lau, Y.L. and Krishnappan, B.G., "Does Reentrainment Occur During Cohesive Sediment Settling?," *J. Hyd. Eng.* ASCE, 120 (2), 1994, pp. 236-244.

Lavelle, J.W., "A Model for Estuarine Sedimentation Involving Marine Snow," In: *Nearshore and Estuarine Cohesive Sediment Transport*, A.J. Mehta, ed., Coastal and Estuarine Studies Series, 41, AGU, Washington DC, USA, 1993.

Le Hir, P., Bassoulet, P. and L'Yavanc, J., "Application of a Multivariate Transport Model for Understanding Cohesive Sediment Dynamics," In: *Nearshore and Estuarine Cohesive Sediment Transport*, A. J. Mehta ed., Coastal and Estuarine Studies Series, 41, AGU, Washington DC, USA, 1993.

Le Hir, P. and Karlikow, N., "Sediment Transport Modelling in a Macrotidal Estuary: Do we Need to Account for Consolidation Processes?," *Proc. XXIII Int. Conf. Coastal Eng.*, ASCE, Venice, Italy, 1992, pp. 3121-3134.

Lick, W. and Huang, H., "Flocculation and Physical Properties of Flocs," In: *Nearshore and Estuarine Cohesive Sediment Transport*, A.J. Mehta, ed., Coastal and Estuarine Studies Series, 41, AGU, Washington DC, USA, 1993.

Malcherek, A., Markofsky, M. and Zielke, W., "Numerical Modelling of Settling Velocity Variations in Estuaries," *Archiv für Hydrobiologie*, 1995 (in print).

McCave, I.N., "Erosion, Transport and Deposition of Fine-Grained Marine Sediments," In: *Fine-Grained Sediments: Deep Water Processes and Facies*, D.A.V. Stow and D.J.W. Piper eds., Geological Society Special Publication N° 15, Blackwell, Oxford, UK, 1984.

McLean, S., "Theoretical Modelling of Deep Ocean Sediment Transport," *Mar. Geol.*, 66, 1985, pp. 243-265.

Mehta, A.J., "Depositional Behavior of Cohesive Sediments," *PhD Dissertation*, Coastal and Oceanographic Engineering Department, University of Florida, Gainesville, Florida, USA, 1973.

Mehta, A.J., "Characterisation of Cohesive Sediment Properties and Transport Processes in Estuaries," In: *Estuarine Cohesive Sediment Dynamics*, A.J. Mehta ed., Lecture Notes on Coastal and Estuarine Studies, N° 14, Springer-Verlag, Berlin, Germany, 1986.

Mehta, A.J., "On Estuarine Cohesive Sediment Suspension Behavior," *J. Geophys. Res.*, 94, (C10), 1989, pp. 14303-14314.

Mehta, A.J., " Review Notes on Cohesive Sediment Erosion," *Proc. Coastal Sediments '91*, ASCE, Seattle, Washington, USA, 1991a, pp.40-53.

Mehta, A.J., " Summary of Ad-Hoc Technical Panels at the Nearshore and Estuarine Sediment Transport Workshop - St. Petersburg, Florida, April 9-12, 1991", Coastal and Oceanographic Engineering Department, University of Florida, Gainesville, Florida, USA, 1991b (unpublished).

Mehta, A.J., Hayter, E.J., Parker, W.R., Krone, R.B. and Teeter, A.M., "Cohesive Sediment Transport I: Process Description", *J. Hyd. Eng. ASCE*, 115 (8), 1989a, pp. 1076-1093.

Mehta, A.J. and Lott, J.W., "Sorting of Fine Sediments During Deposition," *Proc. Coastal Sediments '87*, ASCE, New Orleans, Louisiana, USA, 1987, pp. 348-362.

Mehta, A.J., McAnnaly, W.H., Hayter, E., Teeter, A.M., Schoellhamer, D., Heltzel, S.B., and Carey, W.P., "Cohesive Sediment Transport. II: Application," *J. Hyd. Eng.* ASCE, 115 (8), 1989b, pp. 1094-1112.

Mehta, A.J. and Partheniades, E., "An Investigation of the Depositional Properties of Flocculated Fine Sediments," *J. Hyd. Res.*, 12 (4), 1975, pp. 361-381.

Mehta, A.J. and Srinivas, R. "Observations on the Entrainment of Fluid Mud by Shear Flow," In: *Nearshore and Estuarine Cohesive Sediment Transport*, A.J. Mehta ed., Coastal and Estuarine Studies Series, 41, AGU, Washington DC, USA, 1993.

Mellor, G.L. and Blumberg, A.F., "Modelling Vertical and Horizontal Diffusivities with the Sigma Coordinate System," *Mon. Wea. Rev.*, 113, 1985, pp. 1379-1383.

Mersey Dock and Harbour Board, "Report of the Committee Appointed by the Mersey Docks and Harbour Board to Investigate the Effects of the Discharge of Crude Sewage into the River Mersey," *MDHB Report*, MDHB, Liverpool, UK, 1930.

Møller-Jensen, P., "Wadden Sea Mud - Methods for Estimation of Transport, Erosion and Consolidation of Marine Cohesive Sediments," *PhD Thesis*, Department of Civil Engineering, Aalborg University, Aalborg, Denmark, 1993.

Neves, R.J., "Experimental Study and Mathematical Modelling of the Transient and Residual Circulations in the Sado Estuary" (in french), *PhD Thesis*, University of Liege, Liege, Belgium, 1985.

Nicholson, J., "Three-Dimensional Models of Particulate and Cohesive Suspended Sediment Transport," *PhD Thesis*, University of Manchester, Manchester, UK, 1983.

Nicholson, J. and O'Connor, B.A., "Cohesive Sediment Transport Model," *J. Hyd. Eng.,* ASCE, 112 (7), 1986, pp.621-640.

O'Connor, B.A., "Mathematical Model for Sediment Distribution," *Proc. XIV IAHR Cong.*, Paris, 1971, pp. D23.1-D23.8.

O'Connor, B.A., "Sediment Intrusion in a Tidal Lock," *Proc. XV IAHR Cong.*, São Paulo, Brazil, 3, 1975, pp. 301-308.

O'Connor, B.A., "Short and Long Term Changes in Estuary Capacity," *J. Geol. Soc.*, 144, 1987, pp. 187-195.

O'Connor, B.A., Ali, K.H.M. and Nicholson, J., "Mud Process Modelling: Final Report," *Report CE/5/91*, Department of Civil Engineering, University of Liverpool, UK, 1991.

O'Connor, B.A. and Nicholson, J., "Mud Transport Modelling," In: *Physical Processes in Estuaries*, J. Dronkers and W. van Leussen, eds., Springer-Verlag, Berlin, Germany, 1988.

O'Connor, B.A. and Tuxford, C., "Modelling Siltation in Dock Entrances," *Proc. Third Int. Symp. Dredging Tech.*, Bordeaux, France, 1980, pp. 359-372.

Ockenden, M., "A Model for the Settling of Non-uniform Cohesive Sediment in a Laboratory Flume and Erosional Field Setting," *J. Coastal Res.*, 9 (4), 1993, pp. 1094-1105.

Odd, N.V.M., "Mathematical Modelling of Mud Transport in Estuaries," In: *Physical Processes in Estuaries*, J. Dronkers and W. van Leussen, eds., Springer-Verlag, Berlin, Germany, 1988.

Odd, N.V.M. and Cooper, A.J., "A Two-Dimensional Model of the Movement of Fluid Mud in a High Energy Turbid Estuary," *Report N° SR 147*, Hydraulics Research Ltd., Wallingford, UK,1988.

Odd, N.V.M. and Owen, M.V., "A Two-Layer Model of Mud Transport in the Thames Estuary," *Proc. Inst. Civil Eng.*, Supplement (IX), Paper 7517S, 1972, pp. 175-205.

Odd, N.V.M. and Rodger, J.G., "Vertical Mixing in Stratified Tidal Flows," *J. Hyd. Division ASCE,* 104 (HY3), 1978, pp. 337-351.

Odd, N.V.M. and Rodger, J.G., "An Analysis of the Behaviour of Fluid Mud in Estuaries," *Report N° SR 84,* Hydraulics Research Ltd., Wallingford, UK,1986.

Oduyemi, K.O.K., "Turbulent Transport of Sediment in Estuaries," *PhD Dissertation,* Civil Engineering Department, University of Birmingham, Birmingham, UK, 1986.

Owen, M.V., "A Detailed Study of the Settling Velocities of an Estuarine Mud," *Report INT 78,* Hydraulics Research Station, Wallingford, UK, 1970.

Owen, M.V., "The Effect of Turbulence on the Settling Velocities of Silt Flocs," *Proc. XIV Cong. International Association for Water Research,* IAWR, Paris, France, 1971, pp. D4.1-D4.5.

Parchure, T.M. and Mehta, A.J., "Erosion of Soft Cohesive Sediment Deposits," *J. Hyd. Eng. ASCE,* 111(10), 1985, pp. 1308-1326.

Parker, W.R., "On the Observation of Cohesive Sediment Behavior for Engineering Purposes," In: *Estuarine Cohesive Sediment Dynamics,* A.J. Mehta ed., Springer-Verlag, Berlin, Germany, 1986.

Parker, W.R., "Definition and Determination of the Bed in High Concentration Fine Sediment Regimes," *J. Coastal Res.*, Special Issue N°5, 1989, pp. 175-184.

Parker, W.R. and Kirby, R.R., "Time Dependent Properties of Cohesive Sediment Relevant to Sedimentation Management - European Experience," In: *Estuarine Comparisons*, V.S. Kennedy ed., Academic Press, New York, USA, 1982.

Partheniades, E., "Engineering Properties of Estuarine Sediments," *NATO Advanced Institute on Estuary Dynamics (Lecture L16)*, Laboratório Nacional de Engenharia Civil, Lisbon, Portugal, 1973.

Partheniades, E., "A Fundamental Framework for Cohesive Sediment Studies," In: *Estuarine Cohesive Sediment Dynamics*, A.J. Mehta ed., Lecture Notes on Coastal and Estuarine Studies, N° 14, Springer-Verlag, Berlin, Germany, 1986.

Phillips, N.A., "A Coordinate System Having Some Special Advantages for Numerical Forecasting," *J. Meteor.*, 14, 1957, pp. 184-185.

Price, W.A. and Kendrick, M.P., "Field and Model Investigations into the Reasons for Siltation in the Mersey Estuary," *Proc. Inst.Civil Eng.*, 24, May 1963, pp. 473-518.

Richardson, J.F. and Zaki, W.N., "The Sedimentation of a Suspension of Uniform Spheres Under Conditions of Viscous Flow," *Chem. Eng. Sci.*, 3, 1954, pp. 65-73.

Roache, P.J., "Computational Fluid Dynamics," Hermosa Publishers, Albuquerque, New Mexico, USA, 1976.

Roberts, W., "Fluidisation of Mud by Waves. Development of a Mathematical Model of Fluid Mud in the Coastal Zone," *Report N° SR 296*, Hydraulics Research Ltd., Wallingford, UK, 1992.

Ross, M.A., "Vertical Structure of Estuarine Fine Sediment Suspensions," *PhD Dissertation*, Coastal and Oceanographic Engineering Department, University of Florida, Gainesville, Florida, USA, 1988.

Ross, M.A., and Mehta, A.J., "On the Mechanics of Lutoclines and Fluid Mud," *J. Coastal Res.*, Special Issue N° 5, 1989, pp. 51-62.

Sandford, L.P. and Halka, J.P., "Assessing the Paradigm of Mutually Exclusive Erosion and Deposition of Mud, with Examples from Upper Chesapeake Bay," *Mar. Geol.*, 114, 1993, pp. 37-57.

Sheng, Y.P., "Modelling Bottom Boundary Layer and Cohesive Sediment Dynamics in Estuarine and Coastal Waters," In: *Estuarine Cohesive Sediment Dynamics*, A.J. Mehta ed., Lecture Notes on Coastal and Estuarine Studies, N° 14, Springer-Verlag, Berlin, Germany, 1986.

Sills, G.C and Elder, D. McG.,"The Transition from Sediment Suspension to Settling Bed," In: *Estuarine Cohesive Sediment Dynamics*, A.J. Mehta ed., Springer-Verlag, Berlin, Germany, 1986.

Smith, I.M., "The Diffusion-Convection Equation," In: *A Survey of Numerical Methods for Partial Differential Equations*, I. Gladwell and R. Wait, eds., Oxford University Press, Oxford, UK, 1979.

Smith, T.J., "On the Representation of Reynolds Stress in Estuaries and Shallow Coastal Seas," *J. Phys. Ocean.*, 12, 1982, pp. 914-921.

Smith, T.J. and Kirby, R., "Generation, Stabilisation and Dissipation of Layered Fine Sediment Suspensions," *J. Coastal Res.*, Special Issue N° 5, 1989, pp. 63-73.

Smith, T.J. and O'Connor, B.A., "A Two-Dimensional Model for Suspended Sediment Transport," *Proc. XVII IAHR Cong.*, Baden-Baden, Germany, 1, 1977, pp. 77-84.

Smith, T.J. and Takhar, H.S., "On the Calculation of the Width-Averaged Flow Due to Long Waves in an Open Channel," *J. Hyd. Res.*, 17(4), 1979, pp. 329-339.

Smith, T.J. and Takhar, H.S., "A Mathematical Model for Partially Mixed Estuaries Using the Turbulence Energy Equation," *Estuarine Coastal Shelf Sci.*, 13, 1981, pp. 27-45.

Sly, P.G., "Marine Geological Studies in the Eastern Irish Sea and Adjacent Estuaries, with Special Reference to Sedimentation in Liverpool Bay and River Mersey," *PhD Thesis*, University of Liverpool, UK, 1966.

Spaulding, M.L., "A Vertically-Averaged Circulation Model Using Boundary-Fitted Coordinates," *J. Phys. Oceanogr.*, 14, 1984, pp. 973-982.

Srinivas, R., "Response of Fine-Sediment Water Interface to Shear Flow," *MSc Thesis*, Coastal and Oceanographic Engineering Department, University of Florida, Gainesville, Florida, USA, 1989.

Srinivas, R. and Mehta, A.J., "Observations on Estuarine Fluid Mud Entrainment," *Int. J. Sed. Res.*, 5(1), 1989, pp. 15-22.

Teeter, A.M., "Vertical Transport in Fine-Grained Suspension and Newly-Deposited Sediment," In: *Estuarine Cohesive Sediment Dynamics*, A.J. Mehta ed., Lecture Notes on Coastal and Estuarine Studies, N° 14, Springer-Verlag, Berlin, Germany, 1986.

Teisson, C., "Cohesive Suspended Sediment Transport: Feasibility and Limitations of Numerical Modelling," *J. Hyd. Res.*, 29 (6), 1991, pp. 755-769.

Teisson, C., "A Review of Cohesive Sediment Transport Models," *4th Nearshore and Estuarine Cohesive Sediment Transport Conference*, Wallingford, UK, 1994.

Thorn, M.F.C. and Parsons, J.G., "Erosion of Cohesive Sediments in Estuaries: An Engineering Guide," *Proc. Third Int. Symp. on Dredging Tech.*, H.S. Stephens, ed. BHRA, Bordeaux, France, 1980.

Toorman, E., "Modelling of Fluid Mud Flow and Consolidation," *PhD thesis*, Catholic University of Leuven, Leuven, Belgium, 1992.

Unsöld, G., "Der Transportbeginn rollingen Sohlmaterials in gleichformigen turbulenten Strommungen: eine kritische Uberprufung der Shields-Funktion und ihre experimentelle Erweiterung auf feinstkornige, nicht-bindige Sedimente," *Doctoral Dissertation*, University of Kiel, Kiel, Germany, 1982.

Urick, R.J., "Principles of Underwater Sound," McGraw-Hill, New York, USA, 1983.

van Leussen, W., "Aggregation of Particles, Settling Velocity of Mud Flocs: a Review," In: *Physical Processes in Estuaries*, W. van Leussen and J. Dronkers, eds., Springer-Verlag, Berlin, Germany, 1988.

van Leussen, W. and Cornelisse, J.M., "The Role of Large Aggregates in Estuarine Fine-Grained Sediment Dynamics", In: *Nearshore and Estuarine Cohesive Sediment Transport*, A.J. Mehta, ed., Coastal and Estuarine Studies Series, 41, AGU, Washington DC, USA, 1993.

van Olphen, H., "Clay Colloid Chemistry," Interscience Publishers, New York, USA, 1963.

Vanoni, V.A., "Sedimentation Engineering," *Report of Engineering Practice N° 54*, ASCE, New York, USA, 1975.

Verboom, G.K., "The Advection-Dispersion Equation for an An-Isotropic Medium Solved by Fractional-Step Methods," *Publication N°157*, Delft Hydraulics Laboratory, Delft, The Netherlands, 1975.

Villaret, C. and Paulic, M., "Experiments on the Erosion of Deposited and Placed Cohesive Sediments in an Annular Flume and a Rocking Flume," *Report UFL/COEL-86/007*, Coastal and Oceanographic Engineering Department, University of Florida, Gainesville, Florida, USA, 1986.

Water Pollution Research Laboratory, "The Effect of the Discharge of Crude Sewage into the Estuary of the River Mersey on the Amount and Hardness of the Deposits in the Estuary," *Wat. Pollut. Res. Lab. Tech. Pap. 7*, HMSO, London, UK, 1938.

White, F.M., "Fluid Mechanics," Mc Graw Hill, New York, USA, 1979.

Wilks, P.J., "Grab Sampling in the Mersey Estuary," *Report*, Mersey Barrage Company, Liverpool, UK, 1991.

Williamson, H.J. and Ockenden, M., "Laboratory and Field Investigation of Mud and Sand Mixtures," *Proc. First Int. Conf. Hydroscience Eng.*, Washington DC, USA, 1993, pp. 622-629.

Wolanski, E., Asaeda, T. and Imberger, J., "Mixing Across a Lutocline," *Limnol. Oceanogr.*, 34, 1989, pp. 931-938.

Yanenko, N.N., "The Method of Fractional Steps," Springer-Verlag, New York, USA, 1971.

APPENDIX A
REMARKS ON THE NATURE OF THE TRANSPORT EQUATION

The mathematical complexity of the advection-diffusion equation presented in section 3.2 for a cartesian domain makes it useful to summarise its main properties in connection with the modelling of suspended cohesive sediment transport. Taking the settling velocity as $W_s=W_s(C)$ alone, equation 3.8 can be rewritten as:

$$\varepsilon_x\frac{\partial^2 C}{\partial x^2}+\varepsilon_y\frac{\partial^2 C}{\partial y^2}+\varepsilon_z\frac{\partial^2 C}{\partial z^2}+\left(\frac{\partial \varepsilon_x}{\partial x}-u\right)\frac{\partial C}{\partial x}+\left(\frac{\partial \varepsilon_y}{\partial y}-v\right)\frac{\partial C}{\partial y} + \left(\frac{\partial \varepsilon_z}{\partial z}-w+W_s\right)\frac{\partial C}{\partial z}-\frac{\partial C}{\partial t}+\frac{\partial W_s}{\partial z}C=0 \qquad \text{(A.1)}$$

(with the same notation of Chapter 3) which corresponds to the general form

$$a(\cdot)\frac{\partial^2 C}{\partial x^2}+b(\cdot)\frac{\partial^2 C}{\partial y^2}+c(\cdot)\frac{\partial^2 C}{\partial z^2}+d(\cdot)\frac{\partial C}{\partial x}+e(\cdot)\frac{\partial C}{\partial y} +f(\cdot)\frac{\partial C}{\partial z}+g(\cdot)\frac{\partial C}{\partial t}+h(\cdot)C+i(\cdot)=0 \qquad \text{(A.2)}$$

of a second order partial differential equation (PDE) in a space x, y, z, t, where C is the dependent variable.

In general terms, when the coefficients of an n^{th} order PDE depend upon n^{th} order derivatives of the dependent variable the equation is nonlinear. When the coefficients depend upon the dependent variable or its m^{th} order derivatives ($m < n$), the equation is quasilinear. Finally, the equation is linear when they depend on the independent variables alone or are constant (Lapidus and Pinder, 1982). A classification of equation A.1 consequently depends on the functionality of coefficients $a(\cdot)$ to $i(\cdot)$.

It can be recognised that, while $a(\cdot), b(\cdot), d(\cdot), e(\cdot), g(\cdot)$ and $i(\cdot)$ are functions of the independent variables alone or are constant, the remaining may depend on the concentration and its derivatives in different ways. If the effect of vertical mass exchange inhibition due to stratification is negligible and no functional dependence of the vertical mass diffusivity on the vertical concentration gradient (i.e. through the Richardson number) is considered, equation A.1 will be quasilinear, given that $W_s=W_s(C)$. In the opposite case, and through the vertical gradient of the vertical mass diffusivity (see expressions 2.23, 2.27 and 2.19) which can, generally be described as

$$\frac{\partial \varepsilon_z}{\partial z} = \frac{\partial}{\partial z}[F(z), r(Ri)] = \frac{\partial}{\partial z}\left[F(z), R\left(\frac{\partial \rho}{\partial z}\right)\right] = \frac{\partial}{\partial z}\left[F(z), S\left(\frac{\partial C}{\partial z}\right)\right] \qquad \text{(A.3)}$$

a nonlinear behaviour can be expected (in equation A.3 F, r, R and S are generic functions and the remaining symbols have the same definitions as in Chapters 2 and 3). Equation A.1, consequently, shows a different behaviour relative to similar equations describing transport phenomena of substances for which settling of particles or inhibition of vertical turbulent exchanges due to stratification are not important, which are linear; moreover it is instructive to remark that such differences arise from terms physically related to the vertical component of transport.

From equation A.1 it is also apparent that its solution will behave differently, depending on the relative magnitude of the advective and diffusive terms and will, in extreme cases, have the properties of the limiting hyperbolic (purely advective) or parabolic (purely diffusive) solutions. Although, in strict mathematical terms, the transition between the parabolic and hyperbolic behaviours of the solution is linked

to the existence of null mass diffusivities it is hypotesised that such transition is gradual for the broad range of conditions found when describing natural flows, in actual agreement with the physics of transport phenomena (Baptista, 1987). For example, it is of interest to notice that, when solving the equation for unsteady flows, as happens with estuarine and coastal applications, the relative magnitude of advective and diffusive terms can significantly change in time (i.e. during a tidal cycle), leading to difficulties in uniquely characterising the type of solution to be expected. All the above facts justify the splitting techniques widely used when numerically solving the advection-diffusion equation, enabling adequate methods to be used to separately solve purely parabolic and purely hyperbolic problems.

References

Baptista, A.M., "Solution of Advection-dominated Transport by Eulerian-Lagrangian Methods Using the Backwards Method of Characteristics," *PhD Dissertation*, Department of Civil Engineering, MIT, Cambridge, Massachusetts, USA, 1987.

Lapidus, L. and Pinder, G.F., "Numerical Solution of Partial Differential Equations in Science and Engineering," John Wiley and Sons, New York, USA, 1982.

APPENDIX B
DIMENSIONAL ANALYSIS OF THE TRANSPORT EQUATION IN THE COMPUTATIONAL DOMAIN

In order to determine the relative magnitude of the several terms in the transport equation, which represent advective and diffusive fluxes in the three spatial directions and vertical settling fluxes, it is convenient to use, for clarity, a simplified version of equation 3.8 in the vertical cartesian plane (x, z), in the form:

$$\frac{\partial C}{\partial t} = -u\frac{\partial C}{\partial x} - w\frac{\partial C}{\partial z} + \frac{\partial}{\partial z}(W_s C) + \frac{\partial}{\partial x}\left(\varepsilon_x \frac{\partial C}{\partial x}\right) + \frac{\partial}{\partial z}\left(\varepsilon_z \frac{\partial C}{\partial z}\right) \qquad \text{(B.1)}$$

with the same notation used in Chapter 3. Results derived from the analysis of the x components of equation B.1 can be extended to both horizontal dimensions since, due to the irregularity of the horizontal boundaries in most estuaries, the magnitude of the lateral (y) fluxes is very similar to that of longitudinal (x) fluxes, when a cartesian description is adopted. This equation is transformed into a computational domain (x^*, σ, t^*) form as:

$$\begin{aligned}\frac{\partial C}{\partial t^*} = & -u\frac{\partial C}{\partial x^*} - (\mathrm{T} + u\mathrm{A} + w\Gamma)\frac{\partial C}{\partial \sigma} \\ & + \Gamma\frac{\partial}{\partial \sigma}(W_s C) + \Gamma\frac{\partial}{\partial \sigma}\left(\varepsilon_z \Gamma \frac{\partial C}{\partial \sigma}\right) \\ & + \frac{\partial}{\partial x^*}\left(\varepsilon_x \frac{\partial C}{\partial x^*}\right) + \frac{\partial}{\partial x^*}\left(\varepsilon_x \mathrm{A}\frac{\partial C}{\partial \sigma}\right) \\ & + \varepsilon_x \mathrm{A}\frac{\partial^2 C}{\partial x^* \partial \sigma} + \mathrm{A}\frac{\partial}{\partial \sigma}\left(\varepsilon_x \mathrm{A}\frac{\partial C}{\partial \sigma}\right)\end{aligned} \qquad \text{(B.2)}$$

where T, A and Γ are transformation parameters, i.e. the derivatives of the transformation with respect to t, x and z:

$$\mathrm{T}=\frac{\partial\sigma}{\partial t}$$
$$\mathrm{A}=\frac{\partial\sigma}{\partial x} \qquad \text{(B.3)}$$
$$\Gamma=\frac{\partial\sigma}{\partial z}$$

Non-dimensional variables and parameters, denoted by a prime, are defined as

$$C'=\frac{C}{C_0} \qquad t'=\frac{t^*}{t_0} \qquad u'=\frac{u}{u_0}$$

$$x'=\frac{x^*}{L} \qquad \sigma'=\frac{\sigma}{\sigma_0} \qquad w'=\frac{w}{w_0} \qquad \text{(B.4)}$$

$$W_s'=\frac{W_s}{W_{s0}} \qquad \varepsilon_x'=\frac{\varepsilon_x}{H^2}t_0 \qquad \varepsilon_z'=\frac{\varepsilon_z}{H^2}t_0$$

$$\mathrm{T}'=\frac{\mathrm{T}}{\mathrm{T}_0} \qquad \mathrm{A}'=\frac{\mathrm{A}}{\mathrm{A}_0} \qquad \Gamma'=\frac{\Gamma}{\Gamma_0}$$

where L and H are the estuarine length and depth and subscript 0 denotes characteristic maxima. Non-dimensional variables and parameters defined in B.4 are, consequently, of order 1. In B.4 t_0 is a reference time scale to be defined later, u_0, w_0 and W_{s0}, are characteristic horizontal, vertical and settling velocities and, finally, T_0, A_0 and Γ_0 are characteristic values of the transformation parameters.

Substituting the variables and parameters in equation B.2 by those resulting from the definitions in B.4 (i.e., for example, $C=C_0C'$), the following equation is obtained:

$$\left[\frac{C_0}{t_0}\right]\frac{\partial C'}{\partial t'}=-\left[\frac{u_0 C_0}{L}\right]u'\frac{\partial C'}{\partial x'}$$
$$-\left(\left[\mathrm{T}_0\right]\mathrm{T}'+\left[u_0\mathrm{A}_0\right]u'\mathrm{A}'+\left[w_0\Gamma_0\right]w'\Gamma'\right)\left[\frac{C_0}{\sigma_0}\right]\frac{\partial C'}{\partial\sigma'}$$
$$+\left[\frac{\Gamma_0 W_{s0} C_0}{\sigma_0}\right]\Gamma'\frac{\partial}{\partial\sigma'}\left(W_s'C'\right)+\left[\frac{\Gamma_0^2 H^2 C_0}{t_0\sigma_0^2}\right]\Gamma'\frac{\partial}{\partial\sigma'}\left(\varepsilon'_z\Gamma'\frac{\partial C'}{\partial\sigma'}\right) \qquad \text{(B.5)}$$
$$+\left[\frac{H^2 C_0}{L^2 t_0}\right]\frac{\partial}{\partial x'}\left(\varepsilon'_x\frac{\partial C'}{\partial x'}\right)+\left[\frac{\mathrm{A}_0 H^2 C_0}{L t_0\sigma_0}\right]\frac{\partial}{\partial x'}\left(\varepsilon'_x\mathrm{A}'\frac{\partial C'}{\partial\sigma'}\right)$$
$$+\left[\frac{\mathrm{A}_0 H^2 C_0}{L t_0\sigma_0}\right]\varepsilon'_x\mathrm{A}'\frac{\partial^2 C'}{\partial x'\partial\sigma'}+\left[\frac{\mathrm{A}_0^2 H^2 C_0}{t_0\sigma_0^2}\right]\mathrm{A}'\frac{\partial}{\partial\sigma'}\left(\varepsilon'_x\mathrm{A}'\frac{\partial C'}{\partial\sigma'}\right)$$

where the terms outside brackets (i.e., primed), are of order 1. Multiplying equation B.5 by factor t_0/C_0 :

$$\frac{\partial C'}{\partial t'}=-\left[\frac{u_0 t_0}{L}\right]u'\frac{\partial C'}{\partial x'}$$
$$-\left(\left[\mathrm{T}_0\right]\mathrm{T}'+\left[u_0\mathrm{A}_0\right]u'\mathrm{A}'+\left[w_0\Gamma_0\right]w'\Gamma'\right)\left[\frac{t_0}{\sigma_0}\right]\frac{\partial C'}{\partial\sigma'}$$
$$+\left[\frac{\Gamma_0 W_{s0} t_0}{\sigma_0}\right]\Gamma'\frac{\partial}{\partial\sigma'}\left(W'_s C'\right)+\left[\frac{\Gamma_0^2 H^2}{\sigma_0^2}\right]\Gamma'\frac{\partial}{\partial\sigma'}\left(\varepsilon'_z\Gamma'\frac{\partial C'}{\partial\sigma'}\right) \qquad \text{(B.6)}$$
$$+\left[\frac{H^2}{L^2}\right]\frac{\partial}{\partial x'}\left(\varepsilon'_x\frac{\partial C'}{\partial x'}\right)+\left[\frac{\mathrm{A}_0 H^2}{L\sigma_0}\right]\frac{\partial}{\partial x'}\left(\varepsilon'_x\mathrm{A}'\frac{\partial C'}{\partial\sigma'}\right)$$
$$+\left[\frac{\mathrm{A}_0 H^2}{L\sigma_0}\right]\varepsilon'_x\mathrm{A}'\frac{\partial^2 C'}{\partial x'\partial\sigma'}+\left[\frac{\mathrm{A}_0^2 H^2}{\sigma_0^2}\right]\mathrm{A}'\frac{\partial}{\partial\sigma'}\left(\varepsilon'_x\mathrm{A}'\frac{\partial C'}{\partial\sigma'}\right)$$

For a reference time scale, defined as a characteristic sediment settling time (Ross, 1988)

$$t_0 = \frac{H}{W_{s0}} \tag{B.7}$$

and considering that characteristic values of the transformation parameters are defined as

$$\begin{aligned} T_0 &= \frac{\sigma_0}{t_0} = \frac{\sigma_0 W_{s0}}{H} \\ A_0 &= \frac{\sigma_0}{L} \\ \Gamma_0 &= \frac{\sigma_0}{H} \end{aligned} \tag{B.8}$$

equation B.6 is transformed into:

$$\begin{aligned} \frac{\partial C'}{\partial t'} = &-\left[\frac{u_0 H}{L W_{s0}}\right] u' \frac{\partial C'}{\partial x'} \\ &-\left(\left[\frac{\sigma_0 W_{s0}}{H}\right] T' + \left[\frac{u_0 \sigma_0}{L}\right] u' A' + \left[\frac{w_0 \sigma_0}{H}\right] w' \Gamma'\right)\left[\frac{H}{W_{s0}\sigma_0}\right]\frac{\partial C'}{\partial \sigma'} \\ &+[1]\Gamma' \frac{\partial}{\partial \sigma'}(W_s' C') + [1]\Gamma' \frac{\partial}{\partial \sigma'}\left(\varepsilon'_z \Gamma' \frac{\partial C'}{\partial \sigma'}\right) \\ &+\left[\frac{H^2}{L^2}\right]\frac{\partial}{\partial x'}\left(\varepsilon_x' \frac{\partial C'}{\partial x'}\right) + \left[\frac{H^2}{L^2}\right]\frac{\partial}{\partial x'}\left(\varepsilon'_x A' \frac{\partial C'}{\partial \sigma'}\right) \\ &+\left[\frac{H^2}{L^2}\right]\varepsilon'_x A' \frac{\partial^2 C'}{\partial x' \partial \sigma'} + \left[\frac{H^2}{L^2}\right] A' \frac{\partial}{\partial \sigma'}\left(\varepsilon'_x A' \frac{\partial C'}{\partial \sigma'}\right) \end{aligned} \tag{B.9}$$

The relative importance of terms in equation B.9 (and, therefore, of the corresponding terms in equation B.2) is given by the factors within square brackets, as primed terms are of order 1. Characteristic values for estuarine geometries and flows can be considered as L=10000 m; H=10 m, u_0= 1 m/s, w_0=0.001 m/s, W_{s0}=0.001 m/s and σ_0=1. Evaluation of coefficients in B.9 therefore indicates:

(i) Vertical settling and vertical diffusion terms

The coefficients of both terms in equation B.9 are unity.

(ii) Horizontal diffusion terms

$$\left[\frac{H^2}{L^2}\right]=O(10^{-6}) \tag{B.10}$$

(iii) Horizontal advection term

$$\left[\frac{u_0 H}{L W_{s0}}\right]=O(1) \tag{B.11}$$

(iv) Vertical advection term

$$\left[\frac{\sigma_0 W_{s0}}{H}\frac{H}{W_{s0}\sigma_0}\right]=1$$

$$\left[\frac{u_0\sigma_0}{L}\frac{H}{W_{s0}\sigma_0}\right]=O(1) \tag{B.12}$$

$$\left[\frac{w_0\sigma_0}{H}\frac{H}{W_{s0}\sigma_0}\right]=1$$

i.e. the global coefficient is of order 1.

Analysis of the magnitude of the coefficients in equation B.9 therefore indicates that terms arising from horizontal diffusion terms in equation B.1 are much smaller than the remaining terms and could, in principle, be neglected. Furthermore, it should be noted that the relative magnitude of the remaining terms in equation B.9 is not the same during a tidal cycle. The characteristic value which was adopted for the horizontal velocity corresponds to fully developed ebb or flood situations. However, during a tidal cycle the horizontal velocity actually varies from very small values, in

the vicinity of slack water, to those corresponding to maximum ebb or flood; therefore, coefficient B.11 may, during the former periods, take values which are two or three orders of magnitude smaller than the coefficients of the vertical terms.

Reference

Ross, M.A., "Vertical Structure of Estuarine Fine Sediment Suspensions," *PhD Dissertation*, Department of Coastal and Oceanographic Engineering, University of Florida, Gainesville, Florida, USA, 1988.

APPENDIX C
A GENERALISED SIGMA TRANSFORMATION

A common problem in computational fluid mechanics is the existence, within the solution domain, of areas where large gradients of the independent variable are found. This requires that fine computational grids are used to represent such areas, in order to avoid major losses of accuracy in the numerical solution. A possible way to solve the problem is to uniformly refine the grid throughout the computational domain. This may, however, become costly when applications to large domains and extended time periods are sought and, furthermore, generates large amounts of unnnecessary information in areas of the domain where refinement of the computational grid is not required. Another possibility is the use of coordinate transformations, mapping cartesian domains into computational domains in such a way that a uniform grid in the latter corresponds to a grid where point clustering in areas of interest of the former is obtained.

A second problem found in many computational fluid mechanics problem is the geometrical irregularity or the time-varying nature of the cartesian domain in which the equations are being solved. This is the case when the simulation of circulation and transport phenomena in natural environments (as in estuaries an coastal areas under tidal effects) is sought. Again the use of coordinate transformations, mapping geometrically complex and time-varying domains into computational domains where uniformly spaced grids can be defined, is a convenient approach.

In the case of three-dimensional (3D) numerical modelling of suspended cohesive sediment transport in estuaries both problems are found and, therefore, the benefits resulting from the use of coordinate transformations are apparent. In general terms a full geometric transformation, mapping the cartesian x, y, z space into a computational x^*, y^*, z^* space, could be used. However, as described in Chapter 2, the key aspects to be addressed, if significant gains of accuracy in modelling are to be obtained, are related to the vertical mode of transport. A less complex approach, using vertical coordinate transformations alone, therefore, seems adequate. A generalised vertical coordinate transformation was, consequently, defined in the the following form:

$$\sigma = g(Z) = g[f(z)] \tag{C.1}$$

In equation C.1 the first function, $f(z)$, vertically maps the cartesian domain ranging from the bottom ($-H$) to the free surface (η) into an intermediate computational domain, with vertical coordinate Z ranging from -1 to 0, in such a way that uniformly spaced grid points in the intermediate domain are still uniformly spaced in the cartesian domain. The first function, therefore, corrects for the effects of a time-varying free surface, as bottom variations are assumed to be negligible at the time scale of tidal simulations. The second function in C.1 allows vertical grid refinement in zones of the domain where higher gradients are expected and, as a result, equally spaced grid points in the σ computational domain are not equally spaced in either the Z or the z domains.

The inverse transformation of C.1 will be:

$$z = f^{-1}[g^{-1}(\sigma)] = f^{-1}(Z) \qquad \text{(C.2)}$$

A function satisfying the requirements for the first function, $f(z)$, in equation C.1 is the Phillips (1957) coordinate transformation, widely used in metereology and oceanography, which has the form:

$$Z = \frac{z-\eta}{\eta+H} \qquad \text{(C.3)}$$

The second function in equation C.1, $g(Z)$, has to be defined in agreement with the physics of the phenomena to be represented and, in the case of cohesive sediments, should allow grid refinement near the lower boundary. Based on a family of general stretching transformations (Roberts, 1971; Anderson et al., 1984) one such transformation can be defined as:

$$\sigma = -\frac{\ln[(\beta - Z)/(\beta + Z)]}{\ln[(\beta + 1)/(\beta - 1)]} \qquad \text{(C.4)}$$

where β is the transformation stretching parameter ($1 < \beta < \infty$), which clusters more points near the lower boundary as it approaches unity. This transformation produces a transformed σ domain ranging from -1 at the lower boundary to 0 at the upper boundary and will be called a *Type I* transformation. For programming reasons, however, it is more intuitive to use a σ domain ranging from 0 at the lower boundary to 1 at the upper boundary and this will be called a *Type II* transformation. This transformation has the same grid clustering properties as the previous one and is defined as:

$$\sigma = 1 - \frac{\ln[(\beta - Z)/(\beta + Z)]}{\ln[(\beta + 1)/(\beta - 1)]} \qquad \text{(C.5)}$$

A *Type II* transformation was used in the development of the current version of model SUSMUD3. A plot of the normalised depth Z versus the transformed coordinate σ as

a function of the transformation parameter β , obtained using a *Type II* transformation, is presented in figure C.1.

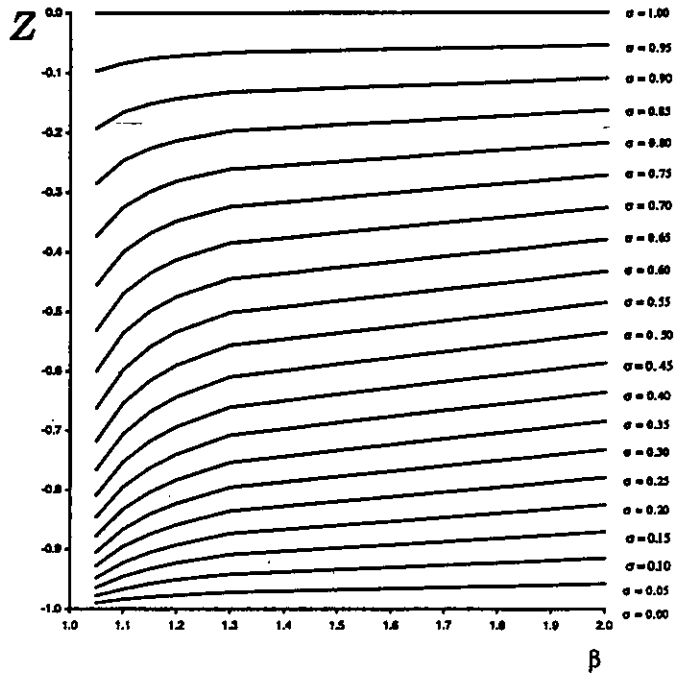

Figure C.1 Normalised depth versus the transformed coordinate, as a function of the clustering parameter.

The expression for the inverse transformation of a *Type I* transformation is:

$$Z = g^{-1}(\sigma) = \frac{\beta - \beta[(\beta+1)/(\beta-1)]^{-\sigma}}{\{[(\beta+1)/(\beta-1)]^{-\sigma}\}+1} \tag{C.6}$$

while the inverse transformation for the *Type II* is:

$$Z = g^{-1}(\sigma) = \frac{\beta - \beta[(\beta+1)/(\beta-1)]^{1-\sigma}}{\{[(\beta+1)/(\beta-1)]^{1-\sigma}\}+1} \tag{C.7}$$

Furthermore, the inverse of function f is:

$$z = f^{-1}(Z) = \eta + (H+\eta)Z \tag{C.8}$$

leading to the direct expressions for the inverse transformation:

$$z=\eta+(H+\eta)\frac{\beta-\beta[(\beta+1)/(\beta-1)]^{-\sigma}}{\{[(\beta+1)/(\beta-1)]^{-\sigma}\}+1} \tag{C.9}$$

if a *Type I* transformation is used, and:

$$z=\eta+(H+\eta)\frac{\beta-\beta[(\beta+1)/(\beta-1)]^{1-\sigma}}{\{[(\beta+1)/(\beta-1)]^{1-\sigma}\}+1} \tag{C.10}$$

for the case of a *Type II* transformation. Finally, the derivatives of the transformed coordinate with respect to the cartesian coordinates and time, which appear in the transport equation written for the computational domain, are the same for both types of the transformation:

$$\begin{aligned}
T&=\frac{\partial\sigma}{\partial t}=K\left[-\frac{\partial\eta}{\partial t}\frac{(H+z)}{(H+\eta)^2}\right]\\
A&=\frac{\partial\sigma}{\partial x}=K\left[\frac{\partial H}{\partial x}\frac{(\eta-z)}{(H+\eta)^2}-\frac{\partial\eta}{\partial x}\frac{(H+z)}{(H+\eta)^2}\right]\\
B&=\frac{\partial\sigma}{\partial y}=K\left[\frac{\partial H}{\partial y}\frac{(\eta-z)}{(H+\eta)^2}-\frac{\partial\eta}{\partial y}\frac{(H+z)}{(H+\eta)^2}\right]\\
\Gamma&=\frac{\partial\sigma}{\partial z}=K\left[\frac{1}{(H+\eta)}\right]
\end{aligned} \tag{C.11}$$

where:

$$K=K(Z)=\frac{2\beta}{\ln[(\beta+1)/(\beta-1)](\beta^2-Z^2)} \tag{C.12}$$

References

Anderson, D.A., Tannehill, J.C. and Pletcher, R.H., "Computational Fluid Mechanics and Heat Transfer," Hemisphere Publishing Corporation, New York, USA, 1984.

Phillips, N.A., "A Coordinate System Having Some Special Advantages for Numerical Forecasting," *J. Meteor.*, 14, 1957, pp. 184-185.

Roberts, G.O., "Computational Meshes for Boundary Layer Problems," In: *Proc. Second Int. Conf. Num. Methods Fluid Dyn.*, Lecture Notes in Physics, 8, Springer-Verlag, New York, USA, 1971.

APPENDIX D
CONVERGENCE, CONSISTENCY AND STABILITY ANALYSIS OF THE NUMERICAL METHODS USED IN THE TRANSPORT MODEL

D.1 General Aspects

When solving differential equations through the use of numerical methods it is required that the solutions produced by such methods approach the true solution of the original equation (for the same initial and boundary conditions) as the mesh is refined. Numerical methods possessing this property are said to be *convergent* (Anderson et al, 1984; Lapidus and Pinder, 1982). Two other important properties are *consistency* and *stability* as, for the numerical solution to be acceptable, the numerical methods must satisfy such properties.

Taking the particular case of interest, namely the solution of a partial differential equation (PDE) using a finite difference representation or equation (FDE), consistency analysis deals with the extent to which the FDE approximates the PDE it seeks to represent. A FDE is said to be consistent if the difference between the PDE and the FDE (truncation error) vanishes as the mesh is refined (Anderson et al., 1984; Lapidus and Pinder, 1982).

Stability is strictly applicable only to marching problems, i.e. those transient or transient-like problems where the solution of a PDE is required on an open domain subject to a set of initial conditions and a set of boundary conditions. This type of

problems is governed by hyperbolic or parabolic PDE's, as is the case of the advection-diffusion equation described in Chapter 3. A stable numerical method is one for which errors of any source (round-off, truncation, mistakes) are not permitted to grow as the calculation proceeds from one time step to the next (Anderson et al., 1984). Weak stability analysis deals with the growth of a single, general, round-off error and is carried out through Fourier or von Neumann Analysis. It is assumed that proof of weak stability using this method implies strong stability, i.e. that the overall error due to round-off does not grow (Anderson et al., 1984).

For marching problems governed by linear PDE's a proof of convergence is given by Lax's Equivalence Theorem. This theorem states that "given a properly posed initial value problem and a finite-difference approximation to it that satisfies the consistency condition, stability is the necessary and sufficient condition for convergence" (Anderson et al., 1984). The same authors also indicate that "most computational work proceeds as though this theorem applies also to nonlinear PDE's, although the theorem has never been proven for this more general category of equations". This approach will also be followed in the present analysis, given the mathematical nature of the advection-diffusion equation solved by model SUSMUD3 (see Appendix A).

The use of a fractional step method for solving the advection diffusion equation requires that consistency and stability of each partial step is separately investigated for the method to be consistent and stable (Verboom, 1975). In the case of model SUSMUD3 three of the four model steps were solved using finite difference methods:

vertical, longitudinal diffusion and lateral diffusion, of which the last two steps were of similar nature and can be examined in the same way. The consistency and stability analysis of the vertical step and of the longitudinal diffusion step are presented below.

D.2 Vertical Step

D.2.1 Consistency

In order to study the consistency of the numerical scheme used for the vertical step it is necessary to expand the values of C, $\bar{\varepsilon}^{\nu}$ and W_s in Taylor series about node ijk, at time step n. Consequently, and for the time derivative (omitting the asterisk notation in the independent variables and indexes i, j for clarity):

$$\frac{C_{k+1}^{n+1}-C_k^n}{\Delta t}=\frac{\partial C}{\partial t}+\frac{\Delta t}{2}\frac{\partial^2 C}{\partial t^2}+\ldots=\frac{\partial C}{\partial t}+O(\Delta t) \tag{D.1}$$

where the notation corresponding to the fractional step method (* and **) has also been replaced by the more conventional notation for consecutive time steps (n, $n+1$). Similarly the diffusive term produces:

$$\begin{aligned}
&\frac{\Gamma_k}{\Delta\sigma^2}\left[C_{k+1}^{n+1}\,\bar{\varepsilon}_{k+1/2}^{\nu}-C_k^{n+1}(\bar{\varepsilon}_{k+1/2}^{\nu}+\bar{\varepsilon}_{k-1/2}^{\nu})+C_{k-1}^{n+1}\bar{\varepsilon}_{k-1/2}^{\nu}\right]\\
&\quad=\Gamma\left[\frac{\partial C}{\partial\sigma}\frac{\partial\bar{\varepsilon}^{\nu}}{\partial\sigma}+\bar{\varepsilon}^{\nu}\frac{\partial C^2}{\partial\sigma^2}+\Delta t\,\bar{\varepsilon}^{\nu}\frac{\partial}{\partial\sigma}\left(\frac{\partial C^2}{\partial\sigma\,\partial t}\right)\right.\\
&\qquad\left.+\frac{\Delta\sigma^2}{6}\frac{\partial C^3}{\partial\sigma^3}\frac{\partial\bar{\varepsilon}^{\nu}}{\partial\sigma}+\frac{\Delta\sigma^2}{12}\bar{\varepsilon}^{\nu}\frac{\partial C^4}{\partial\sigma^4}+\ldots\right]\\
&\qquad=\Gamma\frac{\partial}{\partial\sigma}\left(\bar{\varepsilon}^{\nu}\frac{\partial C}{\partial\sigma}\right)+O(\Delta t,\Delta\sigma^2)
\end{aligned} \tag{D.2}$$

which is obtained by considering only the leading terms in the expansion of the vertical diffusion coefficients about point k:

$$\begin{aligned}
\bar{\varepsilon}^{v}_{k+1/2} &= \bar{\varepsilon}^{v}_{k} + \Delta\sigma \frac{\partial \bar{\varepsilon}^{v}}{\partial \sigma} + O(\Delta\sigma)^2 \\
\bar{\varepsilon}^{v}_{k-1/2} &= \bar{\varepsilon}^{v}_{k} - \Delta\sigma \frac{\partial \bar{\varepsilon}^{v}}{\partial \sigma} + O(\Delta\sigma)^2 \\
\bar{\varepsilon}^{v}_{k+1/2} + \bar{\varepsilon}^{v}_{k-1/2} &= 2\bar{\varepsilon}^{v}_{k} + O(\Delta\sigma)^3
\end{aligned} \tag{D.3}$$

The settling term, with the settling velocity computed at the current time step, n, as usually done in cohesive sediment models, is expanded as:

$$\begin{aligned}
&\frac{\Gamma_k}{\Delta\sigma}\left(W^{n}_{s_{k+1}} C^{n+1}_{k+1} - W^{n}_{s_k} C^{n+1}_{k}\right) \\
&= \Gamma\left[\frac{\partial}{\partial\sigma}\left(W_s C\right) + W_s \frac{\Delta\sigma}{2}\frac{\partial^2 C}{\partial\sigma^2} + W_s \Delta t \frac{\partial^2 C}{\partial\sigma\,\partial t}\right. \\
&\left. + \Delta\sigma \frac{\partial}{\partial\sigma}\left(C\frac{\partial W_s}{\partial\sigma}\right) + \Delta\sigma\,\Delta t \frac{\partial}{\partial\sigma}\left(\frac{\partial W_s}{\partial\sigma}\frac{\partial C}{\partial t}\right) + \Delta t \frac{\partial W_s}{\partial\sigma}\frac{\partial C}{\partial t} + \ldots\right] \\
&= \Gamma\frac{\partial}{\partial\sigma}\left(W_s C\right) + O(\Delta t, \Delta\sigma)
\end{aligned} \tag{D.4}$$

Collecting terms it is recognised that:

$$\begin{aligned}
&\frac{C^{n+1}_{k+1} - C^{n}_{k}}{\Delta t} - \Gamma_k\left[\frac{W_{s_{k+1}} C^{n+1}_{k+1} - W_{s_k} C^{n+1}_{k}}{\Delta\sigma} + \bar{\varepsilon}^{v}_{k+1/2}\frac{C^{n+1}_{k+1} - C^{n+1}_{k}}{\Delta\sigma^2} - \bar{\varepsilon}^{v}_{k-1/2}\frac{C^{n+1}_{k} - C^{n+1}_{k-1}}{\Delta\sigma^2}\right] \\
&= \frac{\partial C}{\partial t} - \Gamma\frac{\partial}{\partial\sigma}\left(W_s C\right) - \Gamma\frac{\partial}{\partial\sigma}\left(\bar{\varepsilon}_v\frac{\partial C}{\partial\sigma}\right) + O(\Delta t, \Delta\sigma)
\end{aligned} \tag{D.5}$$

i.e. the FDE tends to the PDE as Δt, $\Delta\sigma$ tend to zero. Therefore, the finite difference equation corresponding to the vertical step is consistent with the partial differential equation of the same step and has a truncation error of $O(\Delta t, \Delta\sigma)$.

D.2.2 Stability

The finite-difference equation for the implicit method used in the solution of the vertical step can be written in a condensed form as:

$$C_k^{n+1} - C_k^n = A\,C_{k+1}^{n+1} + B\,C_k^{n+1} + D\,C_{k-1}^{n+1} \qquad \text{(D.6)}$$

where, again, the asterisk notation (** and *), corresponding to the fractional step method, has been replaced by the more conventional notation for consecutive time steps (n, $n+1$).

The numerical solution N can be decomposed into an exact solution Ω (i.e., that computed with infinite accuracy) and a round-off error ε, as:

$$N = \Omega + \varepsilon \qquad \text{(D.7)}$$

Replacing C in the condensed equation D.6 by definition D.7:

$$(\Omega_k^{n+1} + \varepsilon_k^{n+1}) - (\Omega_k^n + \varepsilon_k^n) = A\,(\Omega_{k+1}^{n+1} + \varepsilon_{k+1}^{n+1}) + B\,(\Omega_k^{n+1} + \varepsilon_k^{n+1}) + D\,(\Omega_{k-1}^{n+1} + \varepsilon_{k-1}^{n+1}) \qquad \text{(D.8)}$$

Since the exact solution Ω must satisfy the difference equation one obtains:

$$\varepsilon_k^{n+1} - \varepsilon_k^n = A\,\varepsilon_{k+1}^{n+1} + B\,\varepsilon_k^{n+1} + D\,\varepsilon_{k-1}^{n+1} \qquad \text{(D.9)}$$

i.e. both the exact solution and the error must satisfy the same finite difference equation. Therefore the numerical error and the exact numerical solution both possess the same growth property in time. Any perturbation of the input values at the n^{th} time level will either be prevented from growing without bound - stable system - or will grow larger - unstable system (Anderson et al., 1984). Considering the distribution of errors at time level n it is assumed that the error can be written as a series in the form:

$$\varepsilon(x,y,\sigma,t) = \sum_{m,p,q} \zeta^n_{m,p,q} e^{i(\gamma_m x+\gamma_p y+\gamma_q \sigma)} \tag{D.10}$$

where $i = \sqrt{(-1)}$. The periods of the fundamental frequencies ($m, p, q=1$) are $2L_x$, $2L_y$ and $2L_\sigma$, respectively, and

$$\begin{aligned} \zeta^n_{m,p,q} &= \zeta(n\Delta t) = \zeta(t) \\ \gamma_m &= \frac{m\pi}{L_x} \quad m=0,1,...,M \\ \gamma_p &= \frac{p\pi}{L_y} \quad p=0,1,...,P \\ \gamma_q &= \frac{q\pi}{L_\sigma} \quad q=0,1,...,Q \end{aligned} \tag{D.11}$$

M, for example, is the number of intervals, Δx units long, contained in length L_x. Assuming the finite-difference equation is (locally) linear it is sufficient to examine the behaviour of a single term in the series, in the form:

$$\varepsilon_{m,p,q}(x,y,\sigma,t) = \zeta^n_{m,p,q} e^{i(\gamma_m x+\gamma_p y+\gamma_q \sigma)} \tag{D.12}$$

Replacing ε in equation D.9, the following equation is obtained:

$$(\zeta^{n+1}-\zeta^n) e^{i(\gamma_m x+\gamma_p y+\gamma_q \sigma)} = \zeta^{n+1}(Ae^{i\gamma_q \Delta\sigma}+B+De^{-i\gamma_q \Delta\sigma}) e^{i(\gamma_m x+\gamma_p y+\gamma_q \sigma)} \tag{D.13}$$

Simplifying and re-arranging equation D.13 one obtains:

$$\zeta^{n+1}(1-Ae^{i\gamma_q \Delta\sigma}-B-De^{-i\gamma_q \Delta\sigma}) = \zeta^n \tag{D.14}$$

The amplification factor G is defined as

$$G = \frac{\zeta^{n+1}}{\zeta^n} = \frac{1}{1-Ae^{i\gamma_q \Delta\sigma}-B-De^{-i\gamma_q \Delta\sigma}} = \frac{1}{1-B-(A+D)\cos\theta+i(D-A)\sin\theta} \tag{D.15}$$

where $\theta = \gamma_q \Delta\sigma$. Coefficients A, B and D are also defined as (see Chapter 4):

$$A = \Delta t\left[\frac{\Gamma_k \bar{\varepsilon}^{v}_{k+1/2}}{\Delta\sigma^2} + \frac{\Gamma_k W^{n}_{s_{k+1}}}{\Delta\sigma}\right] = E_1 + F_1$$

$$B = \Delta t\left[-\frac{\Gamma_k(\bar{\varepsilon}^{v}_{k+1/2} + \bar{\varepsilon}^{v}_{k-1/2})}{\Delta\sigma^2} - \frac{\Gamma_k W^{n}_{s_k}}{\Delta\sigma}\right] = -E_1 - E_2 - F_2 \qquad \text{(D.16)}$$

$$D = \Delta t\left[\frac{\Gamma_k \bar{\varepsilon}^{v}_{k-1/2}}{\Delta\sigma^2}\right] = E_2$$

and, therefore,

$$G = \frac{\zeta^{n+1}}{\zeta^{n}} = \frac{1}{1 + E_1 + E_2 + F_2 - (E_1 + E_2 + F_1)(\cos\theta) + i(E_2 - E_1 - F_1)\sin\theta} \qquad \text{(D.17)}$$

Furthermore it is recognised that mass diffusivities and settling velocities in consecutive vertical positions are very similar and that, consequently:

$$\begin{aligned} E_1 &\approx E_2 = E \\ F_1 &\approx F_2 = F \end{aligned} \qquad \text{(D.18)}$$

Therefore it is possible to write

$$G = \frac{\zeta^{n+1}}{\zeta^{n}} \approx \frac{1}{1 + (2E + F)(1 - \cos\theta) - iF\sin\theta} \qquad \text{(D.19)}$$

For unconditional stability $|G| \leq 1$ is required and, consequently

$$\begin{aligned} |G| = \frac{|\zeta^{n+1}|}{|\zeta^{n}|} &\approx \frac{1}{|1 + (2E + F)(1 - \cos\theta) - iF\sin\theta|} \\ &= \frac{1}{\sqrt{[1 + (2E + F)(1 - \cos\theta)]^2 + [-F\sin\theta]^2}} \end{aligned} \qquad \text{(D.20)}$$

Since both E and F are positive quantities (see the definition of Γ in equations C.11 and C.12) and $(1-\cos\theta)$ takes values in the interval $[0, 2]$ it is possible to conclude that $|G| \leq 1$, as required, and that, consequently, the numerical scheme can be expected to be stable.

D.3 Horizontal Diffusion Steps

D.3.1. Consistency

In order to analyse the consistency properties of the unidimensional Barakat and Clark method, as used in both horizontal diffusion steps, it sufficient to consider the differential equation corresponding to the longitudinal step as:

$$\frac{\partial C}{\partial t}-\frac{1}{D}\frac{\partial}{\partial x}\left[D\varepsilon^{h}\frac{\partial C}{\partial x}\right]=\frac{\partial C}{\partial t}-\varepsilon^{h}\frac{\partial^{2}C}{\partial x^{2}}-\frac{1}{D}\frac{\partial D\varepsilon^{h}}{\partial x}\frac{\partial C}{\partial x}=0 \qquad \text{(D.21)}$$

where, again, the asterisk notation in the independent variables has been omitted for clarity. The equation for the first step in the Barakat and Clark method (where the asterisk notation of the fractional step method has also been replaced by the conventional n, $n+1$ notation for time levels and subscripts j and k have been omitted) is:

$$\frac{C_i^{n+1}-C_i^{n}}{\Delta t}-\frac{1}{D_i}\left[(D\varepsilon^{h})_{i+1/2}\frac{(C_{i+1}^{n}-C_i^{n})}{\Delta x^{2}}-(D\varepsilon^{h})_{i-1/2}\frac{(C_i^{n+1}-C_{i-1}^{n+1})}{\Delta x^{2}}\right]=0 \qquad \text{(D.22)}$$

since the r values are, in fact, concentrations. Expanding C_{i+1}^{n}, C_i^{n+1}, C_{i-1}^{n} and product $D\varepsilon^{h}$ (considered at time step n) in Taylor series about point i and time step n, and simplifying the following expression is obtained:

$$\frac{\partial C}{\partial t} - \varepsilon^h \frac{\partial^2 C}{\partial x^2} + \frac{\Delta t}{2}\frac{\partial^2 C}{\partial t^2} - \varepsilon^h \frac{\Delta t}{2}\frac{\partial^3 C}{\partial x^2 \partial t} - \varepsilon^h \frac{\Delta x^2}{12}\frac{\partial^4 C}{\partial x^4}$$
$$- \frac{1}{D}\frac{\partial D\varepsilon^h}{\partial x}\frac{\partial C}{\partial x} - \frac{1}{D}\frac{\Delta t}{2}\frac{\partial D\varepsilon^h}{\partial x}\frac{\partial^2 C}{\partial x \partial t} - \frac{1}{D}\frac{\Delta x^2}{6}\frac{\partial D\varepsilon^h}{\partial x}\frac{\partial^3 C}{\partial x^3} + \qquad \text{(D.23)}$$
$$+R+O(\Delta t^2, \Delta x^3) = 0$$

where R represents additional terms which cancel when averaging. Similarly, the finite difference equation for the second step is (since s values are also concentrations):

$$\frac{C_i^{n+1} - C_i^n}{\Delta t} - \frac{1}{D_i}\left[(D\varepsilon^h)_{i+1/2}\frac{(C_{i+1}^{n+1} - C_i^{n+1})}{\Delta x^2} - (D\varepsilon^h)_{i-1/2}\frac{(C_i^n - C_{i-1}^n)}{\Delta x^2}\right] = 0 \qquad \text{(D.24)}$$

which produces, following the same procedure:

$$\frac{\partial C}{\partial t} - \varepsilon^h \frac{\partial^2 C}{\partial x^2} + \frac{\Delta t}{2}\frac{\partial^2 C}{\partial t^2} - \varepsilon^h \frac{\Delta t}{2}\frac{\partial^3 C}{\partial x^2 \partial t} - \varepsilon^h \frac{\Delta x^2}{12}\frac{\partial^4 C}{\partial x^4}$$
$$- \frac{1}{D}\frac{\partial D\varepsilon^h}{\partial x}\frac{\partial C}{\partial x} - \frac{1}{D}\frac{\Delta t}{2}\frac{\partial D\varepsilon^h}{\partial x}\frac{\partial^2 C}{\partial x \partial t} - \frac{1}{D}\frac{\Delta x^2}{6}\frac{\partial D\varepsilon^h}{\partial x}\frac{\partial^3 C}{\partial x^3} - \qquad \text{(D.25)}$$
$$-R+O(\Delta t^2, \Delta x^3) = 0$$

Averaging equations D.23 and D.25, as required by the Barakat and Clark method, the following equation is obtained:

$$\frac{\partial C}{\partial t} - \varepsilon^h \frac{\partial^2 C}{\partial x^2} - \frac{1}{D}\frac{\partial D\varepsilon^h}{\partial x}\frac{\partial C}{\partial x} + T.E. = 0 \qquad \text{(D.26)}$$

where the truncation error ($T.E.$) of the overall method is $O(\Delta t^2, \Delta x^2)$ as shown by Barakat and Clark (1966). The finite difference representation tends to the partial differential equation being solved when $\Delta t \to 0$ and $\Delta x \to 0$ and the numerical method is, therefore, consistent.

D.3.2 Stability

The finite-difference equation for the first step of the Barakat and Clark method can be written in a condensed form (omitting subscripts j and k)as:

$$C_i^{n+1} - C_i^n = A(C_{i+1}^n - C_i^n) - B(C_i^{n+1} - C_{i-1}^{n+1}) \tag{D.27}$$

Following the same method used to analyse the vertical step and replacing C in the condensed equation by the definition of the error, as in D.12, one obtains:

$$\begin{aligned}(\zeta^{n+1} - \zeta^n) e^{i(\gamma_m x + \gamma_p y + \gamma_q \sigma)} \\ = \left[A(\zeta^n e^{i\gamma_m \Delta x} - \zeta^n) - B(\zeta^{n+1} - \zeta^{n+1} e^{-i\gamma_m \Delta x})\right] e^{i(\gamma_m x + \gamma_p y + \gamma_q \sigma)}\end{aligned} \tag{D.28}$$

Simplifying and re-arranging, one obtains:

$$\zeta^{n+1}(1 + B - Be^{-i\gamma_m \Delta x}) = \zeta^n(1 + Ae^{i\gamma_m \Delta x} - A) \tag{D.29}$$

and the amplification factor becomes:

$$G = \frac{\zeta^{n+1}}{\zeta^n} = \frac{1 - A(1 - e^{i\gamma_m \Delta x})}{1 + B(1 - e^{-i\gamma_m \Delta x})} = \frac{1 - A(1 - \cos\theta - i\sin\theta)}{1 + B(1 - \cos\theta + i\sin\theta)} \tag{D.30}$$

where $\theta = \gamma_m \Delta x$. Coefficients A and B are defined as (see Chapter 4):

$$\begin{aligned}A &= \frac{\Delta t (D\varepsilon)_{i+1/2}}{\Delta x^2 D_i} \\ B &= \frac{\Delta t (D\varepsilon)_{i-1/2}}{\Delta x^2 D_i}\end{aligned} \tag{D.31}$$

and since, at consecutive longitudinal positions, such quantities are very similar, it can be considered that:

$$B \approx A \tag{D.32}$$

Considering D.32 and taking the module of the amplification factor:

$$|G| = \frac{|\zeta^{n+1}|}{|\zeta^n|} = \frac{|1-A(1-\cos\theta)+iA\sin\theta|}{|1+A(1-\cos\theta)+iA\sin\theta|}$$
$$= \sqrt{\frac{1+4A^2\sin^2\theta/2-4A\sin^2\theta/2}{1+4A^2\sin^2\theta/2+4A\sin^2\theta/2}} \le 1 \qquad \text{(D.33)}$$

since A is a positive quantity. The first step of the method is, therefore, expected to be unconditionally stable.

The finite-difference equation for the second step of the Barakat and Clark method can, again, be written in a condensed form (omitting subscripts j and k)as:

$$C_i^{n+1} - C_i^n = A(C_{i+1}^{n+1} - C_i^{n+1}) - B(C_i^n - C_{i-1}^n) \qquad \text{(D.34)}$$

Following the same method used to analyse the first step one obtains:

$$(\zeta^{n+1} - \zeta^n) e^{i(\gamma_m x + \gamma_p y + \gamma_q \sigma)}$$
$$= \left[A(\zeta^{n+1} e^{i\gamma_m \Delta x} - \zeta^{n+1}) - B(\zeta^n - \zeta^n e^{-i\gamma_m \Delta x})\right] e^{i(\gamma_m x + \gamma_p y + \gamma_q \sigma)} \qquad \text{(D.35)}$$

Simplifying and re-arranging:

$$\zeta^{n+1}(1 - Ae^{-i\gamma_m \Delta x} + A) = \zeta^n(1 - B + Be^{i\gamma_m \Delta x}) \qquad \text{(D.36)}$$

The amplification factor becomes:

$$G = \frac{\zeta^{n+1}}{\zeta^n} = \frac{1-B(1-e^{-i\gamma_m \Delta x})}{1+A(1-e^{i\gamma_m \Delta x})} = \frac{1-B(1-\cos\theta+i\sin\theta)}{1+A(1-\cos\theta-i\sin\theta)} \qquad \text{(D.37)}$$

where $\theta = \gamma_m \Delta x$, as before, and coefficients A and B are defined in D.31 and approximated as in D.32. Taking the module of the amplification factor:

$$|G| = \frac{|\zeta^{n+1}|}{|\zeta^{n}|} = \frac{|1-A(1-\cos\theta)-iA\sin\theta|}{|1+A(1-\cos\theta)-iA\sin\theta|}$$
$$= \sqrt{\frac{1+4A^2\sin^2\theta/2-4A\sin^2\theta/2}{1+4A^2\sin^2\theta/2+4A\sin^2\theta/2}} \leq 1 \qquad \text{(D.38)}$$

The second step of the Barakat and Clark method is, therefore, also expected to be unconditionally stable. Since both steps of the method have the same stability properties the overall method is also expected to be unconditionally stable.

D.5 Advection Step

A formal analysis of convergence, consistency and stability, similar in nature to those of the previous sections, becomes extremely difficult for the case of a three-dimensional backward method of characteristics for unsteady, non-uniform flow field.

In very general terms, a backward method of characteristics in which interpolations for Courant numbers ($Cu=u\Delta t/\Delta x$) greater than unity are performed at the appropriate intervals encompassing the interpolation position (i.e. out of the neighbouring region of the head of the characteristic, $[i, i+1]$ or $[i-1, i]$ in the 1D case, for a characteristic starting at point i), as in SUSMUD3, is expected to produce an unconditionally stable method, as indicated by Verwey and Daubert (1978). Therefore, stability limitations on the time step recognised in early versions of the method, are, in principle, avoided through this approach, as the concentrations at the feet of the characteristics are obtained by interpolation rather than by extrapolation (Baptista, 1986). Verwey and Daubert (1978) also indicate that the former method had been successfully used at the

Laboratoire National d'Hydraulique (Chatou, France) with linear and quadratic (as is the case of model SUSMUD3) interpolation polinomials.

In order to develop a more detailed analysis of the method it is recognised that accuracy losses may result from both steps of the method: backtracking and interpolation.

Losses of accuracy resulting from backtracking are related to errors in the calculation of the characteristic lines and, ultimately, of the positions of their feet, where interpolations will be carried out. This aspect is particularly important in unsteady, non-uniform velocity fields and leads to mass conservation problems, a critical issue in the method of characteristics. Verwey and Daubert (1978), while recognising that errors in mass balance cannot be avoided for varying velocity and spatial step conditions also indicate that, according to their own experience, such errors are very limited. This seems to be confirmed by the test performed with the advection module of SUSMUD3 and described in detail in Chapter 4.

The second cause for losses in accuracy is interpolation, in connection with the properties of the methods used. Although a large number of interpolators is available, a review of their properties within the framework of finite-element based Eulerian-Lagrangian methods did not recognise an optimal choice (Baptista, 1986). Truncation error analysis and the study of amplitude and phase errors of the several interpolators and of their propagation, leading to the evaluation of global accuracy, was carried out

by the same author for the simple 1D advection equation with constant velocities (see Baptista, 1986, for details).

For the case of a second order polinomial interpolation method (3P-LI3 in Baptista's notation) similar to that used in the successive one-dimensional interpolation scheme of model SUSMUD3 the leading term of the truncation error was found to be, for the general case ($Cu > 1$):

$$\xi(\xi^2-1)\frac{\Delta x^3}{6\Delta t}\frac{\partial^3 C}{\partial x^3} \qquad \text{(D.39)}$$

where $\xi = (x_p - x_{i-l})/\Delta x$, i.e. the normalised x coordinate relative to the central point x_{i-l} of the interpolation interval $[x_{i-l-p}, x_{i-l+1}]$. In this case, as noted by the same author, and for a given simulation time, accuracy should be improved by taking fewer (and larger) time steps. Consistency, as previously defined, can still be verified, provided $\Delta x^3/\Delta t \to 0$, when both Δx and Δt tend to zero. For the particular case of $Cu \leq 1$, (i.e. $l=0$) the leading term of the truncation error was found to be

$$\frac{u}{6}(u^2\Delta t^2-\Delta x)\frac{\partial^3 C}{\partial x^3} \qquad \text{(D.40)}$$

which indicates unconditional consistency.

Based on his previous analyses Baptista also investigated stability and convergence. His work indicated that method 3P-LI3 is unconditionally stable and unconditionally convergent.

D.6 Conclusions

The consistency and stability analyses carried out in previous sections for the vertical and longitudinal diffusion steps, the latter being also applicable to the lateral diffusion step, seem to indicate that, within the set of assumptions used in such analyses, the finite difference methods used in model SUSMUD3 are consistent and stable. Applying Lax's Equivalence Theorem, within the conditions indicated by Anderson et al. (1984), such numerical methods should also be convergent.

Regarding advection, and despite the differences between the simple case studied by Baptista (1986) and the complex application cases model SUSMUD3 is intended for, it is expected that consistency, stability and convergence properties which are similar to those of method 3P-LI3 used by the same author are also found in the advection module of the former. In particular, and in agreement with the indications of Verwey and Daubert (1978), both unconditional stability and convergence are expected.

References

Anderson, D.A., Tannehill, J.C. and Pletcher, R.H., "Computational Fluid Mechanics and Heat Transfer," Hemisphere Publishing Corporation, New York, USA, 1984.

Baptista, A. M., "Accurate Numerical Modelling of Advection-Dominated Transport of Passive Scalars. A Contribution," *Thesis*, Laboratório Nacional de Engenharia Civil, Lisbon, Portugal, 1986.

Barakat, H.Z. and Clark, J.A., "On the Solution of the Diffusion Equation by Numerical Methods," *J. Heat Transfer ASME*, 87-88, 1966, pp. 421-427.

Lapidus, L and Pinder, G.P., "Numerical Solution of Partial Differential Equations in Science and Engineering," Wiley-Interscience, New York, USA, 1982.

Verboom, G.K., "The Advection-Dispersion Equation for an An-Isotropic Medium Solved by Fractional-Step Methods," *Publication N° 157*, Delft Hydraulics Laboratory, Delft, The Netherlands, 1975.

Vervey, A. and Daubert, O., "Discussion of Accurate Calculation of Transport in Two Dimensions, by Forrest M. Holly, Jr. and Alexandre Preissman," *J. Hyd Eng.*, ASCE, 104 (7), 1978, pp. 1116-1118.

APPENDIX E

FLOWCHART OF MODEL SUSMUD3

PROGRAM SUSMUD3

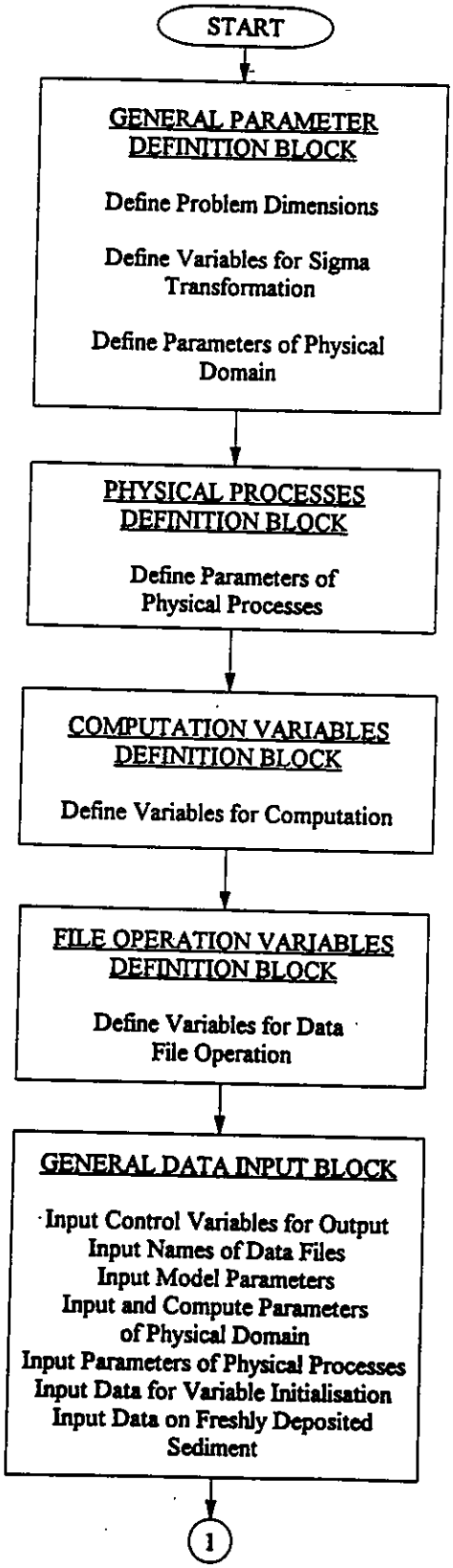

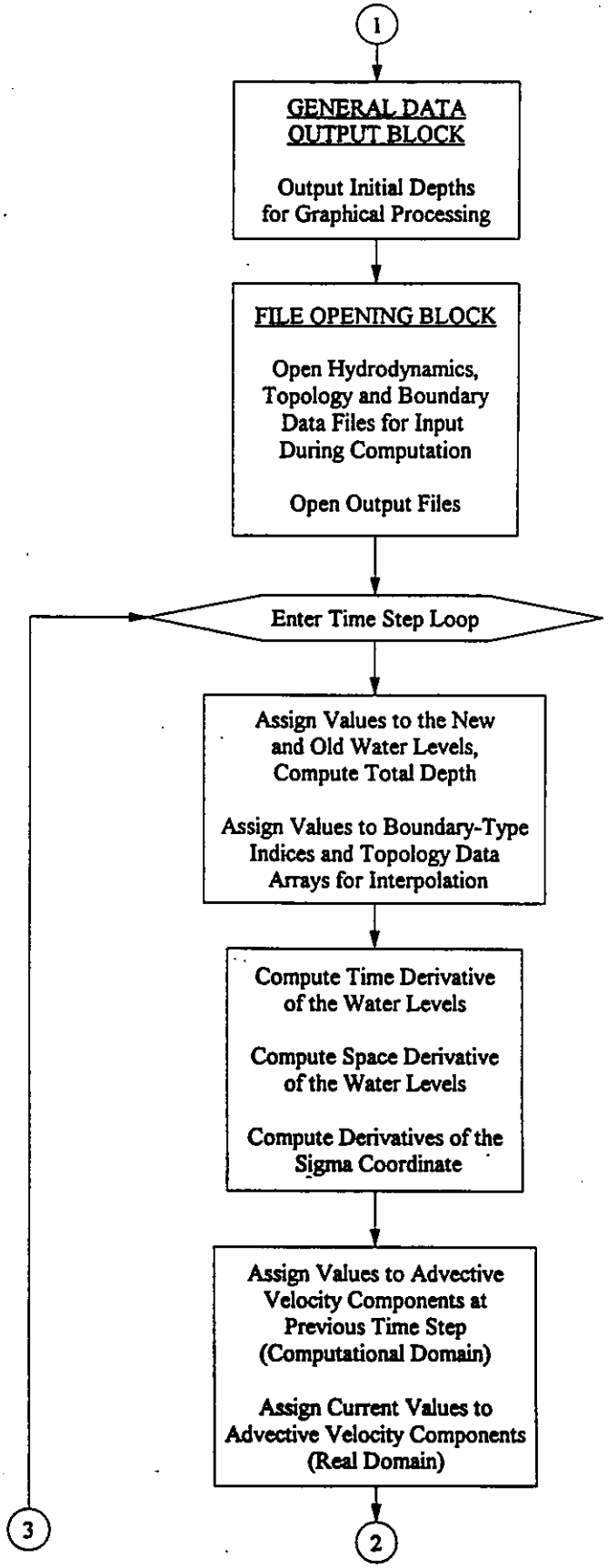
1
GENERAL DATA OUTPUT BLOCK
Output Initial Depths for Graphical Processing
FILE OPENING BLOCK
Open Hydrodynamics, Topology and Boundary Data Files for Input During Computation
Open Output Files
Enter Time Step Loop
Assign Values to the New and Old Water Levels, Compute Total Depth
Assign Values to Boundary-Type Indices and Topology Data Arrays for Interpolation
Compute Time Derivative of the Water Levels
Compute Space Derivative of the Water Levels
Compute Derivatives of the Sigma Coordinate
Assign Values to Advective Velocity Components at Previous Time Step (Computational Domain)
Assign Current Values to Advective Velocity Components (Real Domain)
3
2

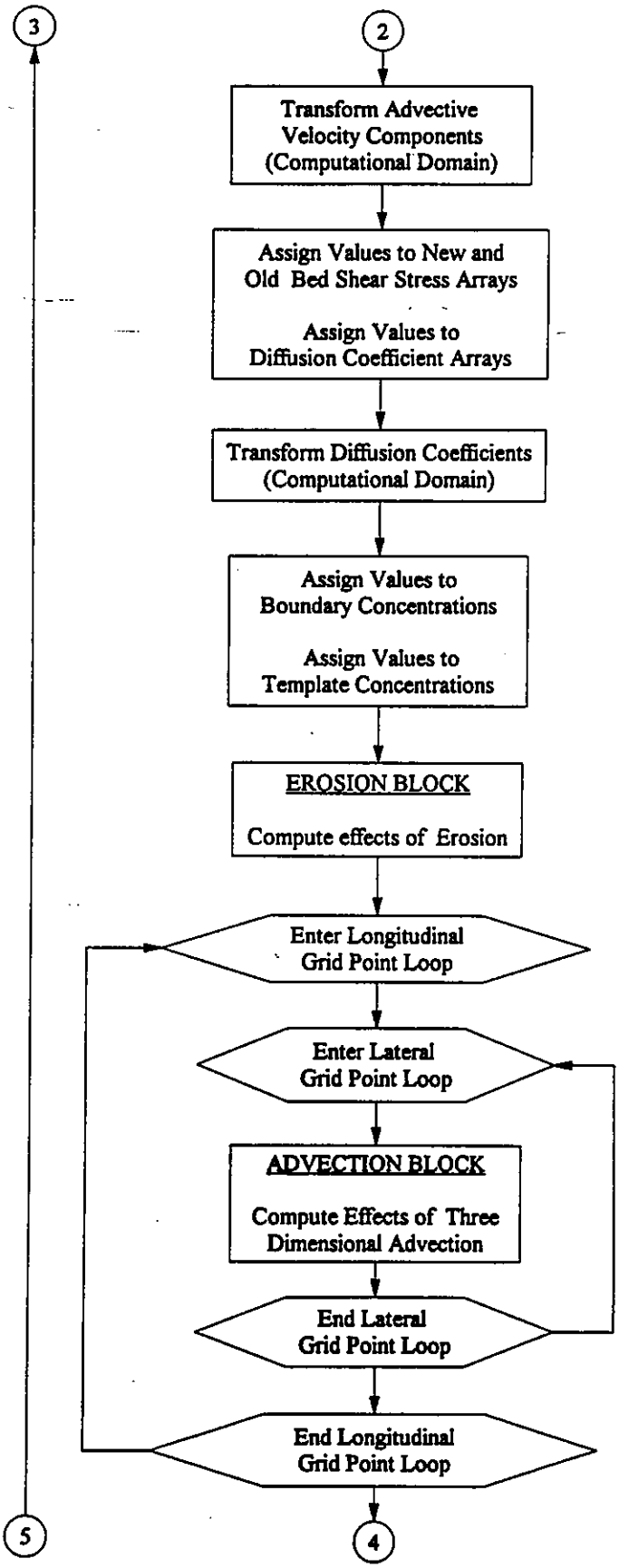
3
2
Transform Advective Velocity Components (Computational Domain)
Assign Values to New and Old Bed Shear Stress Arrays
Assign Values to Diffusion Coefficient Arrays
Transform Diffusion Coefficients (Computational Domain)
Assign Values to Boundary Concentrations
Assign Values to Template Concentrations
EROSION BLOCK
Compute effects of Erosion
Enter Longitudinal Grid Point Loop
Enter Lateral Grid Point Loop
ADVECTION BLOCK
Compute Effects of Three Dimensional Advection
End Lateral Grid Point Loop
End Longitudinal Grid Point Loop
5
4

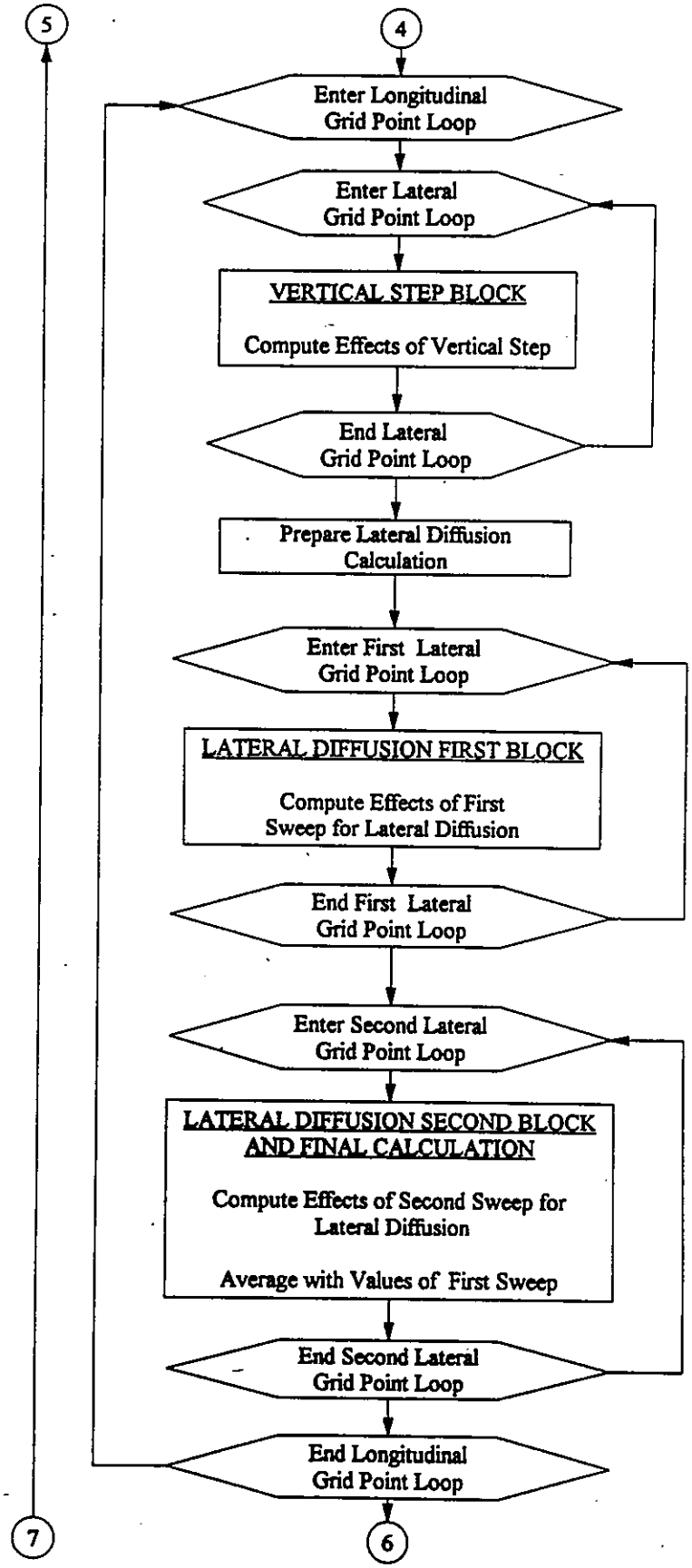
5
4
Enter Longitudinal Grid Point Loop
Enter Lateral Grid Point Loop
VERTICAL STEP BLOCK
Compute Effects of Vertical Step
End Lateral Grid Point Loop
Prepare Lateral Diffusion Calculation
Enter First Lateral Grid Point Loop
LATERAL DIFFUSION FIRST BLOCK
Compute Effects of First Sweep for Lateral Diffusion
End First Lateral Grid Point Loop
Enter Second Lateral Grid Point Loop
LATERAL DIFFUSION SECOND BLOCK AND FINAL CALCULATION
Compute Effects of Second Sweep for Lateral Diffusion
Average with Values of First Sweep
End Second Lateral Grid Point Loop
End Longitudinal Grid Point Loop
7
6

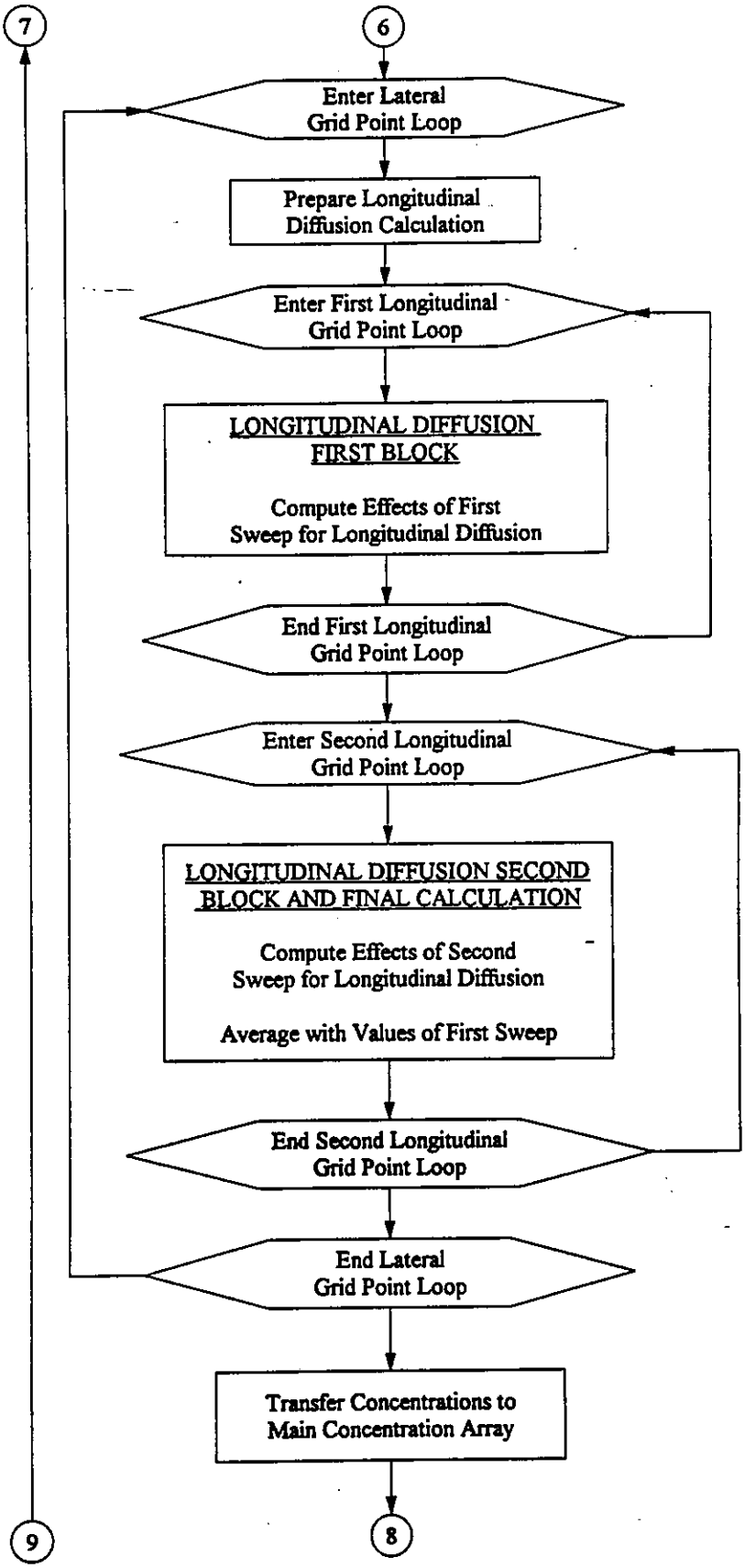
7
6
Enter Lateral
Grid Point Loop
Prepare Longitudinal
Diffusion Calculation
Enter First Longitudinal
Grid Point Loop
LONGITUDINAL DIFFUSION
FIRST BLOCK
Compute Effects of First
Sweep for Longitudinal Diffusion
End First Longitudinal
Grid Point Loop
Enter Second Longitudinal
Grid Point Loop
LONGITUDINAL DIFFUSION SECOND
BLOCK AND FINAL CALCULATION
Compute Effects of Second
Sweep for Longitudinal Diffusion
Average with Values of First Sweep
End Second Longitudinal
Grid Point Loop
End Lateral
Grid Point Loop
Transfer Concentrations to
Main Concentration Array
9
8

E.6

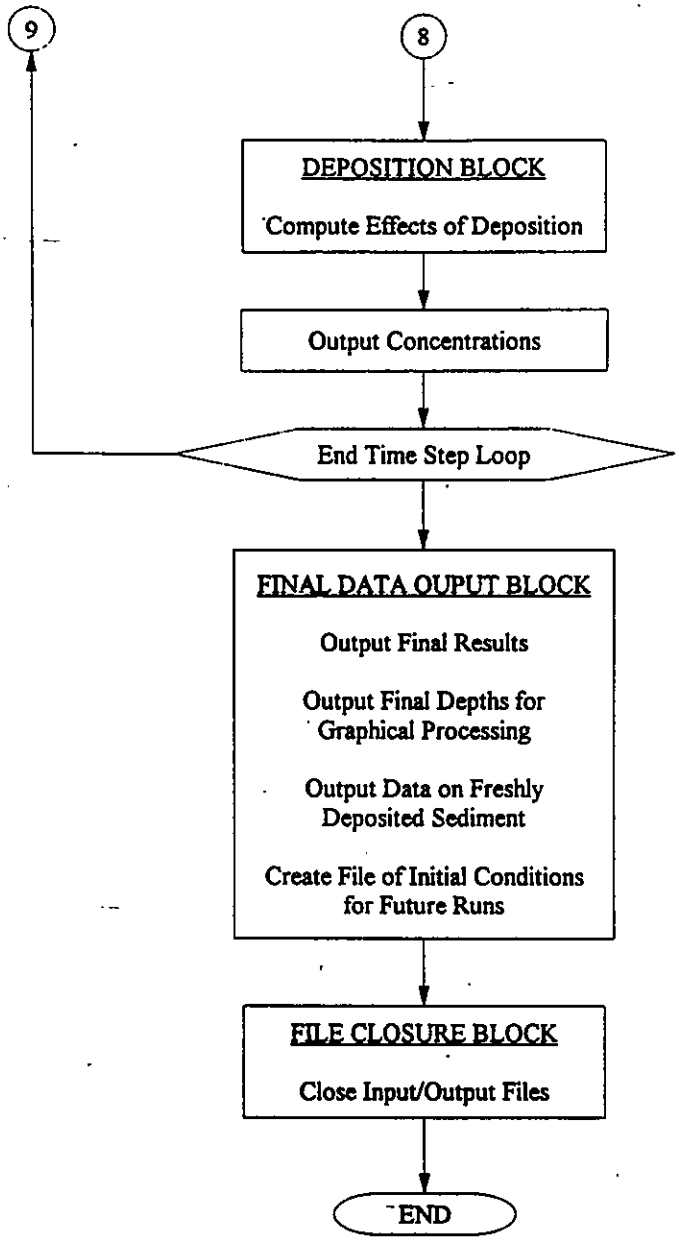
9
8
DEPOSITION BLOCK
Compute Effects of Deposition
Output Concentrations
End Time Step Loop
FINAL DATA OUPUT BLOCK
Output Final Results
Output Final Depths for Graphical Processing
Output Data on Freshly Deposited Sediment
Create File of Initial Conditions for Future Runs
FILE CLOSURE BLOCK
Close Input/Output Files
END

APPENDIX F

FLOWCHART OF MODEL FLDMUD2

PROGRAM FLDMUD2

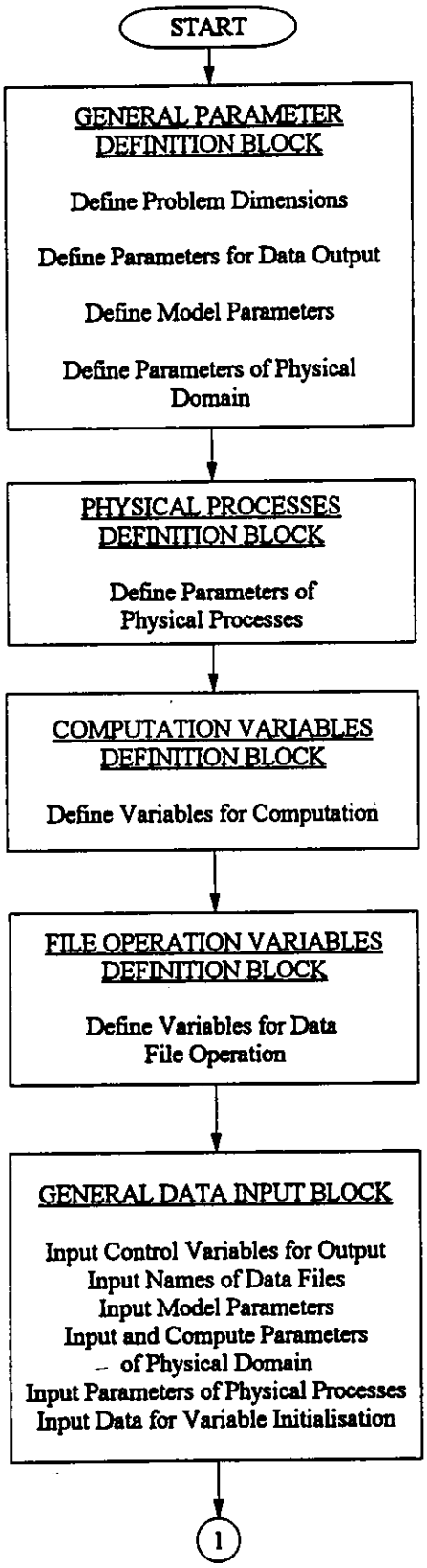

F.2

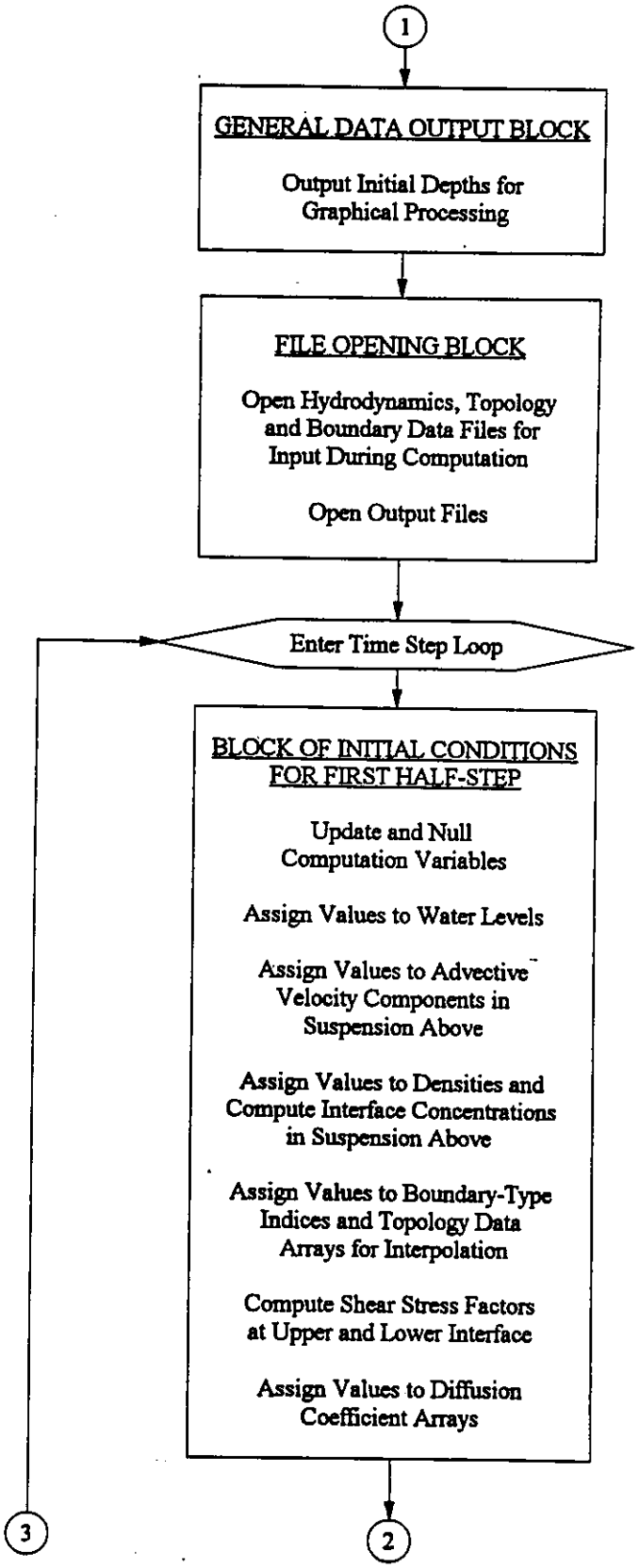
1
GENERAL DATA OUTPUT BLOCK
Output Initial Depths for Graphical Processing
FILE OPENING BLOCK
Open Hydrodynamics, Topology and Boundary Data Files for Input During Computation
Open Output Files
Enter Time Step Loop
BLOCK OF INITIAL CONDITIONS FOR FIRST HALF-STEP
Update and Null Computation Variables
Assign Values to Water Levels
Assign Values to Advective Velocity Components in Suspension Above
Assign Values to Densities and Compute Interface Concentrations in Suspension Above
Assign Values to Boundary-Type Indices and Topology Data Arrays for Interpolation
Compute Shear Stress Factors at Upper and Lower Interface
Assign Values to Diffusion Coefficient Arrays
3
2

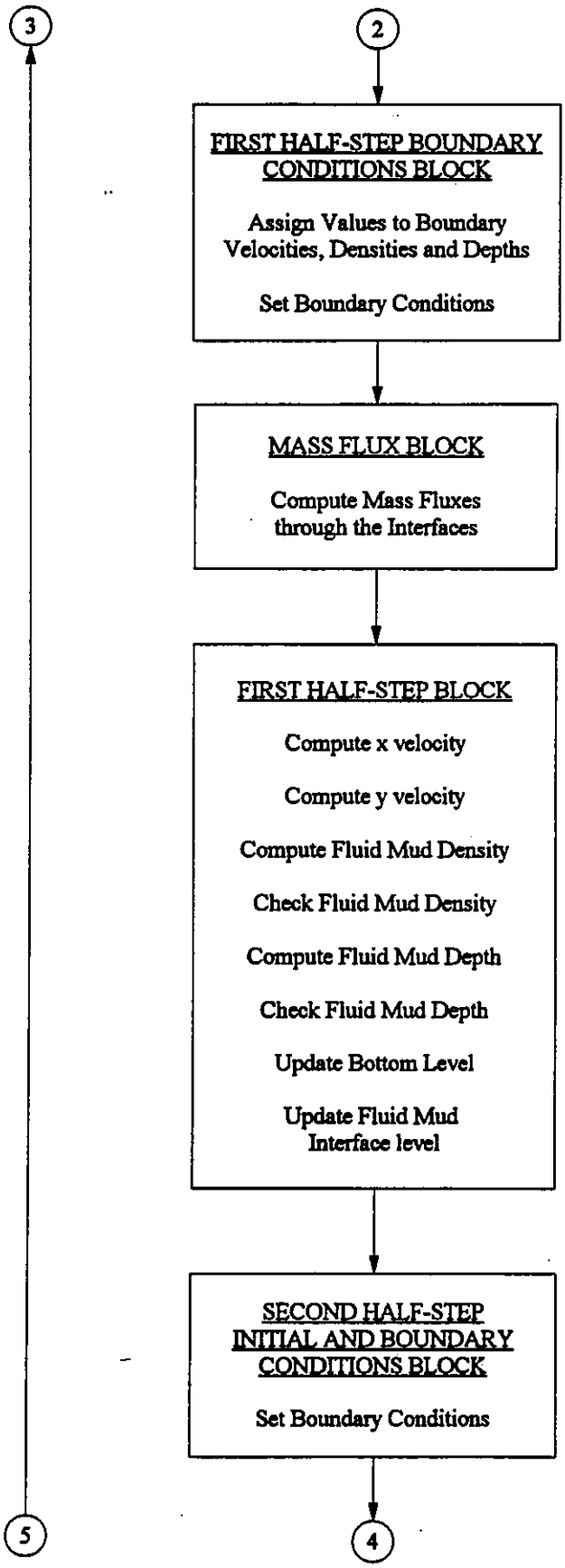
3
2
FIRST HALF-STEP BOUNDARY CONDITIONS BLOCK
Assign Values to Boundary Velocities, Densities and Depths
Set Boundary Conditions
MASS FLUX BLOCK
Compute Mass Fluxes through the Interfaces
FIRST HALF-STEP BLOCK
Compute x velocity
Compute y velocity
Compute Fluid Mud Density
Check Fluid Mud Density
Compute Fluid Mud Depth
Check Fluid Mud Depth
Update Bottom Level
Update Fluid Mud Interface level
SECOND HALF-STEP INITIAL AND BOUNDARY CONDITIONS BLOCK
Set Boundary Conditions
5
4

F.4

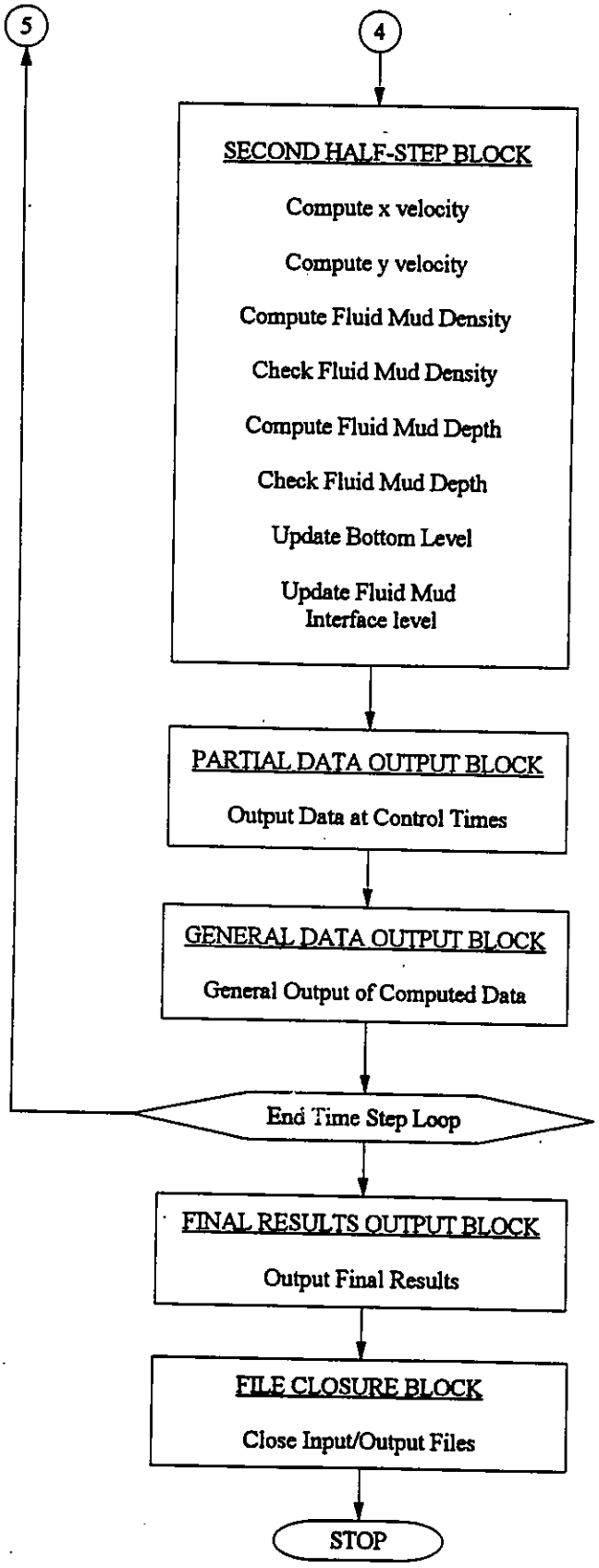
5
4
SECOND HALF-STEP BLOCK
Compute x velocity
Compute y velocity
Compute Fluid Mud Density
Check Fluid Mud Density
Compute Fluid Mud Depth
Check Fluid Mud Depth
Update Bottom Level
Update Fluid Mud Interface level
PARTIAL DATA OUTPUT BLOCK
Output Data at Control Times
GENERAL DATA OUTPUT BLOCK
General Output of Computed Data
End Time Step Loop
FINAL RESULTS OUTPUT BLOCK
Output Final Results
FILE CLOSURE BLOCK
Close Input/Output Files
STOP

F.5